NOTE TO USERS

The original manuscript received by UMI contains pages with slanted print. Pages were microfilmed as received.

This reproduction is the best copy available

UMI

UNIVERSITÉ DE MONTRÉAL

ANALYSIS OF HYDRAULICALLY EXPANDED TUBE-TO-TUBESHEET JOINTS

MAHDY ALLAM
DÉPARTEMENT DE GÉNIE MÉCANIQUE
ÉCOLE POLYTECHNIQUE DE MONTRÉAL

THÈSE PRÉSENTÉE EN VUE DE L'OBTENTION
DU DIPLÔME DE PHILOSOPHIAE DOCTOR (Ph.D.)
(GÉNIE MÉCANIQUE)
DÉCEMBRE 1996

© Mahdy Allam 1996

National Library of Canada
Acquisitions and Bibliographic Services
395 Wellington Street
Ottawa ON K1A 0N4
Canada

Bibliothèque nationale du Canada
Acquisitions et services bibliographiques
395, rue Wellington
Ottawa ON K1A 0N4
Canada

Your file Votre référence

Our file Notre référence

The author has granted a non-exclusive licence allowing the National Library of Canada to reproduce, loan, distribute or sell copies of this thesis in microform, paper or electronic formats.

The author retains ownership of the copyright in this thesis. Neither the thesis nor substantial extracts from it may be printed or otherwise reproduced without the author's permission.

L'auteur a accordé une licence non exclusive permettant à la Bibliothèque nationale du Canada de reproduire, prêter, distribuer ou vendre des copies de cette thèse sous la forme de microfiche/film, de reproduction sur papier ou sur format électronique.

L'auteur conserve la propriété du droit d'auteur qui protège cette thèse. Ni la thèse ni des extraits substantiels de celle-ci ne doivent être imprimés ou autrement reproduits sans son autorisation.

0-612-32983-6

Canada

UNIVERSITÉ DE MONTRÉAL

ÉCOLE POLYTECHNIQUE DE MONTRÉAL

Cette thèse intitulée:

ANALYSIS OF HYDRAULICALLY EXPANDED TUBE-TO-TUBESHEET JOINTS

Présentée par: ALLAM Mahdy

en vue de l'obtention du diplôme de: Philosophiae Doctor

a été dûment acceptée par le jury d'examen constitué de:

M. SHIRAZI-ADL, Aboulfazl, Ph.D., président du jury

M. CHAABAN, Ahmad, Ph.D., membre et directeur de recherche

M. BAZERGUI, André, Ph.D., membre et co-directeur de recherche

M. BOUZID, Abdel-Hakim, Ph.D., membre

M. KHARSHAFDJIAN, Gary, M.Sc.A, membre

To my father who has been looking forward to this moment.

ACKNOWLEDGEMENT

I would like to express my true gratitude to my advisors, Dr. André Bazergui, Professor and director of the Ecole Polytechnique de Montréal, and Dr. Ahmad Chaaban, Professor at the Mechanical Engineering Department. I am grateful to Dr. Chaaban for his encouragement and guidance throughout the research program and above all for his steadfast friendship. I am deeply indebted to Prof. Bazergui for his valuable technical advice, unlimited support and for his help providing me with every possible assistance.

I want to thank Mr. W. Schneider, G. McClellan and R. McGregor, Babcock and Wilcox International Division, Cambridge, Ontario, for their encouragement and generosity in allowing me to use some of their data, their facilities during my industrial training and for providing the specimens required for the experimental study.

A special appreciation is due to my friends Mr. M. Dammak, A. Hashemi and G. Noureddine. Also, I want to thank the technicians, particularly, Mr. G.Gironne, D. Julien and F. Da-Costa who helped me while preparing the experimental part of the research work.

Last, but not the least, I would like to express my deep gratitude towards my parents and my beloved wife for their encouragement, support, understanding and patience during the course of this project.

RÉSUMÉ

Souvent, quand ils sont en service, les joints tube/plaque à tube perdent leur étanchéité à cause de la diminution de la pression initiale de contact produite lors du procédé d'expansion. Ceci est dû non seulement à la charge mécanique, à la dégradation thermique et à la différence de l'expansion thermique entre le tube et la plaque à tube, mais aussi à la propagation de la fissuration sous corrosion. Durant les dernières années, la plupart des recherches académiques et industrielles dans ce domaine étaient orientées vers l'obtention d'une résistance axiale élevée du joint alors qu'on a négligé complètement le comportement complexe du joint quand il est en opération. Les conditions de fonctionnement deviennent de plus en plus sévères suite à l'accroissement requis de la pression et de la température dans les équipements industriels. En conséquence, une analyse plus exacte tenant compte des conditions de fabrication et d'opération est nécessaire.

L'étude présentée dans cette thèse est une investigation de l'expansion hydraulique des joints tube/plaque à tube utilisant différentes techniques: analytique, numérique et expérimentale. Dans le but de calculer la pression de contact résiduelle et les contraintes maximales en tension dans la zone de transition du tube, l'étude analytique doit prendre en compte la plupart des paramètres de conception. Un modèle analytique simple est développé. Ce modèle est basé sur l'interaction élastique et élasto-plastique des éléments

du joint représentés par le tube et la plaque à tube. En général, les résultats obtenus par le modèle sont en accord avec ceux obtenus numériquement par la méthode des éléments finis. Dans la mesure du possible, les résultats analytiques ont été comparés avec ceux obtenus expérimentalement.

Trois différents modèles d'éléments finis sont utilisés dans l'analyse numérique; le modèle de plan de contrainte/déformation, le modèle axisymétrique et le modèle 3-D. Le modèle axisymétrique 2-D est utilisé dans l'analyse d'une manière intensive afin depasser les limites des modèles de plan de contrainte et de plan de déformation (calcul de contraintes résiduelles dans la zone de transition du tube). Il permet de remplacer le modèle 3-D qui exige un temps de calcul en CPU (Central Processing Unit) énorme et qui nécessite plus d'espace mémoire. Les modèles éléments finis sont principalement utilisés pour étudier l'effet d'implication des paramètres de conception sur la résistance du joint et sur les contraintes résiduelles maximales. Ces modèles sont aussi utilisés en vue de simuler le comportement complexe du joint lors des charges mécanique et thermique. L'effet de la flexion de la plaque tubulaire sur le joint a été étudiée en imposant un déplacement équivalent sur le joint. Les résultats ont été comparés avec ceux obtenus expérimentalement et analytiquement par d'autre chercheurs

Des essais de traction sont réalisés en vue de vérifier les modèles analytiques et numériques proposés. La résistance à la traction ainsi que le déplacement relatif entre le

tube et la surface de contact de l'anneau a été mesuré expérimentalement. Un autre montage d'essai est réalisé en vue de déterminer le coefficient de friction pour être utilisé dans les études numériques et analytiques. La rugosité de surface est mesurée avant et après l'expansion dans le but d'examiner le changement produit lors de l'expansion.

Une étude initiale paramétrique montre que le niveau d'écrouissage et le jeu radial ont un effet significatif sur le niveau de la pression de contact résiduelle. Cependant, leur effet sur la contrainte maximale résiduelle est moins importante. L'effet de ces deux paramètres sur la pression de contact résiduelle est pris en compte dans l'étude analytique qui s'avère en bon accord avec la méthode des éléments finis. Une analyse paramétrique additionnelle est présentée dans le but d'étudier l'effet des paramètres de conception sur les contraintes résiduelles lors du chargement et du déchargement. L'analyse démontre que les contraintes lors du chargement sont indépendantes du matériau du tube et de la plaque à tube quand ces contraintes sont normalisées par rapport à la contrainte d'écoulement du matériau du tube. Aussi, les résultats de cette analyse indiquent que la contrainte résiduelle maximale, dont la valeur varie entre 86 et 109 % de la contrainte d'écoulement du tube, est toujours dans la direction axiale.

Les méthodes analytiques et numériques sont aussi utilisées pour étudier la relation entre la résistance à la traction du joint et la pression de contact résiduelle. Elles indiquent une relation linéaire entre ces deux paramètres. Cependant, une différence d'environ 40%

est observée entre la résistance à la traction calculée par la méthode des éléments finis et celle estimée analytiquement par certains manufacturiers. Les mesures expérimentales des charges de traction confirment que la solution par la méthode des éléments finis est adéquate.

Enfin, l'étude paramétrique est poussée plus loin afin d'étudier l'effet des conditions de fonctionnement à température sur à la fois la pression de contact résiduelle et les contraintes résiduelles maximales. L'analyse indique qu'à la température de fonctionnement, les contraintes résiduelles maximales de tension dans la zone de transition du tube ne changent pratiquement pas. À l'opposé, l'effet de la température de fonctionnement sur la pression de contact résiduelle est significatif et dépend de la valeur et du signe du terme $((\alpha_t - \alpha_s).\Delta T)$. En plus, la méthode des éléments finis indique que le chargement mécanique a un effet significatif sur à la fois les contraintes maximales résiduelles et sur la pression de contact résiduelle. Une perte d'étanchéité de 50 % est obtenue en simulant la flexion de la plaque tubulaire produite du côté secondaire. Par ailleurs, un gain de 15% est obtenue lors de la pressurisation de côté primaire.

Le niveau optimal d'expansion défini par l'équation proposée est recommandé pour l'utilisation dans les application industrielles. Une procédure de conception pour l'évaluation des performances du joint basée sur les résultats obtenus dans cette thèse est aussi suggérée.

ABSTRACT

Expanded tube-to-tubesheet joints often fail during service conditions because of losing the initial tightness set up by the expansion process. This results not only from the mechanical loading, thermal degradation and difference in thermal expansion of the tube and tubesheet materials but also from the spread of corrosion cracking. Over the years, most academic and industrial research in this field were oriented towards the attainment of higher axial joint strength at the manufacturing stage while no particular attention was paid to the complex behaviour of the expanded joint in operation. The service conditions become more and more severe due to the required increase in the operating pressure and temperature of industrial equipments. Consequently, the expanded tube-to-tubesheet joint needs more accurate analysis taking into account both the manufacturing and working conditions.

The study presented in this thesis is an attempt to investigate the hydraulically expanded tube-to-tubesheet joints using various techniques, namely: analytical, numerical and experimental. The analytical study takes into account most design parameters in order to calculate the residual contact pressure and the maximum tensile residual stresses in the tube transition zone. A simple analytical model was developed based on elastic and elastic-plastic interaction of the joint elements represented by the tube and tubesheet. In general, the results obtained by the proposed model compare well with those obtained numerically using

the finite element method. In some cases the results of the analytical model were compared with those obtained experimentally. Also, the optimum level of expansion beyond which the joint axial strength would brake off, is suggested.

Three different finite element models are used for the numerical analysis, namely: 2-D plane stress/strain, 2-D axisymmetric and 3-D. The 2-D axisymmetric model is extensively used during the analysis to overcome the limitation (e.g. calculation of residual stress in the tube transition zone) of the 2-D plane stress/strain model and to economically replace the full 3-D model that normally consumes huge CPU (Central Processing Unit) time and requires extensive hardware memory. The FE models are mainly used to investigate the effect of the involved design parameters on the joint strength and level of maximum tensile residual stresses. The models are also used to simulate the complex joint behaviour resulting from mechanically and/or thermally induced loads. In addition, they allow the investigation of the effect of the working condition (e.g. temperature effect and mechanical loading) on both the residual contact pressure and residual stresses. The influence of the tubesheet deflection on the residual contact pressure is also investigated. The results have been compared to experimental and analytical data reported in the literature.

Pull-out tests are performed to verify our analytical and numerical models. The pull-out strength is obtained together with the micro tangential relative displacement at the tube and annular sleeve contacting surfaces. Another experimental setup is performed to

determine the coefficient of friction that can be used for the numerical and analytical analyses. A measurement of the roughness of tube and tubesheet contacting surfaces is considered before and after expansion in order to examine the change in the surface due to the high contact pressure.

An initial parametric study shows that both the strain hardening level and the radial clearance have a significant effect on the level of the residual contact pressure but have less influence on the maximum tensile residual stresses. Therefore, the effect of these two parameters on the residual contact pressure is taken into account by the analytical analysis which consequently shows good agreement with finite element method. An additional parametric analysis is performed to investigate the effect of the design parameters on the loading, unloading and residual stresses. The analysis shows that the loading stresses are independent of the tube and tubesheet materials when these stresses are normalized to the yield strength of the tube material. Also, the results of this analysis indicate that the maximum tensile residual stress is always in the axial direction and ranges between 86% to 109% of the tube yield strength.

Both the finite element and analytical methods are also used to investigate the relationship between the pull-out joint strength and the initial residual contact pressure. They indicate a linear relation between those two parameters. However, a difference of about 40% is observed between pull-out strength calculated by the finite element method and that provided by the simple equation often used in the industrial application to calculate the joint

pull-out load. The experimental measurement for the pull-out load confirms the adequacy of the finite element solution.

Finally, the parametric study is extended further to investigate the effect of the working conditions (e.g. temperature effect and mechanical loading) on both the residual contact pressure and maximum tensile residual stresses. The analysis indicates that during the working temperature, the maximum tensile residual stresses in the tube transition zone are practically unchanged. On the contrary, the effect of the working temperature on the residual contact pressure is significant and depends on the value and the sign of the thermal term $((\alpha_t - \alpha_s)\ \Delta T)$. In addition, the 3-D finite element method indicates that the tubesheet rim displacement has a significant effect on both the maximum tensile residual stresses and residual contact pressure. A correlation factor of about -0.5 is obtained between the joint tightness coefficient and the tubesheet rim displacement. On the other hand, a smaller correlation factor of about +0.15 is found between the primary side pressure and the joint tightness coefficient.

The optimum level of expansion defined by the closed form equation is recommended for use in the industrial application. When this level of expansion pressure is used, there is a high probability to obtain a good joint with a maximum residual contact pressure. A design procedure based on the results presented in this thesis for the evaluation of joint performance is also suggested.

CONDENSÉ EN FRANÇAIS

L'expansion de joint est la technique la plus commune pour rattacher les éléments tubulaires dans les pièces de machine tel que les vaisseaux de pression, les échangeurs de chaleur, les générateurs de vapeur, les systèmes de canalisation, les compresseurs et les moteurs à combustion. Comparativement à d'autres méthodes de fabrication et d'assemblage, le procédé d'expansion est très économique et efficace mais peut être la cause de contraintes résiduelles pouvant donner lieu à la fissuration sous corrosion (Stress Corrosion Cracking, SCC).

Cette thèse couvre spécifiquement le joint tube/plaque à tube. Réalisé correctement, le procédé d'expansion produit une pression de contact résiduelle suffisante pour assurer l'étanchéité du joint, et ce pour toutes les conditions d'utilisation. Il s'avère cependant, que dans le cas des applications à hautes températures, la différence de dilatation entre le tube et plaque à tube cause une relaxation dans la paroi du tube et soulage la pression de contact créé par le procédé d'expansion. C' est pourquoi que pour des applications requérant un haut niveau d'étanchéité, la norme TEMA (1988) recommande d'utiliser une combinaison de soudage et de dudgeonnage (expansion à l'aide de rouleaux). En fait, dans beaucoup de cas, le dudgeonnage est la seule méthode pratique qui permet d'attacher les tubes en un

contact intime avec la plaque à tube. La qualité et la souplesse de cette méthode de connexion est attestée par son utilisation presque universelle.

À part le dudgeonnage, les joints peuvent être installés par une variété de méthodes, notamment, les procédés d'expansion hydraulique, hybride et explosive. L'expansion hydraulique a de nombreux avantages sur le dudgeonnage conventionnel: Rapidité, uniformité des joints, contraintes résiduelles réduites dans le tube, aptitude d'accommoder des tubes non circulaires, et possibilité de régulariser les forces dans le tube pour les équipements ayant deux plaques à tube.

Le joint tube/plaque à tube peut céder de plusieurs manières durant les épreuves, et durant les différentes étapes de fonctionnement. Les mécanismes de ruptures les plus connus sont la fissuration sous corrosion et la fatigue due aux charges induites thermiques et mécaniques. La plupart des ruptures surviennent dans les parties des tubes qui sont directement situées au-delà de la face secondaire de la plaque à tube où les tubes sont sujet à la flexion ou à la torsion et au chargement thermique. Les joints peuvent aussi lâcher dans cette zone en présence de vibrations induites par le fluide. La charge due a la pression différentielle sur les surfaces de la plaque à tube pourrait aussi introduire un mécanisme de rupture additionnel, réduire la pression résiduelle de contact et provoquer ainsi, la perte

d'étanchéité entre les côtés secondaire et primaire de l'échangeur.

Une revue détaillée de la littérature nous a permis de constater que ce sujet a fait l'objet de plusieurs recherches depuis les années quarante. La résistance du joint dépend de divers paramètres de conception et est très reliée aux conditions de fonctionnement. Bien que, dans certains cas, certaines fuites sont tolérées dans des regénérateurs de chaleur (fluide identique à l'intérieur et à l'extérieur du tube), dans d'autres cas, par exemple dans les échangeurs de chaleur où les fluides pourraient former un mélange explosif, la moindre fuite est inacceptable.

Les méthodes de conception des joints ne peuvent prendre en considération tous les paramètres impliqués. Par exemple, peu de travaux de recherche ont été réalisés sur l'influence du cycle thermique sur la pression résiduelle de contact. Aussi, au meilleur de nos connaissances, aucune recherche n'a été réalisée sur l'effet du cycle thermique sur le niveau des contraintes résiduelles maximales en tension. L'effet d'un chargement mécanique, tel que causé par la déformation de la plaque à tube, sur la pression résiduelle de contact et sur la contrainte résiduelle maximale de tension n'a pas été étudié jusqu'ici.

La recherche qui a fait l'objet de cette thèse couvre une analyse détaillée de la

pression résiduelle de contact et des contraintes résiduelles du joint tube/plaque à tube assemblé par expansion hydraulique. La méthode des éléments finis ainsi que les méthodes expérimentales et analytiques ont été utilisées dans notre étude afin d'aboutir à une méthode générale de conception.

L'objectif de notre programme de recherche peut être résumé comme suit:

1- identifier les plus importants paramètres à être pris en compte dans un modèle analytique basé sur une interaction élasto-plastique des deux éléments du joint (tube et plaque à tube) permettant de prédire la pression résiduelle de contact et de spécifier la pression d'expansion optimale basée sur le niveau maximal des contraintes résiduelles introduites dans la zone de transition du tube;

2- étudier les profils des contraintes résiduelles dans la zone de transition du tube, en fonction des paramètres du joint;

3- approximer la résistance du joint à la traction à l'aide de la méthode des éléments finis et des méthodes expérimentales et analytiques;

4- analyser l'effet des cycles de température et des charges mécaniques, sur la pression résiduelle et sur les contraintes maximales résiduelles en tension;

5- proposer une méthode de conception qui pourrait augmenter l'efficacité et la

fiabilité des assemblages tubes/plaque à tube.

Nous avons adopté un modèle axisymétrique par élément fini pour trouver la relation entre les paramètres d'un joint idéalisé, la pression résiduelle et les contraintes maximales résiduelles en tension. Les résultats indiquent que la plupart des paramètres rattachés aux dimensions (jeu radial, dimension du tube,.....) et aux matériaux (limite d'écoulement, module d'élasticité, ...) influencent énormément le niveau de la pression résiduelle de contact mais ont peu d'effet sur la contrainte maximale résiduelle de tension. Une analyse approximative élasto-plastique nous a permis d'étudier le procédé hydraulique d'expansion du joint tube/plaque à tube: Trois équations générales ont ainsi été proposées pour la pression d'expansion minimale, maximale et la pression résiduelle de contact. Le rapport du module d'élasticité du tube et de la plaque à tube a une grande influence sur la pression résiduelle de contact.

Nous avons aussi developpé une méthode analytique simplifiée pour calculer la pression de contact résiduelle du joint et pour évaluer les profils des contraintes résiduelles sur les surfaces intérieures et extérieures du tube dans la zone de transition. L'approche élasto-plastique en état plan de contrainte et la théorie de la poutre sur fondation élastique a été adoptée dans le développement du modèle. Les contraintes résiduelles maximales de

tension obtenues par le modèle analytique ont été validées en les comparant à celles déterminées expérimentalement et par la méthode des éléments finis.

L'approche analytique a été étendue pour calculer la résistance en traction du joint tube/plaque à tube et a démontré une toute différence entre les niveaux de résistance en traction et en compression mais, les deux sont en relation linéaire avec le niveau de la pression résiduelle de contact. Les résultats des éléments finis indiquent que la résistance en traction est approximativement 40% plus basse que celle en compression.

Une série de mesures expérimentales a été réalisée pour obtenir le coefficient de friction entre les surfaces de contact du tube et de la plaque à tube après l'expansion. Deux montages expérimentaux ont été utilisés pour évaluer les caractéristiques de friction entre le tube et la plaque à tube, et pour déterminer la résistance du joint en traction. Les mesures de la rugosité des surfaces du tube et de la plaque à tube ont indiqué un changement dans la rugosité de ces surfaces suite au procédé d'expansion influençant, par conséquent, on a supposé que le coefficient de friction change. Pour le matériau testé, un coefficient de friction de près de 0.1375 ± 0.004 était mesuré et le modèle de friction suivait la loi de friction de Coulomb. Le modèle axisymétrique d'élément fini a donné des résultats comparables à ceux mesurés expérimentalement.

Afin de valider nos analyses par des modèles axisymétriques, nous avons effectué quelques analyses d'éléments finis en 3-D. Ceci a permis de valider le diamètre équivalent du manchon représentant la plaque à tube dans le cas du calcul de la pression initiale de contact, de la déformation et pour les analyses thermiques. Aussi, tous les cas considérés dans l'étude paramétrique indiquent que pendant le chargement thermique et après le cycle de température, les contraintes maximales résiduelles de tension dans la zone de transition de tube sont pratiquement inchangées. Cependant, le niveau du coefficient d'étanchéité du joint est très influencé par le terme thermique $((\alpha_t - \alpha_s)\Delta T)$ ainsi que par le niveau de la déformation plastique introduite dans le tube et la plaque à tube.

Finalement nous avons utilisé la méthode des éléments finis couplée à la méthode de corrélation statistique pour réaliser l'étude paramétrique du chargement mécanique. Les études d'éléments finis en 3-D ont indiqué que la déflexion de la plaque à tube a un effet important aussi bien sur la pression résiduelle de contact que sur les contraintes résiduelles maximales de tension dans la zone de transition de tube. Aussi, l'analyse a montré qu'un coefficient d'étanchéité du joint au-delà de 40% correspond à une faible déformation plastique dans le ligament de la plaque à tube.

Le niveau d'expansion optimum qui est complètement défini par une seule équation

est recommandée pour utiliser dans l'application pratique dans l'industrie. Quand ce niveau de pression d'expansion est utilisé, la probabilité est élevée pour avoir un joint avec une pression de contact résiduel maximale. Une procédure de design basé sur les résultats de cette thèse est aussi recommandée pour l'évaluation de la performance des joints.

TABLE OF CONTENTS

DEDICATION iv

ACKNOWLEDGEMENT v

RÉSUMÉ vi

ABSTRACT x

CONDENSÉ EN FRANÇAIS xiv

TABLE OF CONTENTS xxii

LIST OF TABLES xxviii

LIST OF FIGURES xxxiii

NOMENCLATURE AND ABBREVIATION xlv

LIST OF APPENDICES li

CHAPTER 1: INTRODUCTION 1

1.1 GENERAL 1

1.2 REQUIREMENTS AND FUNCTIONAL BEHAVIOUR 3

1.3 JOINT TYPES 5

1.3.1 Roller Expansion 5

1.3.2 Hydraulic Expansion 7

1.3.3 Grooved joints 9

1.4 FAILURE MECHANISMS IN TUBE-TO-TUBESHEET JOINTS 10

1.5 OBJECTIVE AND METHODOLOGY OF THE RESEARCH WORK 11

CHAPTER 2: LITERATURE SURVEY ..... .24

2.1 INTRODUCTION AND HISTORICAL BACKGROUND 24

2.2 AS-EXPANDED TUBE-TO-TUBESHEET JOINT 26

2.2.1 Experimental Analysis 27

2.2.2 Finite Element method 47

2.2.3 Theoretical Analysis 58

2.3 WORKING CONDITIONS OF EXPANDED JOINT 68

CHAPTER 3: PARAMETRIC STUDY OF TUBE-TO-TUBESHEET JOINT..... 71

3.1 INTRODUCTION 71

3.2 TYPE OF ELEMENT TO BE USED IN THE AXISYMMETRIC FEM 73

3.3 AXISYMMETRIC VERSUS 3-D FEM 76

3.4 FINITE ELEMENT PARAMETRIC ANALYSIS 80

3.5 COMPARISON WITH ELASTIC PERFECTLY PLASTIC

MATERIAL BEHAVIOUR 85

CHAPTER 4: TUBE-TO-TUBESHEET JOINT: FINITE ELEMENT

AND ANALYTICAL ANALYSES 113

PART A: RESIDUAL CONTACT PRESSURE AND RELATED

PARAMETERS 113

4.1 INTRODUCTION 113

4.2 EMPIRICAL EQUATIONS 114

4.3 ANALYSIS OF RESIDUAL CONTACT PRESSURE 116

4.3.1 Limiting Pressure and Appropriate Model Used 116

4.3.2 Analytical Analysis for Residual Contact Pressure 118

4.3.3 Validation of the Analytical Solution 130

4.3.4 Effect of Strain Hardening Parameter 133

PART B: STRESS ANALYSIS OF TUBE TRANSITION ZONE OF AS-EXPANDED JOINT 135

4.4 INTRODUCTION 135

4.5 FINITE ELEMENT ANALYSIS 136

4.5.1 Estimation of Maximum Tensile Residual Stresses 139

4.5.2 Parametric Study of Loading Stresses 141

4.6 ANALYTICAL MODEL FOR RESIDUAL STRESS CALCULATION 143

4.6.1 Loading Stress 143

4.6.2 Unloading Stress 144

4.6.3 Residual Stresses 148

4.6.4 Limitation of the Proposed Analytical Model 148

4.6.5 Verification with Experimental and Numerical Results 149

PART C: OPTIMUM EXPANSION AND RESIDUAL CONTACT PRESSURE LEVELS 152

4.7 INTRODUCTION 152

4.8 OPTIMUM RECOMMENDED EXPANSION PRESSURE 154

4.9 VERIFICATION OF THE PROPOSED EXPANSION PRESSURE 156

4.10 ANALYTICAL EQUATION FOR OPTIMUM RESIDUAL CONTACT PRESSURE 159

CHAPTER 5: EFFECT OF FRICTION BETWEEN TUBE AND TUBESHEET ON THE JOINT STRENGTH 184

5.1 INTRODUCTION 184

5.2 ANALYTICAL ANALYSIS 185

5.3 FRICTIONAL MODEL 189

5.4 FINITE ELEMENT ANALYSIS 191

5.4.1 Effect of Frictional Model 194

5.4.2 Effect of Boundary Condition 195

5.4.3 Comparison between 3-D and Axisymmetric FEM 196

5.4.4 Details Regarding the Axisymmetric Finite Element Analysis 197

5.5 FINITE ELEMENT CALCULATION Vs. EXPERIMENTAL MEASUREMENT 202

5.4.1 Experimental Determination of Friction Properties 202

5.5.1.1 Specimens 203

5.5.1.2 Measurement and instrumentation 205

5.5.1.3 Results and discussion 206

5.5.2 Experimental Determination of Pull-out Strength 207

5.5.2.1 Tube-to-tubesheet joint samples 208

5.5.2.2 Experimental rig and procedure 209

5.5.2.3 Results and discussion 210

5.5.3 Finite Element Determination for Pull-out Strength 211

5.5.4 Comparison between FE and Experimental Results 212

CHAPTER 6: THERMAL LOADING OF TUBE-TO-TUBESHEET JOINT 241

6.1 INTRODUCTION 241

6.2 FE MODELLING FOR THERMAL LOADING ANALYSIS 242

6.2.1 Validation of the Axisymmetric FE Model 242

6.2.2 Selecting the Proper Boundary Conditions 247

6.3 ANALYTICAL APPROACH 249

6.3.1 Simplified Analytical Analysis 249

6.3.2 Joint Tightness Coefficient 254

6.4 PARAMETRIC ANALYSIS OF THERMAL LOADING AND UNLOADING 255

6.4.1 Effect of Temperature change on Residual Stresses in the Transition Zone 257

6.4.2 Effect of Thermal loading on the Joint Tightness Coefficient 258

6.4.3 Effect of Thermal Unloading on the Initial Residual Contact Pressure 261

CHAPTER 7: JOINT BEHAVIOUR UNDER MECHANICAL LOADING 278

7.1 INTRODUCTION 278

7.2 ANALYSIS OF TUBESHEET DEFLECTION 278

7.3 METHOD OF ANALYSIS 280

7.3.1 3-D Finite Element Solution 281

7.4 SIMPLIFIED 2-D FINITE ELEMENT ANALYSIS 284

7.4.1 Mechanical Loading with Simultaneously Expanded Joints 285

7.4.2 Mechanical loading with Sequentially Expanded Joints 289

CHAPTER 8: MULTI-STEP OF EXPANSION 306

8.1 INTRODUCTION 306

8.2 AXISYMMETRIC FINITE ELEMENT ANALYSIS 307

CHAPTER 9: CONCLUSIONS AND RECOMMENDATIONS 316

9.1 MAJOR FINDINGS 316

9.2 RECOMMENDATIONS FOR FUTURE RESEARCH 323

BIBLIOGRAPHY 329

APPENDICES 340

LIST OF TABLES

Table 2.1 Pull-out test results in term of percent wall reduction (Gaffoglio and Thiele (1981)) 37

Table 3.1 Design parameters for three different cases to be analysed by 3-D finite element model and 2-D axisymmetric model 88

Table 3.2 The equivalent sleeve diameter (D_e/d). 89

Table 3.3 Comparison between the results of 3-D and axisymmetric models 89

Table 3.4 Design parameters for an additional case (**CASE-4**) where the yield strength of the tubesheet is lower than that of the tube 90

Table 3.5 Comparison between the results of the 3-D and axisymmetric models for **CASE-4** 90

Table 3.6 Values of the considered design parameters 91

Table 3.7 Effect of design parameters on maximum tensile residual stresses and on residual contact pressure (W= Weak effect; (≤ 10%), SL= Slight effect; (≥10% and ≤25%), and SG= Significant effect; (≥25%)) 92

Table 4.1 Coefficient of Equation (4.1) 162

Table 4.2 Comparison between different models used to obtain residual contact pressure 163

Table 4.3 Data used in Table 4.2 from Soler et al (1984) 163

Table 4.4 Parameters involved in Equation (4.38) 164

Table 4.5 Eight different cases used to verify Equation (4.38) 164

Table 4.6Material properties of some tested cases 165

Table 4.7 Three levels of geometrical parameters and expansion pressure ratio 165

Table 4.8 Optimum combinations of involved parameters, Taguchi (1982) 165

Table 4.9 Finite element results for the first material set (SET1) 166

Table 4.10 Mean and standard deviation values for investigated parameters 166

Table 4.11 A typical case 166

Table 4.12 The results of the finite element obtained by applying the expansion pressure given in Table 4.7 and those of the expansion pressure given by Equation (4.54) 167

Table 4.13 Statistical analysis results 168

Table 5.1 Material properties of some tested cases 214

Table 5.2 Various properties of some tested cases 214

Table 5.3 Relation between shearing and normal traction just before slipping 215

Table 5.4 Comparison between Coulomb's friction law and elastic slip model (see Fig 5.7) 216

Table 5.5 Effect of boundary condition on joint axial strength 216

Table 5.6 Comparison between 3-D and axisymmetric FE solutions for joint axial strength (see Fig. 5.7) 217

Table 5.7 Three levels of geometrical parameters and expansion pressure ratio..... 217

Table 5.8 Joint axial strength as calculated by FEM and Equation (5.1) 218

Table 5.9 Comparison between joint axial strengths on the basis of mean values . . 218

Table 5.10 Correlation parameters for the relationship between initial residual contact pressure and interference normal stresses at moment of sliding . . 219

Table 5.11 Dimensions of tube and sleeve used in friction test (mm) 219

Table 5.12 Material properties for pull-out testing 219

Table 5.13 Dimension, roughness and expansion pressure levels of joint samples . . 220

Table 5.14 Pull-out load as measured experimentally and as calculated by the finite element and by Equation (5.1) 220

Table 6.1 Thermal properties of the cases used in the 3-D model (κ by (W/m K) and α by (1/ °C)x10^{-6}) 264

Table 6.2 Change in temperature for each involved case 265

Table 6.3 Axial stresses and interference pressure as given by 3-D and axisymmetric FEM 265

Table 6.4 Tube and tubesheet deformations as given by 3-D and axisymmetric FEM 266

Table 6.5 CPU time consumed by 3-D and axisymmetric models 266

Table 6.6 Thermal coefficient of expansion (10^{-6} x (1/ °C))for the materials used by Soler (1984); (see Table 4.2) 267

Table 6.7 Axisymmetric FE residual contact pressure versus the calculation of the layered model (Soler (1984)); (OT: Operating temperature, AT: After temperature cycle) 267

Table 6.8 Typical case used for boundary conditions verification, see Figure 6.2 . . 268

Table 6.9 Materials used for parametric study 268

Table 6.10 Material properties of tube and tubesheet; see Table 7.9 268

Table 6.11 Three levels of dimensions and expansion pressure 269

Table 6.12 Maximum tensile residual axial and hoop stresses for as-expanded joint and during and after temperature cycles (Mean values and standard deviation). . . 269

Table 6.13 Residual contact pressure for as-expanded joint and η factor during thermal loading 270

Table 6.14 Mean level of the residual contact pressure for as expanded joint and after temperature cycles 270

Table 7.1 Material and dimensional properties used in 3-D model 292

Table 7.2 Effect of tubesheet rim displacements on the central joint characteristics.. 293

Table 7.3 Mean and standard deviation of investigated parameters (see Table 7.2)....293

Table 7.4 CPU time required for 3-D model 294

Table 7.5 Comparison between 2-D and 3-D finite element solutions 294

Table 7.6 Upper and lower limits of involved parameters 294

Table 7.7 Optimum combination of involved parameter; Taguchi (1982).. 295

Table 7.8 Upper and lower limits of working condition parameters (Calculation No. According to Table 7.7) 295

Table 7.9 Optimum combination of working condition parameters; Taguchi (1982)..296

Table 7.10 Initial residual contact pressure and joint tightness coefficient

(η) at working conditions 296

Table 7.11 Results of the correlation analysis for the joint tightness coefficient (η).... 296

Table II.1 Suggested temperature limits for expanded tube-to-tubesheet joint with similar tube and tubesheet metals 347

LIST OF FIGURES

Figure 1.1Use of expanded joints 15

Figure 1.2 Special tube connections achieved by the expansion process 16

Figure 1.3 Typical tubesheet being assembled. 17

Figure 1.4 Edge welded assembly 18

Figure 1.5 Section through a simple edge-welded joint showing the crevice under the weld 18

Figure 1.6 Butt welded assembly 18

Figure 1.7 Various commercially available roller expander 19

Figure 1.8 Typical roller expansion process 20

Figure 1.9Cross section showing 3, 4 and 5 roller expanders 20

Figure 1.10 Roll expander driven by pneumatic motor 21

Figure 1.11 The hydraulic expansion process 21

Figure 1.12 Primary and secondary sides seals used in hydraulic expansion 22

Figure 1.13 Hydraulic expansion equipment 22

Figure 1.14 Typical hydraulic expansion mandrels of various lengths 23

Figure 1.15 Plain and grooved holes 23

Figure 3.1 Elastic-perfectly plastic and Bi-linear elastic-plastic stress strain relation ... 93

Figure 3.2 Axisymmetric finite element model 93

Figure 3.3 Residual radial stress profile of the tube surfaces inner surface 94

Figure 3.4 Residual radial stress profile of the tube outer surface 94

Figure 3.5 Residual axial stress profile as calculated by different axisymmetric element types 95

Figure 3.6 Residual hoop stress profile as calculated by different axisymmetric element types 95

Figure 3.7 CPU time consumed for various element types used 96

Figure 3.8 Residual axial stress as given by the axisymmetric finite element mode and as provided by Kalnins et al (1989) 97

Figure 3.9 Residual hoop stress as given by the axisymmetric finite element mode and as provided by Kalnins et al (1989) 97

Figure 3.10 Finite circular disk with 19 holes 98

Figure 3.11 3-D finite element model 98

Figure 3.12 Equivalent sleeve diameter versus hole pitch as obtained by Chaaban et al (1992) and by Kohlpaintner (1995) 99

Figure 3.13 Plastic propagation in the real 3-D model of the tubesheet and that created in the equivalent sleeve. 100

Figure 3.14 Comparison between the residual axial stresses obtained by using 3-D and axisymmetric models (CASE3) 101

Figure 3.15 Comparison between the residual hoop stresses obtained by using 3-D and axisymmetric models (CASE3) 101

Figure 3.16 Comparison between the residual axial stresses obtained by using 3-D and axisymmetric models (CASE4) 102

Figure 3.17 Comparison between the residual hoop stresses obtained by using 3-D and axisymmetric models (CASE4) 102

Figure 3.18 3-D profile of residual axial stress on the inner surface of the transition zone.. 103

Figure 3.19 Residual axial stress versus the orientation angle (θ) (CASE-3);Z/d=1.2...104

Figure 3.20 Residual axial stress versus the orientation angle (θ) (CASE-4);Z/d=1.2...104

Figure 3.21 Residual axial stresses and tube profiles for reference case (P_e/S_{yt}=1.0) ... 105

Figure 3.22 Residual hoop stresses and tube profiles for reference case (P_e/S_{yt}=1.0). . .105

Figure 3.23 Maximum residual stresses for different levels of tube wall thickness . . . 106

Figure 3.24 Residual contact pressure for different levels of the tube wall thickness. . 106

Figure 3.25 Maximum tensile residual stress at various value of initial radial clearance 107

Figure 3.26 Residual contact pressure at various value of the initial radial clearance. . 107

Figure 3.27 Maximum tensile residual stresses for three different (D_e/d) ratios. 108

Figure 3.28 Residual contact pressure for three different (D_e/d) ratios. 108

Figure 3.29 Effect of the S_{ys}/S_{yt} on the maximum tensile residual stresses 109

Figure 3.30 Effect of E_{tt}/E_t on the maximum tensile residual stresses 109

Figure 3.31 Residual contact pressure at various value of E_{tt}/E_t 110

Figure 3.32 Effect of E_s/E_t on the residual contact pressure 110

Figure 3.33 Residual contact pressure versus the expansion pressure at different levels of tube strain hardening level 111

Figure 3.34 Residual contact pressure versus the tube strain hardening parameter of tube material at different levels of the initial radial clearance 111

Figure 3.35 Residual contact pressure versus the initial radial clearance at various values of the tube strain hardening parameter 112

Figure 3.36 Maximum tensile residual stresses versus the initial radial clearance at various level of the tube strain hardening parameter of tube material 112

Figure 4.1 Effect of expansion pressure on maximum tensile residual stresses, residual contact pressure, and residual tube enlargement 169

Figure 4.2 Simulation of tube and tubesheet by plane stress or plane strain models .. 170

Figure 4.3 The various steps of creating expanded joint as represented by pressure-radial displacement diagram 170

Figure 4.4 Range of yield strength with the possibility of joint creation 171

Figure 4.5 Residual contact pressure versus tube thickness ratio; Comparison of the present model and previous theories. 171

Figure 4.6 Residual contact pressure as obtained by axisymmetric model, Equation (4.36) and analytical equations given by Krips et al (1976) and Kasriae et al (1983) 172

Figure 4.7 Sensitivity of Equation (4.36) to the modulus of elasticity ratio 172

Figure 4.8 Residual contact pressure as obtained by Equation (4.36) for different tube-to-tubesheet material 173

Figure 4.9 Residual contact pressure as obtained by Equation (4.36) for different

expansion pressure 173

Figure 4.10 Residual contact pressure as calculated by finite element model and as given by Equation (4.38). 174

Figure 4.11 Hoop and equivalent plastic strains of tube middle surface at maximum loading ..... .174

Figure 4.12 Loading, unloading and residual axial stresses as obtained by the finite element method and unloading axial stress as calculated by the analytical solution (inner surface) 175

Figure 4.13 Loading, unloading and residual axial stresses as obtained by the finite element method and unloading axial stress as calculated by the analytical solution (outer surface) 175

Figure 4.14 Loading, unloading and residual hoop stresses as obtained by the finite element method and unloading hoop stress as calculated by the analytical solution (inner surface) 176

Figure 4.15 Loading, unloading and residual hoop stresses as obtained by the finite element method and unloading hoop stress as calculated by the analytical solution (outer surface) 176

Figure 4.16 Expected range of maximum tensile residual stress values in both axial and hoop directions 177

Figure 4.17 Expected axial location for the maximum tensile residual stresses 177

Figure 4.18 Effect of material properties on the loading axial stress 178

Figure 4.19 Effect of material properties on the loading hoop stress 178

Figure 4.20 Effect of the dimensional parameters and expansion pressure levels on the loading axial stress 179

Figure 4.21 Effect of the dimensional parameters and expansion pressure levels on the loading hoop stress 179

Figure 4.22 Description of the tube-to-tubesheet joint for analytical analysis 180

Figure 4.23 Residual axial stress profile as predicted experimentally and as given by the analytical method 180

Figure 4.24 Comparison between the residual axial stress on the inner surface as obtained by the FE and the analytical model. 181

Figure 4.25 Comparison between the residual hoop stress on the inner surface as obtained by the FE and the analytical model. 181

Figure 4.26 Comparison between the residual axial stress on the outer surface as obtained by the FE and the analytical model 182

Figure 4.27 Comparison between the residual hoop stress on the outer surface as obtained by the FE and the analytical model 182

Figure 4.28 Optimum residual contact pressure as obtained by Equation (4.59) and axisymmetric FEM 183

Figure 5.1 Joint axial strength as predicted by different analytical models 221

Figure 5.2 Effective coefficient of friction versus locale coefficient of friction 221

Figure 5.3 Effective coefficient of friction at various levels of modulus of

elasticity ratio 222

Figure 5.4 Effective coefficient of friction at different values of tube wall thickness ration..... 222

Figure 5.5 Damage in tube outer surface as a results of pull-out test 223

Figure 5.6 Typical comparison between Coulomb's friction law and elastic-slip friction model 223

Figure 5.7 Three different ways of evaluating the joint axial strength measured by the finite element method 224

Figure 5.8 Typical relation between the shearing force and the tube micro-motion .. 225

Figure 5.9 Different boundary conditions that can be applied in axisymmetric model for joint axial strength calculation 226

Figure 5.10 Relation between joint axial strength and the initial residual contact pressure as predicted by the finite element analysis 227

Figure 5.11 Statistical relation between interference contact pressure (VAR2) and initial residual contact pressure (VAR1) 227

Figure 5.12 Statistical relation between interference contact pressure (VAR3) and initial residual contact pressure (VAR1) 228

Figure 5.13 Statistical relation between interference contact pressure (VAR4) and initial residual contact pressure (VAR1) 228

Figure 5.14 Tube and tubesheet frictional test specimens (Full area of contact) 229

Figure 5.15 Tube and tubesheet frictional test specimens (Reduced contact area) 229

Figure 5.16 Friction test apparatus 230

Figure 5.17 Equipments used in friction test set up 231

Figure 5.18 Picture showing the tip of displacement transducer is placed near to the interference level between the tube and tubesheet samples 232

Figure 5.19 Stability of normal load over the circular surface of the contacting area; A-Unstable arrangement, B-Stable arrangement 232

Figure 5.20 Typical relation between the shearing force and displacement 233

Figure 5.21 Local coefficient of friction versus normal pressure 233

Figure 5.22 Tube-to-tubesheet joint sample 234

Figure 5.23 Dimension of locking cylinder (mm). 234

Figure 5.24 Collective picture for test sample, locking cylinder and rigid ball. 234

Figure 5.25 Illustration of pull-out test equipment 235

Figure 5.26 Collective picture for pull-out test rig 236

Figure 5.27 Picture showing first arrangement of the displacement transduce 237

Figure 5.28 Typical relation between the shearing force and relative displacement (CASE: 1-1) 238

Figure 5.29 Picture showing second arrangement of the displacement transduce 238

Figure 5.30 Relation between the shearing force and relative displacement as given by MTS displacement cell and the Mμ-Checker 239

Figure 5.31 Equivalent axisymmetric model 240

Figure 5.32 Relation between the shearing force and relative displacement as

given by the finite element solution 240

Figure 6.1 Equivalent axisymmetric model for thermal loading analysis 271

Figure 6.2 Two different boundary conditions that can be applied for axisymmetric model 271

Figure 6.3 As-expanded (AE), and during heating (OT_h) and after temperature cycle (AT_h), tube profile with two different boundary conditions used; see Fig 6.2 272

Figure 6.4 As-expanded (AE), and during cooling (OT_c) and after temperature cycle (AT_c), tube profile with two different boundary conditions used; see Fig. 6.2. 272

Figure 6.5 As-expanded (AE), and during heating (OT_h) and after temperature cycle (AT_h), axial stress profile with two different boundary condition used; see Fig. 6.2. 273

Figure 6.6 As-expanded (AE), and during cooling (OT_c) and after temperature cycle (AT_c), hoop stress profile with two different boundary condition used; see Fig 6.2. 273

Figure 6.7 Simplified plane stress model for tube-to-tubesheet joint 274

Figure 6.8 The steps of creating the expanded joint as well as the joint response to thermal loading as presented in terms of interference contact pressure-stress relation; Yield surface assuming a perfectly plastic material 274

Figure 6.9 Typical axial stress profile, (A) for as-expanded joint and during

thermal loading, (B) for as-expanded joint and after temperature cycling 275

Figure 6.10 Typical hoop stress profile, (A) for as-expanded joint and during thermal loading, (B) for as-expanded joint and after temperature cycling. 276

Figure 6.11 Maximum tensile axial stresses at different thermal loading versus that of as-expanded joint. 277

Figure 6.12 Maximum tensile hoop stresses at different thermal loading versus that of as-expanded joint 277

Figure 7.1 Some mechanical loading acting on the tubesheet surfaces 297

Figure 7.2 3-D finite element model used for tubesheet deformation analysis (Private Communication) 298

Figure 7.3 Central region of the perforated plate 299

Figure 7.4 3-D finite element model 300

Figure 7.5 3-D residual axial stress contour on the tubes transition zone 301

Figure 7.6 Finite element model for simultaneous expansion case 302

Figure 7.7 Statistical relation between the joint tightness coefficient (VAR4) and the displacement (**u**) (VAR1) 302

Figure 7.8 Statistical relation between the joint tightness coefficient (VAR4) and the displacement (**v**) (VAR2) 303

Figure 7.9 Statistical relation between the joint tightness coefficient (VAR4) and the primary side pressure (P_{ps}/S_{yt}) (VAR3) 303

Figure 7.10 2-D finite element model for sequential expansion case 304

Figure 7.11 Relation between joint tightness coefficient and displacement (**u**) at different levels of displacement bi-axialty (β) 305

Figure 7.12 Relation between joint tightness coefficient and displacement ratio at different levels of the displacement (**u**) 305

Figure 8.1 Difficulty in expanding tube in very thick tubesheet; Zone (A) full expansion, Zone (B) Multi-expansion. ..... .310

Figure 8.2 Two expansion process 310

Figure 8.3 Near-overlap region axisymmetric model ..... .311

Figure 8.4 Axial stress and tube deformation profiles after first step of expansion 312

Figure 8.5 Hoop stress and tube deformation profiles after first step of expansion . . . 312

Figure 8.6 Axial stress and tube deformation profiles after second step of expansion.. ..... .313

Figure 8.7 Hoop stress and tube deformation profiles after second step of expansion 313

Figure 8.8 Section through two tubes expanded by 2-step expansion process indicating that the tube inner surfaces are free from any irregularities . . . 314

Figure 8.9 Axial stress profile on the tube inner surface with different levels of overlap length; (OL=Overlap length/d) ..... .315

Figure 8.10 Hoop stress profile on the tube inner surface with different levels of overlap length; (OL=Overlap length/d) ..... .315

Figure 9.1 Proposed design procedures of tube-to-tubesheet joint 325

Figure I.1 Forces on tube subjected to an axial load 346

Figure III.1 Residual contact pressure around central tube (7) after expanding the neighbouring tubes 353

Figure III.2 7-tube block 354

Figure III.3 Pull-out test for 7-tube model 355

NOMENCLATURE AND ABBREVIATION

A_o	Contact area between tube and tubesheet (mm^2)
c	Initial clearance between tube and tubesheet (mm)
$\bar{c}$	= c/d
d	Tube outer diameter (mm)
d_i	Tube inner diameter (mm)
d	Degree of freedom
D_e	Equivalent sleeve diameter (mm)
$\bar{D}_e$	= D_e/d
D_i	Inner diameter of tubesheet hole (mm)
E_s	Modulus of elasticity of tubesheet (GPa)
E_t	Modulus of elasticity of tube (GPa)
E_{ts}	Tangent modulus of tubesheet (GPa)
E_{tt}	Tangent modulus of tube (GPa)
$\bar{E}_t$	= E_t/S_{yt}
f	Local coefficient of friction
$\bar{f}$	Adjusting factor
F	Joint axial strength (N)
F_1	Pull-out load (N); ($\bar{F}_1 = F_1/A_o S_{yt}$)
F_2	Primary side push-out load (N); ($\bar{F}_2 = F_2/A_o S_{yt}$)

F_3 Secondary side push-in load (N); ($\bar{F}_3 = F_3 / A_o S_{yt}$)

F_n Normal force (N)

F_s Shearing force (N)

h Tubesheet thickness (mm)

l Depth of expansion (mm)

M_o Bending moment at edge of transition zone (N.mm/mm)

$\bar{M}_o$ $= M_o / (d^2.S_{yt})$

n Number of observation point

P_{ct} Tube collapse pressure (MPa)

P_e Expansion pressure (MPa)

P_f Interference pressure between tube and tubesheet (MPa)

P_{it} Initial yielding pressure for tube (MPa)

P_{min} Minimum expansion pressure (MPa)

P_{ps} Primary side operating pressure (MPa)

P^* Initial residual contact pressure (MPa)

P Hole pitch (mm)

r Radius measured on tube (mm)

R Radius measured on tubesheet hole (mm)

S Normal stress in transition zone (MPa)

S_n Normal traction at interference between tube and tubesheet (MPa)

S_s Shearing traction at interference between tube and tubesheet (MPa)

S_{ys} Yield strength of tubesheet (MPa)

S_{yt} Yield strength of tube (MPa)

S^*_z Maximum tensile residual axial stress (MPa)

S^*_θ Maximum tensile residual hoop stress (MPa)

t Tube wall thickness (mm)

$\bar{t}$ = t/d

t Factor comparing between two means (t-test)

T_o Initial temperature (°C)

T_h Heating temperature (°C)

T_c Cooling temperature (°C)

u Tubesheet rim displacement in X direction (mm)

U Radial displacement (mm)

U_t Tangential relative displacement (μm)

v Tubesheet rim displacement in Y direction (mm)

V_o Shearing force at edge of transition zone (N/mm)

$\bar{V}_o$ $= V_o / (d.S_{yt})$

Y_s Diameter ratio of tubesheet

Y_t Diameter ratio of tube

Z Axial distance along tube (mm)

Z_z Axial location of maximum tensile residual axial stress (mm)

Z_θ Axial location of maximum tensile residual hoop stress (mm)

α	Correction factor or intercept of linear regression equation
α_{ij}	Coefficient of empirical equation
α	Level of significance
β	Correction factor or slope of linear regression equation
β_i	Independent parameter of empirical equation
β	Displacement ratio (u/v)
α_s	Thermal coefficient of expansion of tubesheet (1/ °C)
α_t	Thermal coefficient of expansion of tube (1/ °C)
ν	Poisson's ratio ($\nu = 0.3$)
Δ	Approximated distance between the end of the uniformly expanded zone and the beginning of the non-expanded zone (mm)
δ	Critical displacement beyond which slipping occurs (μm)
ϵ	Hoop strain
ϵ_s	Hoop strain on the tubesheet inner surface
ϵ_t	Hoop strain on the tube inner surface
η	Joint tightness coefficient
θ	Orientation angle
κ	Thermal conductivity (W/m K)
λ	Standard deviation
μ	Effective coefficient of friction
σ	Mean value

σ_r Radial stress (MPa)

σ_z Axial stress (MPa)

σ_θ Hoop stress (MPa)

Φ Axial rotation of the tube middle surface

Abbreviation:

AE As-expanded

An Analytical.

AT_h After heating temperature cycle

AT_c After cooling temperature cycle

Axy Axisymmetric

FE Finite Element

ID Inner diameter

OL Overlap zone

OD Outer diameter

OT_h Heating operating-temperature

OT_c Cooling operating-temperature

Pr. S. Primary side

Sc. S. Secondary side

SCC Stress Corrosion Cracking.

TZ	Transition zone
TWR	Tube wall reduction
ΔT	Change of Temperature
ΔP	Change of contact pressure
2-D	Two dimensional
3-D	Three dimensional

Superscript

*	Residual

Subscript

c	Cooling
h	Heating
l	Loading
r	Residual or radial
u	Unloading
z	Axial
θ	Circumferential

LIST OF APPENDICES

APPENDIX I EVALUATION OF EFFECTIVE COEFFICIENT OF FRICTION . . . 340

APPENDIX II SUGGESTED TEMPERATURE LIMITS 347

APPENDIX III EFFECT OF SEQUENCE OF EXPANSION 351

CHAPTER I

INTRODUCTION

1.1 GENERAL

Joint expansion is the most common means of connecting tubular elements in a variety of industrial applications. It has been widely used in the fabrication of pressure vessels including heat exchangers, steam generators, piping systems, compressors, and combustion engines, Figure 1.1. Roller joint expansion offers time and costs savings because of its simplicity. It provides good structural integrity and reliable quality for different tubing connection as shown in Figure 1.2. However, when compared to other methods of jointing, roller expansion process is often considered, under certain environmental conditions, a high source of Stress Corrosion Cracking (SCC). So far, it has been widely applied to various tubing connections in different industries such as petrochemical and both conventional and nuclear power stations.

The most important application of the expansion technique is the tube-to-tubesheet expansion process which is the art of cold-working of the tube ends into intimate contact with the metal of the containing tubesheet holes as shown in Figure 1.3. Properly

executed, the expansion process produces pressure-tight joints of great strength and stability. Expanded tube-to-tubesheet joint can be made to give a reasonably good degree of leakage tightness for most applications involving moderate working temperature. However, in high temperature applications, creep causes enough relaxation in the tube wall and relieves the contact pressure set up by the expansion process, so that leaks are likely to be developed. For the application where a very high level of leakage tightness is required, the tube can be attached to the tubesheet by welding which comes mainly into two types: edge and butt welding. Welding has the disadvantage of requiring material compatibility and, in addition, edge welding (Fig. 1.4), involves the difficulty of connecting a very thin tube with a thick tubesheet due to the difference in the respective heating and cooling rates. Edge welding also creates a crevice between the OD surface of the tube and ID surface of the tubesheet hole (Fig. 1.5) which is a source of corrosion in the tubesheet secondary side, especially in steam generators where evaporation tends to precipitate sludge and dissolved salts in the crevice zone. Nevertheless, TEMA (1988) recommends the use of edge welding together with tube expanding. The edge welding is used to add leakage tightness only, and all the tubes and tubesheet loads must be totally carried by the expanded joint.

The shortcomings and the susceptibility of crevice corrosion afflicted by edge welding can be avoided by using butt welding (Fig. 1.6). While very expensive, butt welding, under certain industrial conditions, gives the highest strength and leakage

tightness. In spite of the above, tube expansion turns out to be, in most cases, the only practical method of fastening the tubes with the tubesheet. This is attested by the fact that most utility services, factory outputs, and many material processes depend upon equipment having expanded tube-to-tubesheet joints. Also, the quality of a shell-and-tube heat exchanger relies almost entirely on the integrity of the many tube-to-tubesheet joints. The types, function and requirements and failure mechanisms of tube-to-tubesheet joints are briefly presented in the following sections

1.2 REQUIREMENTS AND FUNCTIONAL BEHAVIOUR

The main function of tube-to-tubesheet joint is to keep a firm contact between the tube and the tubesheet. In order to function efficiently, the tube-to-tubesheet joint must remain tight during the test, startup, operating and shutdown conditions. A second function may be that of contributing to the strength of the tubesheet against the pressure-induced load applied on its large surface. The tube-to-tubesheet joint must therefore be strong enough to effectively transfer the pressure load form the tubesheet to the tube, in addition, to the thermally induced loads that are produced by the difference in thermal expansion between the hot and cold surfaces of both the straight tubes and the tubesheet. A third function may be to firmly attach the tube in order to increase the tube natural frequencies, thus reducing the risk of the flow induced vibration damage.

The required degree of the joint integrity depends upon the working condition and service requirements. Ideally, tube-to-tubesheet joint should have a maximum possible interference residual contact pressure at the tube and tubesheet interface. The joint capability to withstand the different loading is measured by its axial strength which depends upon the level of the residual contact pressure and the surface finish of the contacting surfaces. In addition, the joint tightness against leakage depends on the fluid to be sealed and the surface finish of both the tube and tubesheet. The roughness level of the ID surface of the tubesheet holes and that of the OD surface of the tube greatly influences the holding power and the leakage tightness of the expanded joint. A very rough surface normally increases the friction coefficient between the tube and the tubesheet and consequently increases the joint pull-out strength while it might reduce the joint leakage tightness. The TEMA standard (1988) accepts the tubesheet hole surface if given, at least, a work-mankind finish. Also, it requires the cleaning of the tubesheet holes before expanding the tube and the removal of any burrs in order to avoid cutting the tube during the expansion process.

The only shortcoming of the expanded tube-to-tubesheet joint process is that it induces a high level of tensile residual stress in the tube transition zone, thus increasing the susceptibility to stress corrosion cracking. Unlike the joint structural and leakage strength of the tube-to-tubesheet joint, the tensile residual stresses left in the tube wall should be as low as possible in order to minimize the probability of initiating or accelerating the stress corrosion cracking under the working condition.

1.3 JOINT TYPES

According to the available methods of expansion, tube-to-tubesheet joints can be classified in several categories. They may be installed by a variety of methods, namely, roller expansion, hydraulic, hybrid, explosive and rubber expansion processes. Because they are the most commonly used, roller and hydraulic expansion processes are described in detail in what follows.

1.3.1 Roller Expansion

A variety commercial of roller expanders can be found in the market (Fig. 1.7). They consist of a cylindrical cage which loosely holds three to five (and for special purposes seven) hardened tapered steel rolls that are circumferentially and equally spaced in the cage (Fig. 1.8 and 1.9). The end of the cage is threaded to receive a thrust ball bearing and locking nut. The function of this bearing is to prevent the roller cage from being drawn into the tube. Also, the axial position of the tube part to be rolled is set up by adjusting the position of the thrust bearing. A tapered mandrel having a taper angle double that of the rollers is inserted through the cage to force linear contact of the rollers against the tube inner surface. The roller expander is lubricated and inserted into the tube end and a torque is applied to the mandrel (Fig. 1.10), by an electric, a pneumatic or a hydraulic drive rotating at between 400 to 1000 rpm. As the mandrel rotates and pushes forward, the tube

starts to be radially expanded and its end becomes shorter because of the Poisson's effect. As the tube contacts the tubesheet inner bore, the surrounding tubesheet ligaments withstands the pressure applied by the rollers and resist the tube diameter enlargement. The tube wall is thus squeezed between the roller and the surrounding ligaments. As a results, the tube wall is thinned and tube end is extruded in the axial direction.

The driving motor is set to a desirable torque (usually between 7 to 27 N.m) which is correlated to the apparent tube wall reduction whose optimal value ranges between 4.5% to 5.5% for good joint strength and leakage tightness. The torque sensed by the controler of the rolling machine depends upon the frictional force which is affected by the state of the equipment, the lubricant used, and tube inner surface condition which is likely to be different from one tube to another, thus causing variation in the level of expansion from one tube to the other. In addition, over-rolling, i.e. beyond the abovementioned optimum range, must be avoided since it can greatly weaken either the joint being expanded or the neighbouring already expanded joints. The quality of the rolled joint depends on the following parameters:

1- Tube and tubesheet dimensions.

2- Stress-strain curves of tube and tubesheet materials.

3- Number of rollers.

4- Mandrel speed.

5- Angle of rolls relative to the tube axis.

in addition to, among many, the following:

6- Tube and tubesheet surface cleanliness.

7- Condition of the mandrel, cage and rolls.

8- Rolling lubricant.

9- Roller shape.

10- Operator skills

1.3.2 Hydraulic Expansion

As the name implies, hydraulic expansion or hydro-expanding is a process that uses direct hydraulic pressure on the tube inner surface by a fluid medium which is usually demineralized water. Expansion pressure typically ranges from 65% to 95% of the tube yield strength. Figure 1.11 shows a section through a tube hydraulically expanded in a tubesheet hole. The length of the expanded part of the tube is controlled by the position of the O-ring seals located at the beginning and the end of the mandrel, Fig. 1.12. The O-rings are backed by polyurethane supporting rings. Figure 1.13 is a picture of the system main components: they include the power supply, intensifier assembly and the control gun with the hydraulic expanding mandrel. The power supply is used mainly to control and

operate the system. Also, it contains a special water pump that is driven by pneumatic pump and transfers the water from the main reservoir to the accumulator that stores the water under constant pressure. The intensifier increases the water pressure by a constant multiply. The trigger on the control gun releases the water under very high pressure from the intensifier through the attached flexible high-pressure tubing to the mandrel. Commercial hydraulic expansion units can provide pressures up to 450MPa with a tolerance of $\pm$3.5 MPa. The pressurized water is allowed to dwell inside the expanded part of the tube for approximately 3 to 4.5 sec after which the pressure is automatically released and the expanding water drained back to the reservoir.

Unlike the roller expansion process, the degree of hydraulic expansion is merely controlled by the intensifier water pressure and is thus, amenable to computer-control. Also, there is no limitation on tube length that can be expanded in single process (up to 1.5 m has been quoted in the literatures, Fig. 1.14). This is a distinct advantage over roller expansion which must be restricted to a maximum length of expansion of about 62.5 mm per pass due to the limitation of the driving torque required. Hydraulic expansion exhibits thus numerous advantages in comparison with conventional rolling:

1- Time and cost savings

2- Computability

3- Uniformity of all joints

4- Lower residual stresses in tube

5- Ability of handling non-circularity of the tube without any difficulty

1.3.3 Grooved Joints

Industrial practice has led to the use of grooved joints for the purpose of enhancing joint strength. Various groove shapes have been developed (Fig. 1.15). TEMA (1988), for example, specifies that for a design pressure over 2 MPa and/or for a temperature exceeding 177 °C, all the tube holes must be machined with at least two grooves each approximately 3.175 mm wide by 0.397 mm deep. However, no specification is given about their axial location even though this could lead to significant reduction in the axial joint strength in thin tubesheet if uncontrolled. In fact, the use of grooved tubesheet holes is not totally agreed upon the research, since some field data indicates that the grooves could actually weaken the joint. It could be argued that their effect on the tightness of the expanded joint could be greatly influenced by the following factors:

1- The groove depth

2- The number of grooves

3- The grooves axial location

4- The ratio between the expansion depth to the total groove width

5- The grove shape and configuration

1.4 FAILURE MECHANISMS IN TUBE-TO-TUBESHEET JOINTS

Tube-to-tubesheet joint may fail by several ways during the test, start up, service or shut down conditions. The most common mechanisms of failure is caused by either stress corrosion cracking and/or mechanically and thermally induced loads. Most failures occur in the tube part that is directly located beyond the secondary face of tubesheet where the tubes are subjected to bending and/or torsion and thermal loading. The joints may also fail in this area in the presence of flow induced vibrations. The differential pressure loading on the tubesheet surfaces could also introduce an additional failure mechanism causing the joint to relieve the residual contact pressure and, thus, losing the sealing between the primary and secondary sides.

As mentioned earlier, when the tubes are expanded, there is a transition zone between the tube expanded and non-expanded parts. Also, a crevice zone between the tube and tubesheet, on the tubesheet secondary face is unavoidable. All the expanding techniques leave residual stresses in the expanded, crevice and the transition zones. Those stresses vary from compression to tension along those three zones and strongly provoke the stress corrosion cracking to be initiated on either the ID or OD surfaces of the tube. Transition zone is characterized by a high compressive residual stress on the OD surface

and a very high tensile residual stress on the ID surface. Thus, it becomes sensitive to stress corrosion on ID surface. On the other hand, the crevice zone has lower tensile residual stresses on the tube OD surface, and it is generally cracked by corrosion mechanisms specially in nuclear stream generators where sludge from the water of secondary cycle is accumulated in this zone. In spite of having lower tensile residual stresses than those of the tube transition region, crevice zone is considered as a critical location in steam generator manufacturing.

In thin-walled tubes, an over-secondary-face expanding could lead to cracking the tube on its outer surface. Also, at high temperature application with a large pressure difference between tube and tubesheet sides, creep tends to relieve the residual contact pressure of expanded joints and leads to their failure.

1.5 OBJECTIVE AND METHODOLOGY OF THE RESEARCH WORK

A detailed review of the literature (Chapter 2) shows that expanded joints have been investigated by many researchers since the early 1940's. Strength requirements of the joint depend on various design parameters and very much related to the working conditions. Although, in some cases, a relatively large amount of leakage is tolerated, say, in regenerative heat exchangers (identical fluids inside and outside tubes), in other cases a minute leak may be unacceptable, for example in heat exchangers where the fluids could

form an explosive mixture. It has been reported that some expanded joints fail, even after only a few hours of service.

Joint design methods have so far not been capable of taking into account all of the parameters involved. For example, little has been done with regards to the influence of thermal cycles on the residual contact pressure. Also, to the best of the author's knowledge, no investigation has been done on the effect of thermal cycle on the level of maximum tensile residual stresses. Also, the effect of mechanical loading on both the residual contact pressure and maximum tensile residual stresses has not previously been investigated. It would be desirable to have a more accurate evaluation of the joint integrity under all conditions, so that joint failure may be prevented.

This research work presents detailed analyses for the residual contact pressure and residual stresses in tube-to-tubesheet joints. It uses finite element, analytical, statistical and experimental methods in order to provide a general method that could be used for the design and evaluation of hydraulically expanded tube-to-tubesheet joints. Because of the complexity of the problem encountered in the analysis of expanded joints, the finite element method is considered to be the main tool of our investigations.

First, an axisymmetric finite element model is adopted in order to find a relationship between the joint design parameters and both residual contact pressure and

maximum level of the tensile residual stresses for as-expanded joints. A simplified analytical method for calculating the joint residual contact pressure and the residual stress profiles on the ID and OD surfaces of the tube transition zone will be developed. Because a special emphasis is placed on these two important parameters, the analytical model will be validated by comparing the results to those measured experimentally and obtained by the finite element analysis.

Second, the effect of the working conditions, including thermal and mechanical induced loads, on the levels of residual stresses and residual contact pressure will be investigated. Because it is always required to simplify the analysis by using axisymmetric and plane stress models, it will be important to compare such results to those obtained by performing a full 3-D finite element analysis that represents the problem more completely.

Third, since the tube-to-tubesheet joints may become weaker under the operating conditions, a new term will be introduced related to the joint tightness in order to quantify joint weakness or loss of tightness under these conditions.

The importance of the friction coefficient on the pull-out strength has appeared through the progress of the research work. Therefore, it has been decided to perform a series of experimental measurements to examine the friction effect between the tube and tubesheet contact surfaces after the expansion process. A comparison between the

experimental, finite element and analytical results has been performed to compare the pull-out strength.

The objectives of the current research program may be summarized as follows:

1- Identify the most important expanded joint parameters and provide an analytical model based on a elastic-plastic interacting of the two joint elements (tube and tubesheet) for the purpose of predicting the residual contact pressure and specifying the optimum expansion pressure based on the maximum residual stress levels introduced in the tube transition zone.

2- Study the distribution of loading, unloading and residual stress profiles in the transition zone of the tube, and show how that distribution is affected by the joint parameters.

3- Approximate the joint pull-out strength by using finite element, analytical and experimental methods

4- Analyse the effect of temperature cycles and mechanical load during service on the residual contact pressure and maximum tensile residual stress.

5- Propose a simplified design procedure based on the above.

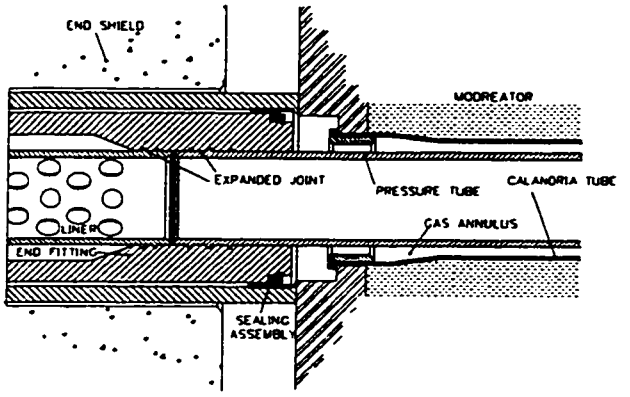


Fig. 1.1.a: Expanded joint arrangement in Pickering reactor

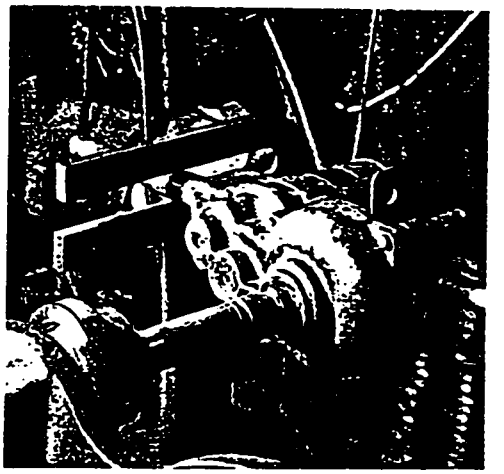


Fig. 1.1.b: Expanded joint is used to support brake assembly of self-propelled railway car



Fig. 1.1.c. : Copper tube is expanded into diesel-engine injector

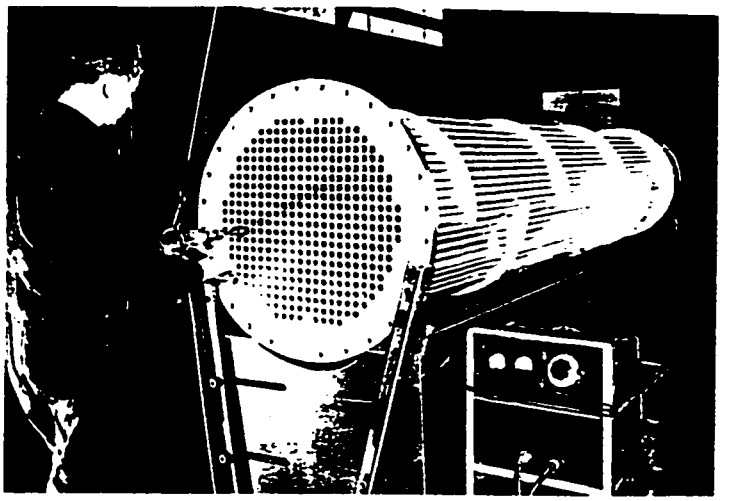


Fig 1.1.d: Tubes being rolled into tubesheet of shell-and-tube heat exchanger

Figure 1.1: Use of expanded joints

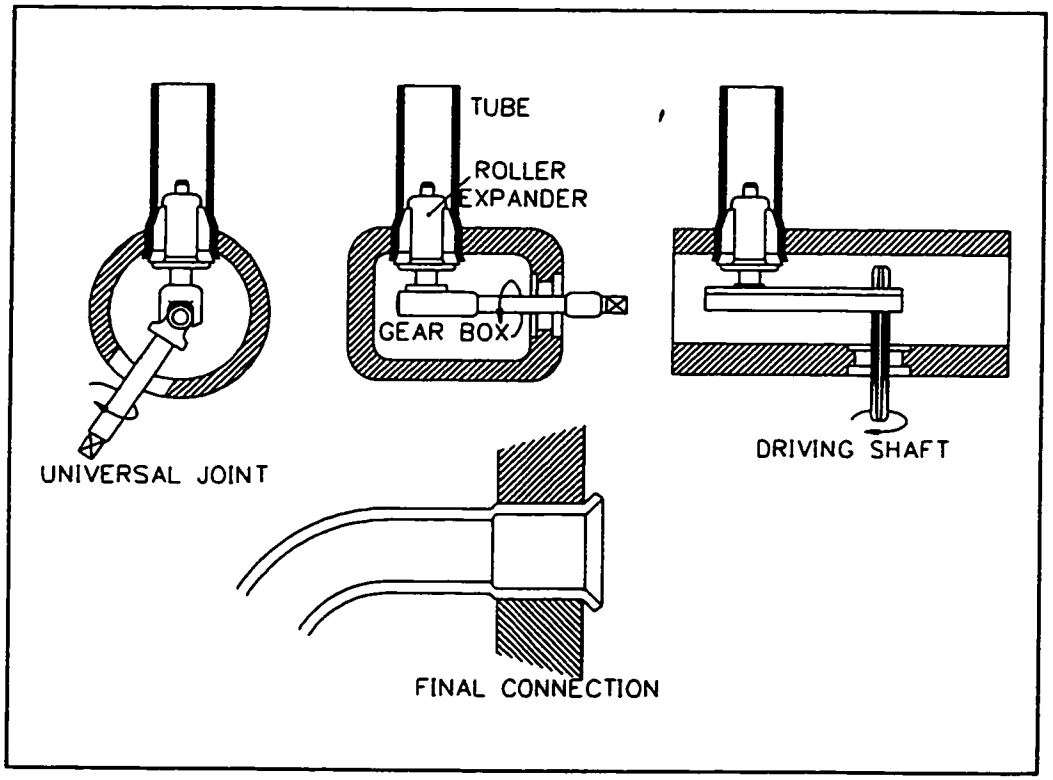


Figure 1.2: Special tube connections achieved by the expansion process

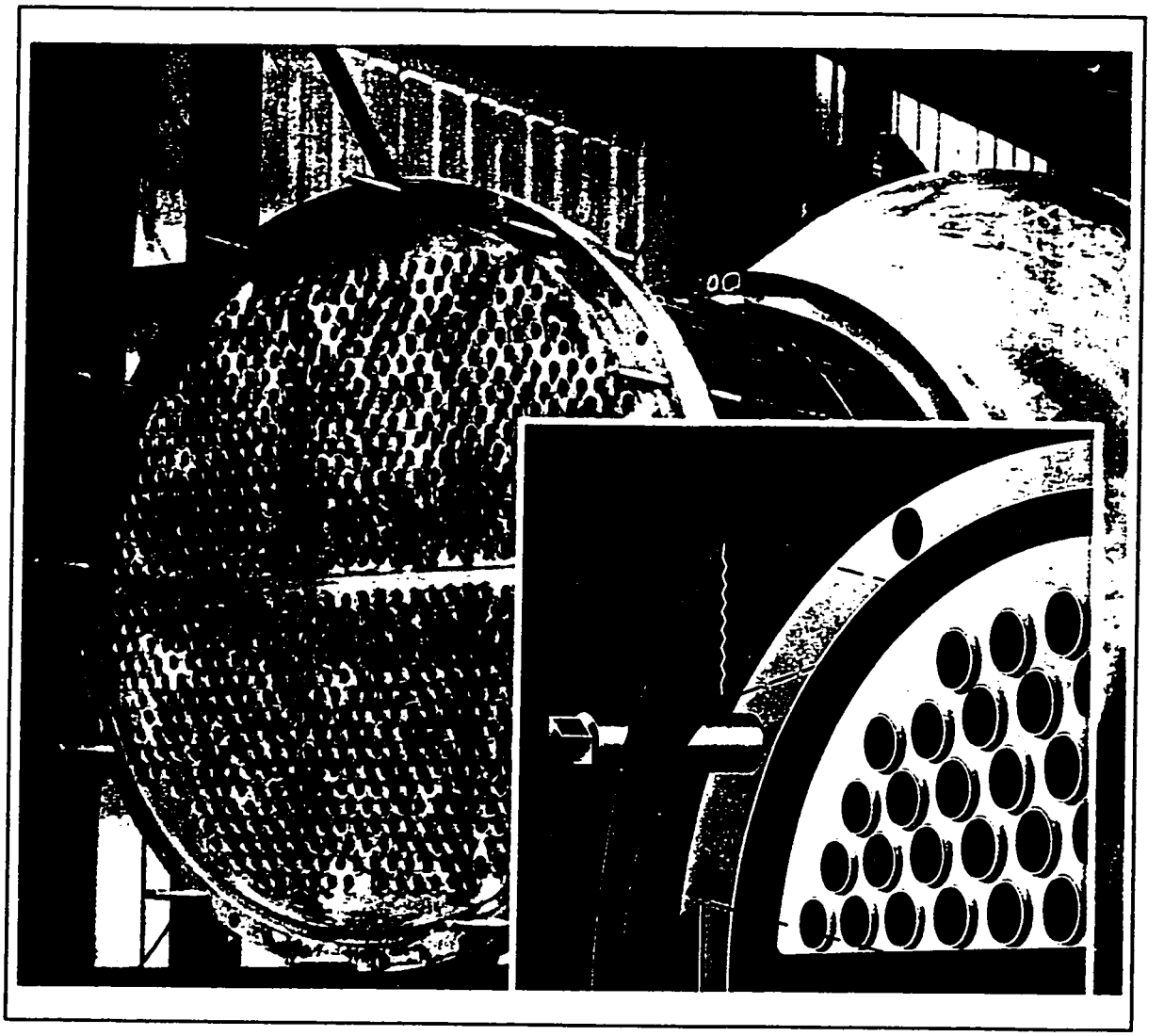


Figure 1.3: Typical tubesheet being assembled

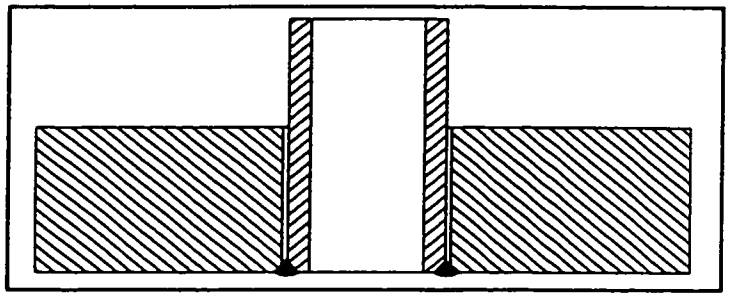


Figure 1.4: Edge welded assembly

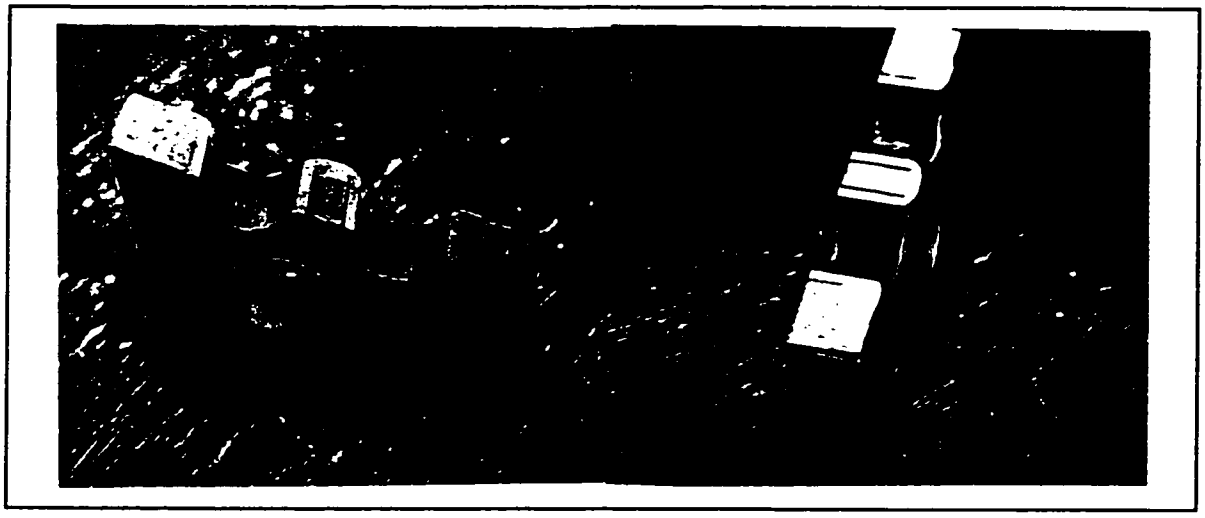


Figure 1.5: Section through a simple edge-welded joint showing the crevice under the weld.

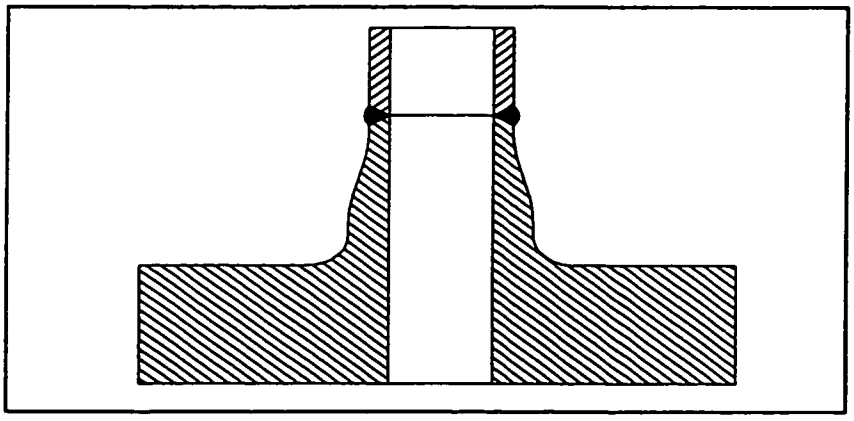


Figure 1.6: Butt welded assembly

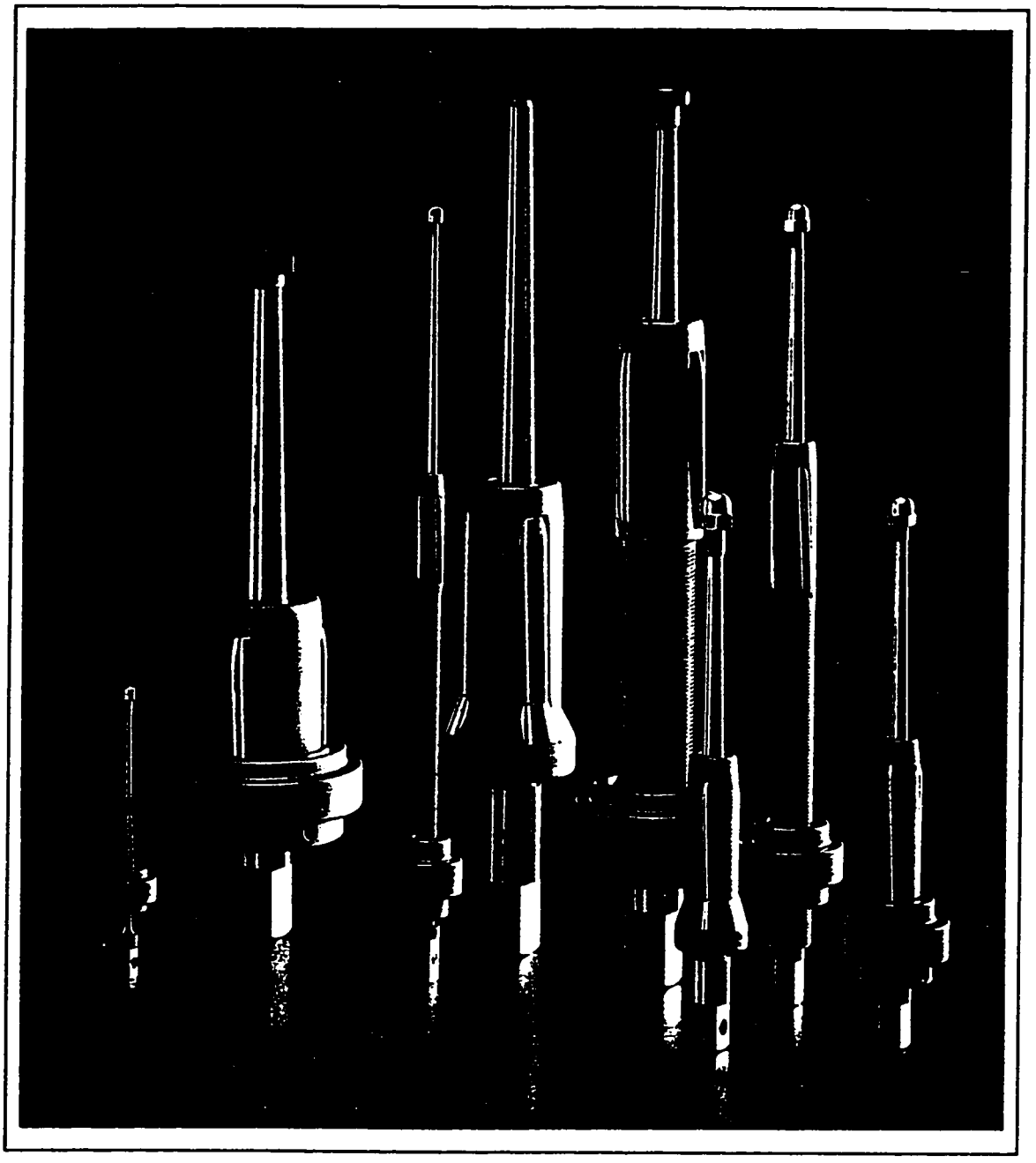


Figure 1.7: Various commercilly available roller expanders

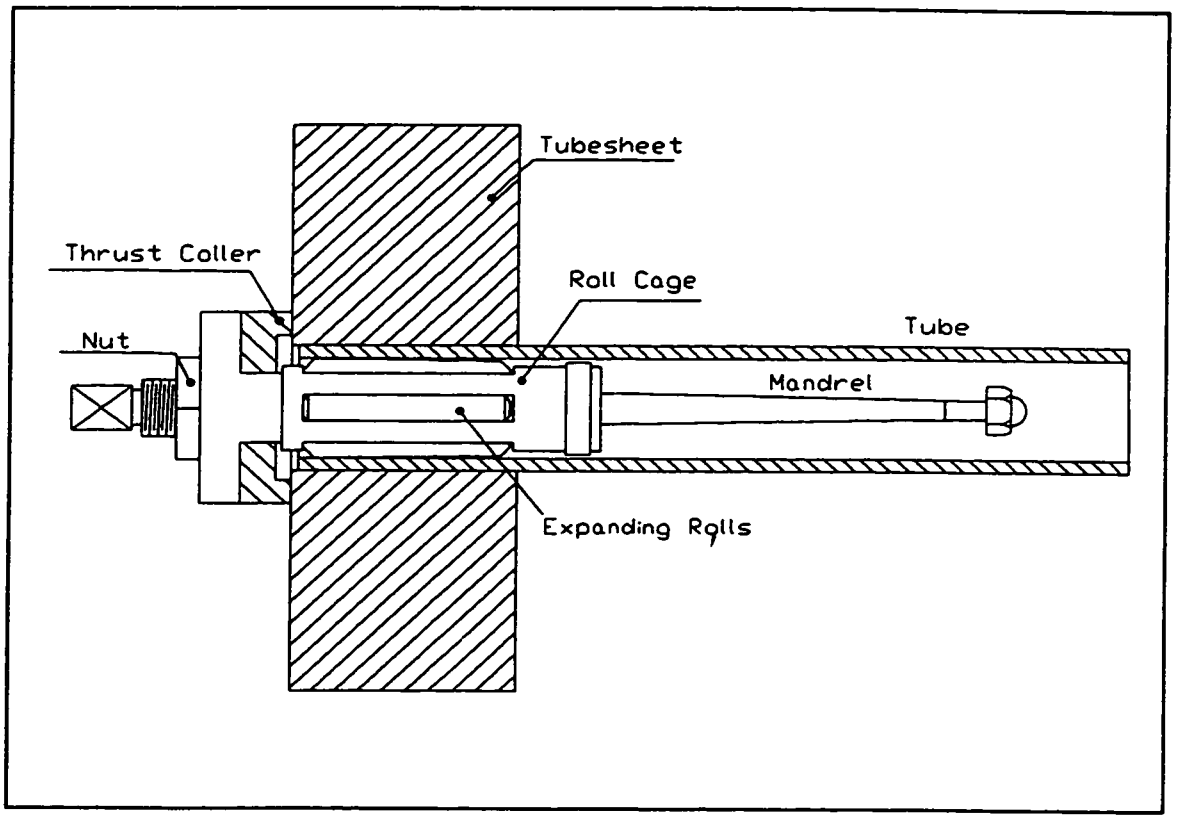


Figure 1.8: Typical roller expansion process

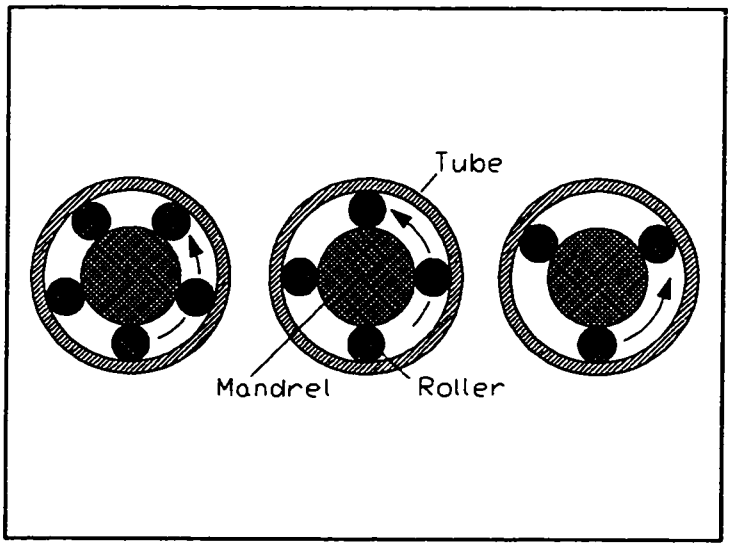


Figure 1.9: Cross section showing 3, 4 and 5 roller expanders

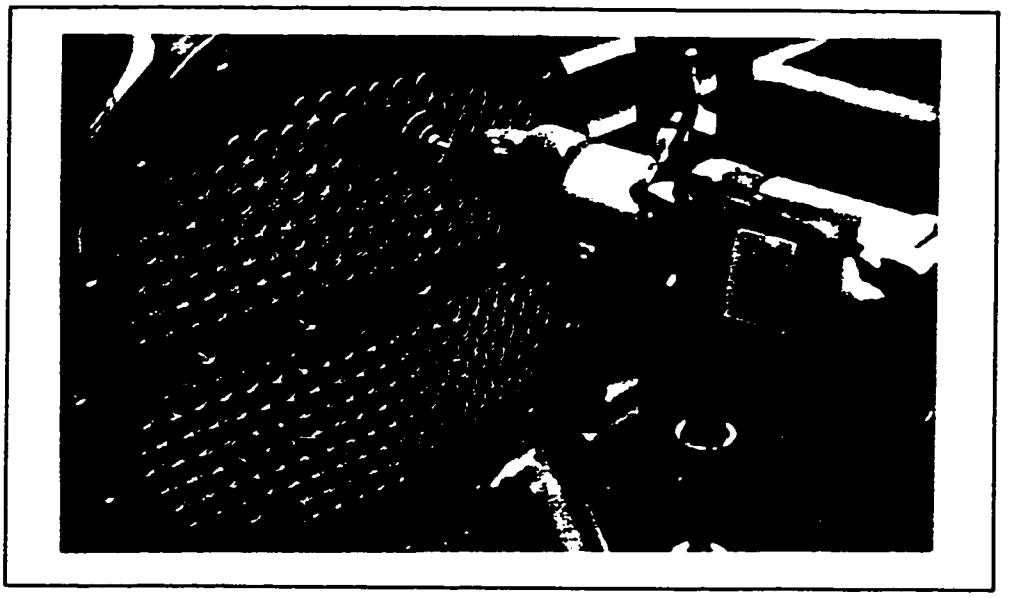


Figure 1.10: Roller expander driven by a pneumatic motor

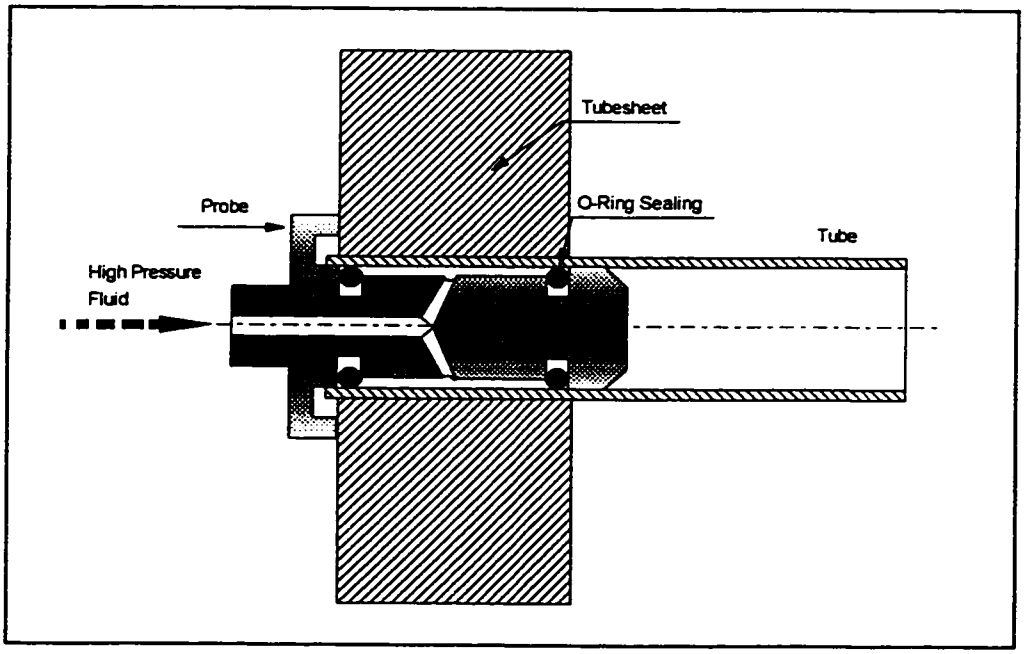


Figure 1.11: The hydraulic expansion process

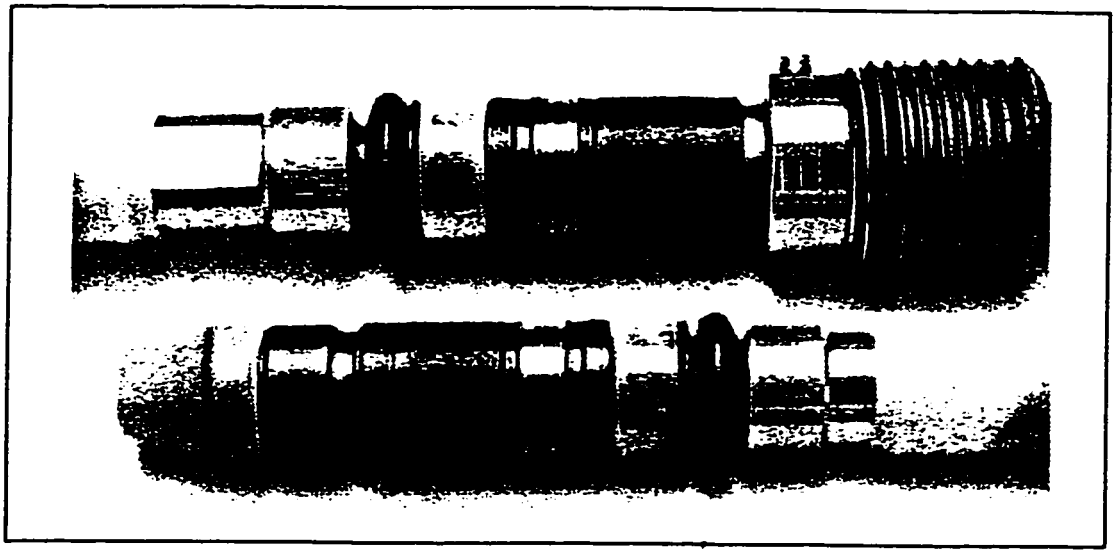


Figure 1.12: Primary and secondary sides seals used in hydraulic expansion

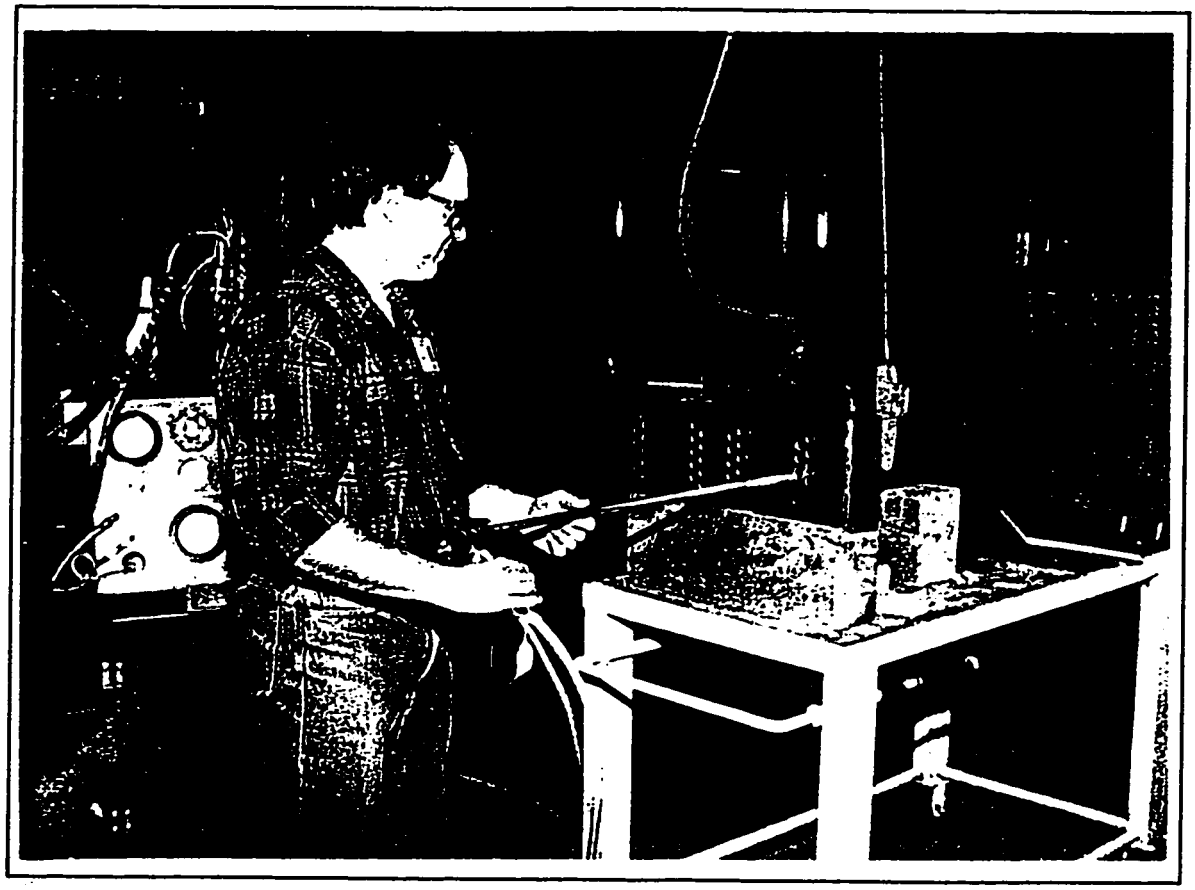


Figure 1.13: Hydraulic expansion equipment

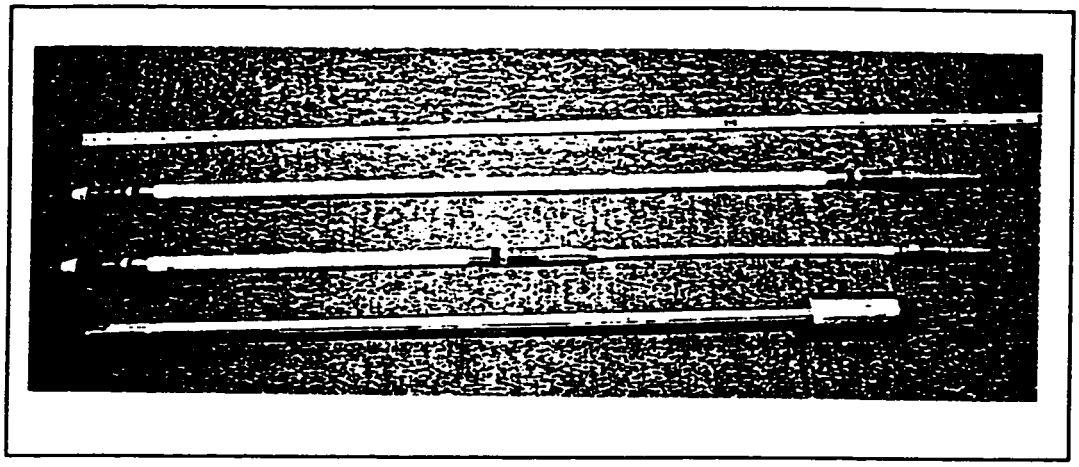


Figure 1.14: Typical hydraulic expansion mandrels of various lengths

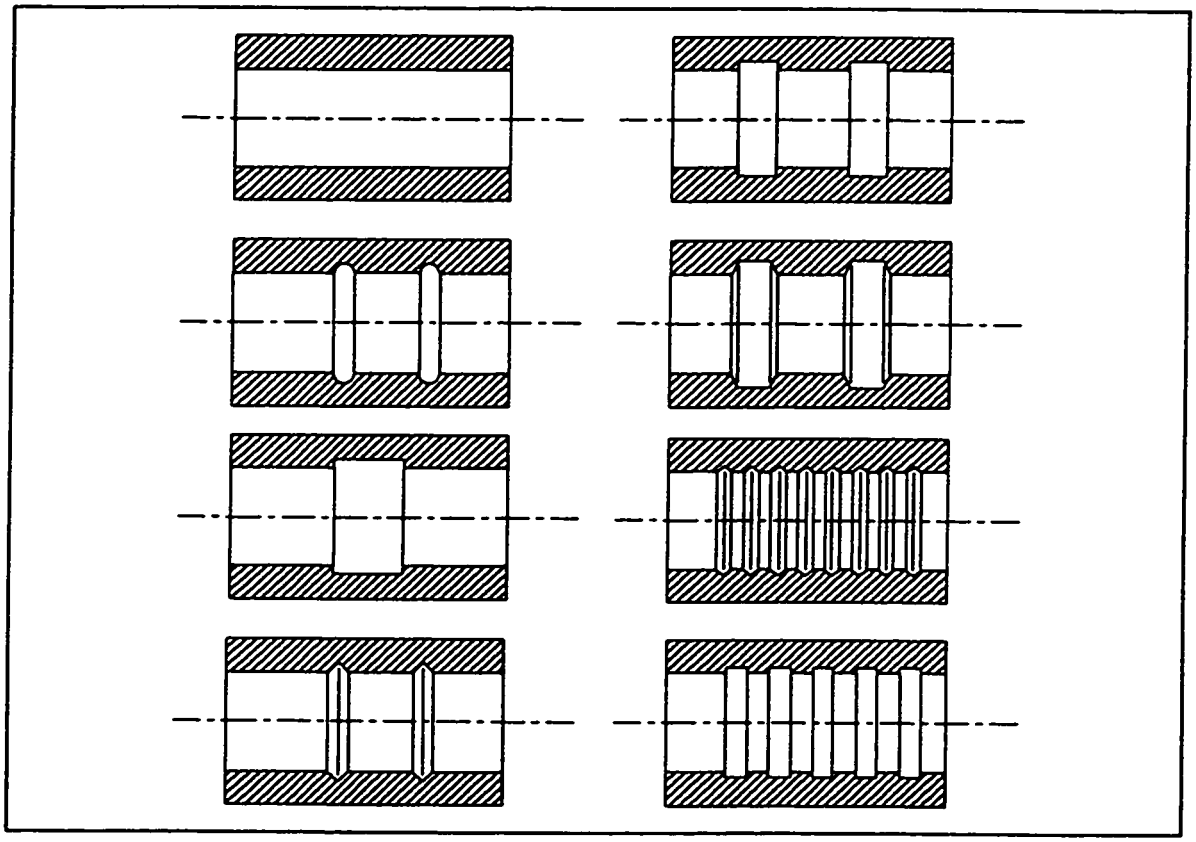


Figure 1.15: Plain and grooved holes

CHAPTER II

LITERATURE SURVEY

2.1 INTRODUCTION AND HISTORICAL BACKGROUND

In this chapter, a comprehensive literature survey is presented which covers the available literature on manufacturing, design and analysis of mechanically rolled and hydraulically expanded joints. The review starts as early as 1927 when Oppenheimer (1927) published the first paper on this subject, and ends with the last available article to us dealing with the expanded joint. The review is divided into three main parts for as-expanded joints, namely: experimental, numerical and theoretical studies. An additional section is devoted to the working behaviour of expanded joint.

The expanded tube joint process which dates back to 1840 was derived from the French-invented process of autofrettage. The first paper to be published on tube-to-tubesheet joint can be traced back to P. H. Oppenheimer in 1927.

During the 1940's, the tube-to-tubesheet joint was extensively investigated. Many papers dealing with roller-expansion process which was the only available technique at the

time. Although, a number of questions were raised with regard to the cause of tube cracking under working conditions, all of the research reported at that time were oriented towards the holding power, the leakage tightness, the axial strength and the residual contact pressure of tube-to-tubesheet joint. The tensile residual stresses in the tube transition zone, which are the real cause for tube cracking, were never mentioned. In 1962 an important contribution to the tube expanding process was published by Toba and indicated for the first time the direct relation between stress corrosion cracking and the tensile residual stresses in the tube transition zone. Hydraulic expansion was first proposed in the early seventies and the first paper related to this technique was published in Germany by Podhorsky and Krips in 1976. Explosive, rubber and hybrid expansion process were also developed at that time.

In the mid-seventies, the tube-to-tubesheet joint was studied by A. Bazergui and his research team (1976). In 1993, an international conference for expanded and rolled joint technology was organized in Toronto through the auspices of the American Society of Mechanical Engineers (ASME), the American Nuclear Society (ANS) and the CANDU Owners' Group (COG). The conference focussed on the practical needs of designers based on the findings of technical analyses and experiments in the field of the expanded joints. The conference proceeding is an excellent source of papers dealing with the design, analysis, and manufacturing (Chaaban et al , 1993).

Section VIII, Div. 1 of the ASME Code (1992) established design standards for boilers and unfired pressure vessels but does not provide much guidance about expanded joints. The Tubular Exchanger Manufacturers Association (TEMA) Standards (1988) cover topics such as the shape, cleanness of the tubesheet holes and depth of expansion, but does not provide a detailed design procedure. As a results, the design of tube-to-tubesheet joints is left to good judgment and some times leads to unsatisfactory service.

2.2 AS-EXPANDED TUBE-TO-TUBESHEET JOINT

The basic design requirements for tube-to-tubesheet joints are specified in Appendix A, Section VIII - Division 1 of the ASME (1992) Boiler and Pressure Vessel Code. The requirement for different joint categories simply specifies that the total axial load on the joint must be limited by the tube yield strength multiplied by the tube metal area reduced by the product of a series of factors that reflect uncertainties of the joint condition. Some of these factors were established experimentally on real joint configurations and others were determined empirically based on experience.

Since the ultimate design objective for the tube-to-tubesheet joint is to maximize the initial contact pressure set up by the expansion process, many researches tackled this problem using different investigation methods. Since the early 1940's, the experimental technique of measuring pull-out strength was used as a direct and only available method to determine the

effectiveness of the joint. Some analytical investigations were also published during that period providing a closed form solution for the contact pressure. The effect of tensile residual stresses in the tube transition zone was experimentally determined in the early 1960's. The finite element method was later used for evaluating both the initial contact pressure and the residual stresses in the tube transition zone. The various approaches are described in more detail in what follows.

2.2.1 Experimental Analysis

As mentioned earlier, the first investigation on the expanded tube-to-tubesheet joint was carried out by Oppenheimer (1927). He recorded the power input to the electric motor driving the roller-expansion tool during the three known steps of the expansion process: 1) expanding the tube until it touches the wall of plate, 2) rolling the tube and deforming the metal of the plate, and finally 3) withdrawing the expander. These results were correlated to the holding force of the expanded joint. Oppenheimer concluded that the holding force of expanded joints having square circular grooves with round edges reaches as much as 12 times the pure shrink-fit resistance. That value was obtained only when the grooves were filled with the tube material. Also, he concluded that the holding force of soft tube and hard plate combination is higher than that of the reversed combination.

Fisher and Cope (1935) presented an introductory study of boiler-tube rolling and

reviewed the methods that were in common use for tube expansion. They covered extensively the elongation method which consists in measuring the rolled-tube axial extrusion and using this as an indication of the degree of expansion by rolling. Experiments were performed on samples of rolled joints produced by expanding short lengths of boiler tubes into blocks of boiler plates. They observed that the leading edges of the rolls leave a sharp shoulder at the inner end of the rolled zone which was suspected to be an ideal starting point for corrosion induced crack propagation. They also showed that the tube-wall thickness decreases at a relatively uniform rate with an increase in tube elongation indicating that tube elongation and tube-wall reduction are directly related to the degree of rolling expansion. A linear relationship between the holding strength and tube elongation was also observed. Axial thrust applied during the rolling process was high enough to deform the heavily rolled-in tubes and/or the tubesheet and lead to the possibility of joint failure.

Fisher and Cope (1943) tried to establish a new rolling technique in which the axial thrust created by rolling expansion was to be eliminated. In their view, the conventional rolling techniques required an operator with considerable skill while their proposed technique did not. The new technique uses an electric motor-driven parallel-rolling self-feeding expander entered to its full length into the tube end. One of the advantages of this technique is that tube expansion could be finely controlled, thus holding the axial thrust at a low value.

Grimison and Lee (1943) performed an extensive experimental investigation to

determine the important parameters involved in tube expanding, various practical methods of measuring the degree of expansion, and the ultimate strength of expanded joints under the various service conditions. The tubes tested in this investigation were 3.25 in. O.D./ 0.17, 0.32 and 0.5 in. wall thickness, and all tubesheet holes were bored to give a nominal diameter clearance of 1/32 in. The residual contact pressure was determined by three different experimental methods which involved the use of thick-cylinder theory by adopting the strain measured during the elastic recovery of either the tube or the tubesheet. The results show wide discrepancies between the methods used. For example, for a typical case, the residual contact pressure was 700 psi by using uniform pressure distribution, 2280 psi by using the thick cylinder theory applied to the tube, and 4300 psi by using the elastic measurements of tangential stains occurring on the periphery of the seat during the removal of the tube. The authors tested the strength of joint samples either in tension, bending, or torsion, and under repeated loading. Not enough data was obtained from the torsion and transverse bending tests to draw any definite conclusion. Repeated loading in torsion to a maximum load of 75% of the yield strength of the tube did not cause failure of the expanded joint after a reasonable number of cycles. It was also found that an increase in joint strength to stand transverse bending may be obtained by increasing the tubesheet thickness. The results indicated an increase in joint axial strength up to a critical value of the total axial extrusion beyond which the joint strength is sharply reduced. As an alternative to tube wall reduction, the total axial extrusion of the tube was recommended to be used as an indicator of the degree of expansion. No method was proposed, however, for measuring the total axial extrusion in the real

expansion process.

Maxwell (1943) discussed the advantages and disadvantages of cold-working the tube by three rolls and a ball-drift expander tool. Also, he explained in detail the effect of tube diameter, tube elongation and tube wall reduction on the axial strength of the expanded joint. The author observed a shearing action between the tube and tubesheet surfaces during roller expansion. This shear may exceed the safe design factor and reduce the holding power of the joint and thus cause a leakage due to the highly reduced contact pressure. Also, the axial thrust of up to 7000lb/tube created during the rolling operation was shown to be a major disadvantage of the rolling technique. The author attributed the flaking of the inner tube wall to the difference in the surface speed of the tapered rolls. Based on his own results and those of other researches, the author reached the following conclusions :

1- The optimum holding-strength values for rolled joints are obtained when the seat depth is 1.25 to 1.5 in. for both grooved and non grooved joint.

2- The three-roll expander is the recommended tool for most joints.

3- The ball-drift expander must be used for small thin tubes.

Following Fisher and Cope (1943) work, Dudley (1954) suggested a more precise electronically-controlled technique relying on the amount of torque required to precisely and consistently roll the joint. The objective of this method was to eliminate the requirement for highly skilled operators. Dudley reported variation in the pull-out strength of identical rolled

joints achieved by an operator with 20 years experience. By contrast, the electronic device, coupled with mechanical expander tools when tested on thousands of condensers tubes end expanded by unskilled personnel produced good leakage resistance during service conditions. The research was extended to cover grooved seats. Push-out strength test on different tubes and seat geometries indicated that the use of serration does not contribute leak-tightness but tends to increase the mechanical strength of the joint. The author concluded that serrations or grooves, are generally not needed but, when used, the type, number and location of the grooves should be carefully considered. In addition, a measurement of tube elongation during tubes expansion indicated that 70 percent of the metal flows away from the back end of the tubesheet producing a compressive loading which therefore tends to separate the tubesheets and create longitudinal stresses in the entire unit and/or in some of the tubes when unequal expansion of the various tubes has occurred.

A detailed review and discussion of more than twenty American and German papers published by different authors since 1927 up to 1943 examining the behaviour of the tube-to-tubesheet joint are given by Cope (1943). His paper is considered as a good source of experimental data for different techniques measuring the joint axial strength and various rolling tools fitted with different number of rolls.

The paper by Fisher and Brown (1954) reflects many years of experience of the authors in the field of tube expansion. They conclude that the parallel roller expander is

preferable to tapered types because it insures uniform cold working of the tube and tubesheet metals and therefore generates stronger rolled joints. This conclusion was later criticized by Alexander and Ford (1956) who proved that parallel roller expanders do not lead to a uniform interference between tube and tubesheet. In an investigation made to determine the relative merits of using 3,4 or 5 roller expanders, the 3-roller was proved to be the best. This confirms Maxwell (1943) finding recommending 3-roller expanders for tubes having non-uniform wall thickness. The authors referred to the problem caused by the leading edges of the rollers. Expanders having rollers with sharp or improperly shaped leading edges create a zone of potential tube corrosion and were believed to be responsible for many tube-end failures. Experimental testing indicated an increase in joint strength with rolling up to a maximum value. Further rolling was limited by the elasticity of metals comprising the joint and thus reduced the joint strength. For best overall results, the hardness of the tube should be somewhat less than that of the tubesheet. A reverse condition usually results in distorted or greatly enlarged tube holes. The authors recommended that tube-hole clearance should be as small as possible, and the length of rolled portion of the tube should be as small as 1-5/8 in. They also recommended the use of so-called retractive expanders in order to eliminate the axial compression load in the tube during expansion. This expansion technique is achieved by first rolling up the back of the joint to the desired degree of expanding, and then rolling forward until the joint is completed.

Alexander and Ford (1956) described in details experimental tests examining the tube

expansion process in relation to many variables and determined whether there would be any significant size effect. They developed a special apparatus for measuring specimens of tube-to-tubesheet joints during and after expansion. Measurement during the expansion was simplified by reducing the mandrel speed to 20 rpm which was lower than normal practice. The strains, both in the radial and in the circumferential directions were measured by means of strain gages located at selected points on the back and front surfaces of the sleeve. Also, the axial extrusion of the tube metal was measured by dial gages. The residual strains on the back and front faces of the disk after removing the expander, were used to measure the holding strength of the joint. The measurement of the extrusion versus cage revolution indicated that the front extrusion is always greater than the back extrusion of the tube metal. The latter observation clearly contradicts what was reported by Dudley (1954) who stated that 70% of the total extrusion flows away from the back of the tubesheet. The results of residual strain distribution clarified the differences between the strains at the front face and their corresponding values on the back face of the sleeve. The last observation indicated that modelling tube-to-tubesheet joint by either plane strain or plane stress may not be acceptable. The authors further concluded that axial extrusion was not a practical criterion to determine the degree of expansion and they recommended the driving torque to be a better indicator. They also concluded that there are no appreciable size effects and that the parallel expander does not produce uniform interference between the tube and tubesheet.

By using the test rig previously developed by Alexander and Ford (1956), Culver and

Ford (1959) investigated certain aspects of the tube-expanding process. The factors investigated were: retubing, the starting position of the roller cage within the tube, and the initial clearance between the tube and tubesheet hole. A few tests were also involved the measurement of the joint relaxation with time. Four complete tests were made in order to study the effect of the starting position of the roller within the joint; the results indicated that a much stronger rolled joint was obtained with less driving torque if the rollers start with their front ends almost at the back side of the joint. Test assemblies were prepared, with a diameter clearance of 0.000, 0.01 and 0.02 in. in order to study the effect of the initial clearance between the tube and the plate hole. The general conclusion was that the effect of the initial clearance is not as expected, and is not a major factor in the joint strength. To study the relaxation of the joint with time, samples were allowed to stand for varying amounts of time (up to 7 days) after expansion. No change in reading was detected either by the displacement calipers or of the surface strains on the plate which lead to the conclusion that the joint pressure relaxation must be very small.

As a consequence of condenser tubes cracking under service conditions, Toba (1966) studied the level of residual tensile stress and stress corrosion in aluminum brass condenser tubes by means of strain gages and stress-corrosion-cracking tests. To our knowledge, he was the first author referring directly to the existence of the tensile residual stresses as a result of the expansion process, and clearly indicating their location. He proposed a new factor related to the level of tensile residual stress in the tube ends. A microphotograph taken from a

section of expanded brass tube specimens that were immersed in an aqueous ammonia solution, indicated that circumferentially initiating cracks were located on the inner surface of the tube between the expanded and non-expanded zones. From this, he concluded that a large tensile residual axial stress always remains in the inner surface of the brass tube in the vicinity of the expanded part. Also, a direct relationship between the tensile residual stress and the initial radial clearance was obtained. Therefore, he concluded that a loosely fitting tube increases the tensile residual stress and consequently increases the possibility of stress corrosion cracking.

The first experimental analysis for hydraulically expanded joints was reported by Krips and Podhorsky (1976) in support of a new theory of hydraulic expansion. The change in tube geometry, the reduction in tube length and the pull-out force were measured on completion of the tests. Also, helium leak test was performed. The measured values were plotted as a function of the number of tubes in the test block. Of particular interest was the fact that the pull-out force increases non-linearly with residual contact pressure calculated analytically, which confirmed the authors' theory. The high disagreement between the calculated residual contact pressure and measured pull-out force was attributed to the variation in hole diameter along the tubesheet thickness. Also, the authors verified experimentally the effect of combining hydraulic with mechanical roll expansion methods for heat exchangers with two fixed tubesheets. This aspect is found particularly interesting in connection with heat exchangers subjected to thermal stresses in operation.

Gaffoglio and Thiele (1981) discussed pullout strength data on five non-ferrous and ferrous tube materials frequently specified for steam condensers. The data was evaluated using air-driven, five-roller, expanders with commercial tube lots expanded into plane and double serrated (square grooved) tubesheet holes produced using standard manufacturing methods. One of the main objectives was to determine if the generally accepted norm of a 5% wall reduction for tubes of copper-based materials produces a joint of acceptable strength with some degree of consistency. Twelve tubesheets of aluminum bronze and Muntz materials were considered in the experiments. Each tubesheet contained a total 88 drilled holes, 44 for each combination of tube material and percentage wall reduction. The drilled holes were in a 60° diagonal array with quarter-inch ligament (implying a 20% ligament efficiency). Prior to rolling , the wall thickness was measured at four locations. Two readings, 90 degrees apart, were taken 1/4" and 3/4" from the tube end. Wall thickness was approximated as the average of four readings. Once testing was completed, recorded values of pullout load for each of the 1056 tubes, as well as dimensional data were submitted to statistical analysis. The average values of pullout strength were represented in two main graphs for aluminum bronze and Muntz metal tubesheets. For certain tube/tubesheet material combination, the results support the contention that a grooved tubesheet hole extends the average pullout strength beyond that of a non-serrated hole. The major finding was that for other tube/tubesheet material combinations, the serrated tubesheet does not increase the pullout strength significantly and could in some cases reduce the joint strength. Table 2.1 summarizes some important results picked-up from the paper where the pullout strength were measured in lbs. The table indicates

the non-significant effect of the groove even with highly rolled tubes that caused tubesheet ligament distortion.

Table 2.1: Pull-out test results in term of percent wall reduction

(Gaffoglio and Thiele (1981))

	Titanium tube Aluminum bronze Tubesheet			304 Stainless steel tube Aluminum bronze Tubesheet			90:10 CuNi tube Muntz Tubesheet		
	Reduction%		Average	Reduction%		Average	Reduction%		Average
	Test	Actual	Strength	Test	Actual	Strength	Test	Actual	Strength
Grooved	8	9.1	1101	5	3.7	1704	3	3.8	2135
Plain	8	7.1	1134	5	5.2	1852	3	3.2	2501
grooved	10	10.7	1688	8	7.53	2309	5	5.6	2601
plain	10	9.8	1538	8	8.2	2037	5	4.5	2476
Grooved	12	12.4	1815	10	10	2914	8	7.7	3067
Plain	12	11.1	1629	10	10	1934	8	6.6	2655

In addition, the measured joint strength varied greatly from tube to tube within the same material group with serrated tubesheet holes, as indicated by the relatively large standard deviation about the main strength of test joints. The authors concluded that for a copper alloy tube material, a good joint strength could be developed with 5% wall reduction. Also, serrated tubesheet holes increases joint strength when using copper alloy tubes especially with aluminum bronze tubesheet. However, the latter conclusion should not be generalized because the joint axial strength is highly affected by the shape, location and number of grooves in serrated tubesheet holes.

Uragami et al (1982) examined experimentally the residual stress of hybrid (hydraulic followed by mechanical rolling) expanded tube-to-tubesheet joints. They also investigated the advantages of the hybrid expansion upon the residual stresses and the axial strength of the joint. One material set for the tube (ASTM A.508) and tubesheet (Inconel 600) was considered. The strength of hydraulically and hybrid expanded joints was examined by performing a fatigue test on both types. The fatigue strength of the hybrid joint was 15 to 20 times that of the joint created by hydraulic expansion only. The second advantage of the hybrid expansion was the visible negligible effect on the maximum tensile residual stresses located in the transition region of the tube. The hybrid expansion was also found to permit the closure of the crevice between the tube and the tubesheet without creating a bulge deformation which typically results from hydraulic over- expansion. However, the results did not indicate at what limit of hydraulic expansion the mechanical rolling has to be alternatively used and up to which value of rolling degree of expansion this phenomenon would still be valid.

Jawad et al (1987) carried out an extensive experimental study to measure the pull-out strength for hydraulically expanded and mechanically rolled tube-to-tubesheet joints. The reported studies included the effect of the surface finish of both the tube and tubesheet hole surfaces. A series of titanium and carbon steel tubes were hydraulically expanded in carbon steel sleeves with no grooves. The results of the pull-out loads indicated that for titanium tubes the hole surfaces finish had no significant effect on the joint strength. On the other hand,

for carbon steel tubes, the pull-out strength seemed to improve with holes having rough surfaces. However, the authors measured only the surface finish before expansion. Consequently, they concluded that improving the surface finish of the hole does not influence the joint strength when the tube and tubesheet are of different materials. Indeed, the surface finish of both the tube and the hole could be greatly affected by the expansion process. Similarly, improved joint strength was achieved when grooved holes were used, particularly with carbon steel tubes. However, a number of tests conducted with titanium tubes attached to a carbon steel tubesheet showed an opposite effect. In our opinion, this could be explained by the fact that the hard titanium tubes were not sufficiently deformed inside the grooves. Nevertheless, the use of grooves with this tube material reduced the contact area between the tube and the tubesheet and consequently reduced the joint strength. In comparison with hydraulically expanded joints and those expanded using the hybrid technique, the welded and expanded joint have shown a superior holding power. Also, the hybrid technique using 3% rolling expansion seemed to increase the axial strength by almost 25% over that of only hydraulically expanded joints.

Haslinger and Hewitt (1983) performed extensive pull-out tests on titanium, AL6X and CuNi tubing using a Muntz tubesheet. The objective of the tests was to determine the leak tightness performance of joints under cyclic loading conditions which exceed the allowable load values recommended by the HEI and ASME codes. The joint integrity test included the study of the effect of rolling torque and tube wall reduction on pull-out strength.

Also studied were the effect of different grooves in the tubesheet for a variety of tubing materials and the use of anaerobic cements. Joint axial strength in general increased with rolling torque until a certain limit beyond which some significant deformation of the tubesheet ligaments were observed. The experimental results indicated too much variation in the measured pull-out strength. Therefore, it was decided to plot the joint axial strength versus the apparent wall reduction in the hope of finding a better correlation. Viewing the enclosures, the authors concluded that the quality of the rolled joint cannot be measured from the driving torque and it would rather have to be evaluated on the basis of the degree of measured wall reduction. Multiple-tube experiments were also performed on 42-array specimens, with and without grooves. The rolling torque was varied from 6 to 11 ft.lbs with the objective of determining the optimum torque. At the high torque, ovality of as much as 0.035" in unrolled tube holes was observed adjacent to the tube being joined. The data and the statistical evaluation of the results gave an unacceptably large data scatter. Consequently, it was concluded that the higher driving torque not only was excessive, but also affected neighbouring joints installed at lower torque. The author thus concluded that 8 to 9 ft.lbs would be the optimum rolling torque for titanium and AL6X tubing materials. Metallurgical examination was also performed to examine the flow of tubing material into the various groove configurations. For AL6X and titanium tubes there was no flow of metal into the single groove when using the roller expansion method. The softer 90:10 CuNi tube allowed more metal flow into the single groove and also, no gaps were observed between the tube and tubesheet. Finally, it was concluded that the joint design loads determined by the ASME

guidelines, using experimental data as input or using applicable "no-test" coefficients can differ substantially.

Druez (1983) and Bazergui et al (1985) determined the residual stress distribution through the wall of the tube in roller expanded region of thin-walled Incoloy-800 Fe-Ni-Cr alloy tubing in as-expanded and heat-treated conditions. The residual stresses were evaluated experimentally by a destructive sectioning (slitting) technique using a strip of strain gages first attached to the expanded tubes at the measurement location. Then, a through-wall section of tube-outer material is removed by progressive chemical etching. The release of residual stresses of that tube section is proportional to the change of strain measured by the strain gages. The measurement were taken by five stain gages in the expanded zone and four stain gages in the non-expanded zone of the tube. Only one strain gage was used to measure the residual stresses in the transition region. This was, of course, because of the size limitation of that region and the size of the strain gage itself. High stress gradients in the transition zone could thus have been masked. The method, however, was innovative and quite effective for determining through-thickness stress distributions. The authors concluded that heat treatment reduced the level of residual stresses by 30% to 50%, but also on the other hand, it reduced the contact pressure between the tube and tubesheet to nearly zero in most cases.

Scott et al (1984) performed extensive experimental testing on hydraulically-expanded joints, including stress corrosion tests, X-Ray diffraction and strain gage measurements. The

stress corrosion tests were used to locate and estimate the extent of maximum tensile residual stress at the surface of expanded tube specimens. Using a corrosive environment for a specified period of time, cracks formed on the surface where tensile stresses exist. The longer the test, the lower is the tensile stress required to initiate cracking. Boiling sodium hydroxide was used in those experiments which take 6 to 9 months to get results. The test samples were frequently taken from the corrosive medium to macroscopic examination for cracks. This could lead to a time error of days, and, consequently, could give rise to errors in estimating the maximum tensile residual stress. The X-Ray diffraction technique was used to measure the residual stress level located on the expanded tube inner surface; stresses within only 0.1 mm depth could be measured. The accuracy of the X-Ray method is highly sensitive to a variety of metallurgical parameters such as grain size, impurities, voids, etc. which were not adequately quantified in the paper for accurate measurements. Strain gages were used to measure the residual stresses which were released by first cutting away the sleeve and making axial cuts in the tubes. Because of the small tube size, the cut-out strip was in segments of as much as 45°. The flexural rigidity of this curved strip being greater than that of a flat strip, the axial residual stresses were not completely released, leading to questionable accuracy: Indeed, the strain gage measurements indicated that there could be strain variation of up to ±50 percent around the circumference which was contrary to the axisymmetric nature of hydraulic process. The authors concluded that hydraulic expansion produces joints with an acceptable level of residual tensile stress. However, the pull-out strength of hydraulically expanded joints was less than that of rolled joints.

Fender et al (1985) performed an experimental testing on pull-out and push-out strength. The tube-to-tubesheet specimens were sampled from a short portion of the tube expanded in tubesheet plate of one inch thickness and one single hole. The samples of the push-out test was also prepared by flaring the tubesheet hole. The comparison of the mean values of the joint strength showed the pull-out load averaging was 6-8% higher than push-out strength. These results are generally expected since the load strength is proportional to the contacting area between the tube and tubesheet meeting surfaces. This area is greater in the sample of the pull-out test where the tube end is straight or non-flared. Also, when the push out load of a joint having flared tube end is compared to that of non-flared tube, a reduction of more than 26% in the joint strength is observed.

Walker et al (1985) measured the strains developed in a tubesheet by the roller expansion of tubes. The measurements were done on the front face of the tubesheet by using Moiré interferometry. The tube plate specimen was a titanium block 125 mm in diameter, with a series of 19 holes, 16 mm in diameter, spaced on 24 mm centre (8mm ligament). The steel tube having twice the stiffness and about the same yield strength of titanium was used for the experiments. The expansion process was carried out using a conventional three roller electrically driven expander which operated up to a preset torque limit. The tube plate was elastically and plastically deformed during the rolling and the elasto-plastic strain field was recorded during the rolling process itself. The major observation from the photographs was that the tubesheet ligaments end up with an area of overall zero strain at the end of the

expansion process even though the same area showed strains after the first and second rolls. This pointed out the limitation of the theory developed by Nadai (1943) and later used by Kasriae et al (1983) which considers the tubesheet to be an infinite plate and predicts that the strain should decay to zero only in the infinite field.

Soler et al (1985) and (1987) developed experimental tests to assess the validity of their theoretical analysis of an expanded tube-to-tubesheet joint. For the simple annular model, the authors investigated the effects of geometry and material composition of the test samples used to simulate the joint. Three different material sets for the tube and the tubesheet were used. The tube and sleeve dimensions were measured mechanically by using a micrometer and a telescoping gage before and after the expansion process. The samples were subjected to hydraulic expansion using commercial tube hydro-expanding equipment and then subjected to slow heating and cooling to a maximum temperature of 400 °F. Because, the interface pressure was central to the theoretical 2-D solution (Soler et al (1984) and Weinstock et al (1985)), the experimental work was expected to also measure this pressure. But, the authors verified only the theoretical analysis by comparing easily measurable quantities, namely: the circumferential strain at the outer diameter of the sleeve, and the change in inside diameter of the tube. Strain was measured when the maximum applied pressure was released, when the maximum steady state temperature was achieved during the thermal cycle, and after the test sample was cooled down to room temperature. From the tabulated results in the paper, it was easy to see that in nearly all cases studied, the theoretical

model predicts higher strain values than the corresponding experimentally determined quantities. When comparing the results using mill test material property values, the experimental and 2-D theory were in good agreement for certain tube-tubesheet combination and in bad agreement for others. Thus serious consideration should be given to the use of mill test properties rather than nominal tabulated properties. The authors concluded, that the correlation of 2-D model with 3-D experiments permits the theoretical model to be used to predict the general behaviour for a given tube-to-tubesheet joints.

Comments and concluding notes:

It appears that one of the most common methods used to expand tubes into a tubesheet is mechanical rolling. The problem with this method is the lack of control of the degree of expansion. Apparent tube wall reduction, front axial extrusion, total axial extrusion and driving torque are independent measurable quantities that have been used to express the degree of rolling expansion. Apparent tube wall reduction became the most commonly used, simply because it can be measured in a production exchanger. In practice there are likely to be some variations in dimension form tube to tube and from hole to hole, it was found more convenient for production operation to measure the torque on the rolling tool rather than the tube wall reduction. Despite of the many efforts to control the rolling process, it still relies on the skill of the operator. To the best of our knowledge, there are no published correlations that provides level of the interference residual pressure in terms of tube wall reduction.

Hydraulic expansion on the contrary, is mainly characterized by the expansion pressure, and exhibits numerous advantages in comparison with conventional rolling.

Experimental techniques employed in the investigation of tube-to-tubesheet joints include joint axial strength, static strain gage measurements, accelerated stress corrosion induced cracking and residual stress measurements. Experimental techniques are costly and time consuming. Some techniques are of questionable accuracy.

The main problem with strain gages and X-Ray methods, is that it is very difficult to make measurements at the location where the contact pressure resides. In addition, the size of the strain gage and the X-Ray beam could mask some high stress gradients especially, in the tube transition zone.

The optimum degree of rolling expansion was generally obtained at approximately 4.5 to 5.5% of tube wall reduction. This optimum value was set without any consideration of the residual stresses in the transition zone. This optimum degree of expansion for hydraulically expanded joints has not been systematically investigated yet.

Residual stresses that are located in the transition zone were not taken into consideration in publications prior to 1960, and most likely were not recognized during that period. Cracks in the transition zone of the tube were thus attributed to the tool used during

the expansion process. The focus of those papers was mainly the axial strength of the expanded joint.

2.2.2 Finite Element Method

The first finite element analysis found in the literature for the tube-to-tubesheet joint was presented by Wilson (1978). Particular emphasis was placed on the tube transition region. The idealized problem that was analysed was an expansion process with a uniform internal pressure which was most analogous to a hydraulic expansion process. Both the tube and tubesheet were represented by a mesh of axisymmetric isoparameteric quadrilateral elements. A special gap-friction element was used to join the tube to the tubesheet. The problem required a large amount of computer time and storage. Consequently, the number of elements was limited to 165. The sleeve outer diameter was selected to be three times the inside diameter. Earlier analytical researches established that the plastic zone could not propagate beyond 2.6 times the hole diameter. The finite element analysis done by Wilson showed that a much smaller sleeve outer diameter could have been used without altering the tube stress distribution significantly. The results also showed that the highest tensile axial stresses were located on the tube inner surface. At the tube to tubesheet boundary, the contact pressure varied in sinusoidal fashion due to the presence of the gap element. Consequently, the radial stress within the tubesheet fluctuates between compression and tension. This oscillation of stress indicates a level of accuracy of about 25% of the tube yield

strength.

Based on their experimental work done in (1976), Podhorsky and Krips (1979) discussed the concept of combining roller and hydraulic expansion to produce a desired amount of pre-strain in the tubes. Since mechanical rolling elongates the tubes, and hydraulic expansion shortens them, Podhorsky and Krips suggested their technique in order to control the prestress, including the special case of stress-free, in straight tubes heat exchangers with two fixed tubesheets. This technique is recently named a hybrid expansion. Recent investigation indicates that a stress-free joint cannot be achieved since the stresses in the tube transition zone for either case of expansion are inevitable. Because the analytical model given in (1976) was on a simple annular model, the precise elastic behaviour of an actual tubesheet was examined with the help of the finite element analysis in order to provide information on the accuracy and reliability of simple annuler model. A 30° portion of the tubesheet was discretized by using plane triangular elements. It appears that the finite element code used in the analysis had no ability to solve the contact nor the elastic-plastic problem. Therefore, the aim of the computation was to obtain the elastic strain diagram for the case of uniformly loaded surfaces due to residual pressure in the central hole. A factor expressing the percentage of elastic recovery given by the finite element model was introduced to correct the analytical result. Practice however showed that such a calculation of tube-to-tubesheet joint ignoring this factor yielded acceptable results within the accuracy of technological process and equipment.

Uragami et al (1982) performed a finite element analysis of a single tube axisymmetric model using the MARC computer code with constant strain triangle elements. Whereas, the residual stresses in the transition zone located on OD surface were calculated and verified experimentally, those located on ID surface received no attention. The experimental measurement of the axial residual stress performed by the authors agree with those calculated by the finite element method favourably. However, the values of the hoop residual stress evaluated experimentally do not correlate well with those calculated by the finite element method. This is due in part to the contact elements used that had no ability to simulate the friction interaction. Also, the authors found that the residual stresses resulting from the hydraulic expansion process were lower than those developed from the rolling expansion. In addition, the hybrid expansion method, when the mechanical roll is performed at the location sufficiently apart from the transition zone formed by hydraulic expansion, is beneficial in the view points of the pull-out force, the gap crevice closure, and the stresses in the transition zone.

Kasriae et al (1983) conducted elastic-plastic finite element analyses in order to establish limitations for rolling tubes in tubesheets of low ligament efficiency. The model included sequential tube expansion in tubesheets having triangular patterns. The ANSYS program was used with a model consisting of 271 four-noded plane strain elements. While the authors assumed sequential expansion, the finite element mesh incorrectly used a 30° wedge which corresponds to the simultaneous expansion case. The difference between the

yield strength of the tube and tubesheet materials was found to affect the contact pressure significantly: The gap between the tube and the hole tends to open during unloading particularly when tubes with higher yield strength are used. Also, it was found that the contact pressure around the central tube are not essentially affected by the presence of the tubes in neighbouring holes. The authors recommended that the expansion process for closely spaced tubes has to be very carefully controlled in order to prevent overstraining thin tubesheet ligaments.

Aufaure et al (1987) developed a finite element computer program to evaluate the residual stresses in the ID surface of tube transition zone and to endeavour to lower their level by varying some design parameters. For simplicity, roll expansion process was approximated by an axisymmetric static problem of unilateral contact. A radial displacement, with exactly the same profile as that of the roll, was prescribed on the inner surface of the tube. The position of tube inner surface was thus known at each increment as a function of the axial direction because of the rolls end-round. The extent of the contact between the tube and tubesheet was also assumed to be known before the expansion. The mathematical model was experimentally verified by measuring the residual stresses on mock-ups made of austenitic stainless steel tubes and plates. For measuring the stresses by X-Rays on the tube inner surface, it was necessary to cut the tube longitudinally into two parts. Thus, the residual stresses in the circumferential direction were altered. But, the axial stresses were assumed to be little affected. This was the reason, why only the axial stresses measurement was done.

No explanation was given as to the observation that the experimental values were greater than the corresponding numerical ones.

Ramu et al (1987) developed a finite element computer software to determine the stress distribution in a Channel Rolled Joints used in Nuclear Engineering. The geometrical model of the problem consisted of only the expanded part of the tube and a sleeve. The analysis was greatly simplified by idealising the mechanical process of rolling by an axisymmetric internal pressure at the location of the rollers along the joint. The procedure adopted also assumed an axially symmetrical stress distribution during all the stages of the rolling process. The geometrical model of the two concentric cylinders were discretized by using axisymmetric 8-noded solid elements. The contact interaction between the tube and the sleeve was completely neglected. The tube and the end fitting seem to have been considered as one integral part. No results other than the extent of the plastic deformation in both the tube and the sleeve was reported.

Wang and Soler (1988) developed a finite element model to study the effect of adjacent holes and outer boundary conditions on the tube-to-tubesheet joints. They focussed on the determination of the appropriate equivalent external annulus diameter to permit the computer code developed by Soler et al (1984) and (1985) together with the general purpose finite element software ANSYS version 4.3 to be used and, consequently, study a large number of geometry combinations. The appropriate outer diameter was obtained using the

annulus model to determine a curve of residual contact pressure versus annulus radius ratios. Then, a finite element plane stress model was used to describe accurately the effect of adjacent tubes, tubesheet ligament and nonsymmetric geometry. In order to simplify the analysis, simultaneous expansion was assumed for a seven tube model and only a portion of the central tubesheet ligament was modelled by the finite element. The expansion pressure was applied only on the central tube and the expansion of adjacent tubes was ignored. The contact pressure was compared to that obtained by the simpler model in order to yield the appropriate radius ratio which would provide the same results. The authors concluded that for most of engineering implementations, the tubesheet equivalent diameter bound by 90% the hole pitch.

Chaaban et al (1989) used the finite element method to study the effect of the material properties, sequence of expansion and the initial clearance on the residual stresses and the contact pressure of hydraulically expanded tube-to-tubesheet joints. The axisymmetric model of a single tube surrounded by an annular sleeve was assumed during the analysis. The effect of the initial gap was only investigated on the basis of a single tube axisymmetric model with elastic-perfectly plastic material behaviour. For an arbitrary sleeve outer diameter, the results of the axisymmetric finite element model indicate that in order to obtain lower residual stresses in the tube transition zone, the initial gap between the tube and tubesheet must be reduced as much as possible. A plane stress seven-tube model, without initial gap between the tubes and the tubesheet, was used to investigate the relationship between the residual

contact pressure and some design parameters particularly the sequence of the expansion. In a preliminary phase of the study, a special finite element model was used for examining whether refining the mesh would help to reduce the residual contact pressure fluctuations around the central tube in the case of simultaneous expansion. It turned out that it did not and, a course mesh having a limited number of reduced integration elements was therefore adopted in the analysis. In the case of simultaneous expansion, the results show an axisymmetric distribution of the contact pressure around the central tube. The assumption of axisymmetric condition was therefore suitable for that case. However, in the sequential expansion case, the single tube axisymmetric model was shown to be non-conservative in predicting the residual contact pressure levels.

Ma et al (1990) developed a three-step method using a seven tube model to replace a fully 3-D elastic-plastic finite element analysis, particularly when a sequential expansion process is applied. A simple axisymmetric model was proposed to simulate the general behaviour of a complete 3-D model. With the seven-tube model the equivalent sleeve external diameter to be used in the axisymmetric model was determined. With more precision for the tubesheet finite element simulation, the authors used a similar but modified technique that was first proposed by Soler and Wang (1988). Both methods were based on the residual contact pressure being the only criterion for calculating the equivalent sleeve diameter. For the first time, the authors used orthogonal design method in order to minimize the number of calculations while keeping the effect of all the parameters involved. Based on a detailed

statistical analysis using a single tube model, the results of the residual contact pressure show that the yield stress of the tube material seems to be the most significant parameter; the second important parameter is the expansion pressure level, followed by Young moduli of the tube and tubesheet materials. The initial clearance between tube and tubesheet as well as the yield strength of tubesheet were found to be less important parameters.

Middlebrooks et al (1991) investigated the residual stresses and strains of hydraulically expanded tube-to-tubesheet joints by using two different finite element codes with three different finite element models and by a theoretical incremental analysis method developed by Singh and Soler (1984). Both plane stress and plane strain conditions were analysed. The finite element plane model was an eighth-symmetry model where the constraint of the adjacent tubesheet material was modelled by a row of elements with a reduced elastic modulus to achieve the equivalent appropriate stiffness. The WECAN (Westinghouse finite element computer code) was used to carry out the calculation. For the given tubesheet hole square pitch, three levels of equivalent sleeve diameter were verified according to either minimum ligament, maximum ligament or the average of the two. Comparison between the residual contact pressure provided by WECAN eighth-symmetry model and the annular model given by Soler indicated that the averaged sleeve diameter would adequately simulate the tubesheet. The residual stresses and transition zone profile were calculated using an axisymmetric model that was constructed and solved with the ABAQUS finite element code. The maximum residual axial stress was found to be higher than the hoop one by about 30 to

40 %. Also, during hydraulic expansion, the tube wall thinned by about 1.5% and the tube length shortened by about 0.9% of the expanded tube length.

Chaaban et al (1992) further developed an empirical equation for the equivalent external sleeve diameter that can be used in the single-tube model for both expansion cases, simultaneous and sequential. Other empirical equations fitted to the results of finite element method and obtained by nonlinear multiple regression were given by Chaaban et al (1993). They were developed to calculate the residual contact pressure and to obtain the maximum tensile residual stresses in the transition zone and the tube wall reduction. The results of both the finite element method and the proposed empirical equations on typical arbitrary cases when compared showed a good correlation. The empirical equations should, however, be used within the limits of the independent parameters.

Hwang et al (1993) presented a finite element analysis of hydraulically expanded tubes through the full thickness of tube plate in nuclear steam generators. The authors performed their investigation by using two different finite element computer codes. For a triangular and square arrangement patterns, the residual contact pressure was first evaluated by using a plane stress model. They assumed that the correct sleeve OD in the axisymmetric model is the one that gives a contact pressure in agreement with that calculated using a plane stress assumption. The effect of the modulus of elasticity of the tube and tubesheet materials on the equivalent sleeve diameter was neglected. For the same design conditions, the average value

of the residual contact pressure around the central tube in triangular pitch model is almost 100% greater than that around the central tube for square pitch model. The finite element analysis was extended to verify a technique named "double-expansion method" that can be used to close the crevice located on the back side of tubesheet. The authors indicated that a virtually zero crevice depth and a tight joint can be achieved numerically by a single or a double expansion process; however, it is impractical during manufacturing due to small variations in the process variables which lead to non-zero crevices or a bulged condition. Also, the authors did not show how the double expansion method could affect the residual stresses in the transition zone.

Abdelsalam and Dokainish (1993) performed a finite element analysis of hydraulically expanded tube-to-tubesheet joints. A 2-D axisymmetric finite element model generated and solved by a general purpose finite element program INDAP (Incremental Nonlinear Dynamic Analysis Program). The initial clearance and the expansion pressure level were the main parameters considered. A peak joint strength, related to the difference between the tube and tubesheet materials strain hardening parameter is shown to exist. A comparison between the residual contact pressure as given by INDAP and those give by two previous analytical solutions (Kasriae et al (1983) and Sachs (1947)) was also presented.

The axisymmetric model for representing the rolling process ignores the radial-hoop shear stress component acting on the tube inner surface. This stress component strongly

influences the plastic deformation of the tube material being rolled. The first realistic numerical simulation for the rolling process was presented by Metzeger and Sauvé (1993) who used transient approach to the roller motion to compute the residual stress profile and the stress history in the expanded part of the tube. Later, Metzeger et al (1995) evaluated the stress state through the tube wall versus the angular position. The main finding of these studies is that the use of the axisymmetric model for rolled joint residual stress evaluation is not accurate. The authors promise further investigation.

Comments and concluding notes:

The finite element method was used to calculate the maximum tensile residual stress in the tube transition zone and to estimate the average value of residual contact pressure in the expanded zone. Four different types of finite element analysis have been used: plane stress, plane strain, axisymmetric and 3-D. The more realistic 3-D model is relatively complex and costly to implement. Plane stress and plane strain models have been used to simplify the problem and to obtain average values of the residual contact pressure in the circumferential direction, and/or to obtain the residual stresses in the tubesheet ligament. The axisymmetric model has been used to evaluate the residual stresses in the transition zone and/or to obtain the average value of the residual contact pressure in the axial direction. The axisymmetric model requires that an equivalent sleeve external diameter which represents the effect of surrounding tubesheet ligaments be determined. The question as to which plane stress or

plane strain model is best suited to calculate the residual contact pressure remains yet unanswered.

Much remains still to be done in order to cover the subject adequately: the use of gap element must be replaced by a more realistic frictional contact element; the study of progress of axial and hoop stresses in the transition zone during expansion and the extent of the plastic zone along the tube axial direction; the simulation of thermal and mechanical loadings during the joint service.

2.2.3 Theoretical Analysis

The elastic-plastic analysis by Jantsscha (1929) of the tube and tubesheet deformations resulting from the tube expansion is the earliest reference we could find on the topic.

Nadai (1931) and (1943) investigated the residual contact pressure created between the tube and tubesheet assuming rolling expansion method. However, uniform internal pressure was assumed during the expansion step. The geometrical model used was a circular infinite plate in plane stress having the innermost layer functioning as a tube thus ignoring the initial clearance between the tube and tubesheet. A maximum value of expansion pressure 1.15 times the tubesheet yield strength was found to exist beyond which it only produced thickening of the tubesheet. Nadai proposed a graphical method by which the residual contact

pressure can be evaluated: The best holding strength is obtained when the expanded joint was given a light to medium amount of rolling, and the axial and peripheral bending stresses at the end of the expanded zone of the tube have a minor effect on the strength of the expanded joint (Note that recent investigation show that these stresses seriously affect the tube-to-tubesheet integrity).

Goodier and Schoessow (1943) used plane stress single tube model having an infinite circular plate representing the tubesheet for the study of the residual contact pressure between the tube and tubesheet. Some cases of plane strain were also investigated with somewhat similar results. All calculations were carried out at a limiting value of the expansion pressure which of 1.15 time the tubesheet yield strength. The residual tangential and radial stresses in the expanded part of the tube as well as the residual contact pressure have been graphically evaluated. For various ratios of the tube-to-tubesheet yield strengths and for selected values of the expansion pressure, the optimum expansion pressure was determined by plotting the plastic limit curve as a function of the radius at any point throughout the tube wall thickness. The linear elastic unloading of the tube indicates that the maximum residual stress in the expanded zone is exceeding the material elastic limit. This was an indicator of the importance of including the reverse yielding correction during the unloading step. The study suggests that the hard plate-soft tube combination is much better than that of the reverse combination.

Sachs (1947) proposed a simplified theoretical evaluation of the conditions for a

maximum tightness of a tube joint. His results were slightly different from those of Goodier and Schoessow (1943). The author proposed a maximum expansion pressure of 1.1 time the tube yield strength instead as compared to 1.15. The tubesheet was again treated as an infinite plate composed of an inner plastic and an outer elastic layers. A closed form equation for the residual contact pressure was given as a function of both the tube dimensions and the yield strength. The author proposed that the tube must have a yield strength approximately twice that of tubesheet in order to achieve the maximum residual contact pressure. Yet, no other results supporting Sachs' conclusion can be found in the literature. Recent investigations have even show some problems are encountered when expanding titanium tubes which have twice yield strength of the Muntz tubesheet (Singh and Soler (1984)).

Krips and Podhorsky (1976) presented a theoretical analysis of hydraulic expansion technique based on plane stress conditions aiming to obtain a closed form solution of the residual contact pressure. They assumed without verification that the effect of the moduli of elasticity of tube and tubesheet was negligible. (Note that this factor cannot be neglected, since the level of the residual contact pressure relies on the linear unloading rate of both the tube and tubesheet).

The theory of the hydraulic expansion developed by Goodier and Schoessow (1943) has been extended by Yokell (1982) to provide the optimum groove configuration that must be used with hydraulic expansion. An optimum expansion pressure (1.15 S_{yt}) is again

recommended for expanding the tubes inside grooved holes. Field experience indicates some improvement in joint strength when the expansion pressure is increased beyond that limit for ungrooved joints. For grooved holes, no further enhancement occurs once the arciform shape of tube wall bulge touches the bottom of the groove. Examination of sections through grooved hole joints made by rolling and hydroexpanding, discloses that the rolling process causes the metal extrusion whereas hydroexpanding bulges the tube in a parabolic shape against the groove. The optimum recommended groove width was wider than that recommended by the TEMA standards. Hydroexpansion was shown to be a successful new technology.

Kasraie et al (1983) followed Nadai's (1943) analysis to obtain the residual contact pressure between the tube and tubesheet as a function of the material and dimensional parameters. The tubesheet was simulated by an infinite circular plate having one central hole. As was previously assumed by Podhorsky and Krips, the effect of the modulus of elasticity of both the tube and tubesheet was neglected. The equation was not compared to previous results or to the finite element results developed in the article.

Soler et al (1984) and Weinstock et al (1985) developed a two-dimensional theoretical model of tube-to-tubesheet expanded joint to assess the effect of strain hardening and temperature dependent material properties on the residual contact pressure between the tube and tubesheet. An incremental approach was used to simulate a mechanical expansion of tube

into the tubesheet and a single cycle of thermal loading. The geometry of the joint was idealized by a set of concentric membrane elements in two-dimensional plane stress, with the innermost one being the tube. The equilibrium and compatibility conditions were satisfied between the concentric adjacent elements. The main purpose of their formulation was to determine the residual contact pressure directly after the rolling expansion and temperature cycle. The effect of various dimensional and material parameters and thermal cycles was investigated. The result of a numerical simulation was presented which showed the importance of the above mentioned parameters.

Aldred (1984) discussed some recently available manufacturing techniques to fabricate the joint. Based on the author's practical experience, the major problems inherent in the rolling process are work hardening of tube material, alternation of tube grain structure, tube end rotating fatigue, limitation of expansion length and degree of tube extrusion and wall thinning. These problems cause tubesheet damage and tube bowing due to over rolling causing the life of the heat exchanger to be greatly reduced due to stresses and crevice corrosion. Hydraulic expansion process subjects the tube material to a single cycle of radial expansion under controlled and measurable pressure, so that as shown by practical experiences, the resulting joints are less susceptible to stress corrosion cracking than roller expanded joints. The theories of Goodier and Schoessow (1943), Sachs (1947) and Krips and Podhorsky (1976) were discussed and shown to have limitations because the effects of varying the tube and tubesheet material properties and the effect of grooved tubesheet were

not included. The author recommended to use a grooved hole with optimum groove width, as given by Yoshitomi (1979):

$$W = K\left(\frac{3(1-\nu^2)}{R^2t^2}\right)^{-0.25}$$

where W = optimum groove width

K = dimensionless constant between 1.5 and 3.0

ν = Poisson's ratio

R= mean tube radius

t = tube wall thickness

Although it could increase the joint strength, grooved holes make the job of removing the tube for repair much more difficult. Also, the advantage of grooved joints cannot be generalized as shown experimentally by Gaffoglio (1981).

Jawad et al (1987) provided a theoretical model for residual contact pressure calculation. It assumes that the tube and the tubesheet have the same material. The results were compared with experimental data obtained by testing titanium and carbon steel tubes expanded into a carbon steel tubesheet. Since, the mechanical properties of the titanium and the carbon steel are different, average material data values were considered for the theoretical model. A poor correlation was observed between the theoretically calculated and

experimentally measured joint strength in part due to the assumed value of the coefficient of friction of 0.75. Also, as will be indicated later in this thesis, the initial contact pressure set by the expansion process changes slightly when pull-out force is applied to the tube.

By using the thick wall cylinder shrink-fit analogy, Yokell (1987) examined the interference required for maximum strength and how it varies with tube and tubesheet material and geometrical properties. With the assumption that the tube must yield before it begins to slip, the author developed a closed form equation for the level of interference required for maximum axial joint strength for different dimensional and material parameters. This approach is not compatible with what really happens in the case of tube expanding. In shrink-fitting the tube requires a sleeve with a smaller inside diameter than the tube outside diameter while in tube expanding, the sleeve with a larger inside diameter than the tube outside diameter is used.

Updike et al (1988) developed a theoretical model of a rolled tube-to-tubesheet joint with the objective of determining the residual stresses in the tube transition zone. The tubesheet was treated as an annular flat plate surrounding a single tube. While a purely analytical solution was presented to calculate the unloading elastic behaviour of the rolled zone, the calculation during the loading step was carried out with PC computer code " Kshel-TZ" developed by Updike and Kalnins (1991) and designed to solve elasto/plastic problems of axisymmetric shell elements under axisymmetric loading. The model was based on the

assumption that the loading of the roller is modelled by a uniform internal pressure. The result from the code solution was saved in a data base to be interpolated with the elastic solution during unloading in order to evaluate the residual stresses. A tensile residual stress of 90% of the yield strength or higher is shown to occur in some cases and is always located on the inner surface of the tube.

A method previously developed by Updike et al (1988) was used by the same authors in (1989) to calculate the residual stresses in the transition zone for several practical tube-tubesheet size and material combination. The apparent wall reduction was adopted as the expansion parameter. Based on parametric study, their major finding was that, in most cases, the maximum residual axial stress at the inner surface of the tube transition zone of investigated tubes lies in the range of 80% to 95% of the yield stress. Values above the upper limit were obtained in the case of a very loosely fitting tube in which the residual stress was found to be greater than the tube yield strength.

In order to evaluate the residual contact pressure in the rolled tube-to-tubesheet joint, Kalnins et al (1989) followed up the analysis of their earlier publication (1988). The inside diameter of the tube after rolling -i.e. apparent wall reduction - was chosen as a measure of the expansion. As in Updike et al (1988) and (1989), a PC program, Kshel-PL, was used to calculate the interference contact pressure during loading and the residual contact pressure was graphically expressed as a function of the degree of expansion. They recommend to roll

condenser tubes up to 5% tube wall reduction but without apparent confirmation by the model which indicates that the optimum wall reduction is 9% for the case of loosely fitting tubes. They also found that the contact pressure roughly increases with the tubesheet yield stress.

Updike et al (1990) and (1992) focused on evaluating the residual stresses in the vicinity of the grooves of grooved tube-to-tubesheet joints. The sleeve effective outer radius was chosen to satisfy a boundary condition of zero radial stress. The square grooves in the tubesheet were modelled by representing the radial clearance as step functions with step equals to the groove depth. For linear kinematic hardening and zero axial stress assumptions, the computer code, Kshel-TZ previously developed by the authors (1988), was used. The results show that the maximum tensile residual stress occurs at the inside surface of the tube. The results also suggest the use of a higher hydraulic expansion pressure for grooved joints than that for non-grooved joints which introduces higher residual stresses in the tube transition zone.

Yokell (1992) discussed some practical aspects of expanded and welded-and-expanded tube-to-tubesheet joints. The elastic-plastic theory which was developed by Goodier and Schoessow (1943) was reviewed in detail. The tube was expanded into a hole in an infinitely large plate. For the limiting value of the expansion pressure (P_e/S_{yt}=1.15), the optimum recommended tube diametral ratio that provides maximum residual contact pressure

was 1.32. Also, the maximum value of the tube diametral ratio was limited to 2.719. Following a detailed practical comparison between hydraulically expanded, mechanically rolled and welded-and-expanded tube-to-tubesheet joints, the author recommended the welded-and-expanded joint to add more sealing strength but this requires that the tube, tubesheet and weld filler metal have a very close thermal coefficient of expansion and the welds must be free of cracks, inclusions and porosity. A full-strength and full-depth expansion was highly recommended even in the presence of welding for better joint behaviour under working conditions. No clear recommendation was given as to whether to expand first or weld first.

Kohlpaintner (1995) used the analytical theory developed by Nadai (1943) in order to provide an elastic-plastic computation of the residual contact pressure in a single-tube model. A closed form equation used to calculate the residual contact pressure was developed. The analysis concentrated on the effect of the equivalent sleeve diameter on the residual contact pressure and the determination of effective value of the equivalent sleeve diameter. The deformation behaviour of a finite perforated plate with 19 holes was analysed by means of special Airy stress functions (Hulbert et al, 1965). A system of 162 linear equations were solved in order to calculate the displacements of the tubesheet inner surface of the holes as a function of the tubesheet ligament efficiency. Disks with ligament efficiency from 0.11 to 0.65 were investigated to confirm the dependency of the equivalent sleeve diameter on the ligament efficiency only. This agrees to some extent with a previous statistical analysis (Ma,

1992) in which a superior correlation coefficient between the hole pitch and the equivalent sleeve diameter was found. The equation used to calculate the equivalent sleeve diameter was based on -and limited to- the elastic deformation of the tubesheet.

Comments and concluding notes:

Because of the complexity of the deformation process encountered in tube-to-tubesheet joints, all theoretical efforts have been directed towards the 2-D plane stress or plane strain models. These two models give an average value of residual contact pressure without addressing the problem of the residual stresses in the tube transition zone. None of the analytical solutions accounted for contact forces generated by the rolling technique so that the analytical models were similar to uniform hydraulic pressure expanding. Most authors considered the tubesheet as an infinite plate and in consequences they provided a maximum value of the expansion pressure of 1.15 time the yield strength of the tube material which is not adequate for tubesheet with small ligaments. Few of the solutions were verified experimentally or numerically.

2.3 WORKING CONDITIONS OF EXPANDED JOINT

Haslinger and Hewitt (1983) extended their previous experimental work, introduced in the experiment section, to determine the leak tight performances of tube to tubesheet joints

under cyclic loading conditions which exceed the allowable load values recommended by the HEI and ASME codes. For this purpose three test specimens were fabricated for different joint types. A 1.13" thick tubesheet was designed to incorporate 18 test tubes with 15.5" length. A special load cycle machine was constructed for applying simultaneously controlled axial load and tubesheet bending moments. Due to physical limitations, the 18 tubes were tested in three phases in which 6 tubes were loaded synchronously. Following the load cycle program, the tubes were exposed to a minimum of 10^7 vibration cycles while applying a static bending moment to the tubesheet in order to simulate maximum expected tube vibration responses due to flow-induced excitations. Throughout the cyclic loading and vibration tests, the tube was periodically Helium leak tested. Finally the tubes were subjected to the pull-out tests. Haslinger and Fisher (1985) later published the results of this experimental program. It appeared that in the case of the titanium joints with plain tubesheet holes, the average pull out strength decreased by as much as 15% as a result of cycling. Also, of all the 182 tubes tested, only four joints exhibited leakage failure. It was expected that leakage would become progressively worse by increasing the load or vibration cycles. However, in most cases leakage rate decreased towards the end of cycling test. On the other hand, an improvement in mechanical strength as a result of cyclic loading was not observed. Vibration testing of some specimens resulted in early fatigue failure of the tubes. A through wall cracks occurred at the transition region between the expanded and unexpanded parts of the tubes. Correlating the joint axial strength and the leakage tightness with the apparent wall reduction was not produced by these experiments.

Middlebrooks et al (1991) analysed the thermal cycle corresponding to the work previously discussed in the Finite Element Section. Temperature cycles up to 1100°F were evaluated using the incremental cylindrical layered model by Soler et al (1984). Neglecting the creep effect, there was no loss in the residual contact pressure after thermal cycle for either Alloy 600 or Alloy 690. Using constitutive equation for the tube material while creep in the tubesheet has been neglected, the creep relaxation effects on residual contact pressure was found to be insignificant up to 900°F.

Flesch et al (1993) presented an extensive study to evaluate the operating stresses in the tube transition zone. In almost all cases, cracks initiated in the transition zone were at the tube outer surface and in the longitudinal direction. Circumferential cracks were generally located on inner surface in the transition zone and were always combined with longitudinal cracks. By adding the residual stresses to the operating stresses a better evaluation for the total stresses in the tubes were obtained: this explains why crack location and direction may vary according to the tube location.

CHAPTER 3

PARAMETRIC STUDY OF TUBE-TO-TUBESHEET JOINT

3.1 INTRODUCTION

Using the finite element method and/or some analytical solutions, a number of researchers have investigated the tube-to-tubesheet joints with special emphasis on the level of the contact pressure and the magnitude of the tensile residual stresses. The axisymmetric and/or plane stress finite element models have often been considered to simulate the nonlinear behaviour of the tube-to-tubesheet joint expansion. Sources of nonlinearities are: material non linearity as a result of the elastic-plastic behaviour of the tube and tubesheet materials, boundary condition non linearity due to the contact interaction between the tube outer surface and the hole inner bore, and finally geometrical nonlinearity due to the large displacement arised during the expansion process.

The elasto-plastic behaviour of a variety of tube and tubesheet materials can be idealized by a linear strain hardening or elastic perfectly plastic behaviour curve as shown in Figure 3.1. Tthe primary objective of this chapter is to show the effect of the strain hardening parameter of both the tube and tubesheet materials on the level of residual contact

pressure and residual stresses in the tube-to-tubesheet joint.

In the first section of this chapter, a comparison between different types of axisymmetric elements will be presented. Once the type of element is chosen, a comparison between the 3-D and axisymmetric solutions will be performed in order to confirm the validity of the axisymmetric finite element solution. Finally, a parametric analysis will be performed using the axisymmetric approach. The results will be presented in a convenient way that demonstrates clearly the influence of each parameter involved.

The parameters considered in the present study are :

1. Tube thickness ratio (t/d)
2. Initial clearance ratio (c/d)
3. Tubesheet equivalent diameter ratio (D_e/d)
4. Yield strength ratio (S_{ys}/S_{yt})
5. Modulus of elasticity ratio (E_s/E_t)
6. Tube tangent modulus ratio (E_{tt}/E_t)
7. Tubesheet tangent modulus ratio (E_{st}/E_s)

The most important design parameters will be identified for further investigation in order to propose a more general design equation in the analytical model that will be presented in the next chapter.

3.2 TYPE OF ELEMENT TO BE USED IN THE AXISYMMETRIC FEM

Figure 3.2 shows the equivalent single-tube axisymmetric model using 2-D axisymmetric 8-node quadrilateral isoparametric elements. Interference elements are used to simulate the initial clearance between the tube and the tubesheet as well as the contact state, when it occurs. The entire model consists of 840 nodes and 292 elements. The frictional interaction between the tube and the tubesheet is accounted for by using the Coulomb's friction law with a coefficient of friction $f = 0.35$. The radial, longitudinal and circumferential stresses (S_r, S_z and S_θ) are presented in the global coordinate system (r-z-θ). In order to provide stability to the numerical solutions, the front ends of the tube and the tubesheet at the tubesheet primary side are restrained in the axial direction. This boundary condition has no effect on the stresses in the transition zone since it is far enough from the tubesheet secondary side. In order to avoid the interaction between the constrained boundary and the tubesheet secondary side, a tubesheet thickness of about 25 mm was found satisfactory for the tube dimensions used throughout the present investigation. A uniform internal pressure is applied over the portion of the tube that lies within the tubesheet, as shown in Figure 3.2, and as specified by TEMA (1988). The pressure is applied incrementally up to its maximum value and then fully released.

In order to generalize the solution, the results will be presented in a non-dimensional form. In this analysis, the geometric parameters which are tube wall thickness (t), initial radial

clearance (c) and tubesheet equivalent diameter (D_e) will be normalized with respect to the tube outer diameter (d). The tubesheet equivalent outer diameter will be taken in the range specified by Chaaban et al (1992) and by Kholpanetar (1995). It has a stress-free boundary and depends mainly on the hole pitch. In the axisymmetric model, additional dimensions must be specified such as the tubesheet thickness (h) which has been proved by Ma (1992) to have no effect on either the residual contact pressure or residual stresses. However, as will be shown in Chapter 6, the tubesheet thickness has almost a linear effect on the joint axial strength. Unless otherwise specified, the tubesheet thickness will be set at 25 mm.

The resulting residual contact pressure and residual stresses depend upon an additional important parameter that describes the degree of expansion. For hydraulically expanded tube-to-tubesheet joint, this parameter is the level of the expansion pressure used (P_e) which will be normalized to the yield strength of the tube material. For the purpose of the parametric study presented in this chapter, the range of the expansion pressure (P_e/S_{yt}) has been selected to be between 0.7 and 1.2 (see Chapter 4).

Since we are interested in evaluating the axial and hoop residual stresses in the transition zone of the tube, different axisymmetric solid elements may be chosen. Four different types of 8-noded elements were tested, namely: 8-node quadrilateral full integration (AXI8), 8-node quadrilateral reduced integration (AXI8R), 8-node quadrilateral full integration hybrid (AXI8H) and 8-node quadrilateral reduced integration hybrid elements

(AXI8RH). Some of the results obtained on the joint expansion of a typical case are presented in Figures 3.3 to 3.6. Since the internal face of the tube is a free surface after expansion, the residual radial stress must be theoretically equal to zero. However, based on Figure 3.3, some element types do not conform with this requirement, particularly element AXI8. Also, the same behaviour for this element is observed on the outer surface of the tube where a tensile residual radial stress in the order of 60% of the tube yield strength is observed in Figure 3.4.

Figures 3.5 and 3.6 show the residual axial and hoop stress distributions at the inner surface of the tube along its longitudinal direction. At the beginning of the tube transition zone, again element AXI8 seems to perform poorly when compared to the others. The residual hoop stresses are less affected by the type of element specially on the tube outer surface. However, the residual hoop stresses on the inner surface are affected at the beginning of the tube transition zone only. According to this comparison, it has been decided to exclude the element AXI8.

Another point that must be considered in the choice of the type of element, is the CPU (Central Processing Unit) time; as shown in Figure 3.7, element AXI8R seems to be the most economical one as compared to the hybrid types for the same accuracy; element AXI8R has thus been adopted in all axisymmetric analysis. The results of a typical case (Wang et al, 1993) using Kshel-TZ code developed by Kalnins et al (1988), for axial and hoop residual stress distributions compare very well with those obtained using the AXI8R element, Figures

3.8 and 3.9. Finally, a proper axisymmetric finite element model requires an equivalent sleeve diameter that correctly represents the stiffness of the surrounding tubesheet ligaments. This point was discussed in Chapter 2 and will be investigated further below.

3.3 AXISYMMETRIC VERSUS 3-D FEM

The 3-D geometry of the tube-to-tubesheet joint has often been simplified by a 2-D plane stress or axisymmetric model (Chaaban et al, 1992; and Kohlpaintner, 1995). The latter model has the advantage of including the transition zone along the portion of the tube that just follows its expanded zone and, consequently, enables us to calculate the residual stresses in that region. Soler et al (1988) and Chaaban et al (1992) proposed different techniques to calculate the equivalent annular sleeve diameter by taking into account the effect of adjacent holes and nonsymmetric boundaries on the expansion of a central tube. The use of a 3-D finite element model is required to validate the choice of the equivalent annular sleeve diameter as a function of the various parameters involved.

The equivalent sleeve diameter obtained may be based either on the residual contact pressure level (Soler et al, 1988; and Chaaban et al, 1992) or on the radial displacement (Kohlpaintner, 1995) of the inner surface of the tubesheet idealized by plane stress model. Consequently, those authors compared the results of axisymmetric model against those of plane stress model on the basis of the residual contact pressure only. In the present research

work, it is decided to validate the results using axisymmetric modelling to those using a 3-D modelling. In the present investigation, the results of 3-D model are compared with those obtained using a 2-D axisymmetric model that is constructed with a particular value of the equivalent sleeve diameter using the following parameters:

1- Axial stress on the inner surface of the tube transition zone at a distance Z/d =1.2.

2- Interference pressure between the tube and tubesheet.

3- Circumferential strain at the inner surface of the tube at a distance Z/d =0.5.

4- Circumferential strain at the inner surface of the central hole of the tubesheet at a distance Z/d =0.5.

5- CPU time on RISK 6000/IBM computer.

In order to determine the effect of the tubesheet dimension on the above mentioned parameters, a central hole in a finite circular tubesheet is considered. The results of Kohlpaintner (1995) indicated that a tubesheet with 37 holes can be considered as un infinite tubesheet and the displacement fields calculated on a tubesheet with 19 holes are fairly equal to those of the tubesheet with 37 holes. In this analysis, a tubesheet with only 19 holes is thus considered. Only the triangular tube pattern is considered as shown in Figure 3.10. A sector of 30° is thus sufficient for the FEM model. Figure 3.11 shows the 3-D finite element model

that simulates the 19-hole case. The outer diameter of this model is equal to three times the pitch. The model is constructed with 3-D 20-node reduced integration solid elements, combined with some 3-D 8-node solid elements. Also, 8-node surface contact elements are used between the tube and the tubesheet contact surfaces. The entire 3-D model consists of 4979 nodes and 1317 solid elements. The two sides of the 3-D finite element model are constrained in the normal directions due to periodical symmetry. A uniform internal pressure is applied over the portion of the tube that lies within the tubesheet, as shown in Figure 3.2, and as specified by TEMA (1988). ABAQUS (1992) finite element code was used throughout this investigation.

The three cases of Table 3.1 are considered for the comparison between the 3-D and the 2-D axisymmetric solutions. The equivalent sleeve diameter for the axisymmetric model is calculated by using the empirical equation proposed by Chaaban et al (1992), and the analytical equation given by Kohlpaintner (1995). The values of the equivalent sleeve diameter for the selected cases are given in Table 3.2. Figure 3.12 shows a typical comparison between the equivalent sleeve diameters as a function of the hole pitch. For a thin tubesheet ligament, Chaaban et al (1992) and Kohlpaintner (1995) provided approximately the same level of the equivalent sleeve diameter. However, a difference of more than 25% is observed between the two equivalent sleeve diameters when a thicker tubesheet ligament is considered.

The results of the 3-D FEM are shown in Table 3.3. The axisymmetric analyses were

performed by using an equivalent sleeve diameters as per Kohlpaintner (1995). The comparison of the CPU times indicates as expected a huge difference between the time required to run the 3-D model and that required for the axisymmetric solution. Yet, a good agreement is observed between the results of the 3-D and 2-D models with the exception of the values of ϵ_s in (**CASE-2**). It turns out that during the expansion process of this particular case, a plastic deformation developed on the inner surface of the 3-D tubesheet model. This observation raised a question concerning the agreement between the 3-D and axisymmetric models when the expansion pressure causes a plastic deformation in the tubesheet material. Other cases have been selected for this investigation where the tubesheet yield strength is lower than that of the tube ((**CASE-4**) in Table 3.4).

Table 3.5 shows the numerical results for **CASE-4**. It appears that for this particular case, the axisymmetric model underestimates the radial displacement and consequently the stresses, which are directly related to the displacements, especially during the loading process. However, the interference pressure is found to be almost identical in both solutions. The underestimation of the radial displacement is attributed to the fact that the equivalent sleeve diameter evaluated by either Chaaban et al (1992) or Kohlpaintner (1995), provides a higher stiffness than that of the 3-D tubesheet. Figure 3.13 shows that in the 3-D model, the plastic deformation has propagated through almost half of the tubesheet ligament, whereas in the axisymmetric sleeve, only partial yielding at the inner surface has occurred. This may indicate that an axisymmetric tubesheet having 50% plastic deformation could mean a totally distorted

real tubesheet.

The axial and the hoop residual stresses in the tube transition zone on both the inner and outer surfaces are shown in Figures 3.14 and 3.15 for CASE-3. The residual stresses of the 3-D model are given at (θ=0.0), see Figure. 3.10. Good agreement between the 3-D and 2-D models as shown in Figure 3.14. Also, an acceptable agreement can be observed for CASE-4 (Figures 3.16 and 3.17).

In order to examine whether the tubesheet geometry has any effect on the distribution of the stresses in the transition zone, the 3-D residual axial stress profile on the inner surface of the transition zone is plotted in Fig. 3.18. Also, the residual axial stresses at a distance Z/d=1.2 are plotted in the circumferential direction (Fig. 3.19). Figures 3.19 and 3.20 indicate a constant stress value along the circumferential direction of the 3-D model. Thus it appears that, whether the tubesheet stays elastic or deforms plastically during the expansion process, the stress distribution in the tube transition zone remains fairly axisymmetric.

3.4 FINITE ELEMENT PARAMETRIC ANALYSIS

This section presents a parametric study using the 2-D axisymmetric finite element model shown in Figure 3.2. First, the residual stress profiles on the tube inner and outer surfaces as well as the residual contact pressure are investigated. Dimensional, material, and

manufacturing parameters are considered. The joint characteristics will be presented in terms of the level of expansion pressure. Attention is focused on how the maximum tensile residual stress and the residual contact pressure vary with these parameters and will be presented as a function of the expansion pressure at different levels of the design parameter being investigated. Table 3.6 presents the numerical values of the eight parameters considered in the study. Three levels were applied for each parameter; namely lower, intermediate (reference) and upper values. The cases presented in Table 3.6 are commonly used for many tube-to-tubesheet joints in practical applications.

The procedure of the parametric study consists of varying one parameter at a time and keeping the others at the reference level. In each case, the expansion pressure (P_e/S_{yt}) is varied between 0.7 and 1.2 with an increment of 0.1, which is the practical range being used in the industrial applications. In order to perform a full parametric study within the specified range of the expansion pressure by using the data matrix given in Table 3.6, almost four hundred runs were performed on the Risk station 6000/IBM Computer.

The residual stress profiles and the tube profile for the reference case at the expansion pressure (P_e/S_{yt}=1.0) are presented in Figures 3.21 and 3.22, respectively. The residual stress profiles for the other cases do not vary significantly from those of the reference case. The plots show the distribution of the axial and hoop stresses located on the tube inner and outer surfaces. The residual axial and hoop stresses along the outer surface of tube transition zone

are compressive while those of the inner surface are always tensile. The peak values of the tensile axial and hoop stresses which are always observed at the inner surface of the tube transition zone are approximately $0.95S_{yt}$ and $0.65S_{yt}$ respectively. Each case in the parametric study is characterized by the level of the maximum tensile residual stress and the residual contact pressure. Of course, these values are dependent on the degree of expansion (P_e/S_{yt}) and on the dimensional and material properties which will be extensively investigated below.

Figure 3.23 shows that the maximum tensile residual axial and hoop stresses are slightly affected by the tube wall thickness and the expansion pressure level. However, the effect of the tube wall thickness on the residual contact pressure is noticeable as shown in Figure 3.24. As the expansion pressure increases from its lower to its upper levels, the residual contact pressure seems to increases almost linearly.

The clearance ratio (c/d) is varied between the closest fit (c/d=0.002) and the loosest fit (c/d =0.008) which cover the range of initial clearances specified by TEMA (1988). Figure 3.25 shows the maximum tensile residual axial and hoop stresses against the expansion pressure for the different levels of the initial radial clearance. Not expected is the fact that increasing the initial clearance does not significantly affect the maximum tensile residual stress particularly in the hoop direction. Yet, the statistical analysis performed by Ma (1992) showed a highly positive correlation coefficient reflecting a strong relation between the maximum

tensile residual stresses and the initial clearance. Therefore, it was decided to reexamine in details the relation between these two parameters by considering a wider range of initial radial clearance, see Section 3.5. The second aspect to be considered is the level of the residual contact pressure which is found to be greatly affected by the level of initial radial clearance. Figure 3.26 shows the variation of the residual contact pressure versus the expansion pressure for different levels of initial clearance. As the expansion pressure increases, the residual contact pressure increases in all cases. The increase in the initial radial clearance reduces the level of the residual contact pressure and disturbs its uniform pattern along the tube axis. It is thus surprising that many analytical analyses (Goodier et al, 1943; Nadai, 1943; Saches, 1947; Krips et al, 1976; and Kasarie et al, 1983) excluded the initial clearance parameter when calculating the level of the residual contact pressure for elastic-perfectly plastic joint material.

The last dimensional parameter to be investigated is the equivalent sleeve diameter represented by the ratio (D_e/d). The effect of this dimensional parameter is merely related to the effect of the hole pitch (tubesheet ligament efficiency). Figure 3.27 shows that the maximum tensile residual stresses are almost independent on the sleeve outer diameter and consequently on the tubesheet ligament efficiency. However, its effect is quite significant on the residual contact pressure up to a certain value (D_e/d=4) beyond which the residual contact pressure becomes fully independent, as shown in Figure 3.28. As such, an annular sleeve having a diametral ratio (D_e/d) = 4.5 may be considered as an infinite plate for which the

external diameter has no effect of the joint characteristics.

The second group of design parameters to be investigated are the material parameters. The effect of the tubesheet yield strength ratio (S_{ys}/ S_{yt}) on the characteristics of the expanded joint must be considered only if the tubesheet is plastically deformed during the expansion process. Since in the present cases there are no high plastic deformations in the tubesheet, both the maximum tensile residual stresses and the residual contact pressure become independent of the yield strength ratio (S_{ys}/ S_{yt}) as shown in Figure 3.29. Similar behaviour was also observed when examining the effect of the strain hardening parameter of the tubesheet material represented by the ratio (E_{ts}/ E_s).

By considering the effect of the strain hardening parameter of the tube material, which has been investigated by varying the value of E_{ts}/ E_t, a negligible effect on the maximum tensile residual stresses was found as shown in Figure 3.30. However, it could significantly reduce the residual contact pressure as shown in the Figure 3.31.

Finally, the effect of the modulus of elasticity ratio (E_s/ E_t) is verified. In spite of not having a great effect on the maximum tensile residual stresses, the modulus of elasticity ratio has a very significant influence on the residual contact pressure. As an example, the residual contact pressure for a joint made with material properties having (E_s/ E_t=1.25) and assembled

by an expansion pressure (P_e/ S_{yt}=0.9) is almost equal to zero. This value increases to 8% of the tube yield strength by reducing the modulus of elasticity ratio from 1.25 to 0.8, as shown in Figure 3.32. In fact, reducing (E_e/ E_t) substantially increases the joint residual contact pressure.

The parametric study presented in this chapter has shown that, within the selected range of the expansion pressure level, the maximum tensile residual stresses ratios are not strongly dependent on the design parameters. Nevertheless, some of these parameters could have a significant effect on the level of the residual contact pressure. For convenience, Table 3.7 summarizes the qualitative results of this parametric study and shows the effects and importance of each design parameter involved.

3.5 COMPARISON WITH ELASTIC PERFECTLY PLASTIC MATERIAL BEHAVIOUR

We indicated previously that the effect of the initial clearance (c/d) on the maximum tensile residual stresses seems to contradict Ma's (1992) elastic-perfectly plastic results for which zero initial clearance (c/d=0.0) was considered. This aspect must be further investigated. Unlike Ma's analysis, our parametric study did not involve the case of zero initial clearance. In addition, elastic perfectly plastic material behaviour has often been assumed in

previous analytical theories (Goodier et al, 1943; Nadai, 1943; Saches, 1947; Krips et al, 1976; and Kasarie et al, 1983), and therefore it is worth investigating the effect of ignoring the strain hardening parameter while looking at different levels of initial radial clearance.

First, let us consider the residual contact pressure. For an arbitrary case, Figure 3.33 shows the residual contact pressure versus the expansion pressure for different levels of the tube tangent modulus. The range of expansion pressure is extended beyond the one used in the first parametric study in order to create some plastic deformations in the sleeve wall representing the tubesheet ligament. The residual contact pressure is directly proportional to the expansion pressure up to a certain level for both the elastic perfectly plastic and strain-hardening materials. As would be expected, a joint having a tube made of an elastic perfectly plastic material provides the highest residual contact pressure for the same level of the expansion pressure. Any increase in the strain-hardening modulus significantly reduces the level of the residual contact pressure. The residual contact pressure is plotted against the tangent modulus for various initial radial clearance (Figure 3.34). The residual contact pressure is very sensitive to changing the initial clearance ratio as shown in Figures 3.34 and 3.35. It is shown that, the initial clearance plays a negative role regarding the level of the residual contact pressure obtained when a strain hardening tube material is considered. However, when the elastic perfectly plastic tube material is assumed, a constant horizontal line is resulted between the initial clearance and the level of the residual contact pressure. Neglecting the effect of the initial clearance on the evaluation of the residual contact pressure

when the tube material has zero strain hardening is thus justified. But a proper analysis must take into account the effect of the initial clearance ratio and strain hardening of the tube material, to obtain the level of the residual contact pressure.

In order to establish a better understanding of the effect of the clearance ratio (c/d) on the maximum tensile residual stresses, the range of this parameter has been extended beyond that used in the parametric study presented in the previous section. The results of the maximum tensile residual axial and hoop stresses are plotted in Figure 3.36. As shown in this figure, the tube transition zone has the lowest level of tensile residual stresses at a zero initial radial clearance, an unrealistic case. Any small increase in radial clearance will dramatically increase the tensile residual stresses as shown in Figure 3.36. However, beyond a certain limit, the effect becomes less significant.

Executive summary

A validation of the axisymmetric model has been performed in this chapter. Different types of axisymmetric solid elements have been examined. A good agreement between 3-D and axisymmetric finite element models was obtained when the proper value of the equivalent sleeve diameter was introduced. The axisymmetric model has been used to perform a detailed parametric study to investigate the effect of the design parameters on the residual contact pressure and maximum tensile residual stress. It has been found that most dimensional and

material parameters have a significant effect on the level of residual contact pressure but have less effect on the maximum tensile residual stresses. It has also been observed that the initial radial clearance combined with strain hardening parameter have a great effect on the residual contact pressure. However, with an elastic perfectly plastic material behaviour, the effect of initial clearance on both the residual contact pressure and maximum tensile residual stresses was not significant.

Table 3.1: Design parameters for three different cases to be analysed by 3-D finite element model and 2-D axisymmetric model.

Material				**Dimensions**				**Expansion Pressure**
CASE-1								
Tube: *Stainless Steel*		Tubesheet: *Steel*		Tube	Tubesheet			P_c/S_{yt}
E_t	S_{yt}	E_s	S_{ys}	t/d	c/d	*P*/d	ξ %	
206.69	199.8	206.69	199.8	0.109	0.004	1.5	33.3	0.775
CASE-2								
Tube: *Stainless Steel*		Tubesheet: *Steel*		Tube	Tubesheet			P_c/S_{yt}
E_t	S_{yt}	E_s	S_{ys}	t/d	c/d	*P*/d	ξ %	
206.69	199.8	206.69	199.8	0.109	0.004	2.00	50.0	0.95
CASE-3								
Tube: *90:10 Cu. Ni.*		Tubesheet: *Muntz*		Tube	Tubesheet			P_c/S_{yt}
E_t	S_{yt}	E_s	S_{ys}	t/d	c/d	*P*/d	ξ %	
124	103.34	103.34	137.8	0.095	0.002	2.0	50.0	0.85

Table 3.2: The equivalent sleeve diameter (D_e/d)

Studied Case	CASE-1	CASE-2	CASE-3
Chaaban et al (1992)	2.142	3.0325	3.015
Kohlpaintner (1995)	2.307	4.168	4.168

Table 3.3: Comparison between the results of 3-D and axisymmetric models

Case-1									
Parameter	S_z/S_{yt}		P_f/S_{yt}		$\epsilon_s .10^3$		$\epsilon_t .10^3$		CPU Time Sec
Loading	Max.	Res.	Max.	Res.	Max.	Res.	Max.	Res.	
3-D	1.172	0.567	0.485	0.040	0.836	0.062	14.07	12.63	36932
Axisy.	1.221	0.495	0.483	0.039	0.829	0.063	13.29	12.05	124
Case-2									
Parameter	S_z/S_{yt}		P_f/S_{yt}		$\epsilon_s .10^3$		$\epsilon_t .10^3$		CPU Time Sec
Loading	Max.	Res.	Max.	Res.	Max.	Res.	Max.	Res.	
3-D	1.123	0.652	0.651	0.075	0.957	0.125	14.44	13.09	12711
Axisy.	1.143	0.714	0.664	0.075	0.887	0.124	13.54	12.19	166
Case-3									
Parameter	S_z/S_{yt}		P_f/S_{yt}		$\epsilon_s .10^3$		$\epsilon_t .10^3$		CPU Time Sec
Loading	Max.	Res.	Max.	Res.	Max.	Res.	Max.	Res.	
3-D	1.239	0.663	0.703	0.110	0.977	0.157	7.54	6.31	9488
Axisy.	1.223	0.770	0.694	0.107	0.965	0.155	7.19	5.97	128

Table 3. 4: Design parameters for an additional case (**CASE-4**) where the yield strength of the tubesheet is lower than that of the tube

Material				Dimensions				Expansion Pressure
Tube *70:30 Cu.Nu*		Tubesheet *90:10 Cu.Nu*		Tube	Tubesheet			
E_t	S_{yt}	E_s	S_{ys}	t/d	c/d	*P*/d	ξ %	P_e/S_{yt}
151.57	124.0	124.0	103.35	0.095	0.002	1.5	33.3	1.00

Table 3.5: Comparison between the results of the 3-D and axisymmetric models for **CASE-4**

Parameter	S_z/S_{yt}		P_f/S_{yt}		$\epsilon_s \times 10^3$		$\epsilon_t \times 10^3$	
Loading	**Max.**	**Res.**	**Max.**	**Res.**	**Max.**	**Res.**	**Max.**	**Res.**
3-D	1.2059	0.5284	0.7334	0.1556	2.7652	1.7389	10.395	8.898
Axis.	1.1676	0.6813	0.7517	0.1455	1.7763	0.7921	8.4405	6.998

Table 3.6 : Values of the considered design parameters

Parameter Involved	Lower Case	Reference Case	Upper Case
t/d	0.072	0.109	0.134
c/d	0.002	0.005	0.008
D_c/d	2.000	3.000	4.000
S_{ys}/S_{yt}	0.80	1.20	1.60
E_s/E_t	0.80	1.00	1.25
E_t/S_{yt}	750.0	1000.0	1250.0
E_{tt}/E_t	0.01	0.015	0.02
E_{ts}/E_s	0.01	0.015	0.02

Table 3.7: Effect of design parameters on maximum tensile residual stresses and on residual contact pressure (W= Weak effect; (≤ 10%), SL=Slight effect; (≥10% and ≤25%), and SG=Significant effect; (≥ 25%))

parameter group	parameter	Residual stresses	Contact pressure
		S^*/S_{yt}	P^*/S_{yt}
Expansion pressure	P_c/Syt	SL	SG
Dimensional Parameters	t/d	SL	SG
	c/d	SL	SG
	D_c/d	W	SG
Material Parameters	S_{ys}/S_{yt}	W	W
	E_{ts}/E_s	W	W
	E_t/S_{yt}	W	SL
	E_{ts}/E_t	SL	SG
	E_s/E_t	W	SG

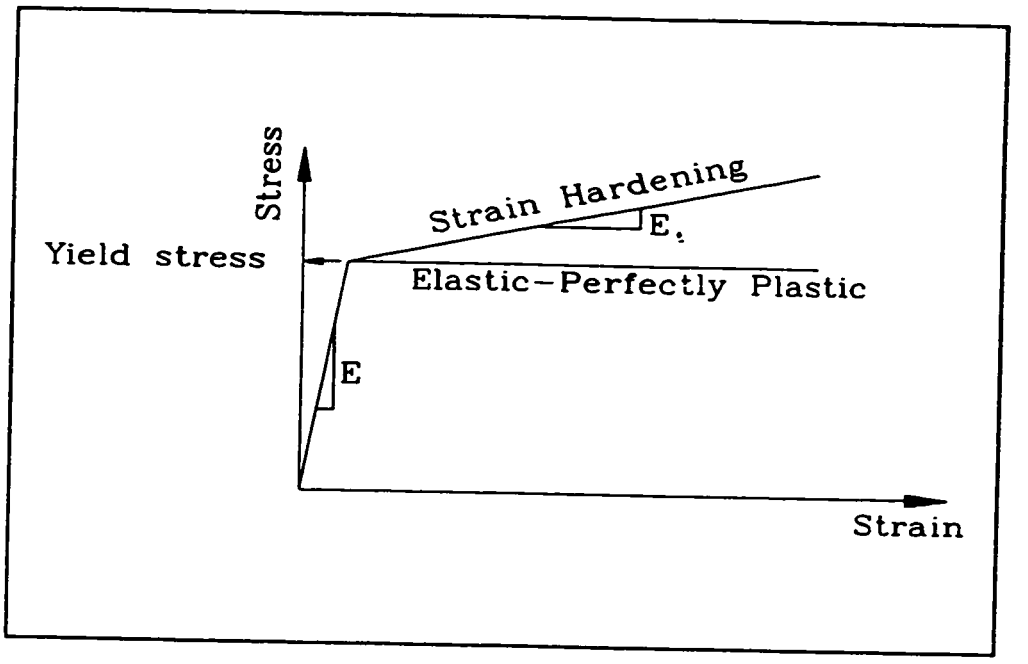


Figure 3.1: Elastic-perfectly plastic and bi-linear elastic-plastic stress strain relation

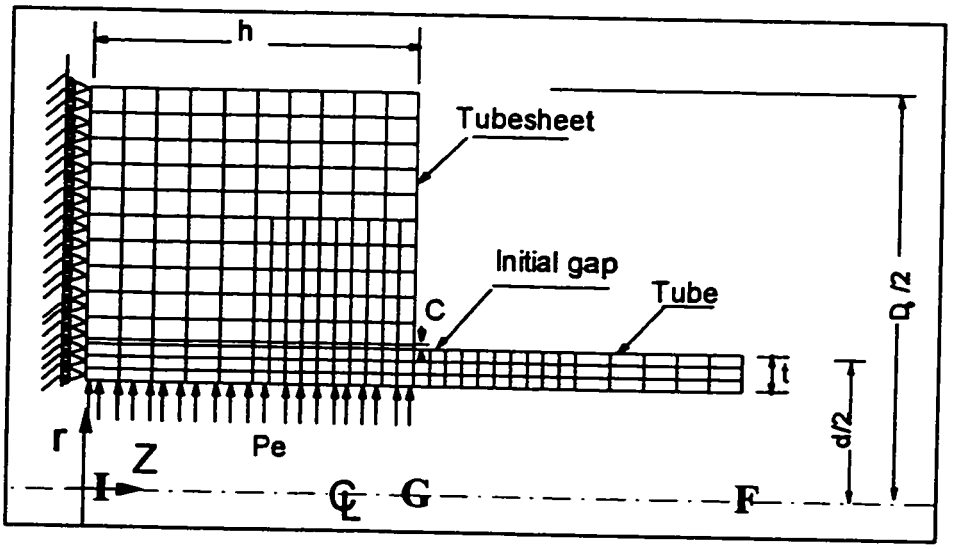


Figure 3.2: Axisymmetric finite element model

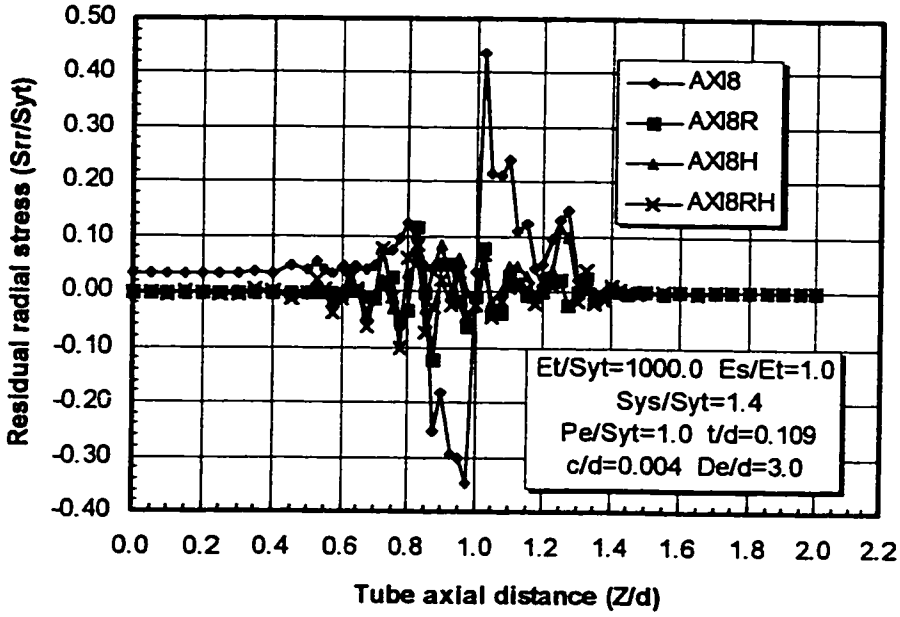


Figure 3.3: Residual radial stress profile on the tube inner surface

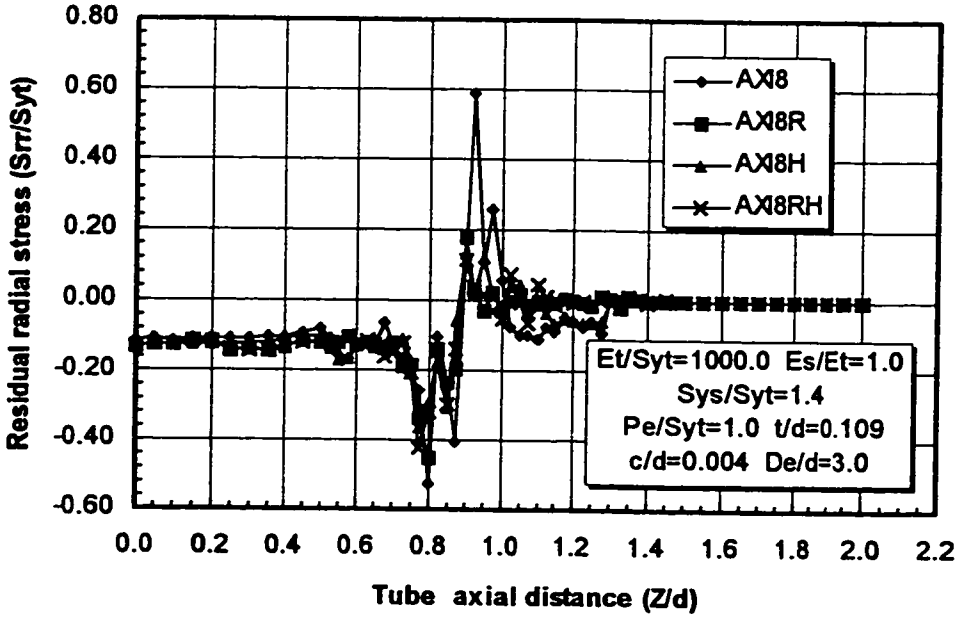


Figure 3.4: Residual radial stress profile on the tube outer surface

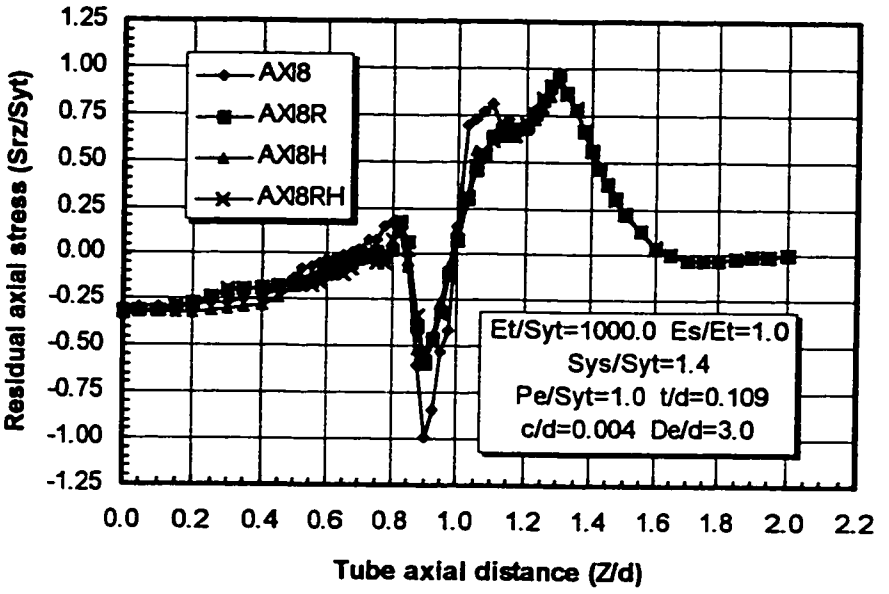


Figure 3.5: Residual axial stress profile as calculated by different axisymmetric element types

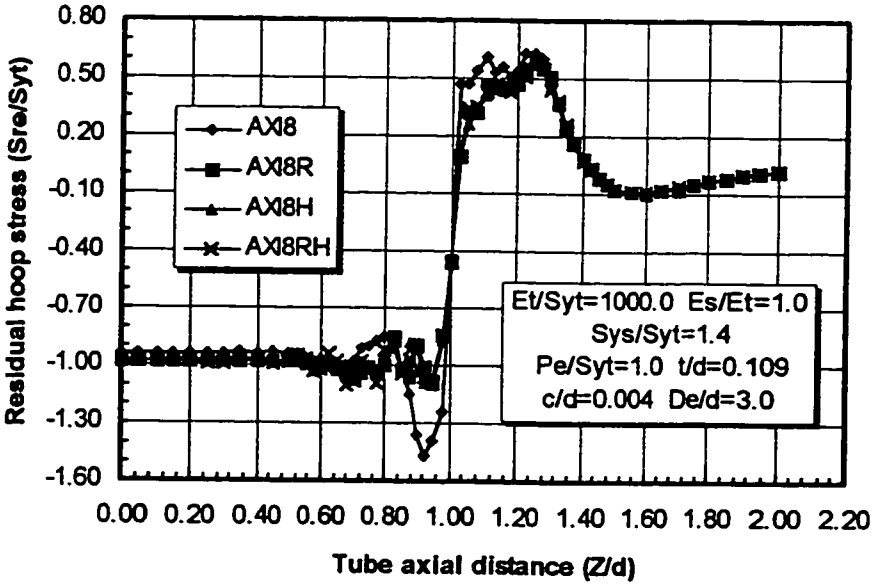


Figure 3.6: Residual hoop stress profile as calculated by different axisymmetric element types

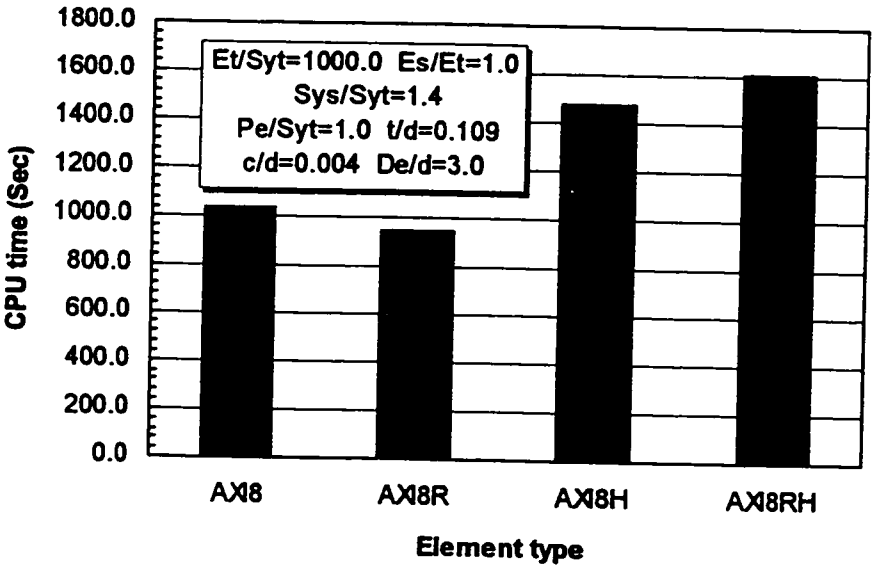


Figure 3.7: CPU time consumed for various element types used

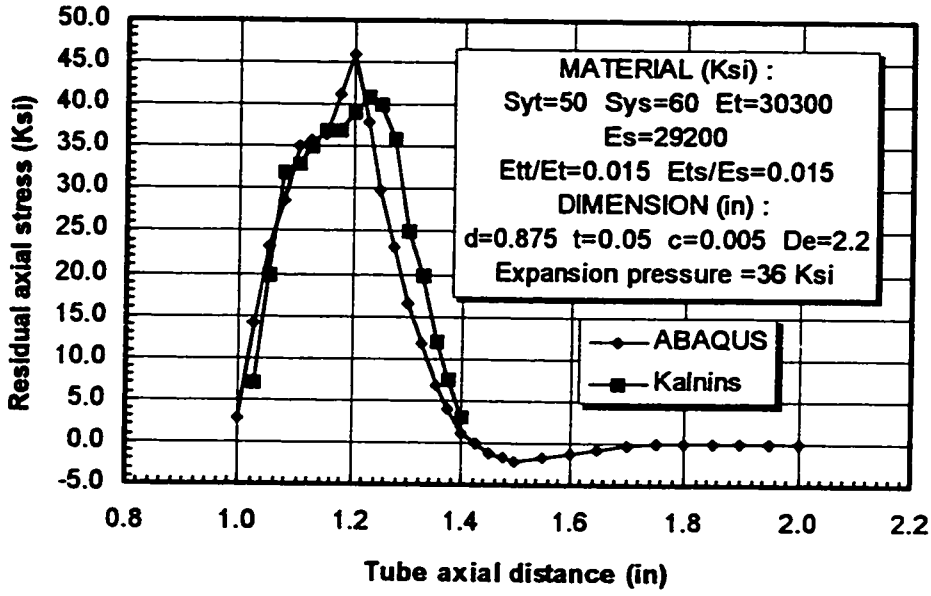


Figure 3.8: Residual axial stress as given by axisymmetric finite element model and as predicted by Kalnins et al (1989)

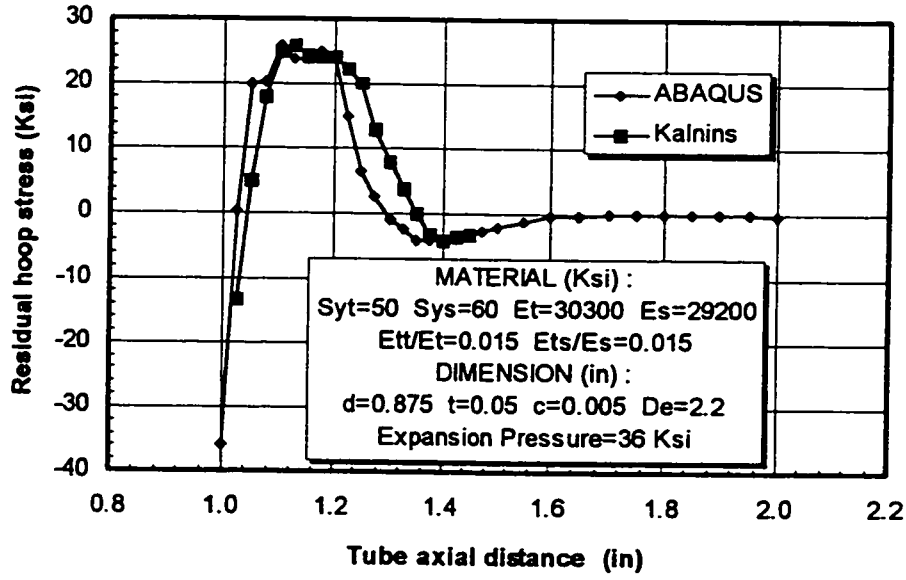


Figure 3.9: Residual hoop stress as given by axisymmetric finite element model and as predicted by Kalnins et al (1989)

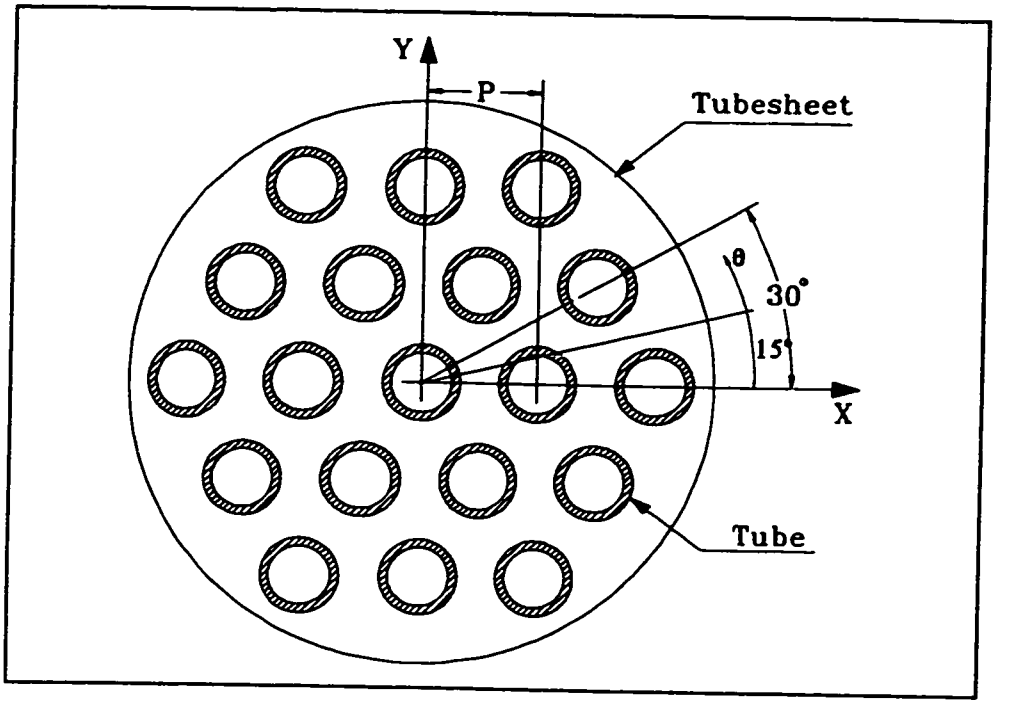


Figure 3.10: Finite circular disk with 19 holes

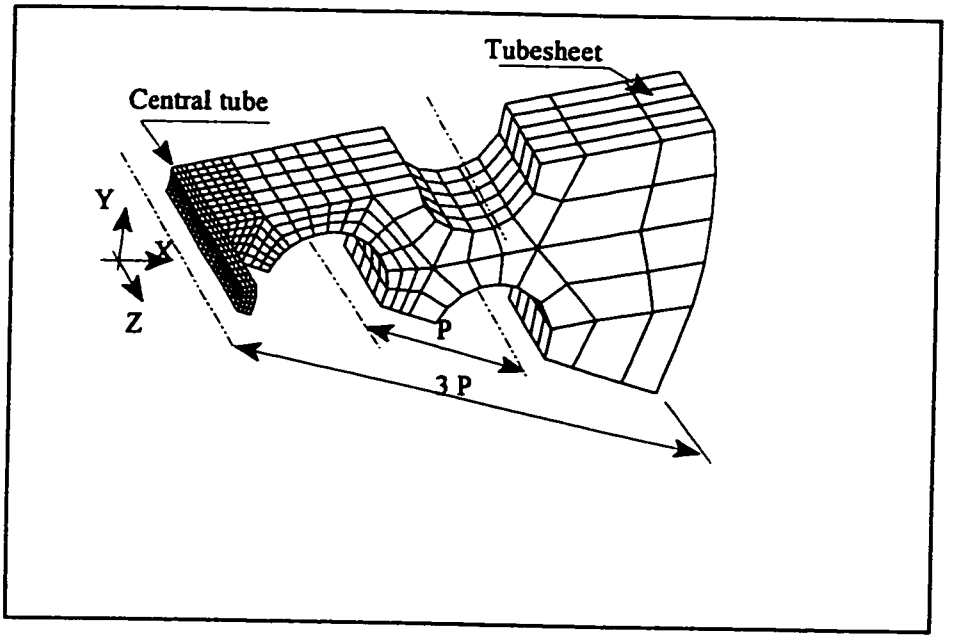


Figure 3.11: 3-D finite element model

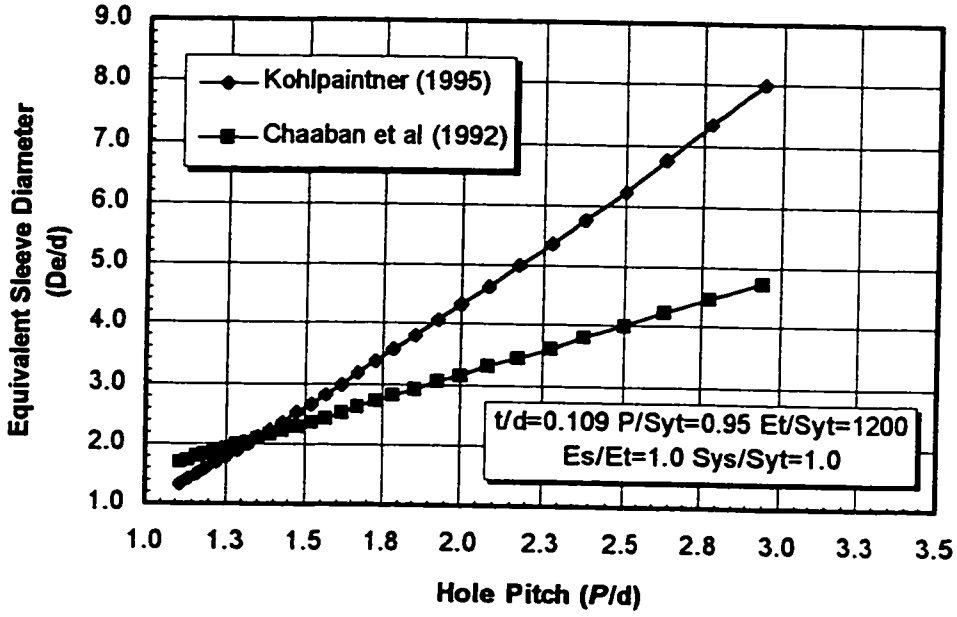


Figure 3.12: Equivalent sleeve diameter versus tube pitch as obtained by Chaaban et al (1992) and by Kohlpaintner (1995)

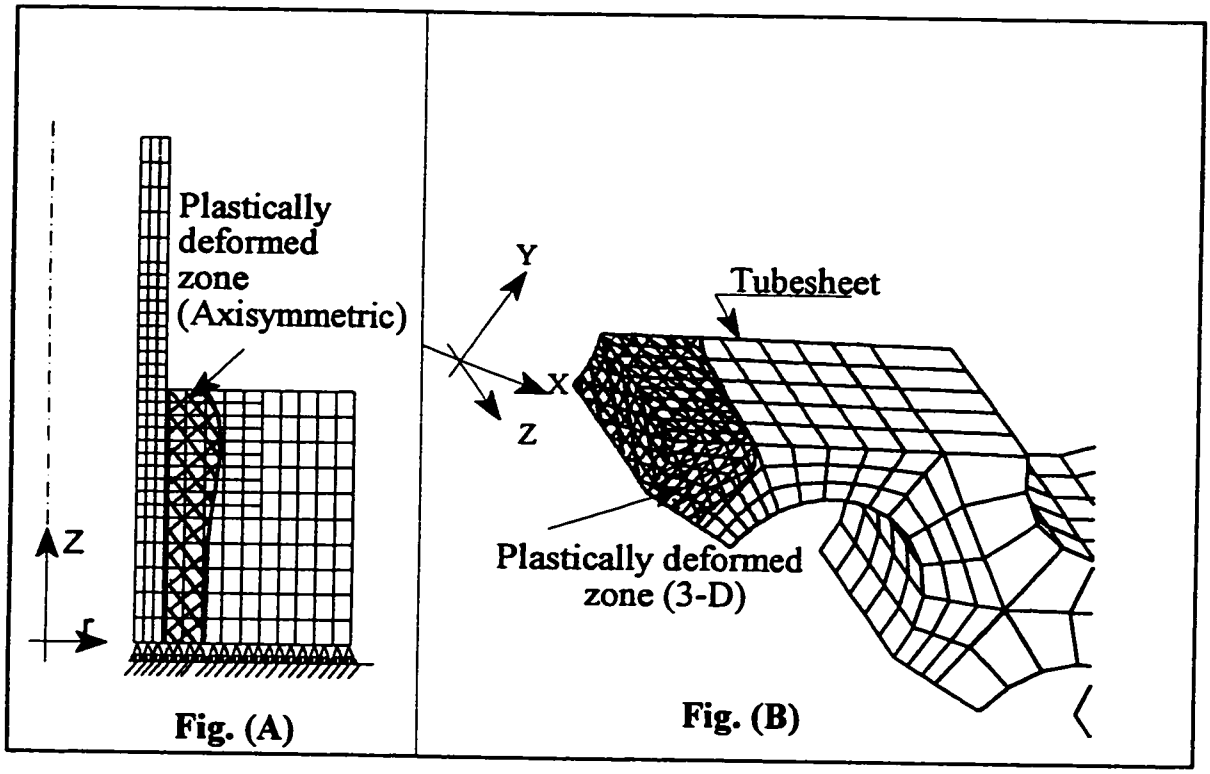


Figure 3.13: Plastic propagation in the real 3-D model of the tubesheet and that created in the equivalent sleeve.

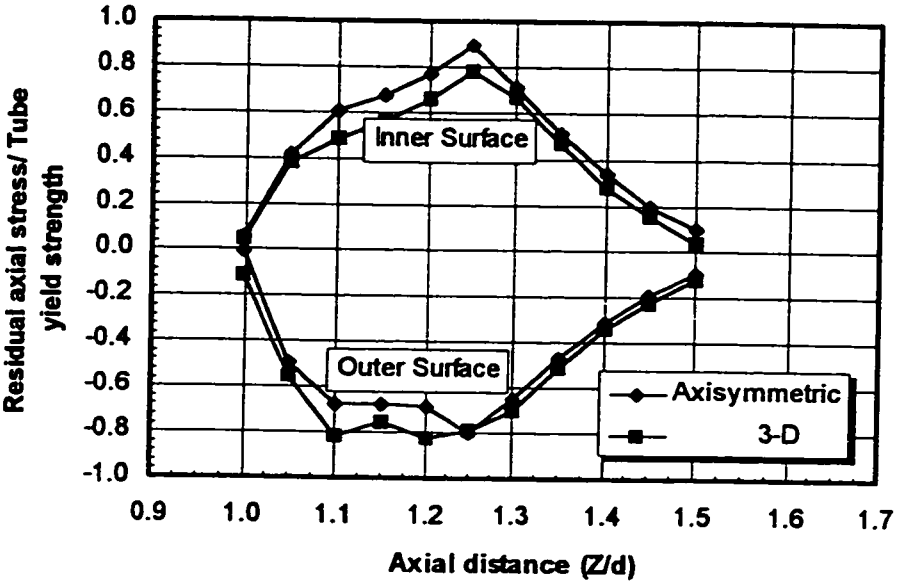


Figure 3.14: Comparison between the residual axial stresses obtained by using 3-D and axisymmetric models (CASE-3)

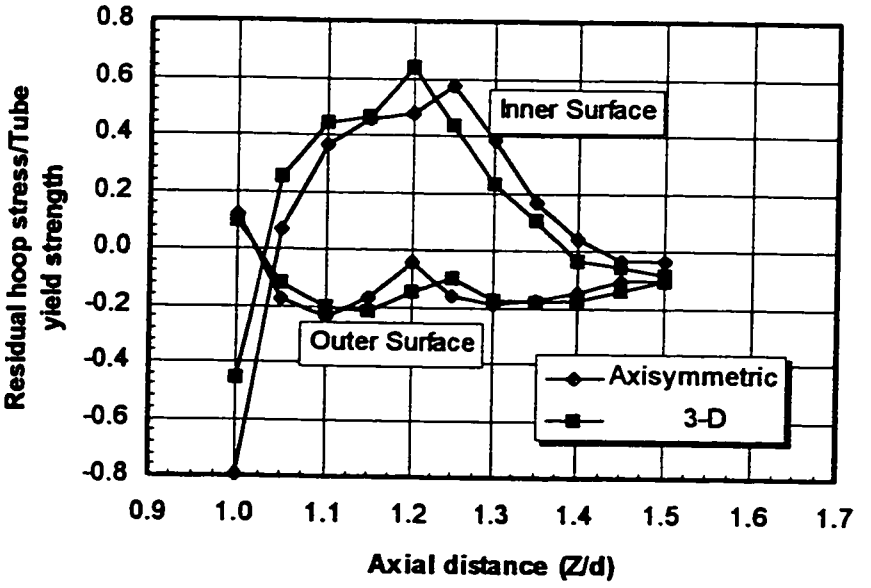


Figure 3.15: Comparison between the residual hoop stresses obtained by using 3-D and axisymmetric models (CASE-3)

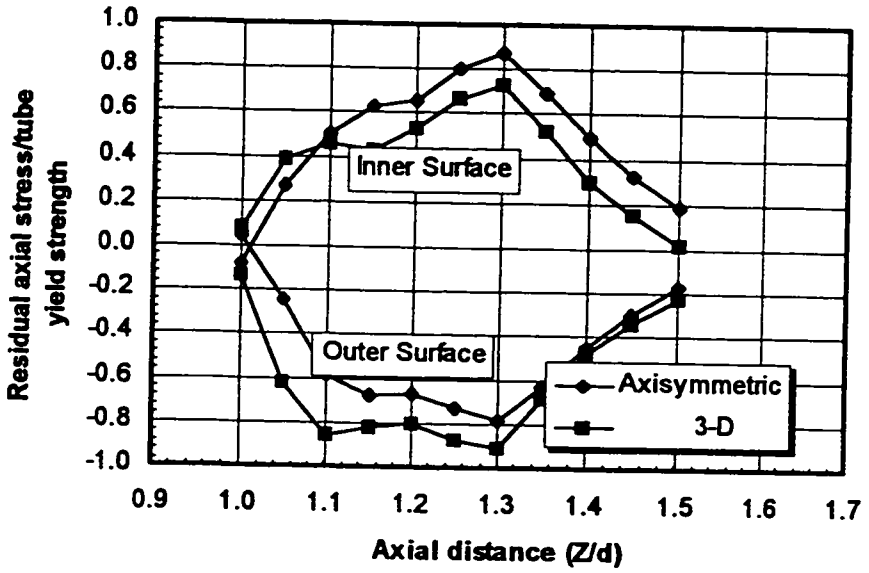


Figure 3.16: Comparison between the residual axial stresses obtained by using 3-D and axisymmetric models (CASE-4)

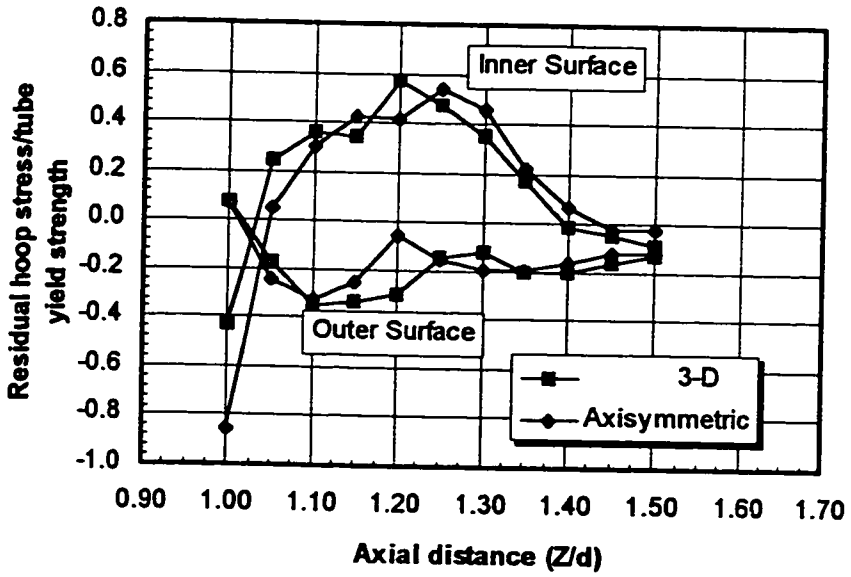


Figure 3.17: Comparison between the residual hoop stresses obtained by using 3-D and axisymmetric models (CASE-4)

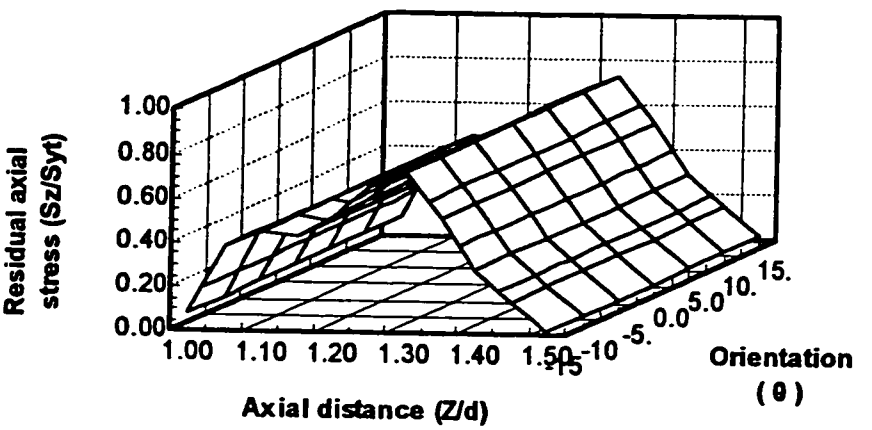


Figure 3.18: 3-D profile of the residual axial stress on the inner surface of the transition zone

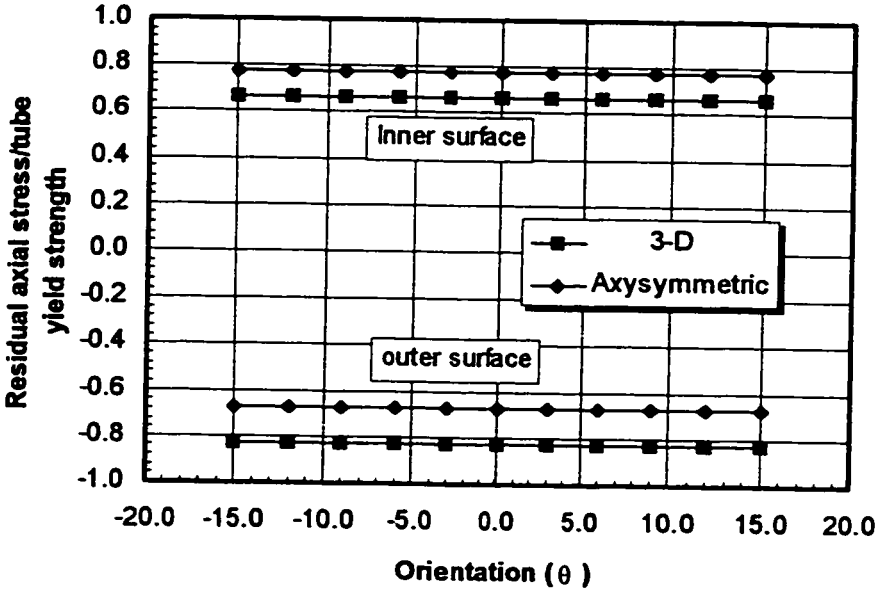


Figure 3.19: Residual axial stress versus orientation angle (θ) (CASE-3); Z/d = 1.2

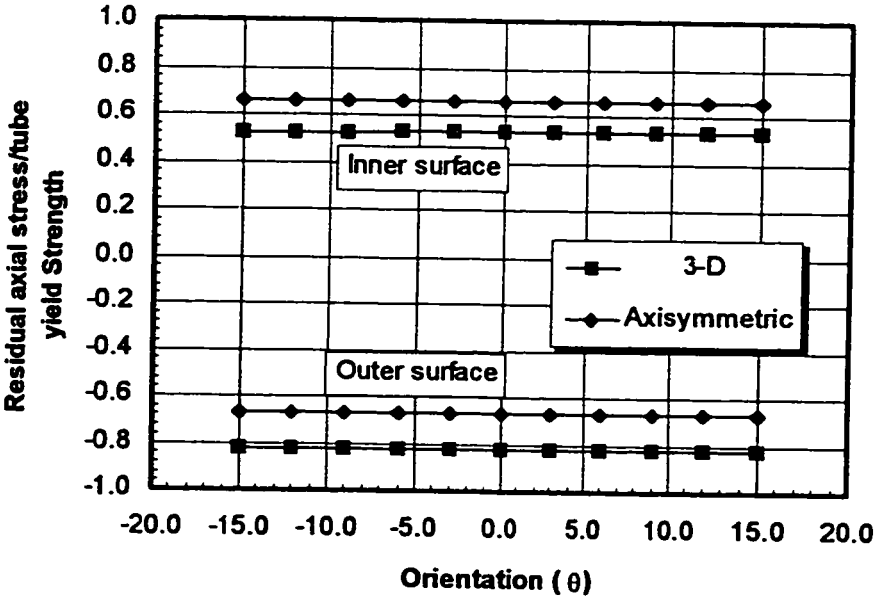


Figure 3.20: Residual axial stress versus orientation angle (θ) (CASE-4); Z/d = 1.2

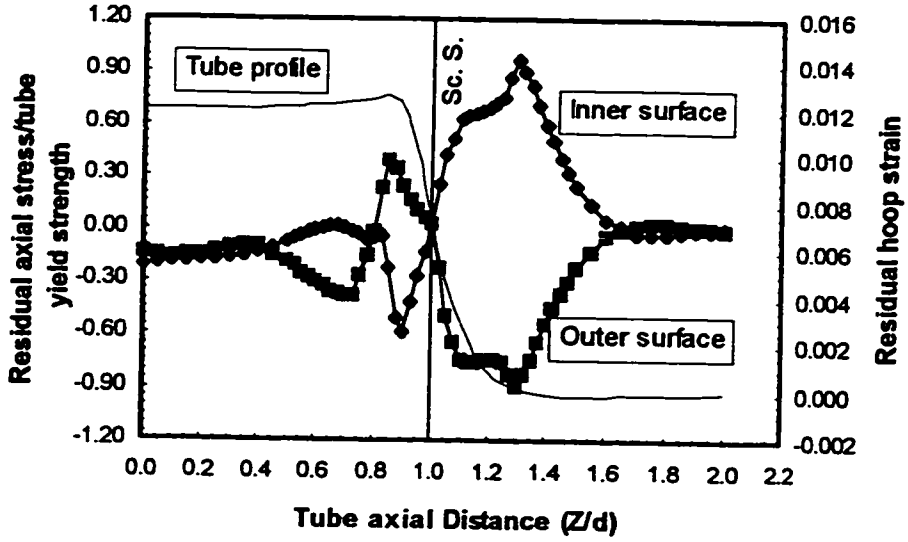


Figure 3.21: Residual axial stresses and tube profile for references case (P_e/S_{yt} = 1.0)

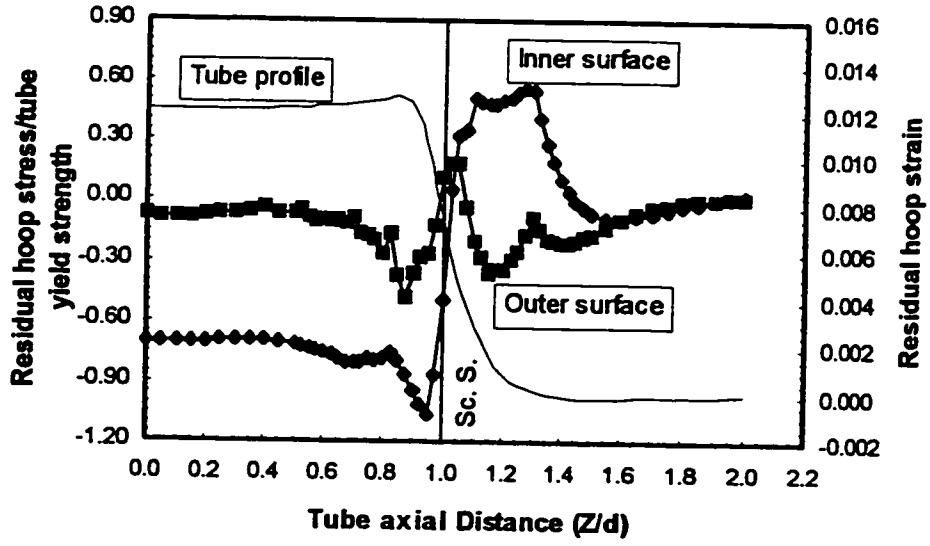


Figure 3.22: Residual hoop stresses and tube profiles for reference case (P_e/S_{yt}=1.0)

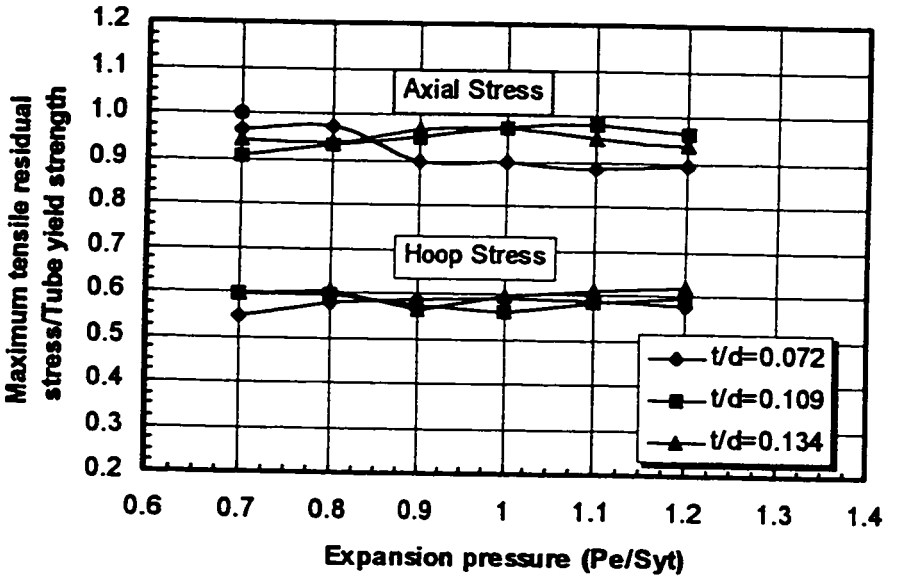


Figure 3.23: Maximum residual stresses for different levels of tube wall thickness

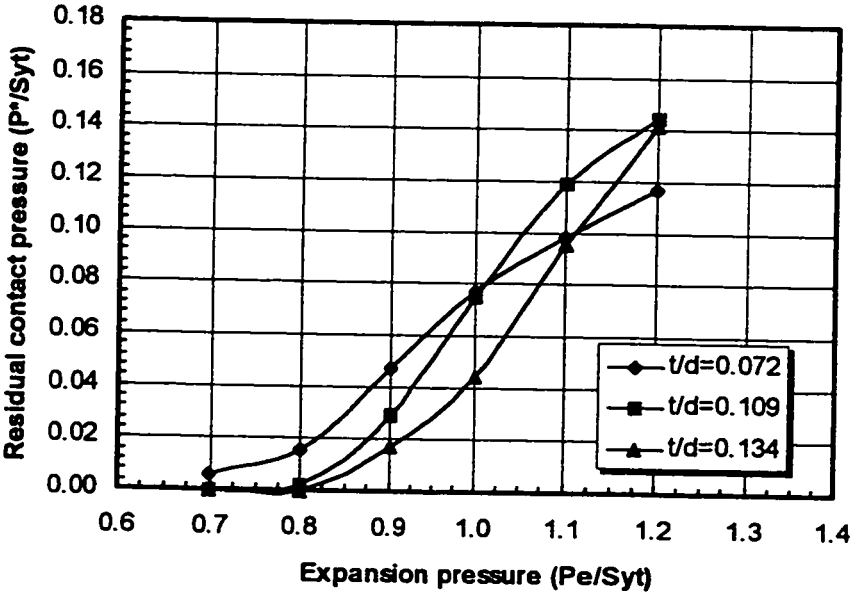


Figure 3.24: Residual contact pressure for different levels of the tube wall thickness

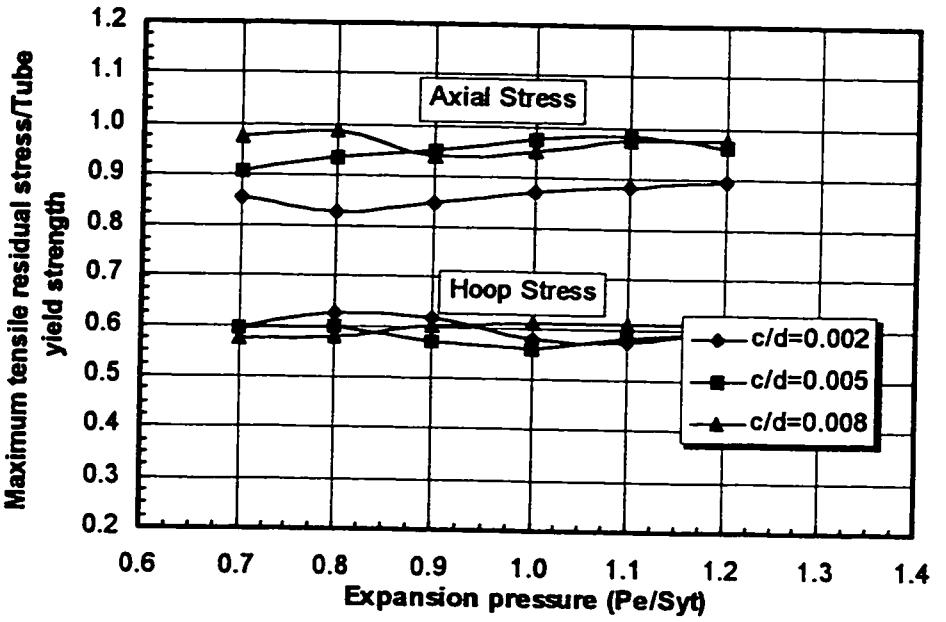


Figure 3.25: Maximum tensile residual stress at various values of initial radial clearance

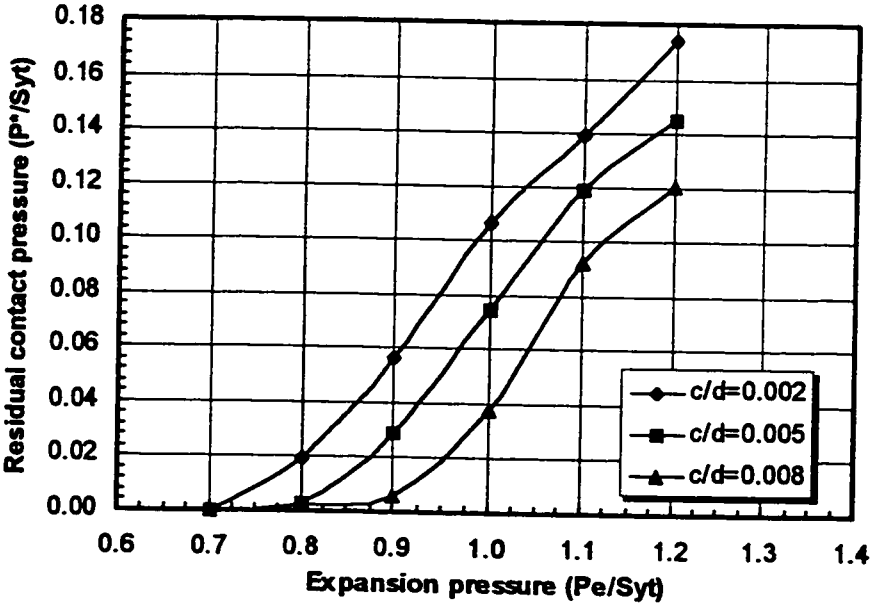


Figure 3.26: Residual contact pressure at various values of the initial radial clearance

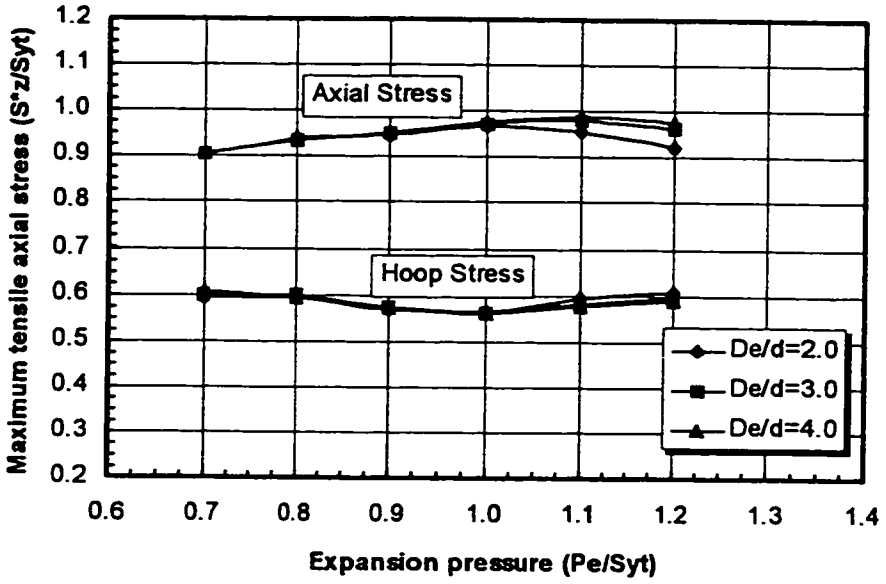


Figure 3.27: Maximum tensile residual stresses for three different (D_e/d) ratios

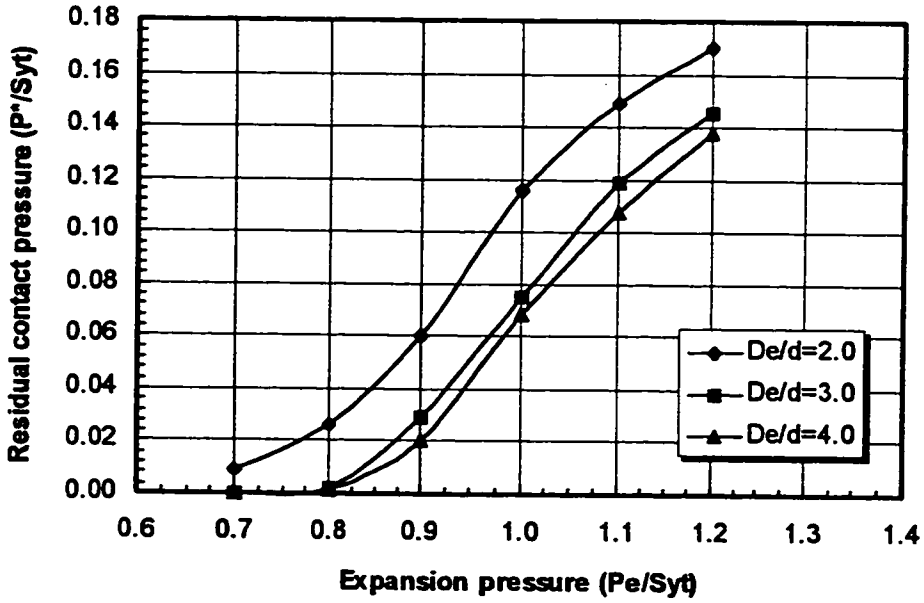


Figure 3.28: Residual contact pressure for three different (D_e/d) ratios

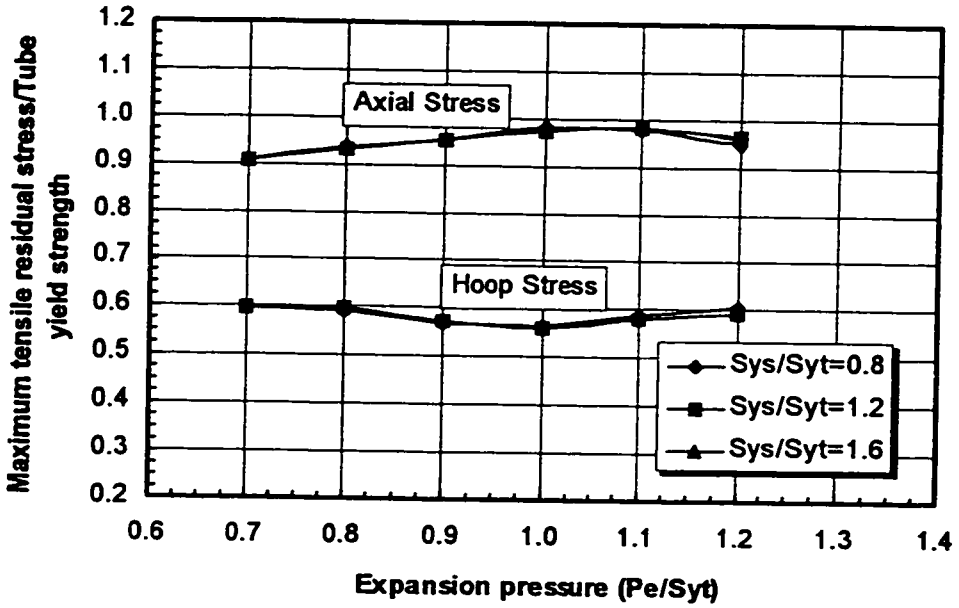


Figure 3.29: Effect of S_{ys}/S_{yt} on maximum tensile residual stresses

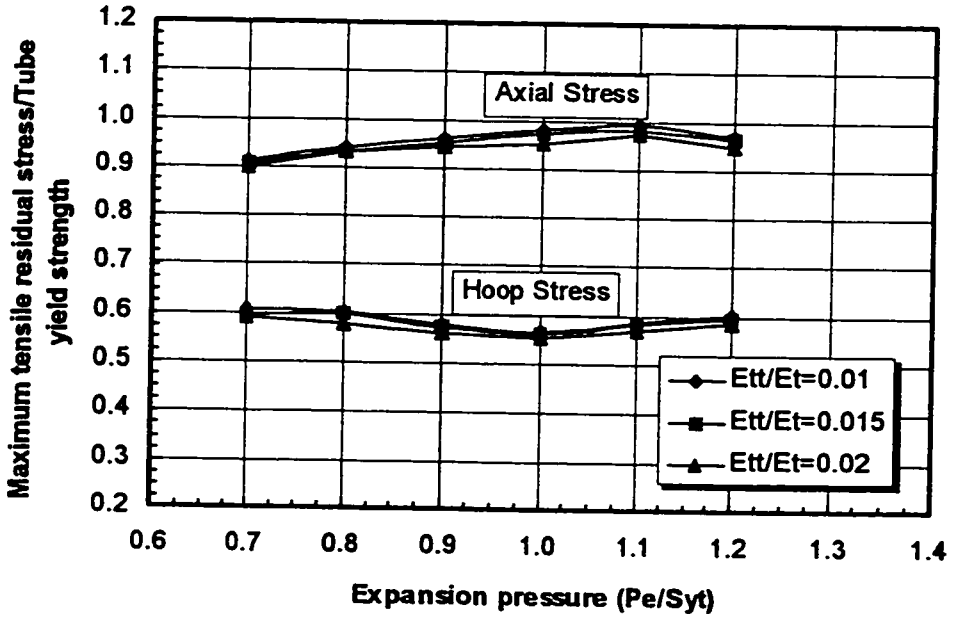


Figure 3.30: Effect of E_{tt}/E_t on maximum tensile residual stresses

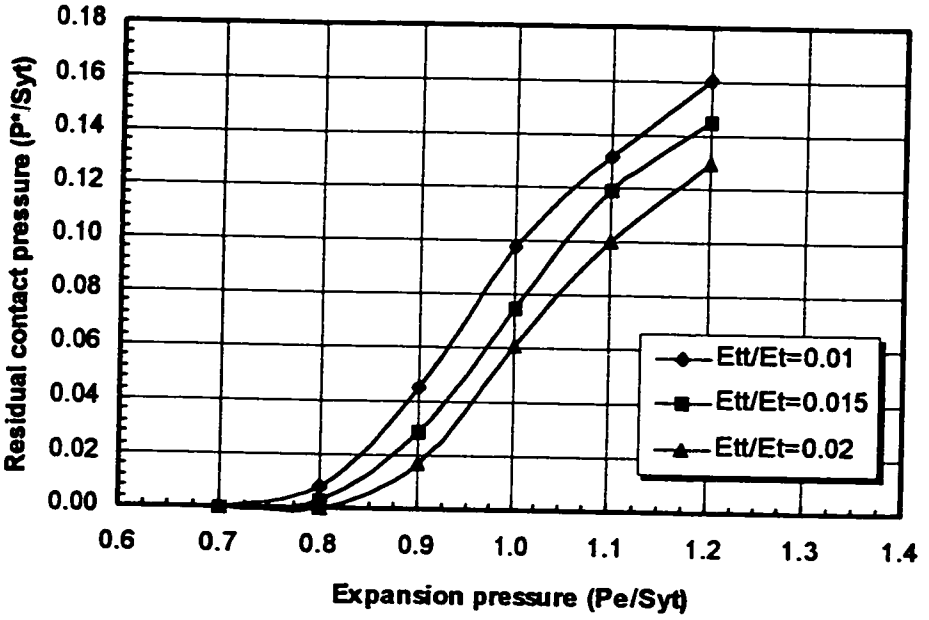


Figure 3.31: Residual contact pressure at various values of E_{tt}/E_t

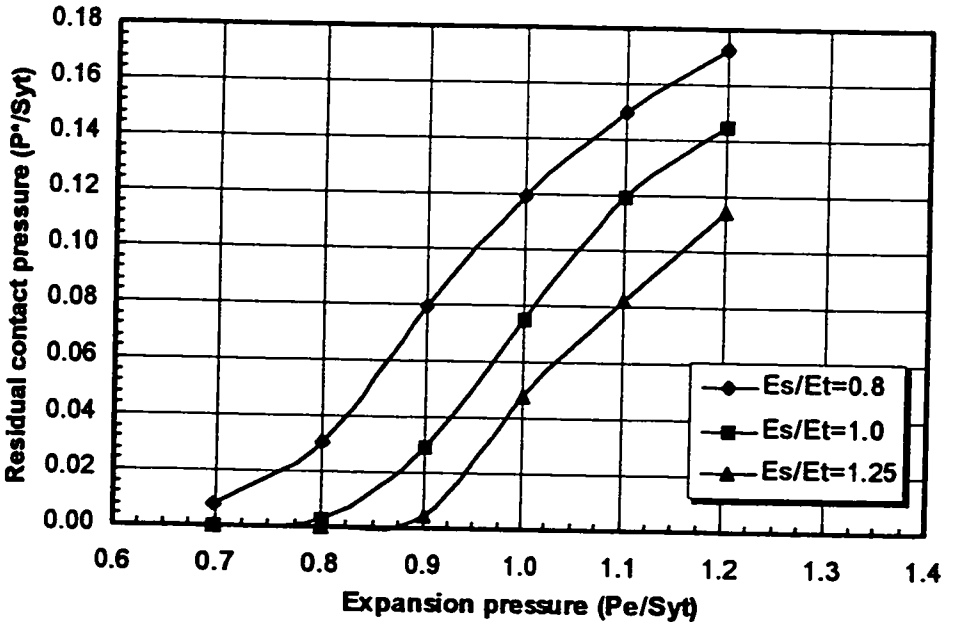


Figure 3.32: Effect of E_s/E_t on the residual contact pressure

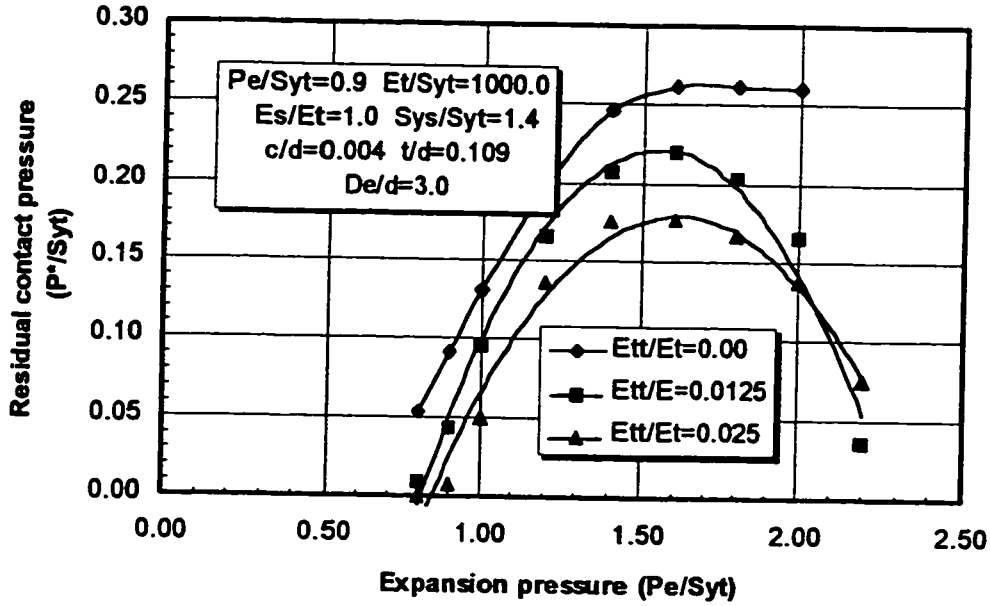


Figure 3.33: Residual contact pressure versus the expansion pressure at different levels of tube strain hardening

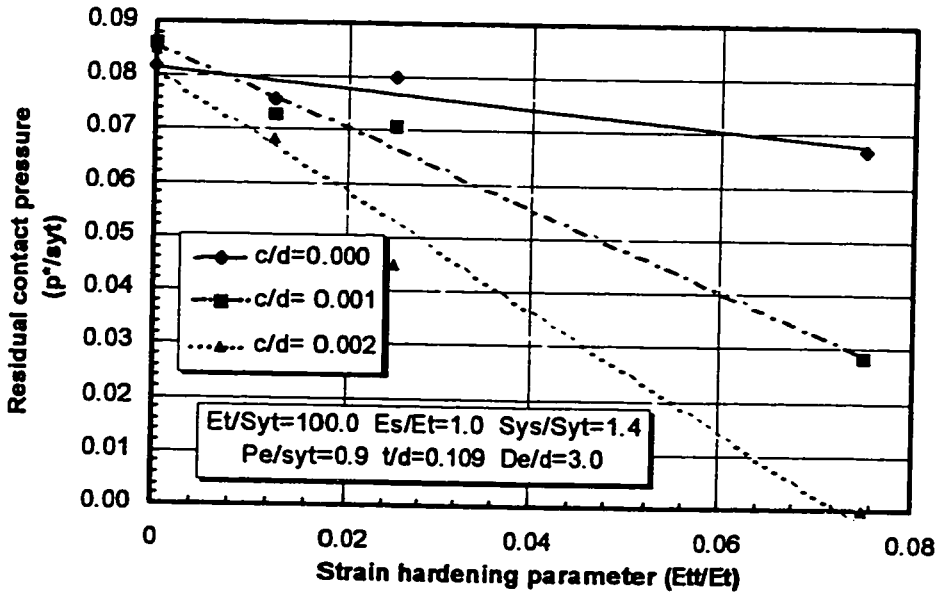


Figure 3.34: Residual contact pressure versus strain hardening parameter of tube material at different levels of initial radial clearance

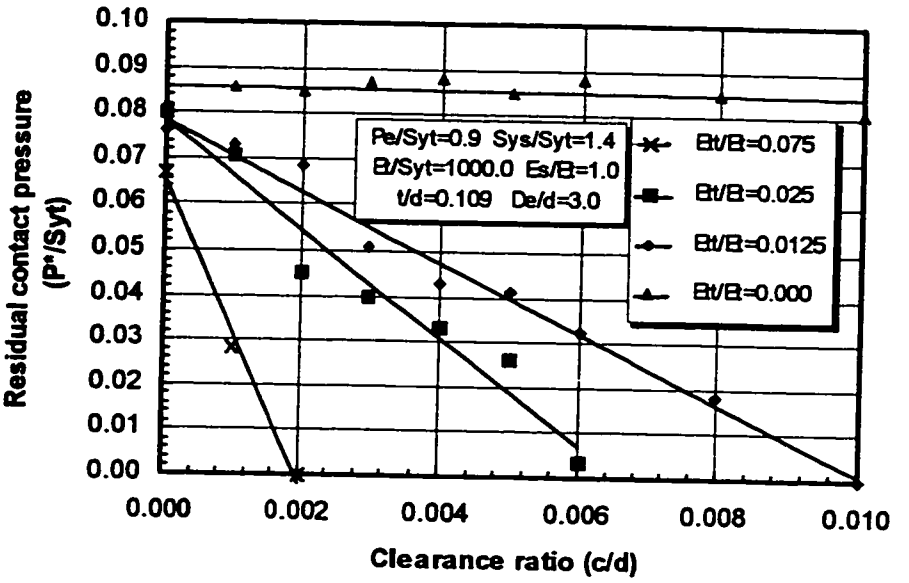


Figure 3.35 Residual contact pressure versus the initial radial clearance at various values of tube strain hardening parameter

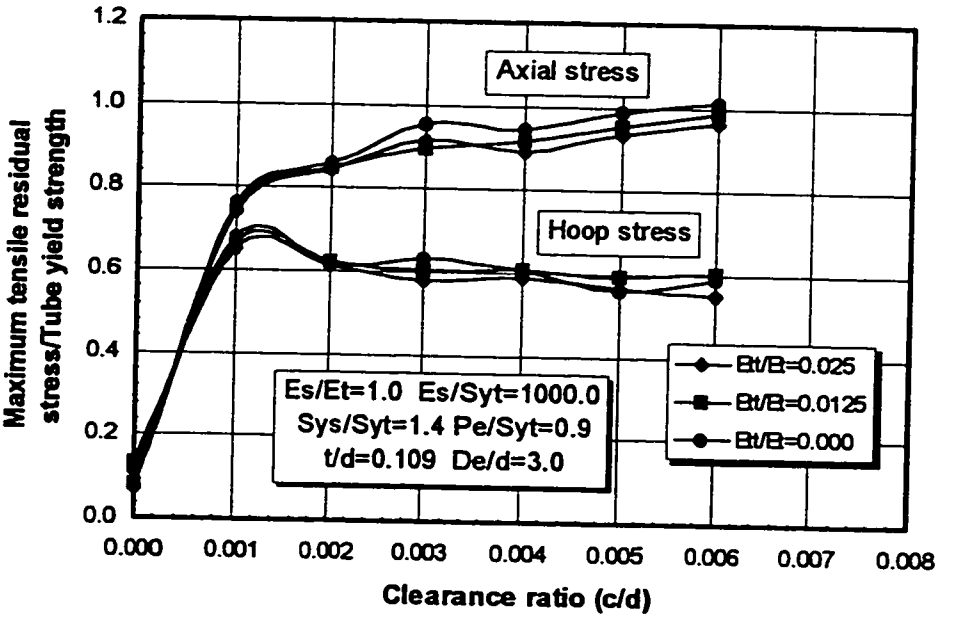


Figure 3.36: Maximum tensile residual stresses versus the initial radial clearance at various level of strain hardening parameter of tube material

CHAPTER 4

TUBE-TO-TUBESHEET JOINT: FINITE ELEMENT AND ANALYTICAL ANALYSES

PART A: RESIDUAL CONTACT PRESSURE AND RELATED PARAMETERS

4.1 INTRODUCTION

A detailed analytical and finite element analysis for the residual contact pressure and residual stress calculations of the tube-to-tubesheet joint will be presented in this chapter. In the first part, both the nonlinear finite element and analytical methods are used to investigate the level of expansion pressure to be applied in order to produce the appropriate contact pressure between tubes and tubesheet. The residual contact pressure in the expanded joint is difficult to determine experimentally. The finite element method will thus be used to validate the proposed analytical solution.

The statistical design approach is used with an empirical equation for evaluating the residual contact pressure and maximum tensile stresses by taking into account the effect of most important parameters. Since, the accuracy of this equation is limited by the number of independent parameters used in the regression model, an analytical investigation

is found necessary for an accurate calculation within a wider range of the independent parameters. The investigation consists of, first, calculating both the maximum residual tensile stress on the inner surface of the tube transition zone and the residual contact pressure and then obtain the recommended expansion pressure. Second, a simplified plane stress analytical solution is developed to obtain the minimum and maximum acceptable limits of the expansion pressure as a function of the geometrical and material parameters including the tube and tubesheet yield strength and modulus of elasticity ratios. Finally, the analytical model is refined by including the material strain hardening parameters.

Based on the analytical solution, a general design procedure is proposed for optimum expansion of tube-to-tubesheet joint. It provides the minimum expansion pressure, recommended expansion pressure, residual contact pressure, residual stress profile in the tube transition zone, and the maximum value of tensile residual stresses and its axial location on the tube.

The proposed solution is validated against published experimental and analytical results. The finite element calculation is also used for some arbitrary cases.

4.2 EMPIRICAL EQUATIONS

A nonlinear regression analysis is performed by using the Statistical Analysis

System (SAS 5.18, 1982) on the basis of the finite element results obtained by Ma (1992). Since the output response represented by the residual contact pressure, maximum tensile residual axial and hoop stresses and tube wall reduction is controlled by a large number of parameters. After some trails, Equation (4.1) was found to be the most appropriate compared to other empirical equation forms.

$$\Phi = EXP\left(\alpha_0 + \alpha_{ij} \ln(\beta_i)\ \ln(\beta_{j-1})\right) \quad ; \ i=1,7 \quad j=1,i+1 \tag{4.1}$$

Where β_i is a vector of independent variables, given by:

$$\beta_i = \left(\left(\frac{t}{d}\right),\left(\frac{P}{d}\right),\left(\frac{c}{d}+10^{-6}\right),\left(\frac{P_e}{S_{yt}}\right),\left(\frac{E_t}{S_{yt}}\right),\left(\frac{E_s}{E_t}\right),\left(\frac{S_{ys}}{S_{yt}}\right)\right)$$

β_0 is a factor produced when j=1, and it has been added to adjust the linear regression part of the empirical equation ($\ln \beta_0 = 1$). The term " Φ " in Equation (4.1) might be P^*/S_{yt}, S^*_z/S_{yt}, S^*_θ/S_{yt} or TWR for simultaneous or sequential expansion cases. The values of coefficients α_0 and α_{ij} in Equation (4.1) are listed in Table 4.1. In addition, this table shows MODEL F and R-SQUARE for each equation. MODEL F indicates how well the model, as a whole, accounts for the dependent variable behaviour. If the significance probability, PF, is small, it indicates significance. R-SQUARE measures how much variation in the dependent variable can be accounted for by the model. R-SQUARE ranges from 0.0 to 1.0 where 1.0 gives the best fit. For example, based on the results of P^*/S_{yt} shown in Table 4.1, the value of R-SQUARE is 0.986 which indicates that we can account for over 98.6% of the residual contact pressure by knowing the value of the parameters

in Equation (4.1). Table 4.1 indicates a good correlation between the assumed empirical equation and the finite element observation points for both simultaneous and sequential expansion cases. The reliability of Equation (4.1) was discussed in (Chaaban et al, 1993): As a regression model, Equation (4.1), when used within the limits of the independent variables, provides the required values without explicit understanding how each independent parameter is acting on the level of the dependent parameters. In the following sections, the analytical solution will be adopted to explore the effect of each dependent parameters on the joint strength.

4.3 ANALYSIS OF RESIDUAL CONTACT PRESSURE

As indicated by the parametric study performed in Chapter 3, the level of the expansion pressure has a direct effect on the level of the residual contact pressure and residual stresses. In order to produce a joint with a good structural integrity and leakage tightness, the effects of this important parameter and all other design parameters including dimensional and material factors, must be verified using the analytical analysis.

4.3.1 Limiting Pressure and Appropriate Model Used

The axisymmetric finite element model developed in Chapter 3 is used first to investigate the residual contact pressure introduced in the tube-to-tubesheet joint by

hydraulic expansion. The frictional interaction between the tube and the tubesheet is also accounted for by using Coulomb's friction law with a coefficient of friction f = 0.35 in all runs reported in this work, except for the cases reported in Table 4.2 where no friction was allowed (f = 0.0). The materials of the tube and tubesheet are assumed to have elastic perfectly plastic behaviour, and the computations are achieved by using the Von Mises yield criterion.

For a typical case, the residual contact pressure (P^*), maximum tensile residual axial stress (S^*_z) and hoop stress (S^*_θ) located on the inner surface of the tube in the transition zone, and the tube enlargement (represented by the residual hoop strain recorded at the front end of the tube (ϵ^*_θ)), were calculated and plotted in terms of the expansion pressure level (See Figure 4.1). This figure is divided into two zones depending on the extent of tubesheet deformation during loading: elastic (left hand side) and plastic (right hand side). The results show a linear increase in the residual contact pressure versus the level of expansion pressure up to the plastic deformation onset in the tubesheet. Further increase in the expansion pressure will cause plastic flow to propagate in the tubesheet. Beyond the limit line shown in Figure 4.1, which represents 25% of overstraining the tubesheet, the maximum hoop residual stress in the transition zone as well as the tube enlargement, continuously increase with no significant increase in the residual contact pressure. However, a decrease in the maximum residual axial stress is observed by increasing the expansion pressure to cause plastic deformations in the tubesheet, and

approximately reaches the same level as that of the maximum hoop stress when the tubesheet starts yielding. For an optimum design, residual contact pressure should be set at its highest value but should not significantly increase the maximum tensile residual stresses in the tube transition zone. Figure 4.1 indicates that this might be achieved at an expansion pressure that causes about 25% of plasticity throughout the tubesheet wall. A large plastic deformation in the tubesheet must be avoided to prevent the tubesheet ligament distortion and eliminate interaction effect while expanding the adjacent tubes (Kasriae et al (1983)). Therefore, when possible, the best expansion pressure should satisfy the following two conditions: 1) The entire tube wall must be plastically deformed, and 2) the innermost layer of the tubesheet bore should have initiated some plastic deformation.

As mentioned earlier, all reported analytical analyses of the residual contact pressure for the tube-to-tubesheet joint have used the assumption of plane stress. In the present study, it has been decided to compare between the results obtained by both (plane stress and plane strain models) prior to performing a detailed analytical investigation.

Figure 4.2 shows a simplified 2-D plane strain (or plane stress) model which is used to calculate the residual contact pressure between the tube and tubesheet. In order to compare the finite element results to those obtained by similar simplified model developed by Soler et al (1984), the effect of adjacent tube holes is not considered. The finite element

mesh for plane stress or plane strain models has been discretized by 8-node elements with 3-node interference contact elements. In order to show the differences between the results obtained with the three models (plane strain, plane stress and axisymmetric), the average value of the residual contact pressure (P^*/S_{yt}) was first calculated for four different cases (Table 4.2). This table also includes the results obtained by Soler et al (1984) using an incremental analytical (numerically solved) solution. Data No. 1, 2, 3, and 4 of Table 4.2, which are given in Table 4.3, were used previously by Soler et al (1984). The plane stress and plane strain finite element solutions seem to give higher values than those obtained by Soler et al (1984). The plane stress model predicts approximately the same results as those obtained by the axisymmetric model. The only exception is the last case (Data No.4) where less agreement between these two models is observed. In order to obtain a simplified analytical equation having acceptable agreement with axisymmetric solution, a closed form analytical plane stress solution seems to be the most appropriate to calculate the residual contact pressure in the tube-to-tubesheet joint. A two dimensional plane stress analytical solution is developed in the following section.

4.3.2 Analytical Analysis for Residual Contact Pressure

The analytical model will be based on the tube and tubesheet interaction shown graphically in Figure 4.3. It was first proposed by Krips and Podhorsky (1976) and modified here, see Allam et al (1995). First, the tube is expanded elastically up to point 1. Beyond this

point, any increase in the expansion pressure will plastically deform the tube wall, starting from the inner surface. After a full plastic deformation, the tube outer diameter will increase until it contacts the tubesheet inner bore, point 2. At this point, the total radial displacement on the outer surface of the tube is equal to the initial radial clearance (c), and any further increase in the expansion pressure will cause the expansion of the tubesheet. If, for example, the expansion pressure is increased so that the radial displacement goes from point 2 to point 3 in Figure 4.3, and then totally released, the tubesheet and the tube will springback to point 2 and just close the initial gap between them. This pressure is called P_{min} (minimum expansion pressure). Further increase in the expansion pressure beyond P_{min}, from point 3 to point 4, will make both the tube and tubesheet spring back to a final position (point 5) at which a permanent residual contact pressure (P^*) between the two surfaces will be created.

The following theoretical analysis represents the expansion steps mentioned above. For simplicity, no plastic deformation is allowed in the tubesheet material.

The elastic hoop and radial stress distributions and the radial displacement of an internally pressurized cylinder are given by Wang (1953):

$$\frac{\sigma_\theta}{P} = \frac{r_i^2}{r_o^2 - r_i^2}\left(1 + (\frac{r_o}{r})^2\right) \qquad (4.2)$$

$$\frac{\sigma_r}{P} = \frac{r_i^2}{r_o^2 - r_i^2}\left(1 - \left(\frac{r_o}{r}\right)^2\right) \tag{4.3}$$

$$\sigma_z = 0.0 \tag{4.4}$$

$$\frac{U}{r} = \frac{P}{E}\frac{r_i^2}{r_o^2 - r_i^2}\left(1 - \upsilon + (1 + \upsilon)\left(\frac{r_o}{r}\right)^2\right) \tag{4.5}$$

In the case of plane stress model, the principal stresses are:

$$\sigma_1 = \sigma_\theta,\ \sigma_2 = \sigma_r,\ \textit{and}\ \sigma_3 = \sigma_z \tag{4.6}$$

The pressure that causes initial yielding on the inner surface of the tube can be obtained by substituting $r = r_i$ in Equations (4.2) and (4.3) and using the Tresca yield criterion for simplicity. This gives:

$$\frac{P_{it}}{S_{yt}} = \frac{1}{2}\left(\frac{(r_o/r_i)^2 - 1}{(r_o/r_i)^2}\right) \tag{4.7}$$

Which can be written in the following more convenient form:

$$\frac{P_{it}}{S_{yt}} = \frac{1}{2}\left(\frac{Y_t^2 - 1}{Y_t^2}\right) \tag{4.8}$$

Where Y_t is given by:

$$Y_t = \frac{1}{1 - 2\bar{t}} \tag{4.9}$$

The equation for the collapse condition of a cylinder subjected to internal and external pressures (P_e, P_f) simultaneously is given by Chaaban (1985), by :

$$\frac{P_e}{S_{yt}} - \frac{P_f}{S_{yt}} = Ln(Y_t) \tag{4.10}$$

Since the tube is subjected to internal pressure only prior to contact, Equation (4.10) becomes:

$$\frac{P_{ct}}{S_{yt}} = Ln(Y_t) \tag{4.11}$$

Based on Equation (4.5), the relationship between the radial displacement on the outer

surface of the tube and the expansion pressure is given by:

$$\frac{U_o}{r_o} = 2\frac{P_e}{E_t}\frac{1}{Y_t^2 - 1} \tag{4.12}$$

The radial displacement (U_1) shown in Figure 4.3, can be calculated by substituting Equation (4.11) into Equation (4.12):

$$\frac{U_1}{r_o} = 2\frac{S_{yt}}{E_t}\frac{Ln(Y_t)}{Y_t^2 - 1} \tag{4.13}$$

As was shown earlier, the joint can be just closed, without any residual pressure, if the inner bore of the tubesheet is radially displaced by a value equals to U_1. In this case, the interference pressure between the tube and tubesheet can be obtained by substituting Equation (4.13) into Equation (4.5), as follows:

$$\frac{P_f}{S_{yt}} = 2\left(\frac{E_s}{E_t}\right)\left(\frac{1}{1+2\bar{c}}\right)\frac{\left(Y_s^2 - 1\right)\quad Ln(Y_t)}{\left(Y_t^2 - 1\right)\left(1 - \upsilon + (1 + \upsilon)\,Y_s^2\right)} \tag{4.14}$$

Where Y_s is given by:

$$Y_s = \frac{\bar{D}_e}{1 + 2\,\bar{c}} \tag{4.15}$$

The value of D_e can be calculated by using the empirical equation provided by Chaaban et al (1992) or by Kohlpaintner (1995).

By substituting Equation (4.10) into Equation (4.14), the minimum expansion pressure (P_{min}) that is required to just close the initial gap will be obtained. This pressure is given in its final form as follows:

$$\frac{P_{min}}{S_{yt}} = 2\left(\frac{E_s}{E_t}\right)\left(\frac{1}{1+2\bar{c}}\right)\frac{\left(Y_s^2-1\right)\ \ln Y_t}{\left(Y_t^2-1\right)\left(1-\upsilon+(1+\upsilon)Y_s^2\right)} + \ln Y_t \qquad (4.16)$$

Now, if the expansion pressure is increased beyond P_{min}, the tubesheet inner bore will be deformed for example, up to point 4, (Figure 4.3) and its radial displacement will be given by the following equation:

$$\frac{U_s}{R_i} = \frac{P_f}{E_s}\frac{1}{Y_s^2-1}\left(1-\upsilon+(1+\upsilon)Y_s^2\right) \qquad (4.17)$$

where R_i is the inner radius of the tubesheet.

If the expansion pressure is released, assuming linear unloading with no reverse yielding in the tube material, the total springback displacement on the tube outer surface will be given by,

$$U_t^* = U_1 + U_2 \tag{4.18}$$

where U_2 is produced by the residual interference pressure between the tubesheet inner surface and the tube outer surface, and can be calculated as follows:

$$\frac{U_2}{r_o} = \frac{P^*}{E_t} \frac{1}{Y_t^2 - 1} \left((1-\upsilon) Y_t^2 + 1 + \upsilon \right) \tag{4.19}$$

Because of the displacement compatibility between the tube outer surface and the tubesheet inner bore, the following relationship must be satisfied, (see Figure 4.3):

$$U_s = U_t^* + U_R \tag{4.20}$$

where U_R is the final radial displacement of the tubesheet inner bore and given by :

$$\frac{U_R}{R_i} = \frac{P^*}{E_s} \frac{1}{Y_s^2 - 1} \left(1-\upsilon + (1+\upsilon) Y_s^2 \right) \tag{4.21}$$

By combining Equations (4.10) and (4.17), and solving Equations (4.17) to (4.21), the residual contact pressure could be obtained as follows:

$$\frac{P^*}{S_{yt}} = \frac{1}{K} \left(\frac{P_e}{S_{yt}} - \frac{P_{\min}}{S_{yt}} \right) \tag{4.22}$$

Where K is a constant given by:

$$K = 1 + \frac{E_s}{E_t}\left(\frac{1}{1+2\bar{c}}\right)\left(\frac{Y_s^2-1}{Y_t^2-1}\right)\left(\frac{(1-\upsilon)Y_t^2+1+\upsilon}{1-\upsilon+(1+\upsilon)Y_s^2}\right) \qquad (4.23)$$

As it can be noticed from Figure 4.3, the residual contact pressure between the tube and the tubesheet may not be created unless U_s is higher than U_1, which means:

$$\frac{2\,S_{yt}\,r_o\,\ln Y_t}{E_t\left(Y_t^2-1\right)} < \frac{P_f}{E_s}\;\frac{R_i}{Y_s^2-1}\left(1-\upsilon+(1+\upsilon)Y_s^2\right) \qquad (4.24)$$

Replacing P_f by its expression given by Equation (4.10), Equation (4.24) can be written in the following form:

$$\frac{E_s}{E_t} < \frac{1}{2}(1+2\bar{c})\left(\frac{P_e}{P_{ct}}-1\right)\left(\frac{Y_t^2-1}{Y_s^2-1}\right)\left(1-\upsilon+(1+\upsilon)Y_s^2\right) \qquad (4.25)$$

For any expansion pressure level and joint dimensions used, this inequality should be satisfied in order to create the joint.

On the other hand, since the tubesheet is treated as a thick-walled cylinder, two limiting

pressures are to be watched:

$$\frac{P_{is}}{S_{ys}} = \frac{1}{2}\left(1 - \frac{1}{Y_s^2} \right) \qquad (4.26)$$

and

$$\frac{P_{cs}}{S_{ys}} = Ln\,(Y_s) \qquad (4.27)$$

The first one (Equation (4.26)) is the internal pressure to cause initial yielding in the tubesheet, and the second one (Equation (4.27)) is the pressure that causes a full plastic deformation of the tubesheet. Since P_f is always the pressure acting on the inner surface of the tubesheet during the expansion process, Equation (4.26) gives the following inequality:

$$S_{ys} \geq 2P_f \frac{Y_s^2}{Y_s^2 - 1} \qquad (4.28)$$

Together with Equation (4.10), we get:

$$\frac{S_{ys}}{S_{yt}} \geq 2\left(\frac{P_e}{P_{ct}} - 1 \right) \frac{Y_s^2\, Ln(Y_t)}{Y_s^2 - 1} \qquad (4.29)$$

Or, in a more convenient form:

$$\frac{P_e}{S_{yt}} \le \frac{1}{2}\frac{S_{ys}}{S_{yt}}\frac{Y_s^2 - 1}{Y_s^2} + Ln(Y_t) \qquad (4.30)$$

Therefore, the expansion pressure should not exceed the value given by Equation (4.30). Consequently, the maximum expansion pressure is given as follows:

$$\frac{P_{max}}{S_{yt}} = \frac{1}{2}\frac{S_{ys}}{S_{yt}}\frac{Y_s^2 - 1}{Y_s^2} + Ln(Y_t) \qquad (4.31)$$

In some special cases, material combinations of tube-to-tubesheet joint where the tubesheet yield strength is lower than that of the tube material may be found, although such combinations are not recommended. However, as was shown by the finite element method in the present study, a tubesheet having a yield strength lower than that of the tube may, up to a certain limit, successfully create the joint; the range of tubesheet yield strength ratio to be adopted in such a case is discussed below.

Since the minimum expansion pressure given by Equation (4.16) does not cause any yielding in the tubesheet, the following inequality is drawn:

$$\frac{P_{min}}{S_{yt}} \le \frac{1}{2}\frac{S_{ys}}{S_{yt}}\frac{Y_s^2 - 1}{Y_s^2} + Ln(Y_t) \qquad (4.32)$$

Combining Equations (4.16) and (4.32) gives the following condition:

$$\frac{S_{ys}}{S_{yt}} \geq 4 \frac{E_s}{E_t} \frac{1}{1+2\bar{c}} \frac{Y_s^2}{Y_t^2-1} \frac{Ln(Y_t)}{\left(1-\upsilon+(1+\upsilon)Y_s^2\right)} \qquad (4.33)$$

This equation gives the value of the tubesheet yield strength ratio that maintains the tubesheet elastic under the minimum expansion pressure. On the other hand, the tubesheet should not support an expansion pressure higher than the value given by Equation (4.27) which can be interpreted in the following form:

$$\frac{S_{ys}}{S_{yt}} \geq \frac{P_e}{S_{yt}\, Ln(Y_s)} - \frac{Ln(Y_t)}{Ln(Y_s)} \qquad (4.34)$$

If a tubesheet has a yield strength ratio lower than that given by Equation (4.34), the tubesheet ligament would be completely destroyed. While expanding a thin walled tube that is harder than a tubesheet, the interference pressure during the expansion process will exceed the tubesheet plastic limit. In an extreme case, when the yield strength of tubesheet is much lower than that of the tube (say $S_{ys}/S_{yt}=0.5$) and by using an expansion pressure of the same order of the tube yield strength, the interference pressure during the expansion will highly exceed the tubesheet plastic limit, so that, when the expansion pressure is released, the tubesheet inner bore will be permanently enlarged and the tube would almost

spring back to a final position creating an additional clearance rather than interference. Therefore, when a tubesheet having lower yield strength is to be used, the expansion pressure must be much lower than the tube yield strength in order to avoid excessive plastic deformation in the tubesheet. In other words, the expansion pressure should be controlled, in this case, by the yielding level of the tubesheet.

Relations (4.29),(4.33) and (4.34) provide the ranges of the tubesheet yield strength ratios that can be used during manufacturing tube-to-tubesheet joints. As an illustration, these relations are plotted for an arbitrary expansion pressure ratio $P_e/S_{yt} = 1.0$, in Figure 4.4. In the range between the solid and dashed lines (Equations. (4.29) and (4.33), respectively) on this figure, better joint with elastically deformed tubesheet will be obtained. On the other hand, the range between the dashed and dotted lines (Equations (4.33) and (4.34), respectively) is not recommended because the tubesheet ligament will be plastically deformed before the expansion pressure reaches its peak level. Finally, the range of the tubesheet yield strength ratio located under the dotted line (Equation (4.34)) will make it impossible to set up the joint. All these conclusions apply, of course, to the specified conditions specified in Figure 4.4.

4.3.3 Validation of the Analytical Solution

The analytical solution given in the previous subsection is somehow an

approximation of the real behaviour of hydraulically expanded joints. This is mainly due to the resistance of the non-expanded part of the tube which cannot be included in the plane stress model. Alternatively, the axisymmetric finite element model would better simulate the tube-to-tubesheet joints and help to modify the proposed analytical model.

First, the value of the minimum expansion pressure given by Equation (4.16) have been compared with that obtained by the finite element method. Many cases have been considered, and all of them indicate that Equation (4.16) predicts a slightly higher values of minimum expansion, about 15%. This could be mainly due to the choice of yield criteria; Von-Mises is used within the finite element solution, whereas Tresca has ben adopted in our plane stress model. As a result, the minimum expansion pressure can be corrected as follows:

$$\frac{P_{mef}}{S_{yt}} = \alpha \frac{P_{\min}}{S_{yt}} \tag{4.35}$$

Where P_{mef} is the effective minimum expansion pressure, and α is a converting factor between Equation (4.16) and the axisymmetric finite element solutions, and its average value has been found to be approximately 0.85. Also, the residual contact pressure, Equation (4.22), has been modified as follows in order to satisfy the results obtained by the finite element analysis.

$$\frac{P^*}{S_{yt}} = \frac{\beta}{K}\left(\frac{P_e}{S_{yt}} - \frac{P_{mef}}{S_{yt}}\right) \tag{4.36}$$

Where β is another converting factor by which the residual contact pressure calculated analytically can be correlated to the finite element solution. The best value of this factor was found to be approximately 1.15.

Equation (4.36) has been tested for some arbitrary design conditions relying on different tube-to-tubesheet joint material and geometrical factors. Almost all tests indicate that the value of the residual contact pressure as obtained by Equation (4.36) is about equal to that calculated by the finite element model.

The results of different analytical theories (Goodier et al, 1943; Sachs, 1947; and Krips and Podhorsky, 1976) are used for comparison with our analytical model, Figure 4.5. Krips and Podhorsky (1976) have assumed a membrane tube wall in their theory. Consequently, their model provides greatly different behaviour as shown in the figure. However, the present model results are in a relatively good agreement with the analytical theories provided by Goodier et al (1943), Kasriae et al (1983) and Sachs (1947).

Figure 4.6 shows the residual contact pressure obtained by the axisymmetric finite element model, Equation (4.36), and by the analytical equations given by Krips and Podhorsky (1976) and by Kasriae et al (1983). Figure 4.6 indicates that the results given by Equation (4.36) and those obtained by the finite element method are almost identical

in the area where the tubesheet is still elastic, and at the beginning of its plastic deformation.

The sensitivity of Equation (4.36) to the modulus of elasticity ratio variation is shown typically on Figure 4.7 which indicates a good agreement between the finite element method and Equation (4.36) for three typical values of E_s/E_t. On the other hand, the results indicate a large decrease in the residual contact pressure level when the modulus of elasticity ratio increases. This behaviour has been predicted by Equation (4.25) which provided the maximum value of the modulus of elasticity ratio beyond which the residual contact pressure could not be established. For the design case given in Figure 4.7, the maximum value of the modulus of elasticity ratio is approximately 1.23 as given by Equation (4.25).

Figures 4.8 and 4.9 show plots of residual contact pressure obtained using Equation (4.36) for different joint materials, and expansion pressure levels for a range of tube thickness ratios obtained from TEMA (1988).

4.3.3 Effect of the Strain Hardening parameter

Based on the results of the parametric analysis presented in Chapter 3, ignoring the combined effects of the strain hardening parameter and the initial clearance ratio result in

an increase in the calculated value of the residual contact pressure, particularly when high levels of these two parameters are considered. Therefore, Equation (4.36) must be modified in order to take into account the effect material strain hardening parameters (E_t/E_i) and the initial radial clearance (c/d). It is obvious from Figures 3.32 and 3.33 that the level of the residual contact pressure can be linearly correlated to both the material strain hardening parameter (E_t/E_i) and the initial clearance ratio (c/d). Consequently, it has been found that the best simplified and precise factor adjusting the residual contact pressure calculated by Equation (4.36) is given by;

$$\bar{f} = A + B\left(\frac{c}{d}\right)\left(\frac{E_{tt}}{E_t}\right) + C\left(\frac{E_{tt}}{E_t}\right) \qquad (4.37)$$

The finial residual contact pressure can be simply given by;

$$P^* = \bar{f} \cdot P_o^* \qquad (4.38)$$

where the value of each factor is given in Table 4.4.

Equation (4.38) was verified using eight arbitrary test cases (Table 4.5). Figure 4.10 shows a good comparison in the tendency of the residual contact pressure as calculated by Equation (4.38) and by the finite element method. This equation may thus

be used with some confidence to approximate the residual contact pressure of expanded joints when the effect of the strain hardening of the tube material is to be taken into account.

PART B: STRESS ANALYSIS OF TUBE TRANSITION ZONE OF AS-EXPANDED JOINT.

4.4 INTRODUCTION

This part presents a simplified theoretical method to calculate the maximum tensile residual stresses introduced in the transition zone of an expanded joint. The maximum tensile residual stresses and their corresponding axial locations are determined by using a standard deviation analysis. The validation of the proposed equations was accomplished by comparing their results to those obtained by the finite element method for a number of arbitrary cases. An upper limit has been imposed on the expansion pressure level depending on the combination of the geometrical and material parameters that are involved in the design of the tube-to-tubesheet joints.

The non-linear finite element method may give reliable results depending on the type of solid and contact elements used, mesh refinement, number of iterations to reach the convergence for an appropriate tolerance, etc.. A full 3-D FE solution is generally

required. Even though, a good development has been achieved in the computer and software technology, none linear contact problems are still challenge. Therefore, based on the above observations, derivation of a simple analytical model that provides the range of maximum tensile residual stresses with their expected locations would be a very useful tool.

As a first step, a simplified 2-D finite element study of the loading, unloading and residual stresses in the tube transition zone is presented. In the second step, a parametric study of the loading and residual stresses profiles is achieved using a statistical technique. The analytical solution obtained in the first part of this chapter, is extended to study the stresses created in the tube transition zone. At the end, an analytical equations used to calculate the residual stresses are given on the basis of plane stress condition and beam on elastic foundation theory.

4.5 FINITE ELEMENT ANALYSIS

A detailed analysis of the 3-D model of the tube-to-tubesheet joint has been already performed in Chapter 3. The results indicate that the 3-D geometry may be simplified by either a 2-D plane stress or an axisymmetric model, during and after expansion of the tube, without compromising the accuracy of the results.

The axisymmetric finite element model shown in Figure 3.2 is used here to investigate the stresses in the tube transition zone. The Letters "I", "G" and "F" are used in Figure 3.2 to indicate particular locations of interest on the tube. The materials of the tube and tubesheet are assumed to have elastic perfectly plastic behaviour. However, based on the parametric study represented in Chapter 3, the effect of the strain hardening parameter of both tube and tubesheet material was only observed on the level of residual contact pressure. The strain hardening parameter has a negligible effect on the residual stresses which are the main subject of this section.

Figure 4.11 illustrates typically the variation of the hoop and equivalent plastic strains on the middle surface of the tube along the axial direction at maximum loading. Based on this result and others not shown here, it can be concluded that, during the loading phase of the expansion process, the plastic deformation in the tube is not only located in the tube loaded portion but also extends up to the end of the transition zone. As a result, the calculation of the stresses during loading in both the uniform expanded part and the transition zone of the tube becomes very complicated. Figures 4.12, 4.13, 4.14 and 4.15 show the loading, unloading and residual stresses in the axial and hoop directions along the tube axis (Z/d) and on the tube inner and outer surfaces. The loading and residual stress components were obtained in two consecutive steps. The loading stress is calculated at the end of the first step when the expansion pressure has reached the yield strength level of the tube (P_e / S_{yt}). The expansion pressure is incrementally reduced to zero in the second step. At this point, the

residual stresses in the transition zone are obtained numerically. Figures 4.12, 4.13, 4.14 and 4.15 show that, during loading, the maximum values of the stresses, in the axial and the hoop directions are of the same order of magnitude but at different locations (this aspect will be detailed later).

The unloading stresses can be obtained by using the following equation:

$$\bar{S}_u = \bar{S}_r - \bar{S}_l \qquad (4.39)$$

These stresses are normalized with respect to the tube yield strength S_{yt}.

The unloading stresses are calculated here to be compared later with those obtained by the analytical solution. Unlike the loading and residual stress distributions which show some gradient discontinuity, the unloading stress distribution suggests that a closed form solution may be developed which could facilitate the analytical calculation of the residual stresses.

The finite element results show that maximum tensile residual stresses are always located on the inner surface of the transition zone, whereas the outer surface of that zone ($1.0 \le Z/d \le 1.5$) is mostly subjected to compressive residual stresses in both axial and circumferential directions. A tensile residual stress of lower magnitude is found on the outer

surface of the crevice zone ($1.0 \leq Z/d$). Therefore, the inner surface will be most likely to be subjected to SCC.

4.5.1 Estimation of Maximum Tensile Residual Stresses

Three different material sets have been selected based on practical combinations of tube-to-tubesheet joint materials, (Table 4.6). For each material set, three levels of each of the remaining parameters, namely: the tube wall thickness, the clearance, the equivalent sleeve diameter and the expansion pressure level have be considered, as shown in Table 4.7. The range of these parameters has been selected in accordance with the geometrical and design specifications of TEMA heat exchanger standard (1988). However, due to the very large number of calculations involved, and also to avoid tedious parametric study similar to that performed in the previous chapter, the orthogonal design method becomes very useful, Taguchi (1982). This approach was used by Ma (1992). The main advantages of this technique are: 1) to reduce the number of calculations and consequently save time, and 2) to determine statistically the optimal combination of the parameters involved.

In order to explain the use of orthogonal arrays, let us consider the four parameters involved, each at three levels. Mathematically, in this case, there are $(4)^3$ possible combinations for each material set. Therefore, 192 calculations would be required in order to determine completely their effects. However, by using the orthogonal design method

only 27 out of 192 calculations are required. These 27 calculations (9 calculations for each set) are chosen according to the orthogonal array of Table 4.8.

The finite element solutions of the 27 observation points are carried out and the residual stresses in the tube transition zone are calculated for each case. The maximum values of these stresses (S^*_z, S^*_θ) in the axial and hoop directions, on the inner surface of the tube, are specified with their axial locations (Z_z, Z_θ). As an example, Table 4.9 shows the values of (S^*_z, S^*_θ, Z_z, and Z_θ) for the first material set (SET1).

In order to provide the range of the maximum tensile residual stresses as well as the range of their axial location in the tube transition zone, the mean values and the standard deviation of each of those variables are performed on the three material sets. Table 4.10 summarizes the results of the standard deviation analysis. Figure 4.16 shows the Gauss curve for the first two parameters (S^*_z/S_{yt} and S^*_θ/S_{yt}) and Figure 4.17 shows the same type of curves but for the second two parameters (Z_z/d and Z_θ/d). Figure 4.16 indicates that the maximum tensile residual stress is always in the axial direction and reaches 85% to more than 100% of the tube yield strength. Figure 4.17 provides the axial location (Z_z/d) of the maximum residual axial stress which is between 1.2 to 1.38 from the front end of the tube. On the other hand, Figures 4.16 and 4.17 indicate that the maximum tensile residual hoop stress varies between 55% to 67% of the tube yield strength and located in the range of (Z_θ/d) between 1.2 to 1.33, measured from the front end of the

tube. Since we are seeking a general analytical solution, it will be useful at this stage to examine the parametric loading stress analysis to give us an idea about how the parameters affect the plastic behaviour along the tube. This is presented in the following section.

4.5.2 Parametric Study of Loading Stresses

The results of the analyses of the three material sets of Table 4.6 together with the different parameters of Table 4.7 are used once again in this section. The stress distributions, on both inner and outer surfaces of the tube at the end of the loading step, are investigated along the axial direction.

First, the effect of the material properties of the tube and tubesheet is examined. As an example, the dimensional parameters and the expansion pressure level of Calculation No. 5 of Table 4.8 are selected. Figures 4.18 and 4.19 show the effect of the three material sets (STE1, SET2 and SET3 of Table 4.6) on the loading stresses, located at the inner and outer surfaces of the tube, in both axial and hoop directions. The results indicate that the material properties of the tube and tubesheet have a negligible effect on the loading stresses when normalized to the tube yield strength. Thus, the geometrical parameters and the expansion pressure level must be the important factors that affect the level of loading stresses.

These effects are examined on one material set which was selected to be (SET1) of

Table 4.6. The effect of changing the level of each parameter (c/d, t/d, D_c/d, and P_c/S_{yt}) on the loading stresses was observed. The results are summarized in Figures 4.20 and 4.21 by plotting the mean value of each stress component in the axial direction and its associated standard deviation value. Figure 4.20 shows the mean and standard deviation values of the axial stresses. The hoop stresses are shown in Figure 4.21. The maximum loading stress on the inner surface, in both the axial and the hoop directions, is in the same order of approximately 125% of tube yield strength, but not at the same location. This explain why the maximum tensile residual stresses is alway in the axial direction. At the end of the loading stage, the maximum loading hoop stress is quite near to the beginning of the transition zone, whereas the maximum loading axial stress is usually found at a point located quite far from the beginning of the transition zone. On the other hand, the unloading stresses either in the axial or circumferential directions are dominant at the beginning of the tube transition zone. Beyond this particular location, all unloading stresses decrease rapidly along the tube axial direction. As a result, the maximum loading hoop stress is reduced significantly to finally give a lower residual hoop stress. On the contrary, the maximum value of loading axial stress is slightly reduced by the unloading stress and consequently a higher tensile residual axial stress is introduced at the end of the tube transition zone.

Concerning the level of the standard deviation, the loading axial stresses either on the inner or on the outer surfaces, have a lower standard deviation value in the intermediate part of the transition zone as shown on Figure 4.20. However, changing the parameters could have

an effect on changing the axial loading stress from its mean value, particularly at the beginning and the end of the transition zone. The same behaviour is observed in Figure 4.21 for the loading hoop stress on the inner surface. On the contrary, Figure 4.21 shows that the loading hoop stress on the outer surface is affected by these parameters mainly in the intermediate section of the transition zone.

4.6 ANALYTICAL MODEL FOR RESIDUAL STRESS CALCULATION

A simple analytical model is proposed in this section to determine the stress state in the transition zone during loading, unloading and at residual condition. The unloading state is assumed, and later confirmed, to be fully elastic. However, the loading one is accomplished with a complete plastic deformation in the expanded and transition zones of the tube.

4.6.1 Loading Stress

As shown in the previous section, the tube and tubesheet material properties have almost no effect on the loading stresses when normalized to the yield stress of the tube material. Also, the dimensional parameters provoke lower variation around the mean level of the loading stresses as shown in Figures 4.20 and 4.21. As such, it can be satisfactorily assumed that the averaged level of the loading stresses can be considered as a good approximation while performing the calculation of the stresses for any arbitrary case.

Therefore, the results of the analysis done on SET1 will be used here. The mean values of the loading stresses at each location Z/d of Figures 4.20 and 4.21 were stored in a computer software to be used while calculating the loading stresses for other study cases.

4.6.2 Unloading Stress

The unloading displacement U_u and unloading rotation Φ_u at the beginning of the transition zone are analysed for the uniformly expanded zone assuming plane stress conditions as explained earlier, and for the transition zone based on a modified beam on elastic foundation theory, see Figure 4.22. A similar approach was used by Updike et al (1992).

By following up the same procedures presented in the first part of this chapter, and finally combining Equations (4.12) and (4.17) to (4.22), the total springback displacement U^*_t may be obtained as follows:

$$\frac{U_t^*}{d} = \frac{S_{yt}}{2K E_t}\left(\frac{P_e}{S_{yt}} - \frac{P_{\min}}{S_{yt}}\right)\frac{(1-\upsilon)Y_t^2 + 1 + \upsilon}{Y_t^2 - 1} + \frac{S_{yt}}{E_t}\frac{Ln(Y_t)}{Y_t^2 - 1} \qquad (4.40)$$

Where K is the same constant as it was given by Equation (4.23).

From Figure 4.3, the unloading displacement at the beginning of the transition zone

is given by the following equation :

$$U_u = - U_t^* \tag{4.41}$$

The unloading edge rotation (Φ_u) may be obtained by knowing the slope of tube profile at the beginning of the transition zone during loading and after unloading. Some approximation is required in order to develop the analytical model. The relation between the edge displacement and the corresponding slope is assumed linear. This assumption must be verified later experimentally. This relation will be then given as follows :

$$\Phi_u \cong \frac{U_t^*}{\Delta} \tag{4.42}$$

where Δ, as shown in Figure 4.22, is approximately equal to the distance between the end of the uniformly expanded zone and the beginning of the non-expanded zone of the tube.

The unloading displacement U_u given by Equation (4.41) is expected to overestimate the real unloading displacement obtained at the junction between the end of the uniformly expanded zone and the beginning of the transition zone. This is mainly due to the resistance of the transition zone and the non-expanded part of the tube, which were not included in the development of Equation (4.41). A correction factor α may thus be used as follows:

$$\bar{U}_u = -\alpha \frac{U_t^*}{d} \tag{4.43}$$

The value of Δ in Equation (4.42) is a function of the material, dimensions of the joint and applied expansion pressure. A first approximations for the values of α and Δ were found to be 0.75 and 0.2 respectively. It is suggested that these values be determined experimentally in a future research program.

By using the unloading displacement U_u and unloading rotation Φ_u at the beginning of the transition zone, the unloading stresses in the transition zone can be calculated based on the discontinuity stress equations in a thin elastic shell, Harvey (1985). For convenience, these equations are written here in dimensionless form:

$$\frac{S_{u\theta}}{S_{yt}} = 2\frac{\bar{E}_t}{1-\bar{t}}\bar{U}_z \pm \frac{6\upsilon}{\bar{t}^2}\bar{M}_z \tag{4.44}$$

$$\frac{S_{uz}}{S_{yt}} = \pm \frac{6\upsilon}{\bar{t}^2}\bar{M}_z \tag{4.45}$$

$$\bar{U}_z = 2\frac{\omega}{\bar{E}_t\,\Gamma}\,\bar{V}_o\,e^{-\omega\bar{z}}\,Cos\omega\bar{z} - 2\frac{\omega^2}{\bar{E}_t\,\Gamma}\,\bar{M}_o\,e^{-\omega\bar{z}}\,(Cos\omega\bar{z} - Sin\omega\bar{z}) \qquad \textbf{(4.46)}$$

$$\bar{M}_z = -\frac{\bar{V}_o}{\omega}\,e^{-\omega\bar{z}}\,Sin\omega\bar{z} + \bar{M}_o\,e^{-\omega\bar{z}}\,(Cos\omega\bar{z} + Sin\omega\bar{z}) \qquad \textbf{(4.47)}$$

$$\bar{V}_o = \frac{\Gamma\,\bar{E}_t}{2\omega}\left(\,2\,\frac{U_u}{d} + \frac{\Phi_u}{\omega}\,\right) \qquad \textbf{(4.48)}$$

$$\bar{M}_o = \frac{\Gamma\,\bar{E}_t}{2\omega^2}\left(\,\frac{U_u}{d} + \frac{\Phi_u}{\omega}\,\right) \qquad \textbf{(4.49)}$$

where the values of ω, Γ and $\bar{r}$ are given by:

$$\omega = \frac{1.285}{\sqrt{\bar{r}\,\bar{t}}}\,,\quad \Gamma = \frac{\bar{t}}{\bar{r}^2}\quad \text{and,}\quad \bar{r} = \frac{1}{2}(1 - \bar{t})$$

The positive and negative signs (±) in Equations (4.44) and (4.45) correspond to the inner and

outer surfaces respectively.

4.6.3 Residual Stresses

Residual stresses are given by:

$$\bar{S}_r = \bar{S}_l + \bar{S}_u \tag{4.50}$$

where, $\bar{S}_l$ is the mean value of the loading stresses that has been already generalized and stored in the computer program. The unloading stress $\bar{S}_u$ must be calculated according to Equations (4.44) and (4.45) for any material, dimension, and expansion pressure level used.

4.6.4 Limitation of the Proposed Analytical Model

Two important limits must be discussed here, 1) the level of the expansion pressure to be applied and 2) the initial clearance between the tube and tubesheet holes. As a precondition, the expansion pressure must not cause any plastic deformations in the tubesheet. This limit was proposed by Allam et al (1996), and expressed by the following equation:

$$\frac{P_{max}}{S_{yt}} = 0.575 \frac{S_{ys}}{S_{yt}} \frac{Y_s^2 - 1}{Y_s^2} + 1.15 \; Ln(Y_t) \qquad \textbf{(4.51)}$$

Regarding the clearance ratio, the analytical solution was obtained by assuming that the entire thickness of the tube becomes plastic, before any contact with the tubesheet inner surface has occurred. The clearance ratio must thus satisfy the following relationship (Chaaban (1985)):

$$\bar{c} \geq \frac{S_{yt}}{2\,E_t} \qquad \textbf{(4.52)}$$

For the type of materials generally used in heat exchangers, the range of $S_{yt} / 2E_t$ varies between $4x10^{-4}$ and 10^{-3}. Also, in many practical cases, $\bar{c}$ varies between $1.9x10^{-3}$ and $1.5x10^{-2}$ (more details can be found in TEMA (1988)). Therefore, the analytical model seems to cover a wide range of real cases.

4.6.5 Verification With Experimental and Numerical Results

An example of comparison of the analytical model (Equations (4.44) and (4.45)) with the finite element method (Equation (4.39)) was previously shown in Figures 4.12, 4.13, 4.14 and 4.15 which show the results of the unloading stresses obtained for one of the analysed

arbitrary cases. The results are in excellent agreement.

The analytical solution is, of course, an approximation of the real problem since the contribution of the non-expanded part of the tube is not included in the plane stress model, also the Tresca yield criterion is used with an elastic-perfectly plastic material. Therefore, further improvement of the analytical model is needed.

The residual stress on the inside surface of the tube of one in the selected cases given previously by Updike et al (1992) is shown in Figure 4.23. The results show the residual axial stress profile on the inner surface of the tube transition zone. The experimental results given by Bazergui et al (1984) and Aufaure et al (1987) are taken directly from Updike et al (1992) paper. The axial distance is represented by $Z/\sqrt{rt}$ for direct comparison with the experimental results. Figure 4.23 shows that there is some disagreement between experimental data and the analytical results in evaluating residual stress profile in the transition zone. This could be caused by many sources of error. Regarding the experimental results, it was very difficult to establish the exact location of the beginning of the transition zone. Also, the material data in the experiments did not match each other exactly, Updike et al (1992). The greatest difference observed in the experimental results provided by Bazergui et al (1984) and Aufaure et al (1987) could also be attributed to the different experimental techniques used. Aufure used X-Ray diffraction to measure the residual axial stresses, whereas Bazergui has used the metal removal technique combined with strain gauge measurements. Nevertheless, all results show

that the maximum value of tensile residual stresses is located on the inner surface of the tube between the expanded and non-expanded zones. On that basis, the present model is in good agreement with the experimental results in establishing the location of the maximum tensile residual stress. Also, it gives approximately the same maximum value of the residual axial stress as provided by Aufaure et al (1987) and Updike et al (1992).

The analytical model was also applied to arbitrary cases of tube-to-tubesheet joint materials and geometrical combinations, different from those presented in Tables 4.6 and 4.7, and several cases have been analysed. Table 4.11 presents the data for one of these cases. Figures 4.24,25, 26 and 4.27 show a fair agreement between the results of analytical and FE models for this particular case.

It is important to say that the present model provides the residual contact pressure and residual stresses in the tube transition zone of as-fabricated tube-to-tubesheet joints. If there is large temperature differences between the working condition and the room temperature, additional pressure and stresses should be added to those provided by the present model. These aspects will be investigated in details in Chapter 6.

PART C: OPTIMUM EXPANSION AND RESIDUAL CONTACT PRESSURE LEVELS

4.7 INTRODUCTION

The purpose of this section is to investigate the effect of the level of the expansion pressure used in the hydraulic expansion process. An analytical equation is proposed for determining the optimum expansion pressure that provides an acceptable level of residual contact pressure and minimum tensile residual stresses. A statistical technique is also carried out to confirm the validity of the proposed solution.

It has been observed that the higher the expansion pressure the sharper the tube transition zone, and a lower pressure would result in a larger crevice and a lower joint axial strength. The optimum degree of expansion has been experimentally investigated for the mechanical rolling process by Grimison and Lee (1943), based on the percentage of tube wall reduction:

$$\textbf{tube wall reduction \%} = \frac{\text{final ID} - \text{initial ID} - 2c}{2\ [\text{measured unrolled wall thickness}]} \times 100$$

where c = initial radial clearance

A tube wall reduction of about 5% was found to provide the optimum level of expansion for a maximum pull-out strength of the rolled joint. However, the effect of expansion on the maximum tensile residual stresses was ignored. As also reported in Chapter 2, Goodier and Schoessow (1943) have showed that to obtain the highest joint axial strength, the expanding pressure should not cause the tubesheet to extrude under the loading pressure. More recently, Kasriae et al (1983) and Yokell (1990) have shown that the expanding pressure is seldom applied to the point of fully developed plastic deformation in the tubesheet ligament, because the resulting tubesheet distortion may be unacceptable. Indeed, permanently enlarged holes in the tubesheet could make retubing difficult. On the other hand, as it has been shown in the previous sections, in some particular cases, the residual contact pressure may not be created even by plastically deforming the tubesheet.

This section is an extension of the analytical work presented in the fist part of this chapter. First, by using the finite element results, a definition for optimum expansion of hydraulically expanded joints will be proposed. The axisymmetric finite element analysis is also used to investigate the effect of the proposed optimum expansion pressure on the residual contact pressure and on the maximum tensile residual stresses at the inner surface of the tube transition zone. By using an analytical approach, a closed form equation for calculating the value of the optimum recommended expansion pressure is developed. Also, the statistical *t*-test is used to examine the significance of the applied expansion pressure. Finally, a comparison between the residual contact pressure obtained by the analytical technique and

by the FEM will be presented.

4.8 OPTIMUM RECOMMENDED EXPANSION PRESSURE

The effect of the expansion pressure on the residual contact pressure was previously shown in Figure 4.1. This figure indicates a linear correlation between the expansion pressure and the residual contact pressure as long as the tubesheet remains elastic. This means that if (S_{ys}/S_{yt}) is high enough, a higher residual contact pressure will be gained by using higher levels of expansion pressure. However, since the practical range of (S_{ys}/S_{yt}) lies between 0.5 and 2.5 (Soler et al, 1984), the tubesheet may always end up being plastically deformed during the expansion process and beyond a certain limit of P_e/S_{yt} no additional residual contact pressure may be gained, as shown by the horizontal part of the curves in Figure 4.1. This figure indicates a linear increase in the residual contact pressure with the expansion pressure up to the onset of plastic deformation in the tubesheet (P_e/S_{yt}=1.15), as shown by the curve of (S_{ys}/S_{yt}=1.4).

As explained and examined in the previous parts of this chapter, a tube yield strength higher than that of the tubesheet is a less favourable combination to produce a good joint. In such cases, the applied expansion pressure could plastically deform the entire tubesheet and consequently the joint cannot be created.

The analysis of the residual contact pressure obtained by varying the expansion pressure level for different cases, indicates that in order to obtain a maximum residual contact pressure, the applied expansion pressure should satisfy the following two conditions: 1) for soft-tube/hard-tubesheet combinations, the level of the expansion pressure should not cause the tube metal to extrude in the tubesheet hole; 2) for hard-tube/soft-tubesheet combinations, the level of expansion pressure should not cause any plastic distortion of the tubesheet. Since generally speaking the applied expansion pressure should be in the same order of the tube yield strength, a plastic deformation may be inevitable in the tubesheet. It is recommended, therefore, to use an expansion pressure that causes initial yielding on the inner surface of the tubesheet in order to obtain a good level of residual contact pressure, to avoid higher tensile residual stresses in the joint and to prevent tubesheet distortion.

The following Equation (4.53) respects these conditions and was previously proposed in part-A of this chapter 4, based on the plane stress assumption and on the Tresca yield criterion :

$$\frac{P_{max}}{S_{yt}} = \frac{1}{2}\,\frac{S_{ys}}{S_{yt}}\,\frac{Y_s^2-1}{Y_s^2} + Ln(Y_t) \qquad \textbf{(4.53)}$$

where Y_s and Y_t are given by:

$$Y_s = \frac{\bar{D}_e}{1 + 2\,\bar{c}} \quad ; \quad Y_t = \frac{1}{1 - 2\,\bar{t}}$$

This equation was verified against many different arbitrary cases of the current investigation and all results show its underestimation for the expansion pressure required to initiate yielding on the tubesheet inner surface. Thus, a correction factor γ has to be introduced as follows:

$$\frac{P_o}{S_{yt}} = \gamma \frac{P_{max}}{S_{yt}} \qquad (4.54)$$

where P_o is the recommended optimum expansion pressure. A value of $\gamma = 1.15$ was found to be the most appropriate.

4.9 VERIFICATION OF THE PROPOSED EXPANSION PRESSURE EQUATION

The nonlinear finite element method together with the *t*-distribution which determines whether the difference between two means is significant or due to random variations will be used here. A detailed derivation of the following equations is given by Dally et al (1983). The standard deviation of the difference in means Π_λ can be expressed by:

$$\Pi_{\lambda}=\Pi_{\rho}\sqrt{\frac{1}{n_1}+\frac{1}{n_2}} \tag{4.55}$$

where Π_{ρ} is the pooled variance, that can be expressed by the following relation:

$$\Pi_{\rho}^{2}=\frac{(n_1-1)\lambda_1^{2}+(n_2-1)\lambda_2^{2}}{n_1+n_2-2} \tag{4.56}$$

The statistical t is then calculated by;

$$t=\frac{|\lambda_2-\lambda_1|}{\Pi_{\lambda}} \tag{4.57}$$

A comparison of t -value calculated by Equation (4.57) with a value of $t(d,\alpha)$ obtained from a special table given by Dally et al (1983), provides a statistical basis for deciding whether the difference in means is significant. The value of $t(d,\alpha)$ depends upon the degree of freedom (d) and the level of significance required (α) . A 2.5% level of significance means that the probability of random variation being taken for a real difference is only 2.5%. The degree of freedom d used in this application is given by:

$$d=n_2+n_1-2 \tag{4.58}$$

This test will be used in order to investigate the effect of the expansion pressure proposed by Equation (4.54) on 1) the residual contact pressure, 2) the maximum tensile residual stress in the axial direction of the tube, and 3) the maximum tensile residual stress in the hoop direction of the tube. In order to achieve this test, two different material sets have been selected (SET1 and SET3 of Table 4.6). For each material set, three levels of each of the remaining parameters, namely: the tube wall thickness, the clearance, the equivalent sleeve diameter and an arbitrary expansion pressure level, are selected according to Table 4.7. Also, Table 4.8 provides the proposed combination for four parameters with three levels each.

The finite element solution of the 18 observation points (nine points for each material set) is carried out first by applying the expansion pressures (P_e/S_{yt}) given in Table 4.7 and second by applying the proposed optimum expansion pressure (P_o/S_{yt}) given by Equation (4.54). The residual contact pressure (P^*/S_{yt}) and the maximum tensile residual stresses (S^*_z/S_{yt}, S^*_θ/S_{yt}) obtained from both conditions are summarized in Table 4.12.

The t-values for the residual contact pressures and those for maximum tensile residual stresses are calculated according to Equation (5.57). The results of the statistical analysis are presented in Table 4.13. For a 2.5% level of significance test with $d = 34$ and $\alpha = 0.025$, $t(d, \alpha)$ is equal to 2.03 (Dally et al (1983)). Table 4.13 indicates that $t > t(d, \alpha)$ for the residual contact pressure. This means that with a 97.5% level of confidence, the residual contact pressure obtained by the optimum recommended expansion pressure (P_o/S_{yt}) is higher than

that obtained when arbitrary expansion pressure is used. On the other hand $t < t(d, \alpha)$ for the maximum tensile residual stresses indicating that the differences in means of the stresses are due to random variation. Thus, the level of the expansion pressure proposed (P_o/S_{yt}) has a small effect on increasing maximum tensile residual stresses either in the axial or in the hoop direction.

4.10 ANALYTICAL EQUATION FOR OPTIMUM RESIDUAL CONTACT PRESSURE

By substituting the recommended expansion pressure (P_o/S_{yt}) given by Equation (4.45) into Equation (4.36), the following Equation (4.59) can be proposed for determining the optimum residual contact pressure based on plane stress assumption:

$$\frac{P^*}{S_{yt}} = \frac{a_o}{K}\left(a_1 X_1 + a_2 X_2 + a_3 X_3\right) \qquad (4.59)$$

where the values of all factors in this equation are function of the material and geometrical properties of the tube and tubesheet, and are given by:

$$K = 1 + \frac{E_s}{E_t}\left(\frac{1}{1+2\bar{c}}\right)\left(\frac{Y_s^2-1}{Y_t^2-1}\right)\left(\frac{(1-\upsilon)Y_t^2+1+\upsilon}{1-\upsilon+(1+\upsilon)Y_s^2}\right)$$

$$X_1 = \frac{S_{ys}}{S_{yt}} \frac{Y_s^2 - 1}{Y_s^2}$$

$$X_2 = Ln(Y_t)$$

$$X_3 = \left(\frac{E_s}{E_t}\right)\left(\frac{1}{1+2\bar{c}}\right) \frac{\left(Y_s^2 - 1\right)}{\left(Y_t^2 - 1\right)\left(1 - \upsilon\right.}$$

The coefficients are given by:

$$a_o = 1.15, \quad a_1 = 0.575, \quad a_2 = 0.3, \quad and \quad a_3 = -1.17$$

Equation (4.59) has been tested with success on many material sets and different tube-to-tubesheet dimensional parameters. As an example, let us consider material SET-3 of Table 4.6 with the dimensions given in Table 4.7. Figure 4.28 compares the results of the finite element model and those of Equation (4.59). The calculation numbers indicated on Figure 4.28 are the same as those of Table 4.12. The results are in a relatively good agreement.

The proposed Equation (4.59) is limited to elastic perfectly plastic tube material with no plastic deformation in the tubesheet. In addition, the initial clearance between the tube and tubesheet must allow a full plastic deformation throughout the wall thickness of the tube before any contact occurrs with the tubesheet.

Executive summary

This chapter gives a detailed analytical approach to evaluate the residual contact pressure and residual stresses in the tube transition zone. Two important equations providing the minimum and maximum expansion pressure levels were obtained. A closed-form equation for the residual contact pressure was also developed. A comparison between this equation and those available in the literature showed a good agreement. A detailed parametric finite element investigation for loading, unloading and residual stress profiles in the tube transition zone was performed. It has been found that within the range of the expansion pressure used, the maximum tensile residual stresses were approximately between 86% and 109% of the tube yield strength. A simplified analytical solution was then obtained to calculate the residual stress profile in the tube transition zone. A good agreement between the analytical solution and the experimental results found in the literature was observed. Finally, the recommended level of the expansion pressure has been proposed as defined by the closed form equation. Finite element analysis together with statistical approach indicated the suggested expansion pressure was likely to increase the residual contact pressure.

Table 4.1: Coefficients of Equation (4.1)

α_{ij}	Sequential case				Simultaneous case			
	S^*_z/S_{yt}	S^*_θ/S_{yt}	P^*/S_{yt}	TWR%	S^*_z/S_{yt}	S^*_θ/S_{yt}	P^*/S_{yt}	TWR%
α_o	-1092.4	-1390.0	-1740.6	1882.5	188.45	-48.788	-1459.1	497.49
11	-18.371	-5.7007	-67.870	17.027	-25.603	-35.619	-12.343	-9.6135
21	-321.34	-352.27	100.41	81.966	-30.252	-31.582	-105.99	-71.419
31	-44.128	-60.222	10.943	32.888	9.6149	4.9628	-24.764	3.8516
41	-8.4677	-76.213	-314.20	323.10	93.298	13.406	-160.28	85.506
51	311.94	394.70	470.02	-520.34	-52.630	7.9882	409.33	-135.17
61	19.453	12.897	30.165	-23.193	4.8657	7.2604	9.0048	-12.171
71	-17.268	-16.864	-9.1223	13.822	-3.3950	-3.7965	-7.6541	0.7033
12	-0.2353	-0.7298	-1.3440	-1.2771	-1.2191	-1.4182	-0.3434	0.5898
22	-0.6988	-0.8423	-1.3226	0.3759	1.1438	-0.0034	0.6501	1.9282
23	-0.3343	-1.0067	-0.8350	0.9468	1.0436	0.9366	-1.0008	2.8021
32	-0.0281	-0.1402	0.0550	0.5899	0.0827	-0.2657	-0.0759	0.3424
33	0.7060	0.4079	-0.1497	0.5608	0.4799	0.7132	-0.4429	0.8435
34	-0.1524	-0.1258	0.0772	-0.1967	0.0686	0.2843	-0.1177	0.1956
42	-1.9222	1.2232	-5.9146	9.4672	2.3656	-1.7690	2.6399	5.6926
43	-22.210	-11.223	6.6845	15.409	-12.953	-5.2322	0.4621	-0.5561
44	-2.1773	-2.2936	-3.1550	0.3275	-0.3333	0.2101	-1.8506	1.5502
45	-7.3125	-16.292	-42.029	28.191	-2.7507	-4.2285	-28.374	3.1662
52	2.2501	0.2473	9.0034	-3.0417	2.6064	3.8077	1.5233	1.8157
53	47.347	52.345	-15.281	-12.591	4.4534	4.7610	15.924	11.150
54	6.3319	8.7661	-1.5948	-4.8608	-1.3232	-0.4604	3.5076	-0.0865
55	1.0698	10.395	39.217	-40.250	-11.411	-1.9071	22.029	-8.6697
56	-22.352	-28.079	-31.740	35.805	3.4884	-0.3116	-28.778	9.3782
62	11.901	3.3087	2.8360	4.3021	9.3610	7.1389	-0.2919	4.8144
63	1.6277	-13.839	5.6688	20.209	11.885	3.4318	-2.8331	-3.9624
64	-4.2639	-4.8280	2.5398	1.0199	-1.1589	-1.5522	-0.4324	-3.7211
65	-4.4090	14.025	33.768	-45.843	-13.878	-5.3002	13.497	-18.864
66	0.0000	0.0000	0.0000	0.0000	0.0000	0.0000	0.0000	0.0000
67	6.4239	4.5438	-11.772	5.6750	1.4895	1.7894	-3.9948	5.3280
72	-5.8020	-2.2407	-1.4071	-3.1628	-5.4221	-3.6404	-0.3450	-4.3679
73	-24.291	-27.028	6.7175	9.3068	-0.7039	-1.6593	-9.9183	-6.0644
74	-2.2199	-3.7542	1.6961	2.8965	1.5740	0.8413	-1.5563	0.5476
75	5.5238	-0.8936	-0.2177	16.125	10.591	4.1236	8.1947	8.4482
76	0.0000	0.0000	0.0000	0.0000	0.0000	0.0000	0.0000	0.0000
77	0.0000	0.0000	0.0000	0.0000	0.0000	0.0000	0.0000	0.0000
78	0.0000	0.0000	0.0000	0.0000	0.0000	0.0000	0.0000	0.0000
PF	0.022	0.014	0.0004	0.006	0.016	0.011	0.0001	0.008
RS	0.976	0.980	0.986	0.986	0.979	0.982	0.990	0.984

Table 4.2. Comparison between different models used to obtain residual contact pressure

Method used	Finite element.			Soler et al (1984)
	Pl. Strain	Pl. Stress	Axisymmetric	
Data No. 1	0.1512	0.1333	0.1407	0.1298
Data No. 2	0.1024	0.0761	0.0642	0.0743
Data No. 3	0.1607	0.0756	0.0866	0.0738
Data No. 4	0.0141	0.0189	0.0132	0.0193

Table 4.3. Data used in Table 4.2 from Soler et al (1984)

Data No.	Dimension Used				Material Used				Expansion Pressure P_e (MPa)
	Tube		Tubesheet		Tube		Tubesheet		
	d	t	D_i	D_e	S_{yt}	E_t	S_{ys}	E_s	
1	19.05	1.24	19.30	58.2	124.11	151.69	103.43	124.11	135.5
2	19.05	0.711	19.30	58.2	124.11	151.69	206.86	200.86	143.3
3	19.05	0.711	19.30	58.2	124.11	151.69	137.9	103.42	143.3
4	19.05	0.711	19.30	58.1	275.8	102.73	137.9	103.42	182.8

Table 4.4: Parameters involved in Equation (4.38)

Parameter	Value
P^*_o	Residual contact pressure for zero-strain hardening given by Equation (4.36)
f	Reduction factor
A	0.91745
B	-5559.02128
C	-1.48397

Table 4.5: Eight different cases used to verify Equation (4.38)

Case	Parameter							
	Geometrical			Material				Manufacturing
	t/d	c/d	D_c/d	S_{ys}/S_{yt}	E_s/E_t	E_t/S_{yt}	E_{tt}/E_t%	P_c/S_{yt}
1	0.366	0.002	3.5	1.333	0.833	1200	1.500	1.100
2	0.366	0.008	3.0	1.333	0.833	1200	1.000	0.800
3	0.428	0.005	3.5	1.333	0.833	1200	1.500	0.987
4	0.391	0.002	3.0	1.667	1.318	122.2	1.200	1.130
5	0.109	0.004	3.0	1.367	1.00	743.1	0.903	0.900
6	0.0664	0.0019	2.5	1.367	1.00	743.1	0.903	0.800
7	0.096	0.0019	3.0	1.367	1.00	743.1	0.903	1.000
8	0.132	0.0042	2.5	1.367	1.00	743.1	0.903	1.000

Table 4.6 : Material properties of some tested cases

SET	Tube		Tubesheet	
	S_{yt}	E_t	S_{ys}	E_s
SET1	123.04	150.4	205.06	198.22
SET2	123.04	150.4	102.5	123.04
SET3	102.5	123.04	136.71	102.5

Table 4.7 : Three levels of geometrical parameters and expansion pressure ratio

Level	Parameters			
	c/d	t/d	D_c/d	P_c/S_{yt}
1	0.002	0.072	2.5	0.8
2	0.005	0.109	3.0	0.9
3	0.008	0.134	3.5	1.1

Table 4.8 : Optimum combinations of involved parameters, Taguchi (1982).

Calculation No.	Parameters			
	c/d	t/d	D_c/d	P_c/S_{yt}
1	1	1	1	1
2	1	2	2	2
3	1	3	3	3
4	2	1	2	3
5	2	2	3	1
6	2	3	1	2
7	3	1	3	2
8	3	2	1	3
9	3	3	2	1

Table 4.9 : Finite element results for the first material set (SET1).

Calculation No.	Value of			
	S^*_z/S_{yt}	S^*_θ/S_{yt}	Z_z/d	Z_θ/d
1	0.9266	0.6222	1.2000	1.2000
2	0.92440	0.57220	1.2500	1.2250
3	0.95070	0.65700	1.2500	1.2500
4	0.96428	0.60090	1.3000	1.2500
5	1.00780	0.57270	1.3000	1.2750
6	0.99440	0.63660	1.3000	1.3000
7	1.03600	0.61260	1.3000	1.2500
8	1.0194	0.63270	1.3500	1.3000
9	1.02780	0.6530	1.3500	1.3000

Table 4.10: Mean and standard deviation values for investigated parameters

	Parameter Involved			
	S^*_z/S_{yt}	S^*_θ/S_{yt}	Z_z/d	Z_θ/d
Mean Value	0.97242	0.61567	1.29259	1.26296
Standard deviation	0.05726	0.03097	0.04375	0.03279

Table 4.11: A typical case.

Parameter Involved	Material			Dimensions			Expansion Pressure
	E_e/E_t	E_t/S_{yt}	S_{ye}/S_{yt}	t/d	c/d	D_c/d	P_c/S_{yt}
Value	1.036	933.3	1.30	0.095	0.006	3.0	0.9

Table 4.12 : The results of the finite element obtained by applying the expansion pressure given in Table 4.7 and those of the expansion pressure given by Equation (4.54).

Pressure Used		P_e/S_{yt} (Table 4.7)			P_o/S_{yt} (Eqn. 4.54)		
Material Set	Calculation No.	P^*/S_{yt}	S^*_z/S_{yt}	S^*_θ/S_{yt}	P^*/S_{yt}	S^*_z/S_{yt}	S^*_θ/S_{yt}
SET-1	1	0.0284	0.9266	0.6222	0.0756	0.8657	0.5842
	2	0.0484	0.9244	0.5722	0.1313	0.9591	0.6354
	3	0.1179	0.9507	0.6570	0.1736	0.9504	0.6356
	4	0.0910	0.9638	0.6008	0.0706	0.9511	0.6099
	5	0.0072	1.0078	0.5727	0.1349	0.9994	0.6301
	6	0.0594	0.9944	0.6366	0.1638	1.0312	0.6268
	7	0.0344	1.0360	0.6126	0.0781	1.0665	0.5723
	8	0.1315	1.0194	0.6327	0.1252	1.0472	0.6351
	9	0.0138	1.0278	0.6530	0.1752	0.9522	0.7533
SET-3	1	0.0830	0.8550	0.6045	0.0901	0.8382	0.5939
	2	0.1137	0.9091	0.5704	0.1446	0.9133	0.5996
	3	0.2050	0.8933	0.6489	0.1899	0.9133	0.6539
	4	0.1487	0.9375	0.5946	0.0921	0.9200	0.6160
	5	0.0734	0.9963	0.5788	0.1510	1.0050	0.6226
	6	0.1358	0.9733	0.6436	0.1790	0.9750	0.6500
	7	0.0995	1.0129	0.6101	0.0950	1.0140	0.6104
	8	0.2229	1.0258	0.6399	0.1441	1.0153	0.6520
	9	0.0986	1.0181	0.6614	0.1937	1.0566	0.6273

Table 4.13: Statistical analysis results.

Parameters	P^*/S_{yt}		S^*_z/S_{yt}		S^*_θ/S_{yt}	
Pressure Used	P_c/S_{yt}	P_o/S_{yt}	P_c/S_{yt}	P_o/S_{yt}	P_c/S_{yt}	P_o/S_{yt}
σ	0.09514	0.13377	0.97072	0.97078	0.61736	0.6282
λ	0.06025	0.04144	0.05333	0.06461	0.03102	0.0386
t-Value	2.24087		0.00315		0.93449	
$t(d,\alpha)$	2.03		2.03		2.03	

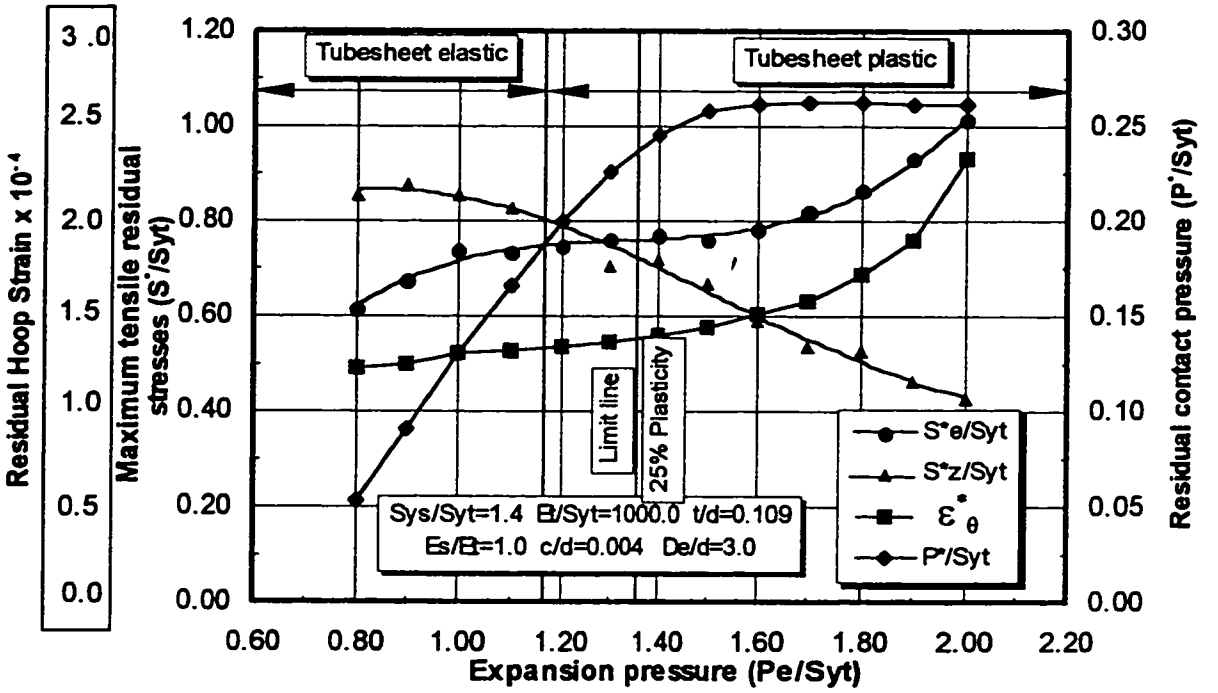


Figure 4.1: Effect of expansion pressure on maximum tensile residual stresses, residual contact pressure, and residual tube enlargement.

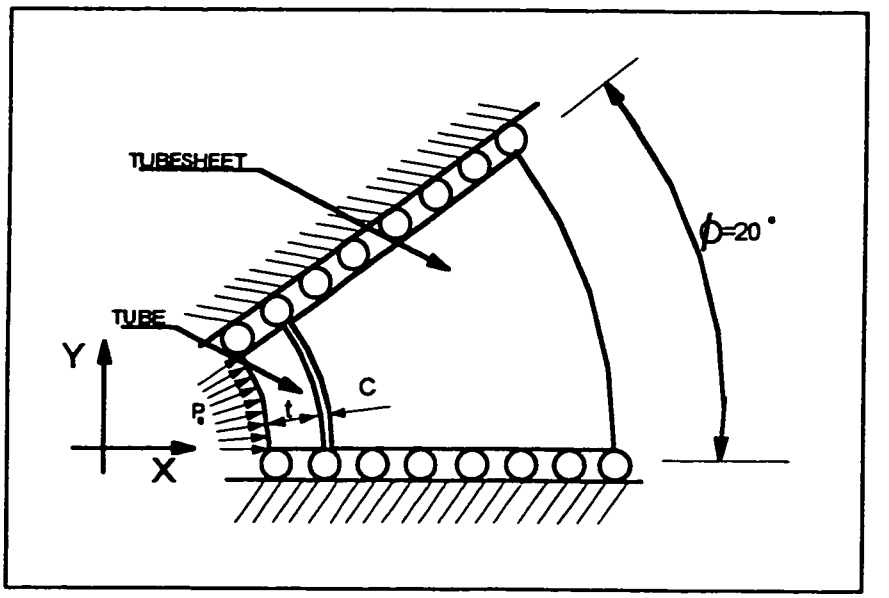


Figure 4.2: Simulation of tube and tubesheet by plain stresss or plane strain models

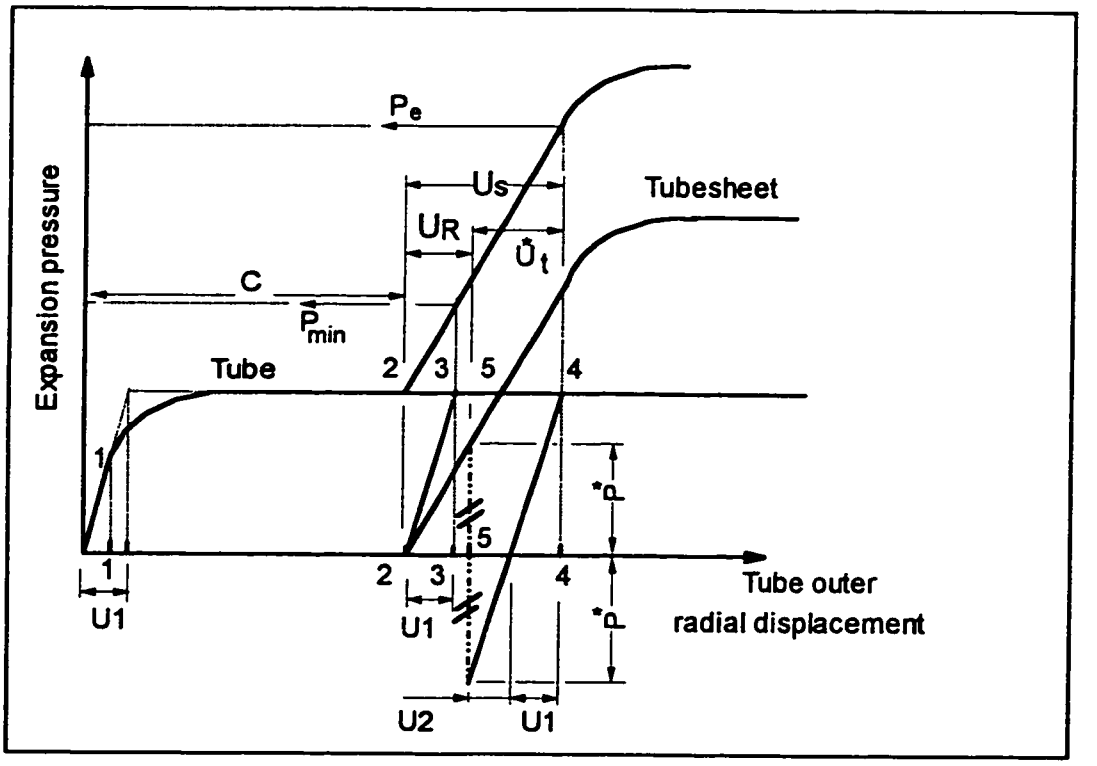


Figure 4.3 : The various steps of creating the expanded joints as represented by the

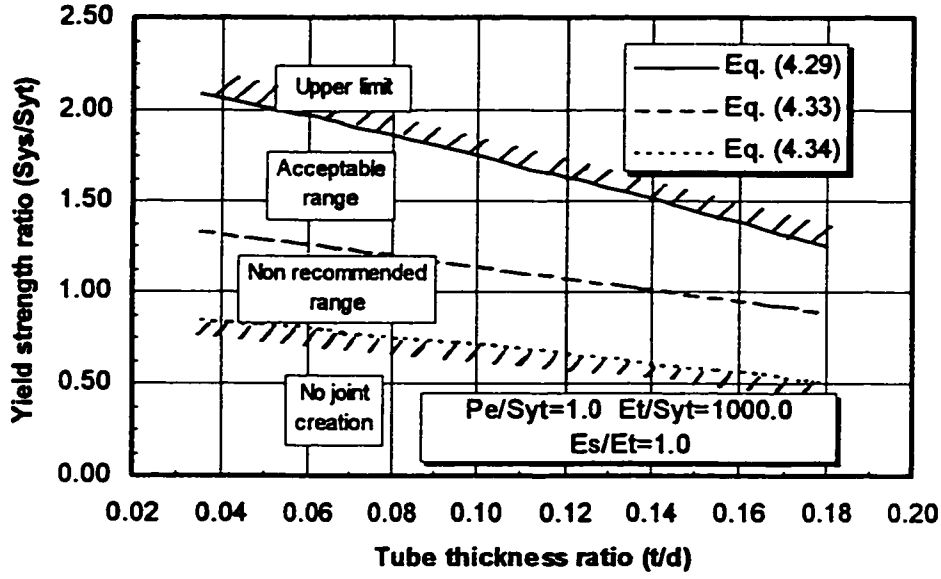


Figure 4.4: Range of yield strength ratio with the possibility of joint creation

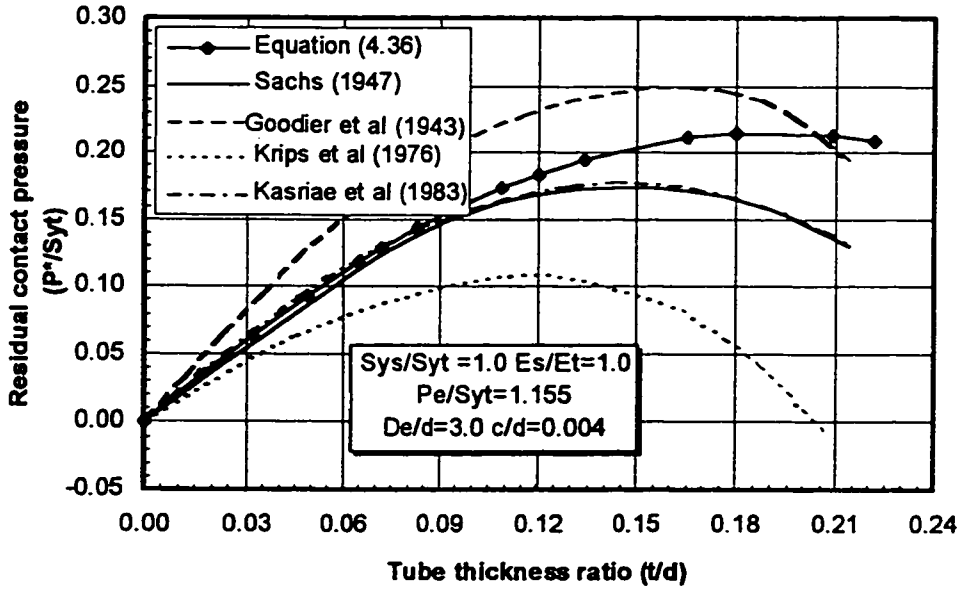


Figure 4.5: Residual contact pressure versus tube thickness ratio; Comparison of the present model with previous theories

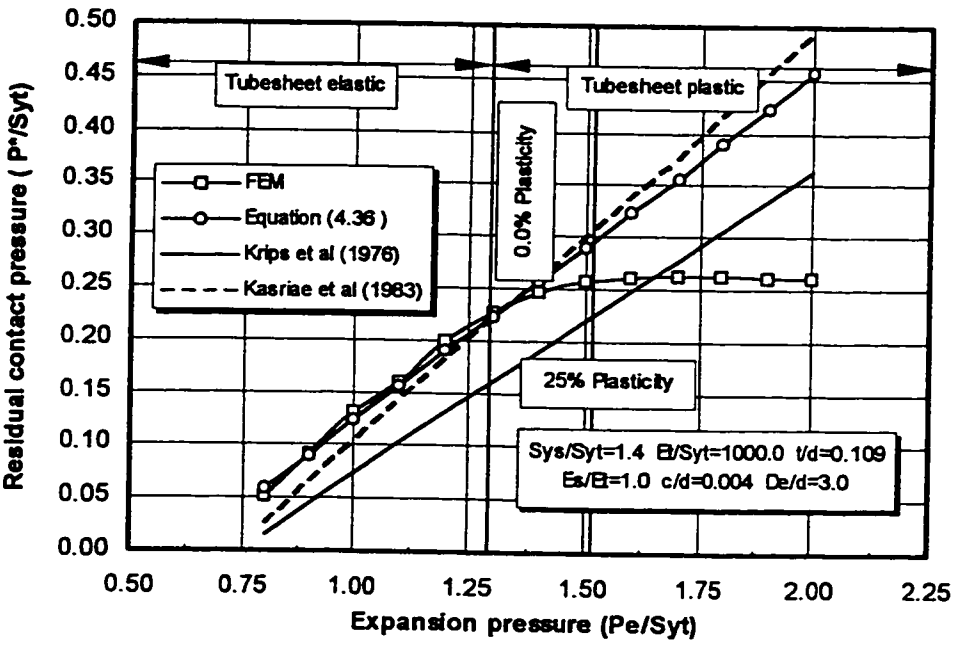


Figure 4.6: Residual contact pressure as obtained by the axisymmetric model, Equation (4.36), and the analytical equations given by Krips et al (1976) and Kasriae et al (1983)

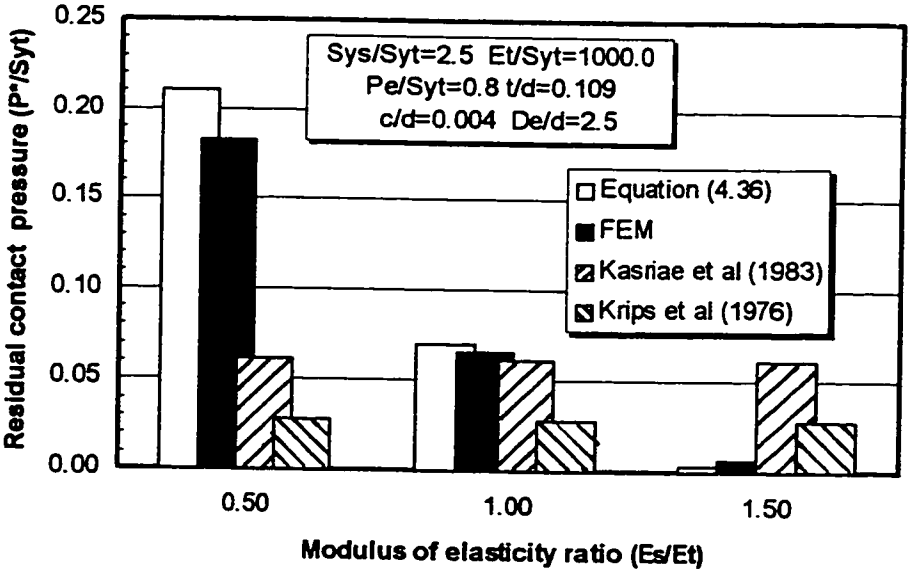


Figure 4.7: Sensitivity of Equation (4.36) to the modulus of elasticity ratio

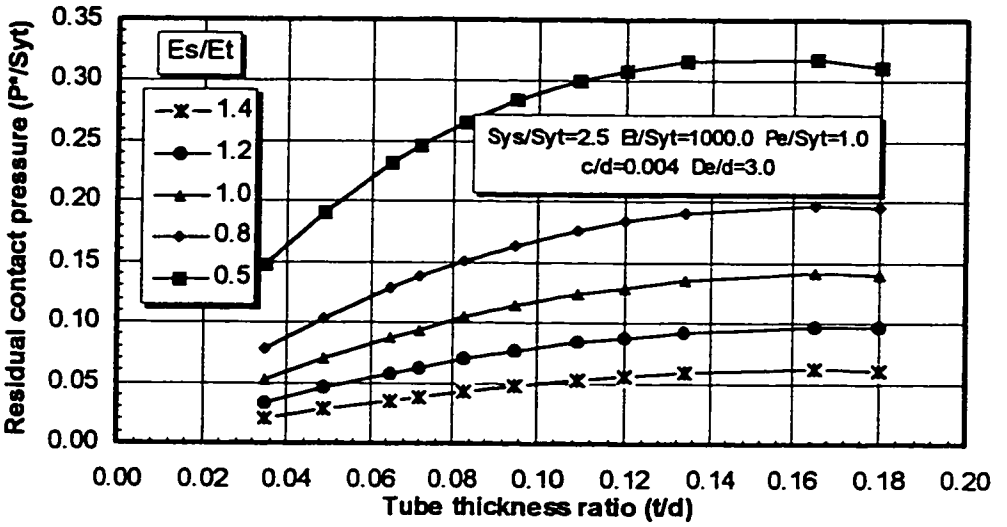


Figure 4.8 : Residual contact pressure as obtained by Equation (4.36) for different tube-to-tubesheet material.

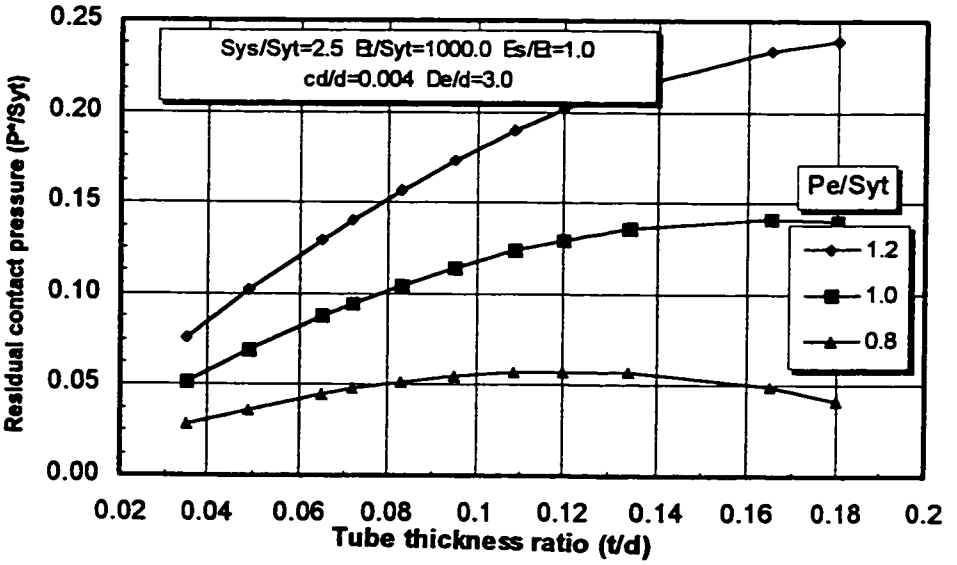


Figure 4.9: Residual contact pressure obtained by Equation (4.36) for different expansion pressure.

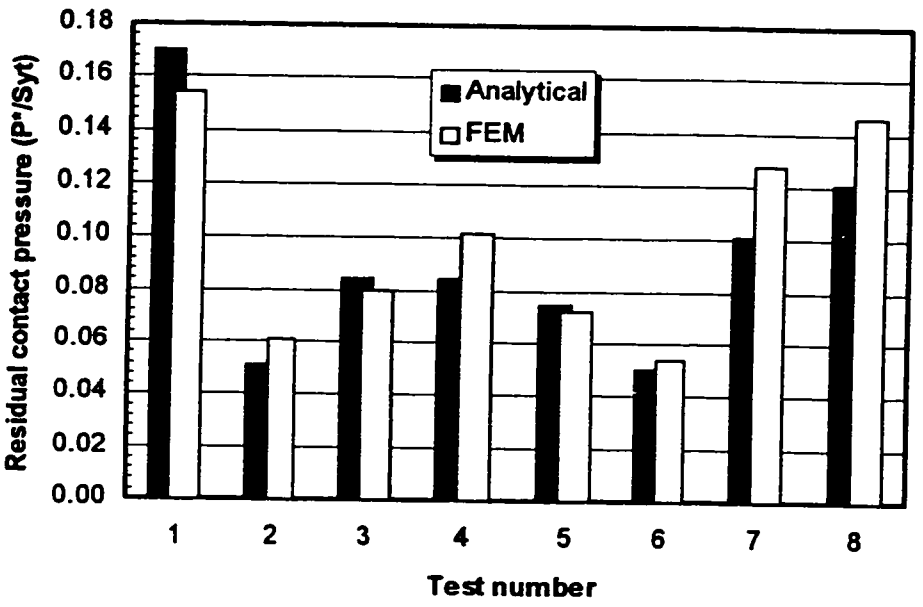


Figure 4.10: Residual contact pressure as calculated by FEM and as given by Equation (4.38)

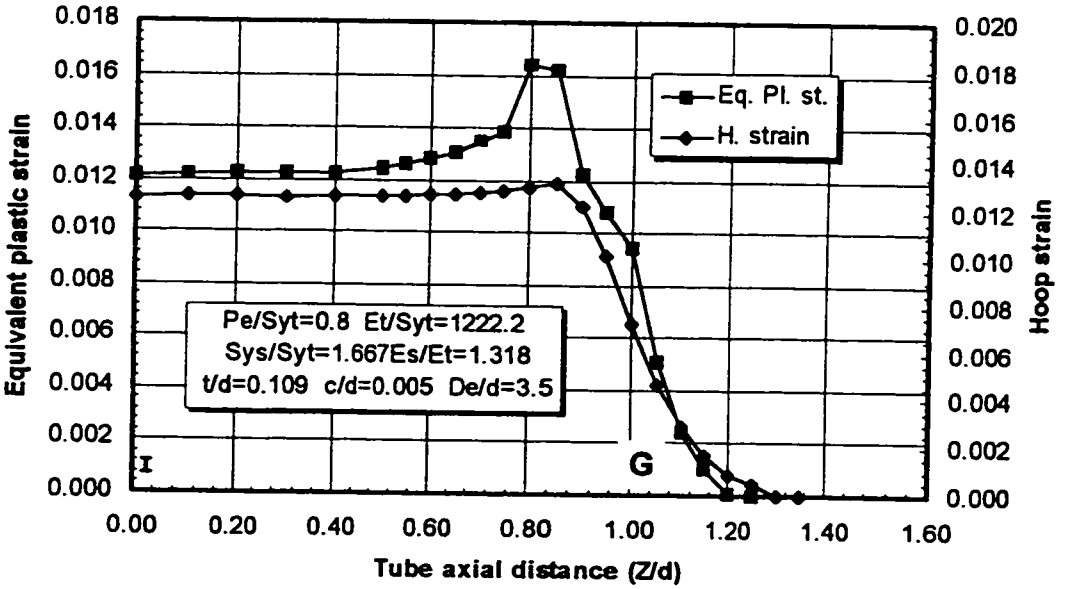


Figure 4.11: Hoop and equivalent plastic strains of tube middle surface at maximum loading

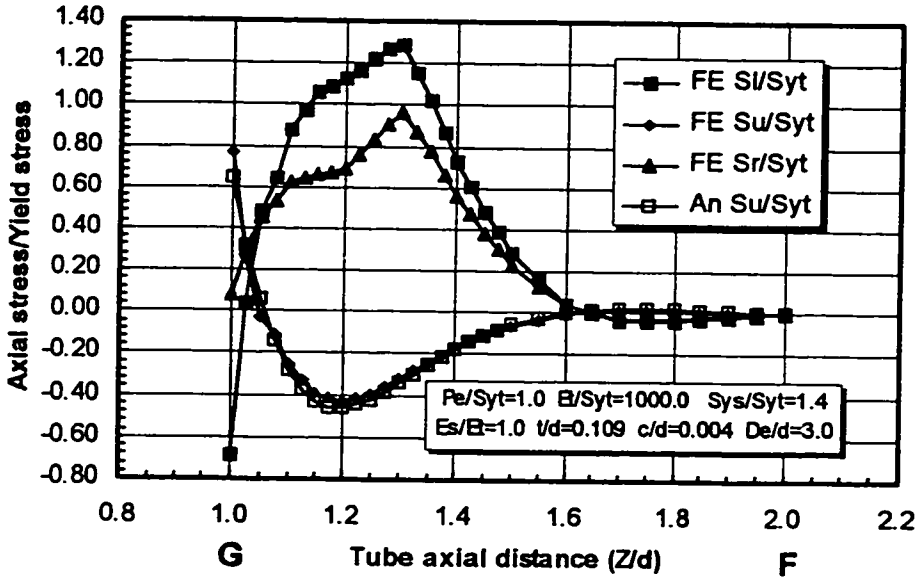


Figure 4.12: Loading, unloading and residual axial stresses as obtained by the finite element method and unloading stresses as calculated by the analytical solution (inner surface)

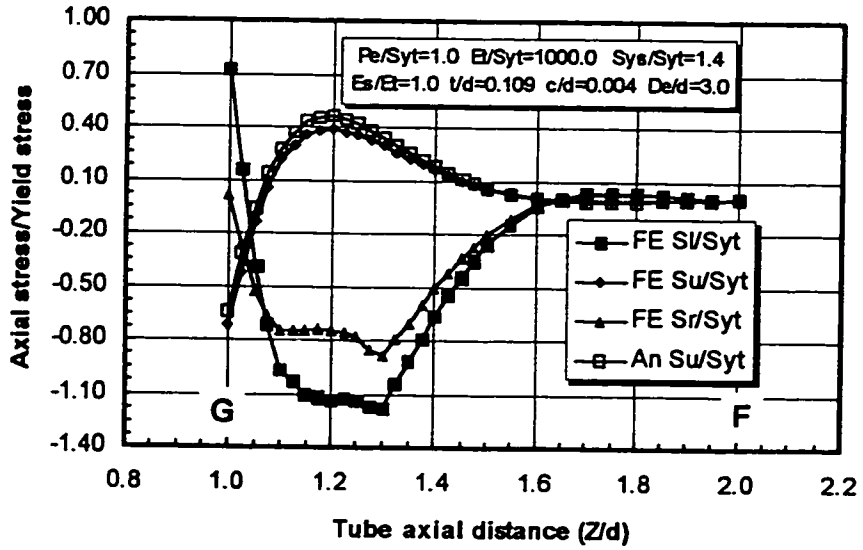


Figure 4.13: Loading, unloading and residual axial stresses as obtained by the finite element method and unloading stresses as calculated by the analytical solution (outer surface)

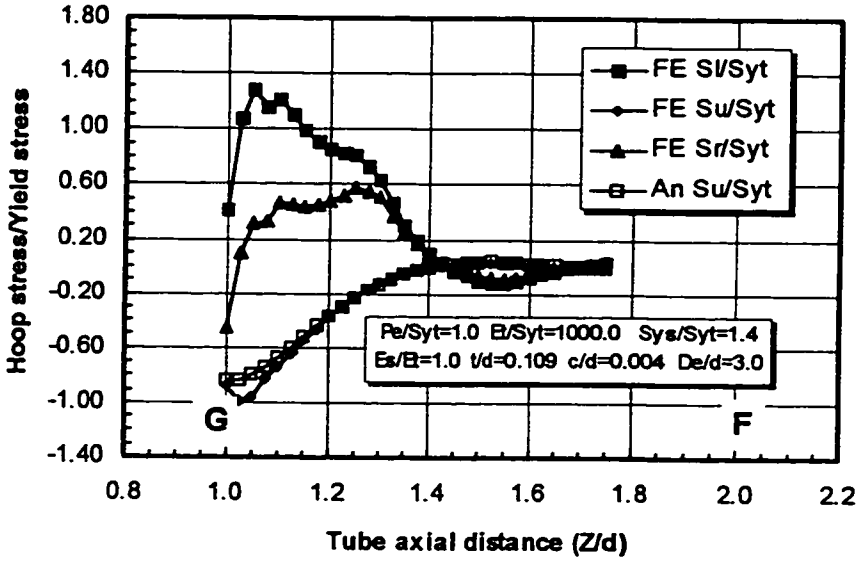


Figure 4.14: Loading, unloading and residual hoop stresses as obtained by the finite element method and unloading stresses as calculated by the analytical solution (inner surface)

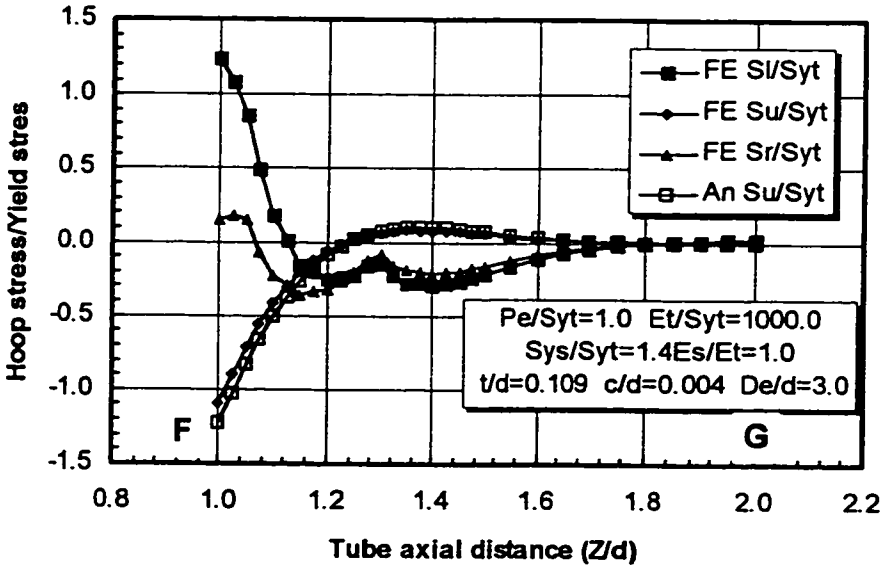


Figure 4.15: Loading, unloading and residual hoop stresses as obtained by the finite element method and unloading stresses as calculated by the analytical solution (outer surface)

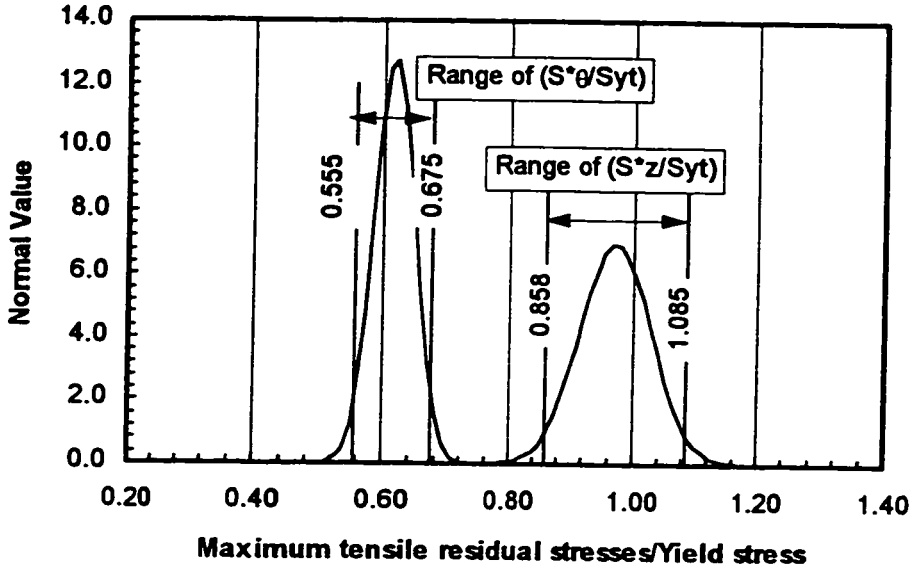


Figure 4.16: Expected range of maximum tensile residual stress values in both axial and circumferential direction

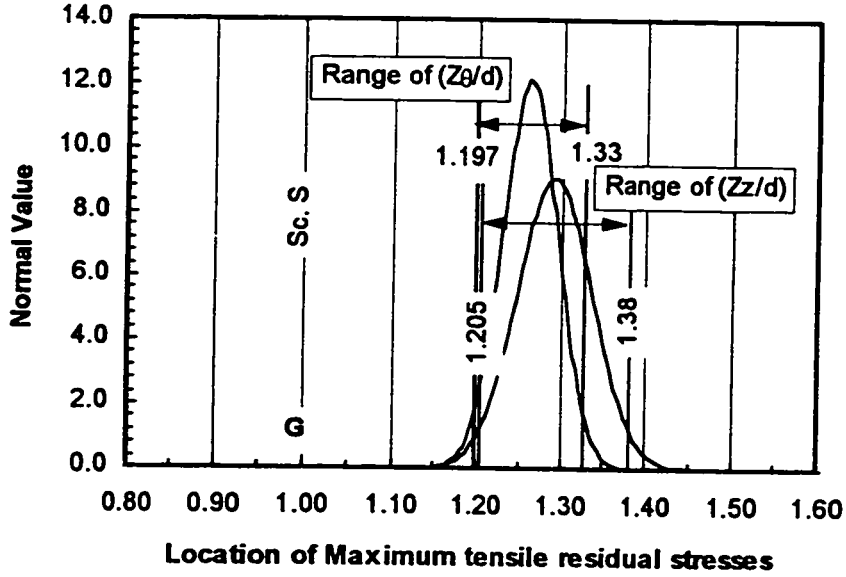


Figure 4.17: Expected axial location for the maximum tensile residual stresses

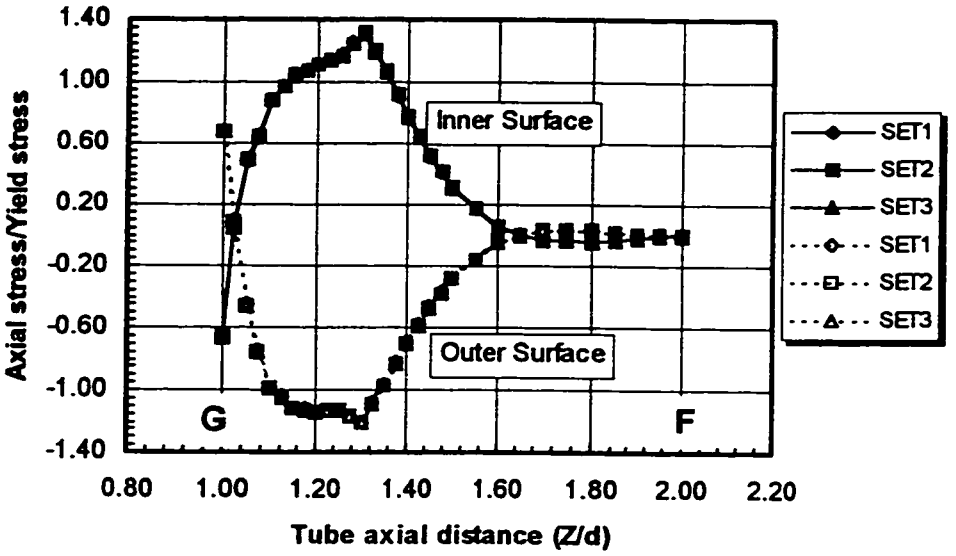


Figure 4.18: Effect of material properties on the loading axial stress

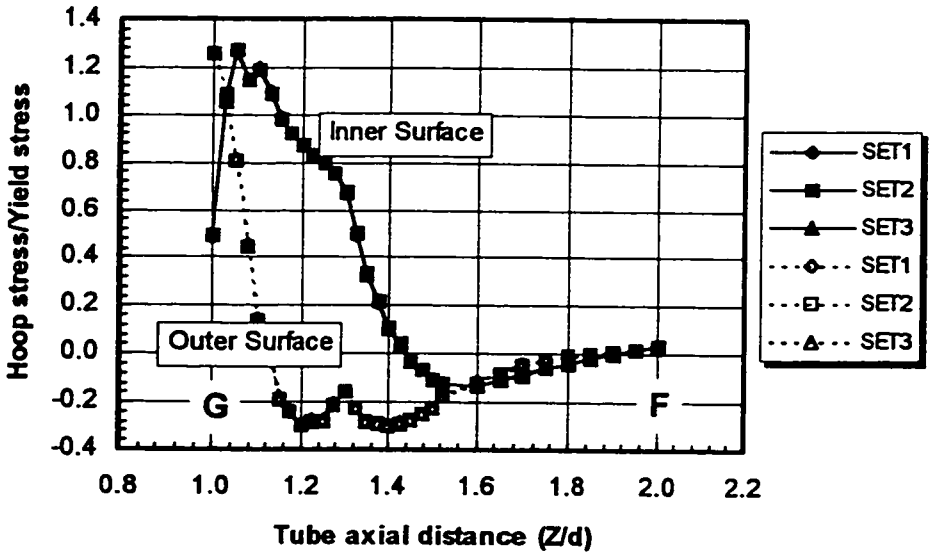


Figure 4.19: Effect of material properties on the loading hoop stress

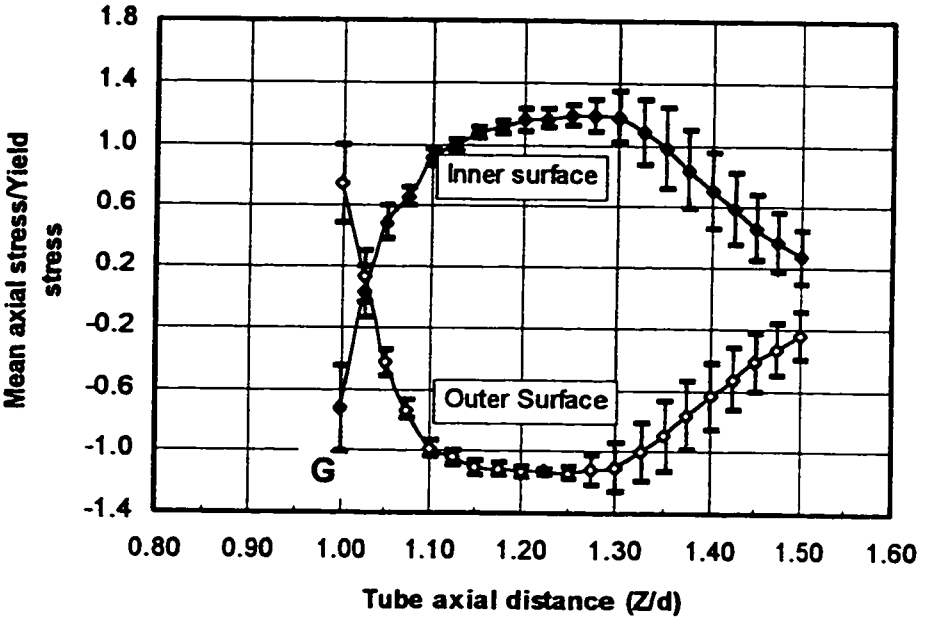


Figure 4.20: Effect of dimensional parameters and the expansion pressure level on loading axial stress

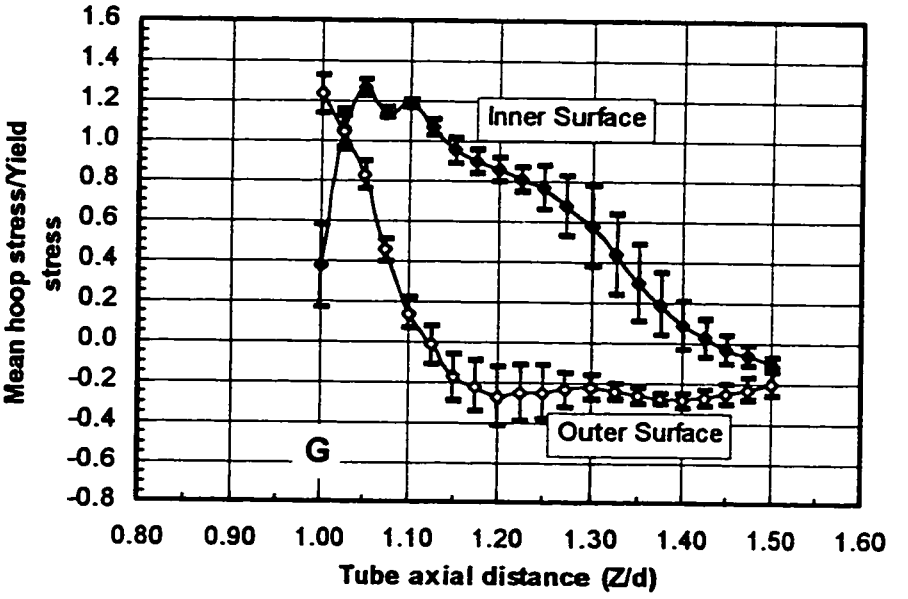


Figure 4.21: Effect of dimensional parameters and the expansion pressure level on loading hoop stress

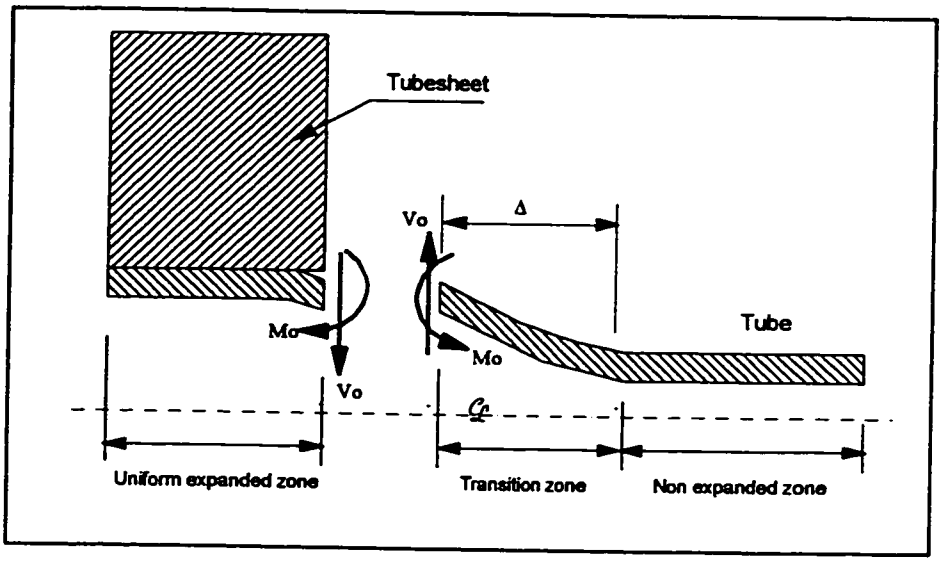


Figure 4.22 : Description of the tube-to-tubesheet joint for analytical analysis

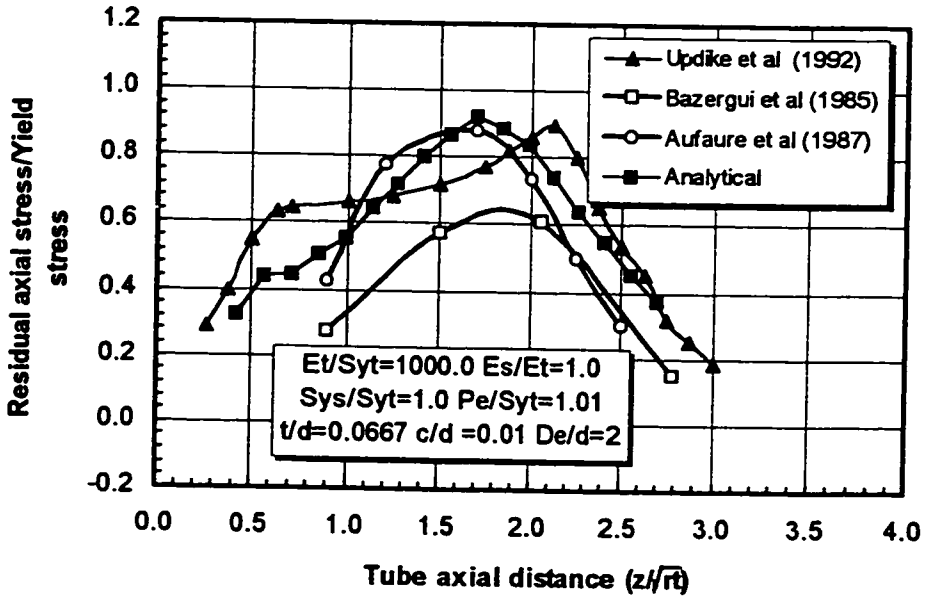


Figure 4.23: Residual axial stress profile as predicted experimentally and as given by the analytical method

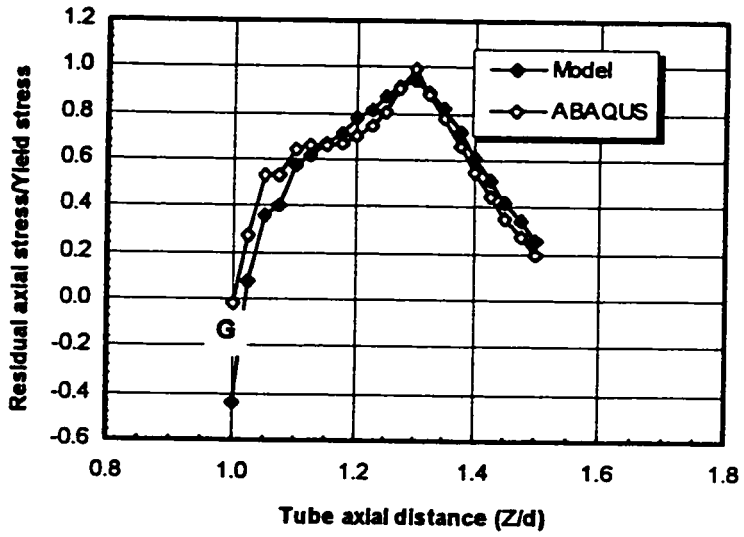


Figure 4.24: Comparison between the residual axial stress on the inner surface as obtained by FE and analytical model

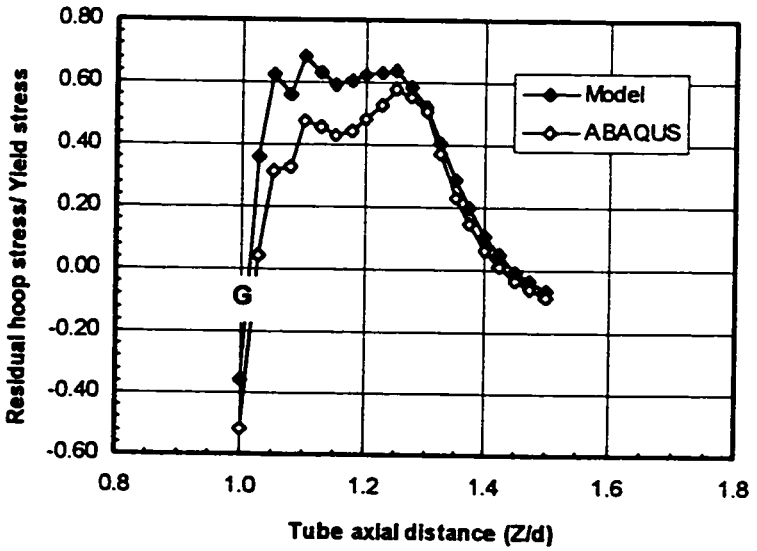


Figure 4.25: Comparison between the residual hoop stress on the inner surface as obtained by FE and analytical model

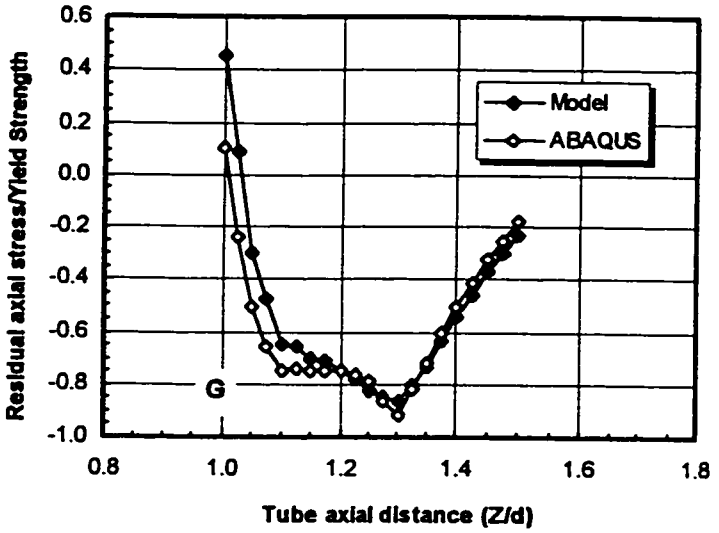


Figure 4.26: Comparison between the residual axial stress on the outer surface as obtained by FE and analytical model

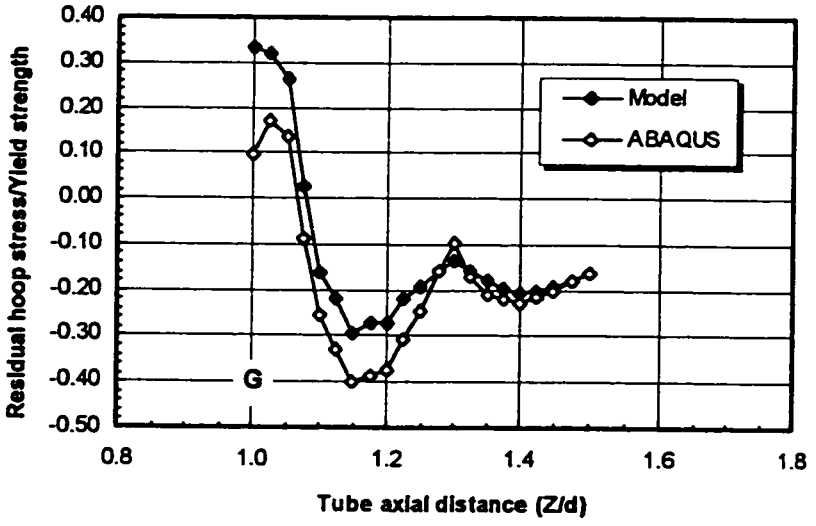


Figure 4.27: Comparison between the residual hoop stress on the outer surface as obtained by FE and analytical model

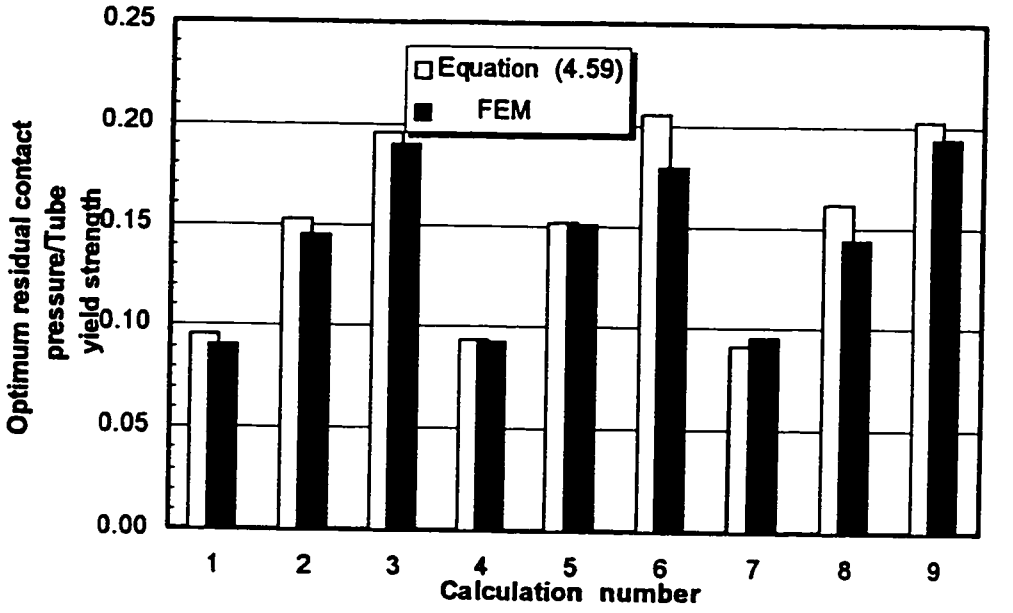


Figure 4.28: Optimum residual contact pressure as obtained by Equation (4.59) and axisymmetric FEM

CHAPTER 5

EFFECT OF FRICTION BETWEEN TUBE AND TUBESHEET ON THE JOINT PULL-OUT STRENGTH

5.1 INTRODUCTION

There is reliable coefficient of friction in many tribology handbooks. However, for our case where the tube and tubesheet are subjected to very high level of deformation, such data are not available in the literature. It would be of great help to measure the friction characteristics between the tube and tubesheet material after expansion. Therefore, an experimental apparatus built by Shirazi-Adl et al (1993) is modified here to determine the friction characteristics between the tube and tubesheet materials. The frictional samples are taken from the expanded region of the tube-to-tubesheet joint where a change in the surface roughness would be expected as a result of the expansion process. In order to validate the reliability of our finite element analysis, the friction measurement is considered essential as input data.

The objective of this chapter is to investigate the joint axial strength by using three

different techniques, namely: analytical, finite element and experimental. No residual stress calculations in the tube transition zone is done in this chapter. Also, the joint axial strength is only evaluated for as-expanded joint that was neither imposed to heat treatment nor subjected to in service mechanical and/or thermal loading. The effect of thermal and mechanical loading on the joint performance will be investigated in Chapter 6 and 7, respectively.

5.2 ANALYTICAL ANALYSIS

When an axial load is applied to the expanded joint, the residual contact pressure will react by an opposite force that is approximated by the average value of the residual contact pressure (P^*) multiplied by the apparent area of contact and the coefficient of friction (f)

$$F = \pi dl \cdot f \cdot P^* \tag{5.1}$$

Where;

F = Joint axial strength (N)

d = Tube outer diameter (mm)

l = Depth of expansion (mm)

f = Locale coefficient of friction

P^* = Average residual contact pressure (MPa)

Since, the tube expansion is a process that causes a high level of plastic deformation in the entire tube wall, and, in some cases, initiates the plastic deformation in the tubesheet, the roughness of the contacting surfaces is, most likely, affected. The analytical solution of joint axial strength presented in Appendix I indicates that the pull-out load depends on various parameters such as the coefficient of friction, tube and tubesheet dimensions, Poisson's ratio, etc. The effect of these parameters can be represented by a single term called effective coefficient of friction. Thus, the previous Equation (5.1) is not adequate for the joint axial strength calculation. Consequently, a modified similar equation taking into account the effect of design partamters must be alternatively introduced. This equation is given by:

$$F = \pi dl \cdot \mu \cdot P^{*} \qquad (5.2)$$

Where (μ) is the effective coefficient of friction which takes into account the change in the tube dimensions due to the applied axial load and, when possible, the modification of the local coefficient of friction as a result of the expansion process.

Two theories have been introduced in the past to calculate the joint axial strength: 1) The simplified 2-D axisymmetric model first proposed by Goodier and Schoessow (1943), which established by using the thick-cylinder theory and by assuming no plastic deformation could occur while pulling or pushing out the tube. 2) The energy minimization principle introduced by Singh and Soler (1984) seeking further development for the first theory.

Appendix I gives more details about these two theories. Based on the final solutions of the joint axial strength, the effective coefficient of friction that can be used in Equation (5.2) is given by:

$$\mu_1 = \frac{1}{l\alpha}\left(1 - e^{-\alpha l}\right) \tag{5.3}$$

$$\mu_2 = \frac{1}{l\beta}\left(e^{\beta l} - 1\right) \tag{5.4}$$

$$\mu_3 = \frac{d_t}{d} f \left(\frac{1+\lambda}{1+\lambda+\nu\phi}\right) \tag{5.5}$$

where the values of α and β are functions of the tube and tubesheet dimensions, while the values of λ and ϕ are functions of the dimensional and material properties of both the tube and tubesheet and the local coefficient of friction (f). The values of each parameter α, β, λ, and ϕ are given in Appendix I.

Also, if the finite element analysis is used to evaluate the joint axial strength, the effective coefficient of friction can be expressed directly as follows:

$$\mu_4 = \frac{F}{\pi d l P^*} \tag{5.6}$$

where both the joint axial strength (F) and the average residual contact pressure (P^*) are calculated by the finite element solution.

It is clear that the joint axial strength is directly proportional to the level of the residual contact pressure that is controlled by many design parameters as detailed in Chapter 4. Also, the dimensions and the elastic moduli of both tube and tubesheet materials have a direct effect on the effective coefficient of friction. In the following, a comparison between the various analytical models used to calculate the joint axial strength will be presented.

In order to observe the difference between the analytical models, the joint axial strength predicted by each model is plotted against the residual contact pressure as shown in Figure 5.1. The calculation is done using Equations (5.1) and (5.2) on the basis of the effective coefficient of friction given by Equations (5.3), (5.4) and (5.5). All models agree that the joint axial strength increases linearly with the residual contact pressure. The rate of the joint pull-out strength is obviously lower than that of the push-out, as show in Figure 5.1 for Equations (5.3) and (5.4), respectively. Equation (5.1) often used to calculate the joint axial strength (Yokell, 1992, and Jawad et al, 1987), may be considered as an averaged relation between different analytical theories predicting the joint pull-out and the push-out strengths.

The variation in the joint strength is attributed to the effective coefficient of friction as given by Figure 5.2. However, within the practical range of the local coefficient of friction

($0.1 \le f \le 0.5$), both the effective and the local coefficients of friction are almost identical, as shown in Figure 5.3 for various modulus of elasticity ratio (E_s/E_J). Therefore, it seems that there is no interaction effect between the modulus of elasticity ratio and the local coefficient of friction on the final value of the effective coefficient of friction (μ). The effect of the tube thickness ratio (t/d) in Equation (5.3) and (5.5) is shown in Figure 5.4. Again, changing the tube thickness ratio has no significant effect on the effective coefficient of friction.

The analytical analysis for the joint axial strength requires the exact value of the local coefficient of friction after expansion which is difficult to obtain. Pulling the tube out from the tubesheet fully damages the tube and tubesheet surface roughness as pictured in Figure 5.5. Consequently, any measurement of the friction coefficient after the pull-out test would be unreliable.

5.3 FRICTIONAL MODEL

As it has been shown in the analytical analysis, the effect of the friction characteristic on the joint axial strength is not attributed to the friction model but to the level of the coefficient of friction used. However, when using the finite element method, both the friction model and coefficient of friction become important. In this section two different frictional laws, friction elastic slip and Coulomb's, are considered. They are schematically represented in Figure 5.6. The first law, friction elastic slip, allows for a relative tangential micro-motion

between the contacting surfaces before sliding occurs.

The law of friction elastic slip may take the following form:

$$\text{if} \quad |F_s| \le f \,.\, |F_n| \quad : \quad 0.0 \le U_t \le \delta \quad ; \quad \text{Stick}$$
$$\text{if} \quad |F_s| > f \,.\, |F_n| \quad : \quad \delta < U_t < \infty \quad ; \quad \text{Slip}$$

Where,

F_s = Shearing force

F_n = Normal force

f = Local static coefficient of friction

U_t = Relative sliding displacement

δ = Critical relative sliding displacement beyond which rigid slipping starts (see Figure 5.6)

The value of (f) and (δ) must be determined experimentally. They depend on the material properties and the roughness of the contacting surfaces and are often independent of the contact loads and the apparent area of contact between the two contacting bodies.

If the critical relative sliding displacement, δ, approaches zero, the previous friction law converts to the Coulomb's law and can be modelled as follows:

$$\text{if} \quad |F_s| \le f \cdot |F_n| \quad : \quad U_t = 0.0 \quad ; \quad \text{Stick}$$
$$\text{if} \quad |F_s| > f \cdot |F_n| \quad : \quad 0.0 < U_t < \infty \quad ; \quad \text{Slip}$$

Generally, for metal to metal contact, the value of δ is in the order of microns and consequently the Coulomb's friction law may be applied with good accuracy.

5.4 FINITE ELEMENT ANALYSIS

As mentioned earlier, the literature survey indicates that the finite element method has not been used to evaluate the joint axial strength of tube-to-tubesheet joint. Indeed, the problem related to joint axial strength cannot be formulated using plane stress/strain models. 3-D or axisymmetric models, can be used to evaluate secondary side pull-out, secondary side push-in and primary side push-out strengths, as shown schematically in Figures 5.7.

Regarding the appropriate friction law to be used (Coulomb's law or elastic slip model) for this particular problem, the finite element verification indicates that there is no significant difference between the two models as long as the critical displacement (δ) related to elastic slip model, is kept below 0.005 times the average length of the contact elements. This limit of the critical displacement corresponds to default value of allowable elastic slip as set in ABAQUS (1995). Generally, as it will be confirmed experimentally, Coulomb's friction law is the right model by which the tube-to-tubesheet joint axial strength can be determined

numerically. However, the zero relative displacement condition cannot be satisfied numerically. Instead, the sliding between the tube and tubesheet is initiated at a very low level of relative displacement at which the shearing force unlocks all the sticking points between the tube and tubesheet contacting surfaces.

In order to demonstrate the procedure followed while evaluating the joint axial strength using the finite element model, the material and the dimensional data given in Tables 5.1 and 5.2 are considered where typical values of coefficient of friction and expansion pressure have been assumed. The build-up condition together with the related results (P^*, S^*_z, S^*_θ, and residual strains) obtained from the expansion process are calculated using the axisymmetric model of Figure 3.2. Up to this point, the finite element model is applied without modifying the kinematic boundary conditions applied on the tube and tubesheet. In order to calculate the joint axial strength, the boundary conditions imposed to the tube must be eliminated. As a result, the tube axial load should be resisted by the shearing force between the tube and tubesheet. Since the joint is created, eliminating the boundary conditions of the tube has no effect on the numerical stablitiy, and that of the tubesheet is adequate to provide the numerical stability for the whole model including the tube and the tubesheet. Thus, the modification of the kinematic boundary condition might be achieved in a nested step between the first two steps when applying and removing the expansion pressure, and the last step when performing the axial strength calculation.

After the kinematic boundary condition applied to the tube is removed, an axial load is then applied to the tube wall at the free end in order to pull out the tube from the sleeve. The load is applied incrementally up to a certain level at which the tube should exhibit rigid body motion in the axial direction.

At the last loading increment, the shearing and the normal tractions at the interference between the tube and the sleeve are printed out for each integration point on the contact elements used, as listed in Table 5.3. The ratio between the shearing and the normal tractions is also calculated and found equal to the local coefficient of friction (f = 0.35) that was specified in the interference input data. In addition, at the slipping instant, the value of the axial load as obtained by the finite element model is also confirmed with following relation:

$$\bar{F} = \frac{1}{\pi dl . S_{yt}} \int S_s \, . \, dA$$

and the relation between the normal and shearing tractions is satisfying Coulomb's friction law:

$$|S_s| = f \, . \, |S_n|$$

where;

S_n Normal traction at initial moment of sliding

S_s Shearing traction at initial moment of sliding

f Local coefficient of friction

A Apparent area of contact

l Depth of expansion

Therefore, it has been confirmed that the finite element model has the capability to calculate the joint axial strength which is equal to the level of the axial load at the last loading increment. The finite element model will be also verified experimentally in section 5.4.

Also, for the same typical case being investigated, the relation between the shearing force and the corresponding relative micro-motion of the tube is presented in Figure 5.8 where $A_o = \pi d\, l$. Relative sliding begins at a lower level of the applied load than the joint axial strength. As the axial load increases, the tube micro-motion increases up to certain level beyond which full sliding occurs and the joint is considered broken.

5.4.1 Effect of Friction Model

Although, a different pull-out loads for different friction models are not expected, a finite element investigation with both models is performed for comparison purpose. Table 5.4 summarizes the axisymmetric finite element calculations for the pull-out strength evaluated on the basis of the two different friction models that may be used in this problem. The material and the dimensional data of Tables 5.1 and 5.2 are used for this calculation. For the elastic slip model, the critical relative displacement is taken 8.5 μm, which is equal to the

average length of the contact element times 0.005. As shown in Table 5. 4, there is a relatively small difference between the two calculated joint axial strengths.

5.4.2 Effect of Boundary Condition

In this subsection, the effect of different arbitrarily combinations of boundary conditions on the pull-out strength is investigated by using the axisymmetric finite element model. Of course, all the prior boundary constrains applied to the tube should be removed before applying the axial load on the joint, since the free axial displacements of all nodes related to the tube must be conditioned by the level of the axial load. Once the tube is expanded against the tubesheet, the tube boundary condition at (Z = 0) is removed from the numerical model using an additional step taking into account all the stresses, contact pressure, strains, etc... of the as-expanded joint. Meanwhile, various new boundary conditions could be applied on the tubesheet as shown in Figure 5.9. For the same typical case presented above, the finite element analysis is performed in order to point out the interaction between the level of the calculated joint strength and the type of boundary conditions applied. The five different boundary conditions illustrated in Figure 5.9 were tested. (BOUND-1) of this figure is used as a reference case and the percentage difference in the joint strength when using other cases is evaluated with respect to that of the reference case and given by:

$$\text{Percentage diff.} = \frac{\text{Calculated joint strength - that of BOUND-1}}{\text{that of BOUND-1}} \times 100$$

The results presented in Table 5.5 show a negligible interaction effect between the boundary conditions used and the joint axial strength. Thus, it is concluded that the kinematic boundary conditions applied on the sleeve nodes in the finite element model, has no important effect on the calculation of the pull-out (F_1), primary side push-out (F_2) or secondary side push-in (F_3) loads. Therefore, the boundary conditions of the reference case (BOUND-1) will be adopted in the following analyses.

5.4.3 Comparison between 3-D and axisymmetric FEM

The 3-D and axisymmetric finite element models of Figures 3.11 and 3.2, respectively, are used for the comparisons. The boundary conditions, loading and unloading are explained in Chapter 3 for the expansion process. The four cases given in Tables 3.1 and 3.4, are considered here. Coulomb's friction law is used with a typical value of the coefficient of friction ($f = 0.35$). Once the expansion pressure is fully relieved from the joint, the boundary kinematic constrain of the tube at $Z=0$ is removed, and thereby the tube axial motion is prevented by the effect of the shearing resistance between the tube and the tubesheet. This is done for both the 3-D and axisymmetric models. The axial load was applied incrementally on the tube wall in three different ways as shown in Figure 5.7.

The comparison between the 3-D and the axisymmetric finite element solution has been performed on the bases of the following parameters:

1- Pull-out load (F_1)

3- Primary side (Pr. S.) push-out load (F_2)

2- Secondary side (Sc. S.) push-in load (F_3)

4- CPU (Centre Processing Time) on IBM 6000 workstation

The results of the 3-D and axisymmetric finite element analysis for the four cases considered are summarized in Table 5.6. The relatively low CPU time consumed by the axisymmetric model compared to the 3-D model, is achieved without compromising the accuracy of the results, since a good agreement in the prediction of the joint axial strengths is obtained. Of course, this agreement between the solutions is still dependent on the proper value of the equivalent sleeve diameter (D_e).

5.4.4 Details Regarding the Axisymmetric Finite Element Analysis

The purpose here is to perform more parametric studies by involving different levels of dimensional, material parameters and expansion pressure and by following the procedure introduced earlier. In fact, all design parameter could influence the joint axial strength because they do have some effects on the residual contact pressure set up during the expansion process as detailed in Chapter 4. The material set given in Table 5.1 with the dimensions and the expansion pressure levels of Table 5.7 have been typically selected. Also, the orthogonal design method, as given in Table 4.8, is used to select the optimum combination of the

parameters involved in the calculations.

The final results of the finite element analysis are summarised in Table 5.8. Also included in the same table, the joint axial strength that is calculated using Equation (5.1) based on the residual contact pressure as provided by the axisymmetric finite element model. The joint axial strength levels are also presented graphically as a function of the residual contact pressure in Figure 5.10, for the pull-out, primary side push-out, secondary side push-in loads and that given by the Equation (5.1) is presented. The symbols on this figure refer to the values as calculated by the finite element, while the solid and dashed lines show the best fit between the results. The push-out load is shown to be remarkably greater than the pull-out load. Yet, pushing the tube from either the primary or secondary sides requires approximately the same breaking load. Equation (5.1) predicts in all cases the highest joint axial strength and disagrees with the numerical results of pull-out strength. As such, a statistical analysis should favourably explain the joint behaviour under the effect of the axial loading and compare between the different levels the joint strength.

First, the *t*-test, previously used in Chapter 4, is applied between the different loads calculated by the finite elements method. The results for this test are given in Table 5.9. For a 5% level of confidence with d=16, the value of $t(d,\alpha)$ is equal to 1.83 as given by Dally (1992). Since $t(d,\alpha)$ is greater than the *t*-value, it can be concluded with a 95% level of confidence that there is no significant difference between any of the joint axial strengths.

However, if the level of the confidence is reduced to 65%, $t(d, \alpha)$ becomes 0.3975 reflecting a lower level than that of the t-value comparing the means of primary side push-out and pull-out loads. Thus, it can be concluded that the primary side-push-out load is higher than the pull-out load by almost 18.4% based on the mean values. The difference between the push-out loads measured from either the secondary or the primary side is still attributed to random variations even with the lowest level of confidence available. It has thus been decided to perform an additional statistical procedure for this problem.

Let us examine the level of the interference contact pressure at which the sliding is initiated versus the initial level of the residual contact pressure. For each study case, the interference contact pressure related to the sliding instant is averaged at the last increment of the axial loading step. For the most conservative case, this level of contact pressure should be equal to the initial residual contact pressure set up by the expansion process. A linear regression analysis is performed between the initial residual contact pressure and that calculated according to the joint axial strength. Using linear regression, the relationship between the two levels of the interference pressure is closely represented:

$$VARn = \alpha + \beta \cdot VAR1 \tag{5.7}$$

where

VARn	Value of the contact pressure at the moment of sliding
VAR1	Initial residual contact pressure

β	Slope of Equation (5.7)
α	Intercept of Equation (5.7)

VARn represents VAR2, VAR3 and VAR4 which are the values of the interference contact pressures calculated on the basis of the pull-out, primary side push-out and secondary side push-in loads, respectively. The slope β and the intercept α in Equation (5.7) are selected in order to minimize the sum squared error resulting from fitting a straight line through the correlated variables. For the most conservative case, the values of β and α, should be equal to unity and zero, respectively. The soundness of the regression model can be evaluated by a correlation coefficient (R) of positive sign with a maximum value of 1.0. If $R \geq 0.8$, then most of the variation in VARn has been accounted for in terms of VAR1, and the relationship between the two variables is thus reliable. The correlation analysis is performed by taking the initial residual contact pressure as the independent variable (VAR1) and those calculated at the sliding instant (VARn) as a response. Table 5.10 summarizes the results of the linear regression analysis.

By first considering the interference contact pressure calculated on the basis of the pull-out strength (VAR2), a linear relationship between VAR2 and the initial residual contact pressure (VAR1) with almost zero intercept is obtained, Figure 5.11. But, as would be expected, slope (β) is only 0.65. This explains why the pull-out strength is much lower than that calculated by the Equation (5.1). A reduction in contact pressure while pulling out the

tube reflects a reduced joint axial strength. In addition, a good correlation coefficient is given for the last two variables VAR3 and VAR4 with almost zero intercept (α). Moreover, Figures 5.12 and 5.13 show that slope β is equal to about 0.8, thus, the push-out load confirmed to be slightly lower than that provided by the simple form Equation (5.1) and higher than the pull-out one.

The variation in the joint axial strength is caused by a number of factors. It seems that prior to initiating the sliding motion, any axial load acting on the tube may slightly reduce the initial residual contact pressure. Additional reduction occurs when the load elongates the tube and consequently reduces its external diameter and causes the reduction in the contact pressure set up by the expansion process. The push-out loads on the other hand enlarges the tube outer diameter and causes an increase in the initial residual contact pressure. However, the linear regression analysis strongly indicates that, even with a push-out load, the interference contact pressure at which the tube starts to slip is always lower than that set up by the expansion process. The push-out strength calculated by the finite element model is thus slightly lower than that provided by Equation (5.1). It can be concluded that, the joint strength is not totally dependent on the initial residual contact pressure but rather to the level of the interference contact pressure at which the tube starts to slip and which in turn depends on the following parameters: 1) modulus of elasticity of the tube and tubesheet, 2) Poisson's ratio of the tube and tubesheet, 3) tube thickness ratio, 4) sleeve equivalent diameter and 5) the applied load direction. The effect of these parameters was considered beyond the scope

of this research work.

5.5 FINITE ELEMENT CALCULATION Vs. EXPERIMENTAL MEASUREMENT

This section describes an experimental and finite element procedures for a number of limited design cases selected to verify the axisymmetric finite element solution for the joint axial strength. The experimental tests are conducted on idealized tube-to-tubesheet joints assembled according to a standard manufacturing process. The experimental tests are for the as-expanded condition only (i.e. not subjected to either heat treatment or cold working).

Because the number of specimens had to be limited, only two design parameters were considered: 1) the level of the expansion pressure and 2) the initial radial clearance. Also, only one set of commonly used tube and tubesheet materials was considered.

5.5.1 Experimental Determination of Friction Properties

The friction characteristics previously used to describe the interference parameters related to the finite element model was so far arbitrarily assumed. In order to minimize the discrepancies between the finite element and experiment joint strength predictions, it is preferable to determine experimentally the real coefficient of friction. An existing experimental apparatus was modified to perform these tests using specimens taken from the

expanded zone of tube-to-tubesheet joint.

5.5.1.1 Specimens

The tube and tubesheet materials chosen for the experimental study are the Inconel 690 and the (SA-508 Class 3) steels. They were obtained from Babcock and Wilcox International division (Cambridge, Ontario). The specimens are taken from the expanded zone of tube-to-tubesheet joint made from straight tube expanded in a short sleeve simulating the tubesheet. Table 5.11 provides the dimensions for both the tube and the sleeve before expansion. The sleeve inner surface is finished to meet with commercial specification. The value of CLA (Central Line Average) is measured for the tube outer surface and the sleeve inner bore by using a surf-indicator (Clevite Brush), and it was 0.20 and 4.0 μm for the tube and sleeve, respectively. The tube is expanded into the sleeve by a commercial hydraulic expender using an expansion pressure of 225.6 ± 3.5 MPa. In order to avoid any damage to the meeting surfaces in the expanded zone from which the specimens for the friction test will be taken, the joint is removed by cutting both the tube and the sleeve longitudinally at two diametrally opposite locations. The cutting is carried out by a milling machine. After removal of the tube from the sleeve, the roughness of both the tube outer surface and the sleeve hole are measured again at the intermediate region of the expanded zone. The fact that the CLA have changed to 0.38 and 2.54 ± 0.002 μm for the tube and sleeve surfaces, respectively, reflects a change in the coefficient of friction as a result of the expansion process.

Each half of the sleeve is then cut longitudinally into three pieces 12.0 mm thick each. Two tubesheet specimens of 12 mm length each are cut from the intermediate region of the sleeve as pictured in Figure 5.14. Three values of the apparent area of contact are considered (12x10, 12x8 and 12x4 mm^2). The apparent area of contact was reduced by grooving the specimens and keeping their length unchanged (12 mm) as shown in Figure 5.15 thus preventing the system instability during the tests.

The 25 mm long tube specimens are cut out from each half of the tube in the expanded region, Figures 5.14 and 5.15. A special attention was paid to the tube and sleeve contacting surfaces during the cutting and machining processes in order to avoid any damage to their roughness

5.5.1.2 Measurement and instrumentation

The friction experimental set up was developed on the basis of an existing apparatus previously used to measure the friction between tibial bone and porous-surfaced metal plates (Shirazi-Adl et al, 1993), Figure 5.16. Figure 5.17 shows a diagram of the main components. Two tube specimens (1) are set in parallel and strongly attached to the tube holder which is fixed to the apparatus support (2) that is tied to the table carrying the apparatus. Two parallel tubesheet specimens (3) are attached to a holder which is firmly fixed to a movable frame (4) over which the normal load is applied by using a dead weight (5). The tangential load applied

to the movable frame is measured by a load gauging cell (6). It can be gradually increased through a linear spring (7) placed between the load cell and the 3-D arm (8), by which the vertical and the horizonal alignments of the load line of action can be visually adjusted. Thereby, the shearing force can be applied, as close as possible, tangent to the interference between the tube and the sleeve specimens. The relative tangential micro-motion between the tube and tubesheet specimens is precisely measured by a displacement transducer (9) which is firmly attached to the support (2). The tip of the transducer is placed on the movable frame (4) and as close as possible to the interface plane between the specimens (see Fig. 5.18). The accuracy of the load cell and the displacement measurement device are about 0.25 N and 4.2 μm, respectively. The tests are performed by controlling the load level that is scaled together with the relative displacement and recorded on a X-Y plotter (10).

The system used is simple, precise and does not introduce any additional shearing force to that resulting from the friction effect and the normal load created between the tube and tubesheet specimens. Also, the apparatus has no installed bearings which could disturb the measurement to anonymous extent. The simplicity of the apparatus makes the range of the loads and the configuration of the contacting areas restrained. Thus, the system cannot be used to measure the frictional properties between single pair of tube and tubesheet specimens because of the circular surfaces of the specimens. Stabilizing the weight over a single pair of specimens having circular contacting surfaces is almost impossible in the available set-up. Therefore, two pairs of specimens are tested simultaneously in order to

provide some stability to the system, as shown in Figure 5.19. The second limitation that one is faced with, is the maximum weight that can be practically applied which is about 200 N.

The normal load ranged between 50 to 200 N including the weights of the specimen, the holders, and the moveable frame. It is applied by placing the appropriate mass on the upper surface of the movable frame. The maximum value of the applied normal load together with the smallest available area are providing a peak level of interference contact pressure of 3.5 MPa. However, the axisymmetric finite element model provided a maximum residual contact pressure, that would exists in the tube-to-tubesheet joint samples, of about 20 MPa. In spite of this difference, no variation in the coefficient of friction measured within this range of the contact pressure, would be expected, based on tribology principles, Halling (1975).

For a given normal load and interference area, a pure tangential load is slowly applied to initiate the sliding of the tubesheet specimen over the tube. In the mean time, the nonlinear displacement-load history is directly recorded for further investigations. In order to confirm the results, each tests is repeated at list three times under the same loading conditions.

5.5.1.3 Results and discussion

Figure 5.20 illustrates typically the force-displacement frictional relation (F_s-U_t). For all the cases considered, similar behaviour was observed: A very small initial relative

displacement ($\leq$ 10 μm) following by full sliding. This frictional behaviour characteristic satisfies Coulomb's friction law. The coefficient of friction ($f = F_t/F_n$) is plotted against the average normal contact stress (S_n), Figure 5.21. Each symbol in Figure 5.21 represents an average value of the repeated tests. The overall mean value of $f=0.1375 \pm 0.004$ is based on twelve different levels for the normal interface pressure. The results of this study indicate that the coefficient of friction (f) is not much affected by the normal interference stress (S_n). Also, as would be expected, the measured level of the displacement (δ) is very small in all friction tests. The experimental measurements indicate that the maximum relative displacement at which sliding starts is always of order 10 ± 4.2 μm. The mean level of the coefficient of friction ($f = 0.1375 \pm 0.004$) together with the Coulomb's friction law are thus selected to define the characteristic of the frictional interface between the tube and sleeve used in the finite element analysis.

5.5.2 Experimental Determination of Pull-out Strength

Four pull-out samples were provided by Babcock and Wilcox (B&W) and manufactured from a tube and tubesheet materials currently used in industrial applications (Inconel 690 and SA-508 Class 3, respectively). The material properties as provided by (B&W) are listed in Table 5.12. The experimental pull-out test is achieved by applying a concentrated load in the tube centre while holding the sleeve. In order to determine the level of the pull-out load precisely, the relative displacement between the tube and the sleeve is also

measured.

5.5.2.1 Tube-to-tubesheet joint samples

The samples consist of a straight tube (approximately 150 mm long) hydraulically expanded into a shorter tubesheet simulation sleeve (approximately 80 mm), Figure 5.22. The sleeve outer diameter has been selected in such a way that its radial stiffness is approximately equivalent to that of the central ligament of a tubesheet having a hole pitch of 25 mm. Prior to the expansion, the sleeve hole was machined to provide the required initial clearance. Because of the variation of hole diameter that could be developed by the machining process, the internal diameter of the sleeve is measured from both sides (Pr. S. D_i and Sc. S. D_i). Table 5. 13 lists the tube and sleeve dimensions measured before expansion, as well as the level of the expansion pressure that was used to create the joint.

In order to perform the pull-out testing, a short steel cylinder (locking cylinder, Fig. 5.23) is machined to be inserted into the tube end on which the pull-out load is applied. A conical centring hole holds a high strength steel ball (8.5 mm) through which the pull-out load will be applied. Figure 5.24 is a picture of the test assembly components. To avoid high temperature exposure through welding (see Appendix III), a room temperature high performance adhesive (Loctite, RC/680) was used instead whose bonding strength of about 100 kN far exceeded the maximum expected pull-out breaking load.

5.5.2.2 Experimental rig and procedure

For the pull-out load measurements, a simple experimental set-up was used on an MTS testing machine as shown in Figures 5.25 and 5.26. The tube end is inserted inside a thick walled steel cylinder (1) that also holds the lower part of the sleeve (2). The cylinder (1) is supported by the MTS cross arm (3) to which is connected a displacement cell (4). A steel rod (5) whose upper end is held to loading cylinder through a the load transducer (6) applies the load through the steel ball to the locking cylinder bonded to the tube. Relative sliding displacement at the interface between the tube and sleeve is measured by two devices: the displacement cell (4) and displacement transducer (7) (Mμ-Checker, Mitutoyo, Mississauga, Ontario, Canada). The tip of transducer (7) is placed on a small magnetized block attached the sleeve outer diameter as shown in Figure 5.27. The precision of the load and displacement measurement cells is about 20 N and 0.1 μm, respectively. During the experiment, the relative sliding displacement together with the synchronised axial load are continuously recorded in an IBM microcomputer (8) and a data acquisition unit (HP 3852A-series 300). The relation between the relative displacement and the axial load can be also plotted directly by the printer (9).

The loading on the MTS machine is limited to 15000 N within 180 seconds which represents a loading rate of 83.3 N/s. The breaking load can be precisely determined by measuring the sliding displacement at the interference level between the tube and the sleeve.

The level of the joint axial strength represented by the maximum shearing force that the joint can stand, is recorded for subsequent comparison with the finite element solution.

5.5.2.3 Results and discussion

A typical pull-out curve (axial load F_a versus the relative displacement U_j) is illustrated in Figure 5.28. The displacements measured by the MTS displacement cell and that of the displacement transducer (Mμ-Checker) are almost identical. Similar non-linear force-displacement curves with large relative displacement are obtained, when additional pull-out tests are performed. The over-estimation in relative displacement has been attributed to the position of the MTS displacement cell and to the layout used while measuring the displacement by the transducer (Mμ-Checker). Since the position of the MTS displacement cell cannot be modified, it has been thus decided to change the set up of the displacement transducer (Mμ-Checker) to that pictured in Figure 5.29. As expected, the displacements measured by the transducer (Mμ-Checker) become much lower than those recorded by the MTS machine, as shown in Figure 5.30. Inevitably, the MTS displacement cell adds the displacements of some of the apparatus components to the relative displacement of the specimen. Nevertheless, this aspect is less important in our case since the main objective of the experiments is to evaluate the maximum resistance shearing force of the joint. The value of the pull-out force will be compared later with those obtained by the finite element model.

5.5.3 Finite Element Determination for Pull-out Strength

The axisymmetric finite element model that was specially prepared for the given geometry is shown in Figure 5.31. It contains 4108 nodes in a total of 1522 axisymmetric quadrilateral isoparametric solid elements. The model also contains a total of 80 quadrilateral interference elements that are used to simulate the initial gap and the contact state when it occurs. The used interface element permits small relative tangential displacements to take place at the interface between the tube and the sleeve. Based on the experimental investigation, the average measured coefficient of friction (f = 0.1375) with Coulomb's friction law are adopted. The tube and sleeve material properties listed in Table 5.12 are used. The Von Mises yield criterion is assumed along with the kinematic hardening flow rule. The lift sides of both the tube and the sleeve are restrained in the axial direction. The length of non expanded part (25.4 mm) was found to be satisfactory since any stress and displacement resulting from the expansion pressure die away well before reaching the tube end. As shown in Figure 5.31, the hydraulic expansion process is simulated by applying a uniform pressure on the inner surface of the tube. The length of the expansion is decided to be as close as possible to that of the experimental samples. A crevice length of about 3 mm is taken from both sides by applying the expansion pressure over a portion of the tube (44.45 mm) that lies under the sleeve. A refined finite element mesh is used for the beginning and the end of the pressure application zone where a variation in the residual contact pressure is expected to be significant.

The peak level of the expansion pressure for each sample is applied in one loading step with about 40 load increments. The expansion pressure is then fully released in another step with 17 unloading increments. In order to reproduce the same boundary conditions used in the experiments, the kinematic constrains acting on both the tube and sleeve primary sides are removed and a new boundary condition is applied for the sleeve upper side only (see Figure 5.9-BOUND-2). The pull-out load is applied incrementally on the tube free end. Figure 5.32 illustrates typically the relation between the resistance load and the relative interference tangential displacement. Similar curves were obtained for the other cases considered here. The comparison with the experimental results and some discussion are given in the following section.

5.5.4 Comparison between FE and Experimental Results

The results of the pull-out force as measured experimentally and as calculated by the finite element model are summarised in Table 5.14. In general, an acceptable agreement between the experimental measurements and the finite element solutions is observed. However, in one of the cases (2-2), the difference was appreciable. For this one sample, the very low pull-out load could be due to some contamination lubricating fluid during manufacturing.

The results of Equation (5.1) based on the residual contact pressure calculated by FE

is also given in Table 5.14. As expected, the pull-out strength provided by Equation (5.1) is greater than both the experimentally measured and the numerically calculated pull-out loads.

The validity of the finite element model for evaluating the pull-out strength of the expanded joint has been confirmed. Also, Equation (5.1) may not be used in a conservative manner to calculate the pull-out strength of the tube-to-tubesheet joint. However, based on the finite element analysis, it could be considered as an approximation while calculating the push-out load only.

Executive summary

The analysis of tube-to-tubesheet axial strength was documented in this chapter. The investigation was achieved by three different techniques, namely; analytical, finite element and experimental. Analytical results indicated that the push-out load was slightly higher than the pull-out force. After comparison with 3-D finite element model, the equivalent axisymmetric model was also used to evaluate the pull-out joint strength. The results indicated that the simplified equation (Eq. (5.1)) often used to calculate the joint strength predicted higher pull-out force than that calculated using the finite element model. The axisymmetric finite element solution was also validated against experimental measurements. In order to reduce the discrepancies between finite element and experimental results, it was necessary to measure the coefficient of friction between the tube and tubesheet materials. A coefficient of friction

of about 0.1375±0.004 was found when the tube and the tubesheet materials were made of Inconel 690 and SA-508 steel, respectively. Using this value and assuming Coulomb's friction law, the axisymmetric finite element model was then used to calculate the pull-out strength. A good agreement between axisymmetric finite element solution and experimental measurement was obtained.

Table 5.1: Material properties of some tested cases

Tube (Inconel 690)			Tubesheet (ASTM A 508)		
S_{yt}	E_t	E_{tt}	S_{ys}	E_s	E_{ts}
285.3	212	1.915	390	212	1.309

Table 5.2: Various properties of some tested cases

t/d	c/d	D_e/d	f	P_e/S_{yt}
0.109	0.004	3.0	0.35	0.9

Table 5.3: Relation between shearing and normal traction just before slipping

Element No.	Integration Point.	S_n/S_{yt}	S_s/S_{yt}	S_s/S_n
101	1	0.114016	-0.03990	0.349936
101	2	0.081392	-0.02429	0.298397
101	3	0.045771	-0.01602	0.349947
102	1	0.045771	-0.01602	0.349947
102	2	0.057733	-0.02021	0.350063
102	3	0.056670	-0.01983	0.349979
103	1	0.056670	-0.01983	0.349979
103	2	0.054833	-0.01919	0.350022
103	3	0.046472	-0.01626	0.349974
104	1	0.046472	-0.01626	0.349974
104	2	0.046713	-0.01635	0.349974
104	3	0.069212	-0.02421	0.349860
105	1	0.069212	-0.02421	0.349860
105	2	0.071073	-0.02487	0.349881
105	3	0.065901	-0.02306	0.349982
106	1	0.065901	-0.02306	0.349982
106	2	0.068995	-0.02415	0.350053
106	3	0.070831	-0.02479	0.350051
107	1	0.070831	-0.02479	0.350051
107	2	0.057782	-0.02023	0.350063
107	3	0.062131	-0.02174	0.349942
108	1	0.062131	-0.02174	0.349942
108	2	0.069913	-0.02448	0.350156
108	3	0.051305	-0.01796	0.350071
109	1	0.051305	-0.01796	0.350071
109	2	0.080425	-0.02815	0.350060
109	3	0.113122	-0.03961	0.350139
110	1	0.113122	-0.03961	0.350139
110	2	0.130836	-0.04580	0.350018
110	3	0.173345	-0.06068	0.350063
111	1	0.173345	-0.06068	0.350063
111	2	0.215829	-0.07554	0.350017
111	3	0.191203	-0.06692	0.349975
112	1	0.191203	-0.06692	0.349975
112	2	0.000000	0.00000	-
112	3	0.000000	0.00000	-

Table 5.4: Comparison between Coulomb's friction law and elastic slip model (see Fig. 5.7)

Friction law	Joint Strength		
	$\bar{F}_1$	$\bar{F}_2$	$\bar{F}_3$
Coulomb's	0.0221	0.0267	0.0265
Elastic Slip	0.0236	0.0282	0.0284
% Difference	6.3%	5.3%	6.67%

Table 5.5: Effect of boundary condition on joint axial strength

Joint Strength	BOUND-1	BOUND-2	BOUND-3	BOUND-4	BOUND-5
$\bar{F}_1$	0.0221	-0.436%	0.232%	1.25%	2.16%
$\bar{F}_2$	0.0267	-3.67%	-7.26%	-2.56%	-1.51%
$\bar{F}_3$	0.0265	1.45%	1.51%	-0.248%	-2.03%

Table 5.6: Comparison between 3-D and axisymmetric FE solutions for joint axial strength (see Fig. 5.7)

Model	Pull-out		Push-out			
			Primary side (Pr. S)		Secondary side (Sc. S)	
	$\bar{F}_1$	CPU	$\bar{F}_2$	CPU	$\bar{F}_3$	CPU
CASE-1						
3-D	0.04126	42750	0.05003	40598	0.05089	40113
Axisy.	0.04577	201	0.05381	272	0.05144	149
CASE-2						
3-D	0.08506	35785	0.10596	26146	0.10717	47184
Axisy.	0.09313	229	0.11128	225	0.11269	189
CASE-3						
3-D	0.13249	32024	0.16438	33857	0.16411	39115
Axisy.	0.12479	189	0.15166	196	0.15142	222
CASE-4						
3-D	0.16584	37861	0.20557	33379	0.21280	3524
Axisy.	0.16515	192	0.20384	187	0.21158	235

Table 5.7: Three levels of geometrical parameters and expansion pressure ratio

Level	Parameters			
	c/d	t/d	D_e/d	P_e/S_{yt}
1	0.00192	0.0664	2.5	0.8
2	0.00416	0.096	3.0	0.9
3	0.0096	0.132	3.5	1.0

Table 5.8: Joint axial strength as calculated by FEM and Equation (5.1)

Calculation No.	Finite element axial load			Equation (5.1)
	$\bar{F}_1$	$\bar{F}_2$	$\bar{F}_3$	
1	0.015722	0.018117	0.01876	0.018851
2	0.020496	0.02358	0.024587	0.024283
3	0.022131	0.026307	0.026013	0.027405
4	0.030982	0.038207	0.037252	0.04473
5	0.011954	0.01445	0.013788	0.01715
6	0.023714	0.0261	0.027977	0.03311
7	0.016599	0.018647	0.019507	0.03031
8	0.036407	0.040073	0.04361	0.05096
9	0.012546	0.01372	0.01415	0.01666

Table 5.9: Comparison between joint axial strengths on the basis of mean values

parameter	$\bar{F}_1$	$\bar{F}_2$	$\bar{F}_3$
σ	0.021172	0.025072	0.024356
λ	0.008262	0.010118	0.009547
t-value	0.426191		0.123291
$t(d,\alpha)$, $\alpha = 0.05$	1.83		1.83
$t(d,\alpha)$; $\alpha = 0.35$	0.3975		0.3975

Table 5.10: Correlation parameters for the relationship between initial residual contact pressure and interference normal stresses at moment of sliding

Axial strength	Correlation Parameters			
	α	β	R	St. Error
Equation (5.1)	0.0	1.000	-	-
VAR2	0.0056	0.6557	0.959	0.0066
VAR3	0.0046	0.8019	0.958	0.0082
VAR4	0.0069	0.7596	0.948	0.0085

Table 5.11: Dimensions of tube and sleeve used in friction test (mm)

t	d	c	D_e
2.286	19.177	0.0635	35.0

Table 5.12: Material properties for pull-out testing

	Tube (Inconel 690)	Tubesheet (SA-508 Class3)
Modulus of elasticity ±5GPa	209	199.6
Poisson's ratio ±0.005	0.289	0.3
Yield strength ±10MPa	294	458
Tangent Modulus ±0.01GPa	2.09	1.996

Table 5.13: Dimension, roughness and expansion pressure levels of joint samples

Case			1		2	
Sample number			1	2	1	2
Dimension ±0.025 mm	Tube	d_i	16.764	16.764	16.764	16.764
		d	19.05	19.05	19.05	19.05
	Sleeve	Pr. S D_i	19.34	19.339	19.261	19.248
		Sc. S D_i	19.339	19.339	19.243	19.207
		D_e	35.05	35.05	35.05	35.05
Roughness ±0.002 μm	Tube outer surface		0.216	0.216	0.216	0.216
	Sleeve inner hole		0.875	0.875	0.875	0.875
Expansion Pressure (P_e) ±3.5 MPa			259.75	259.75	225.57	225.57

Table 5.14: Pull-out load as measured experimentally and as calculated by the finite element and by Equation (5.1)

Case	Sample	Pull-out load (N)		
		Experiments	Finite Element	Equation (5.1)
1	1	6612.5	7630.27	9328.2
	2	7462.5	7630.27	9327.9
2	1	5875.0	5480.52	6462.8
	2	2887.5	5480.52	6462.8

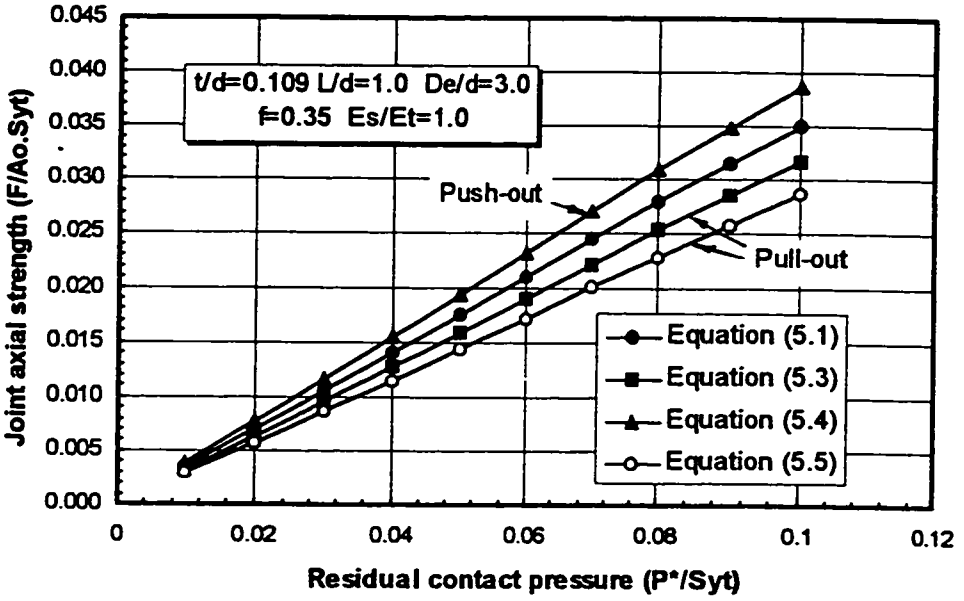


Figure 5.1: Joint axial strength as predicted by different analytical models

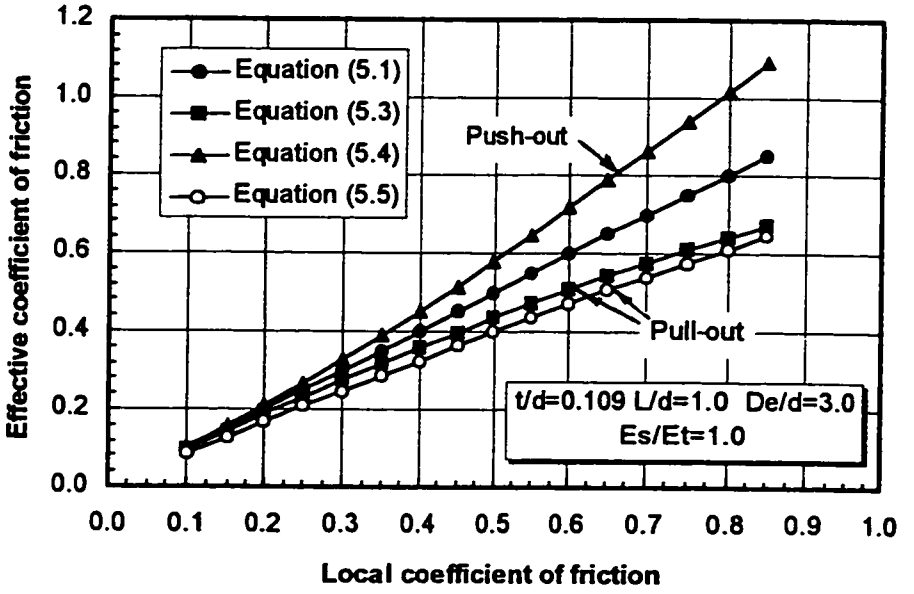


Figure 5.2: Effective coefficient of friction versus locale coefficient of friction

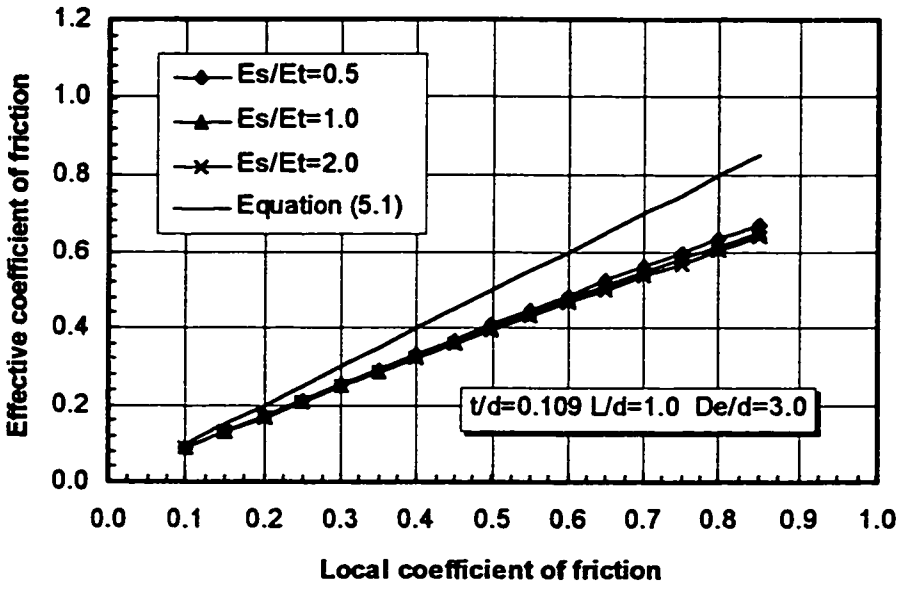


Figure 5.3: Effective coefficient of friction at various level of modulus of elasticity ratio

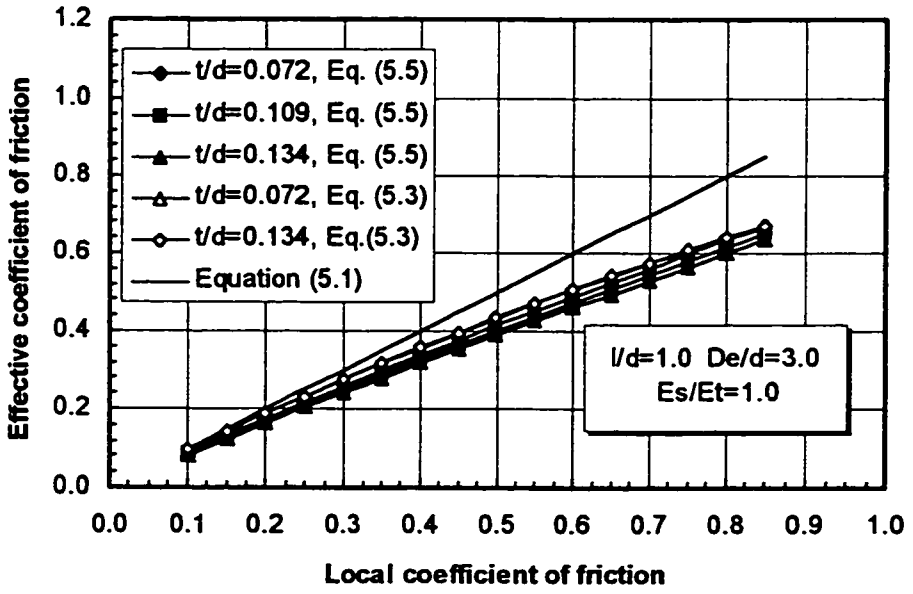


Figure 5.4: Effective coefficient of friction at different values of tube wall thickness ratio

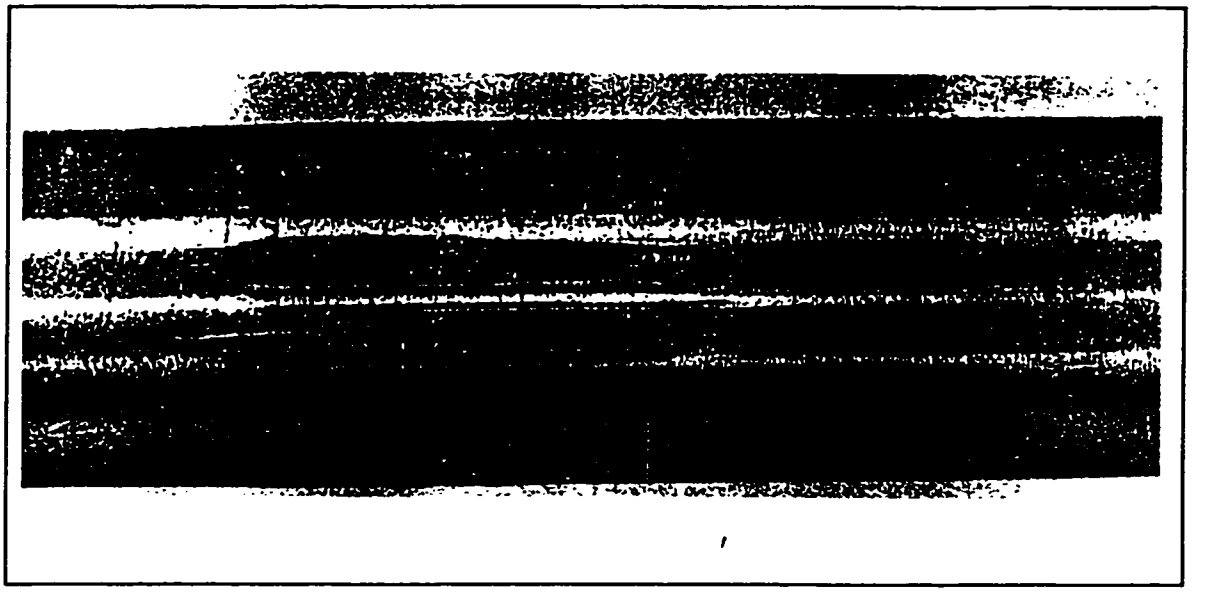


Figure 5.5: Damage of tube outer surface as a result of pull-out test

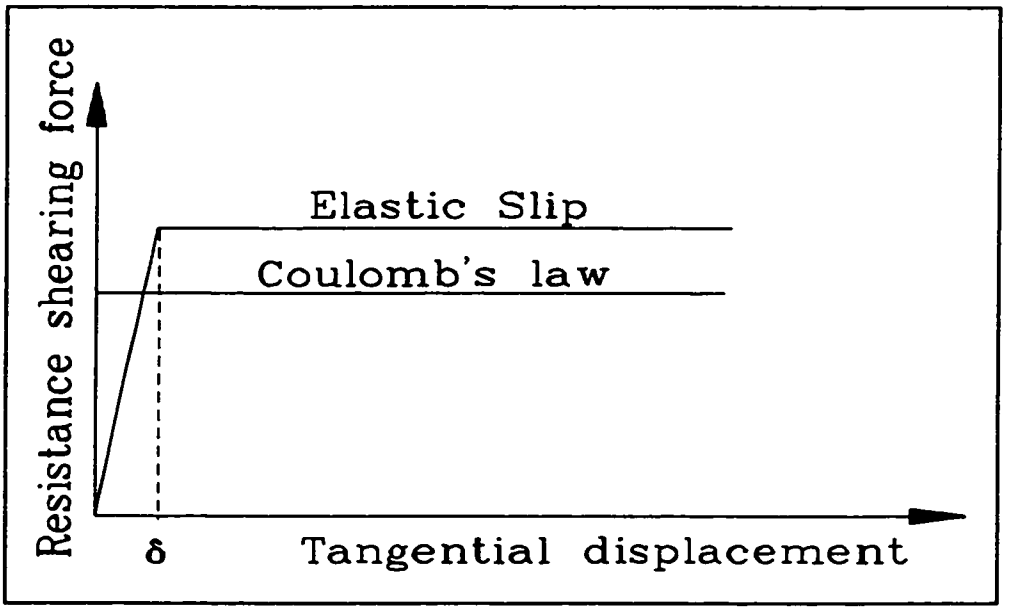


Figure 5.6: Typical comparison between Coulomb's friction law and elastic-slip friction model

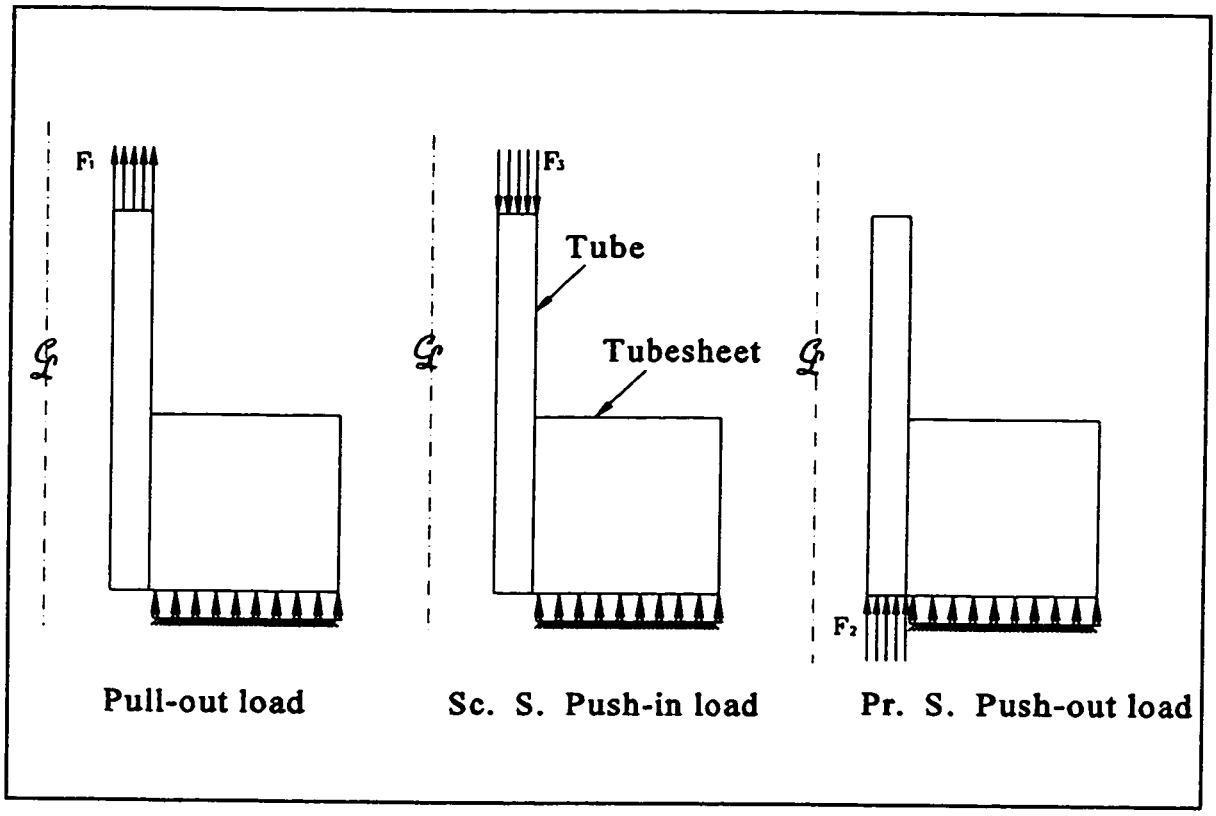


Figure 5.7: Three different ways of evaluating the joint axial strength by the finite element method

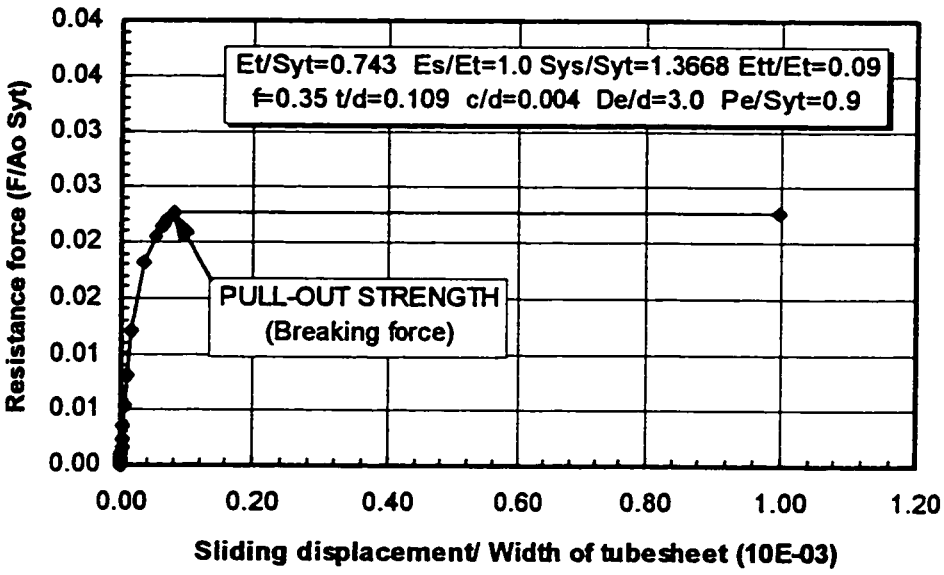


Figure 5.8: Typical relation between shearing force and tube micro-motion

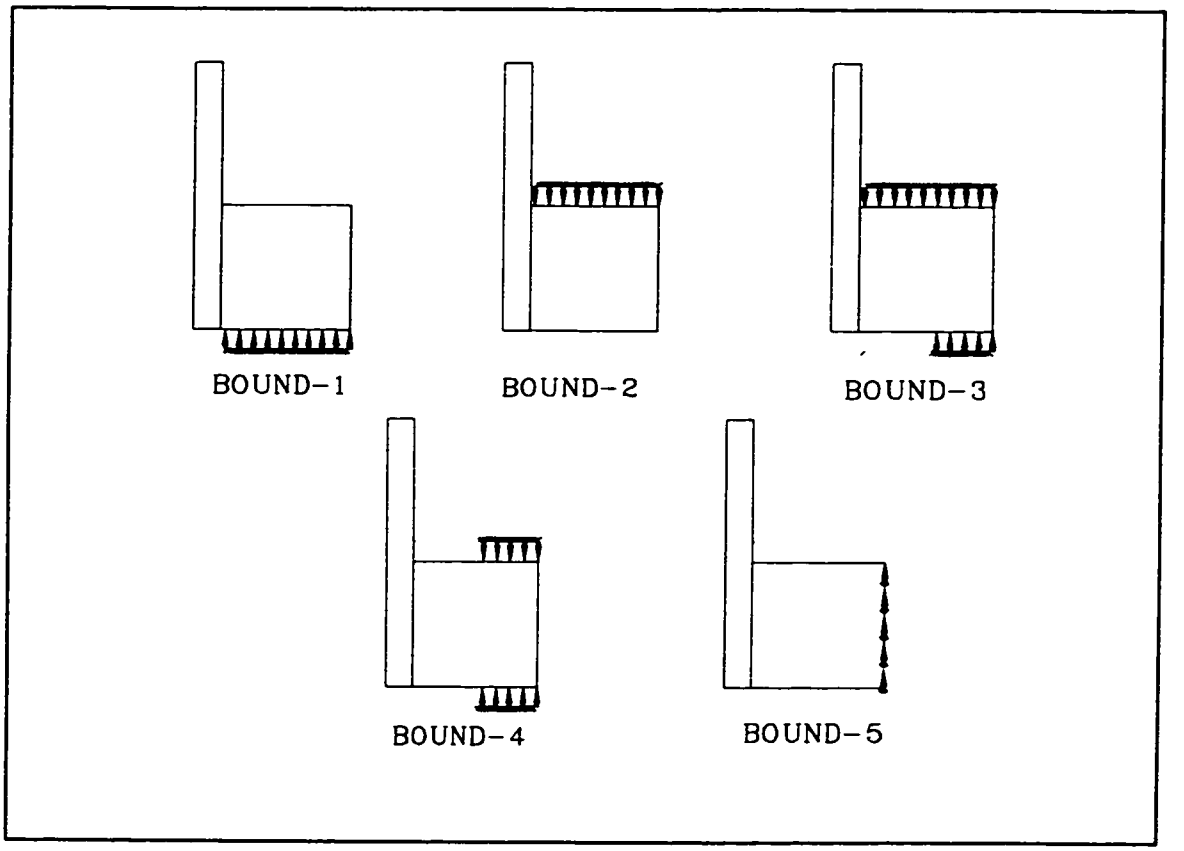


Figure 5.9: Different boundary conditions that can be applied in the axisymmetric model for joint axial strength calculation

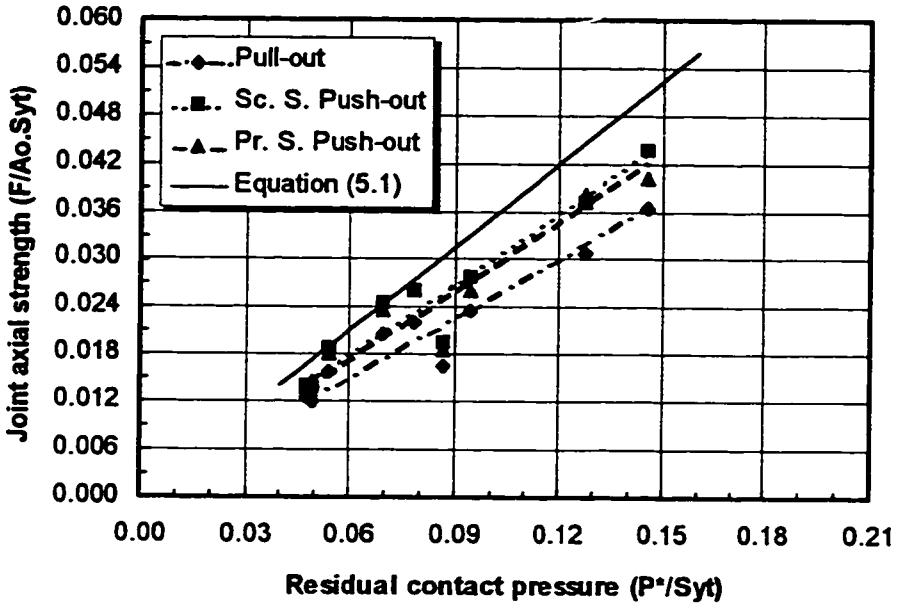


Figure 5.10: Relation between joint axial strength and the initial residual contact pressure as predicted by the finite element analysi

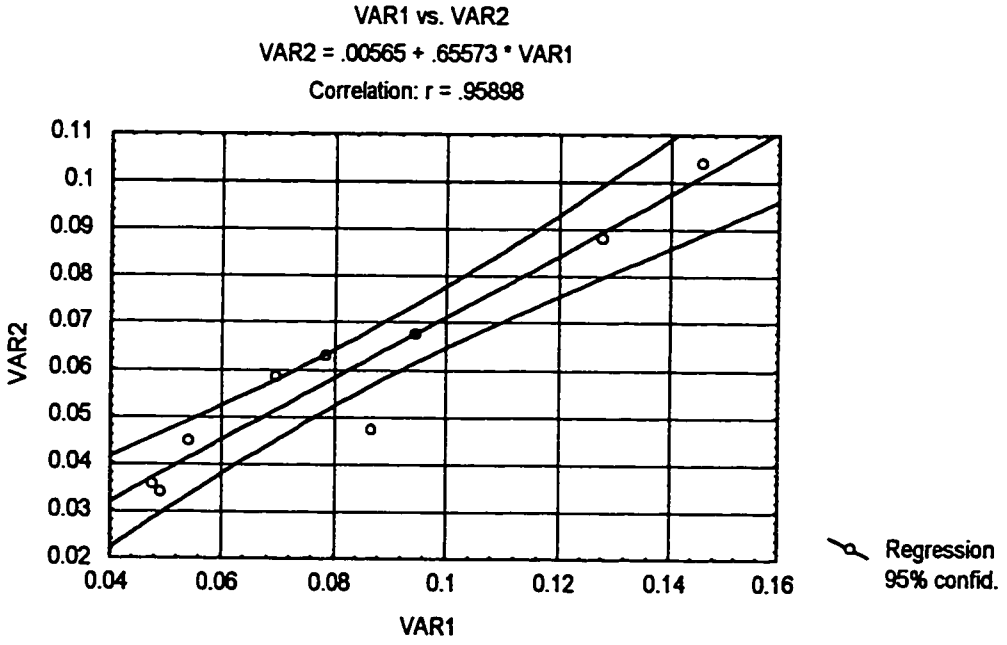


Figure 5.11: Statistical relation between interference contact pressure (VAR2) and initial residual contact pressure (VAR1)

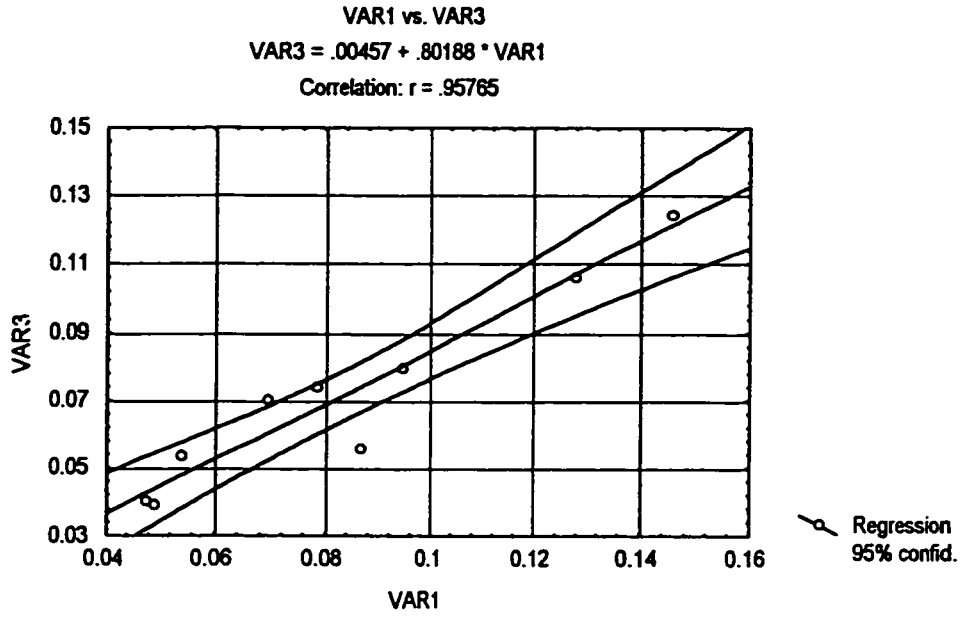


Figure 5.12: Statistical relation between interference contact pressure (VAR3) and initial residual contact pressure (VAR1)

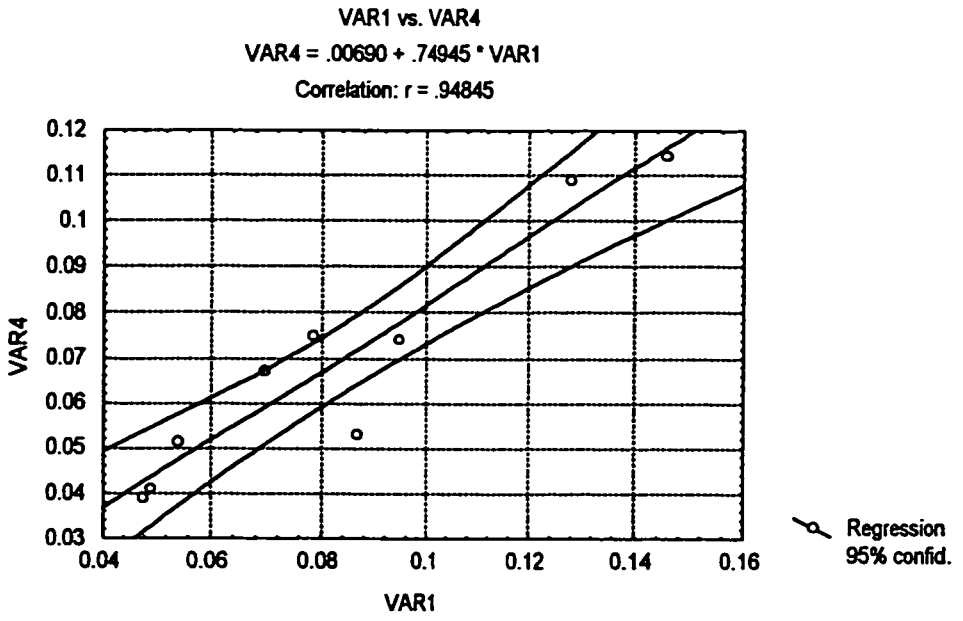


Figure 5.13: Statistical relation between interference contact pressure primary side push-out load (VAR4) and initial residual contact pressure (VAR1)

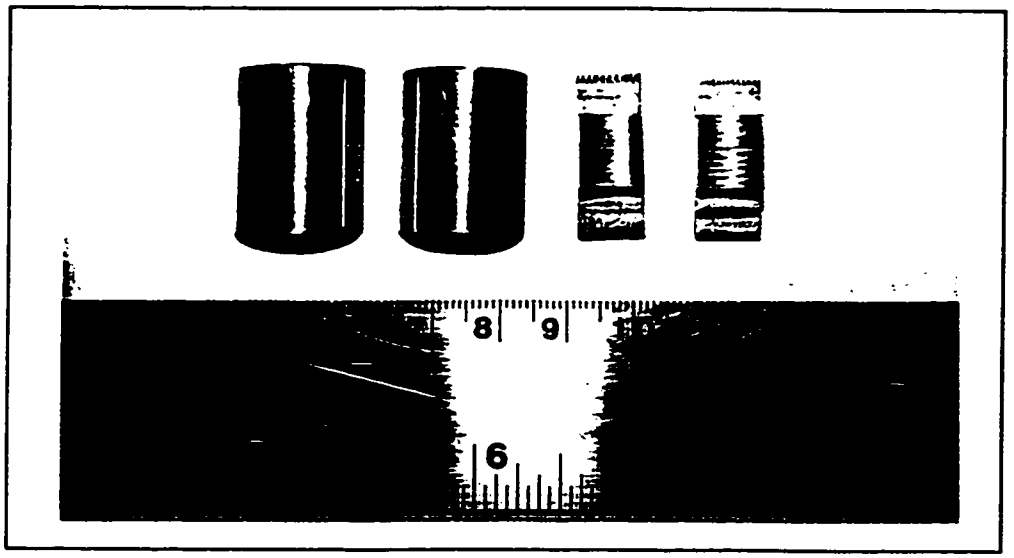


Figure 5.14: Tube and tubesheet frictional test specimens (Full area of contact)

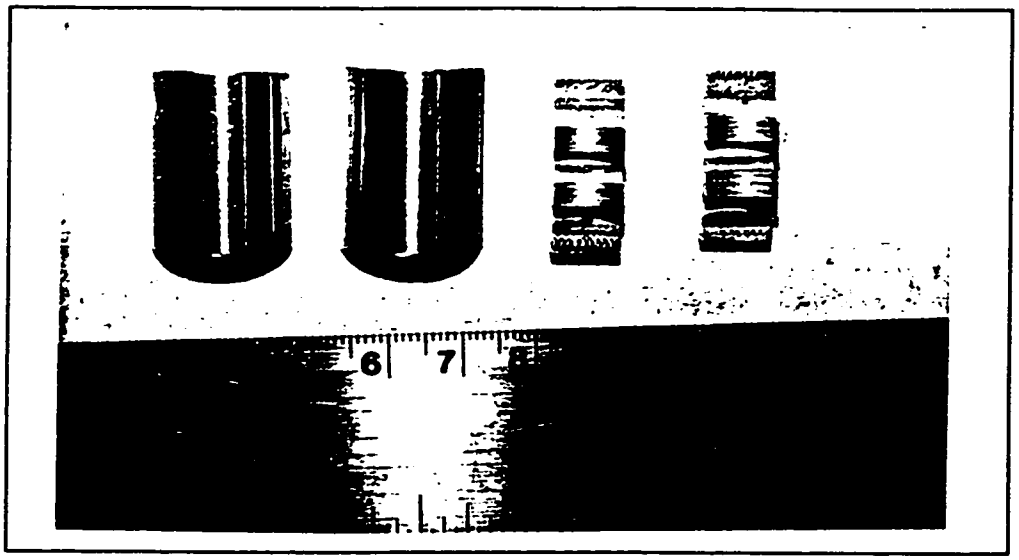


Figure 5.15: Tube and tubesheet frictional test specimens (Reduced contact area)

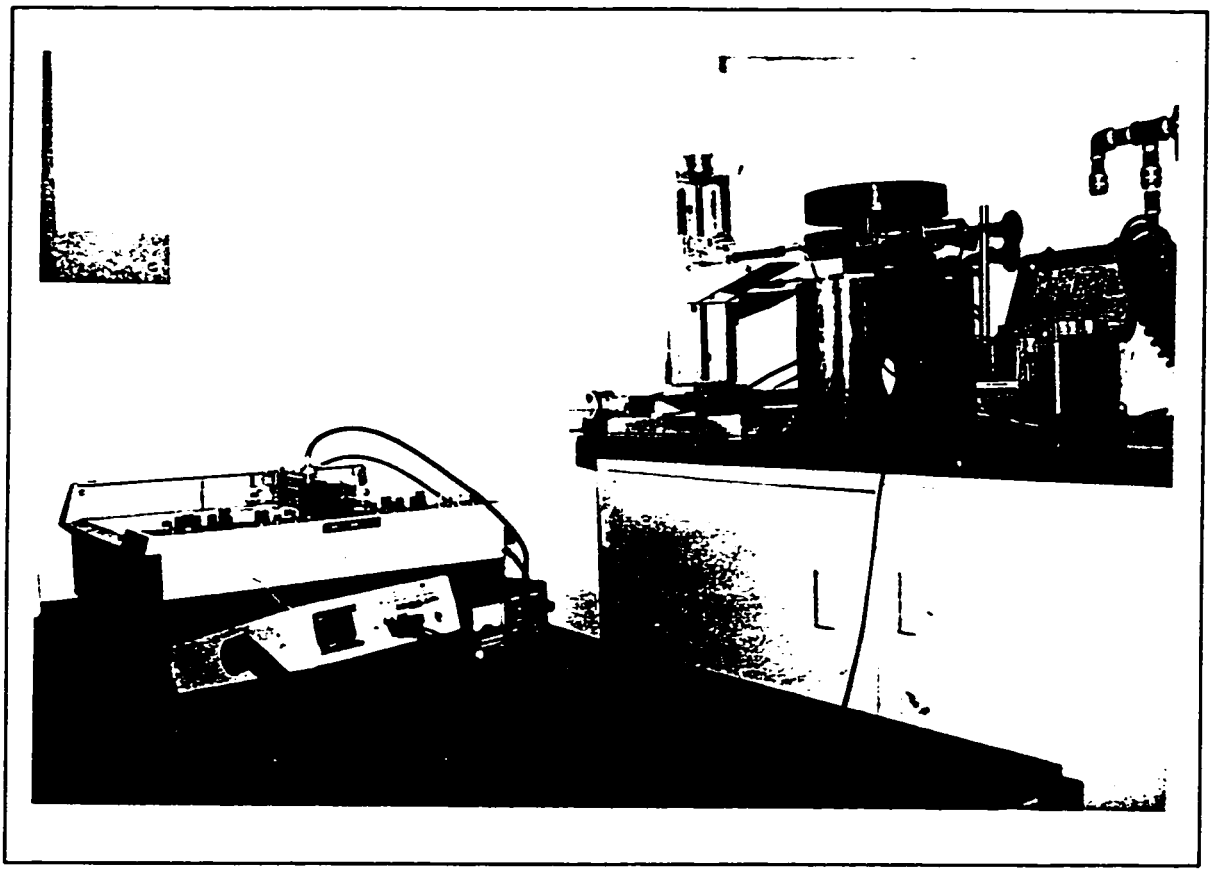


Figure 5.16: Friction test aparatus

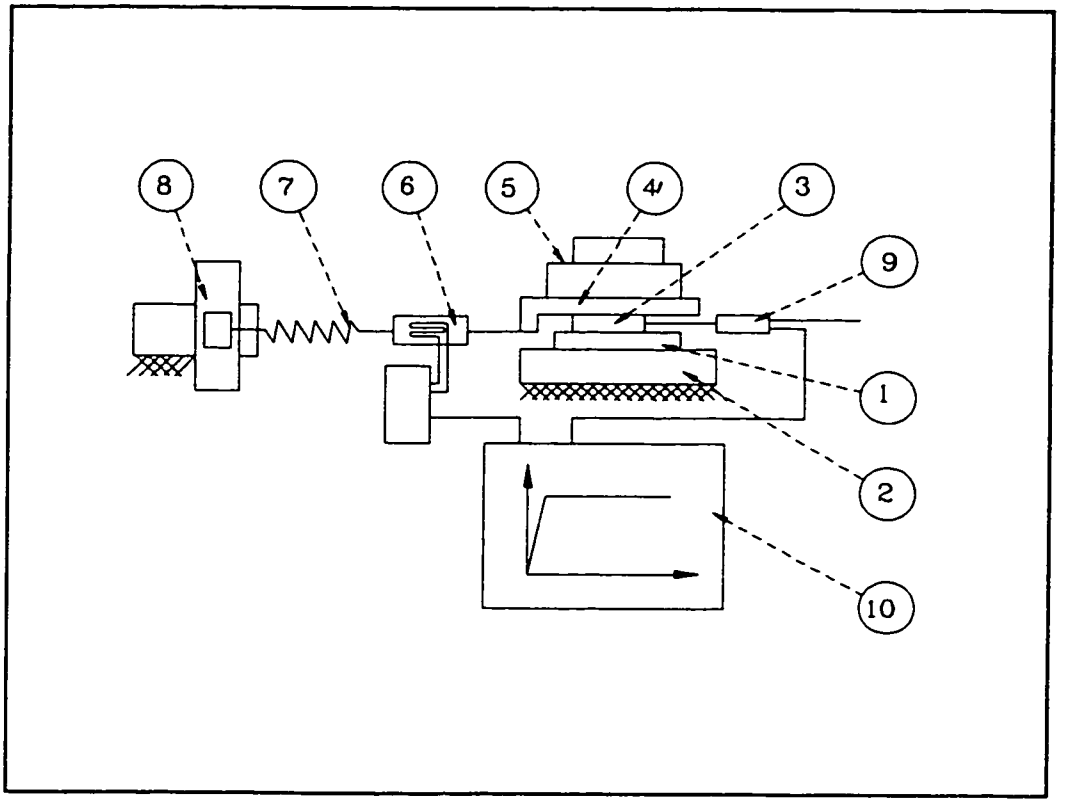


Figure 5.17: Equipments used in friction test set up

1- Two tube specimens
2- Aapparatus support
3- Two tubesheet specimens
4- Movable frame
5- Known weight
6- Load gauging cell
7- Linear spring
8- 3-D arm
9- Displacement transducer (LVDT)
10- X-Y plotter

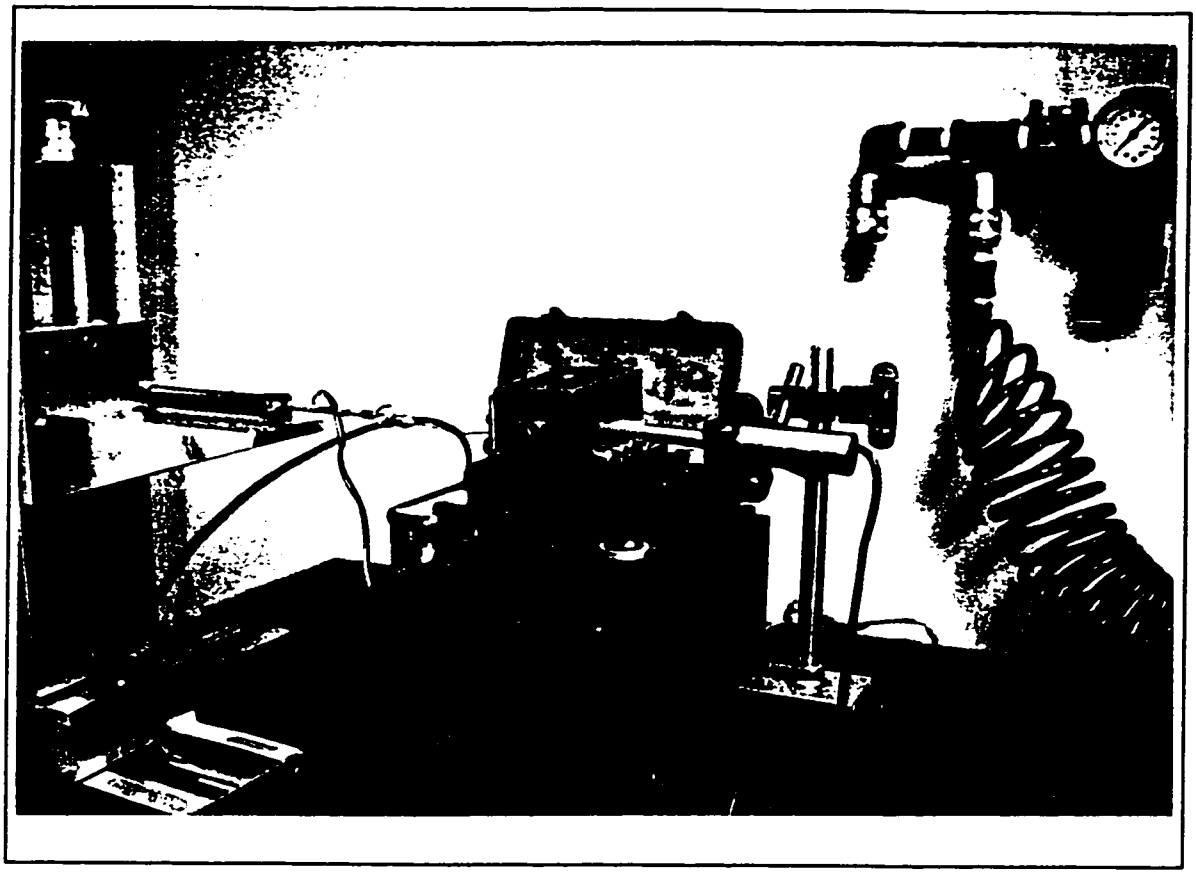


Figure 5.18: Picture showing the tip of displacement transducer placed near to the interference level between the tube and tubesheet samples

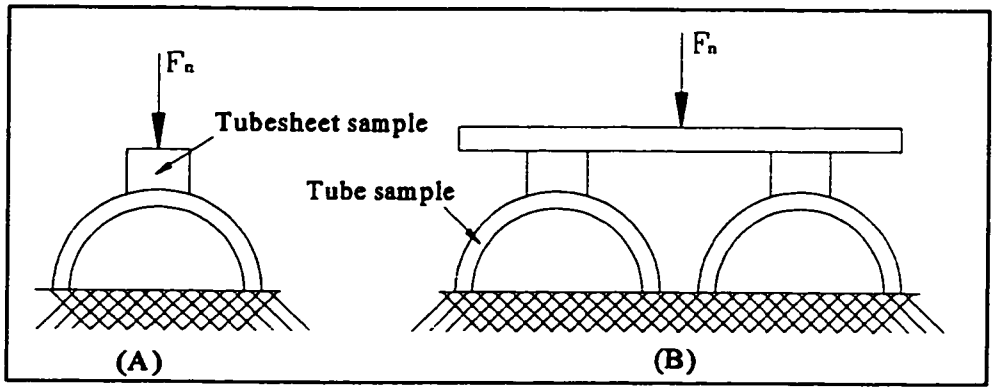


Figure 5.19: Stability of normal load over the cylindrical surfaces of the contacting areas; A- Unstable arrangement B-Stable arrangement

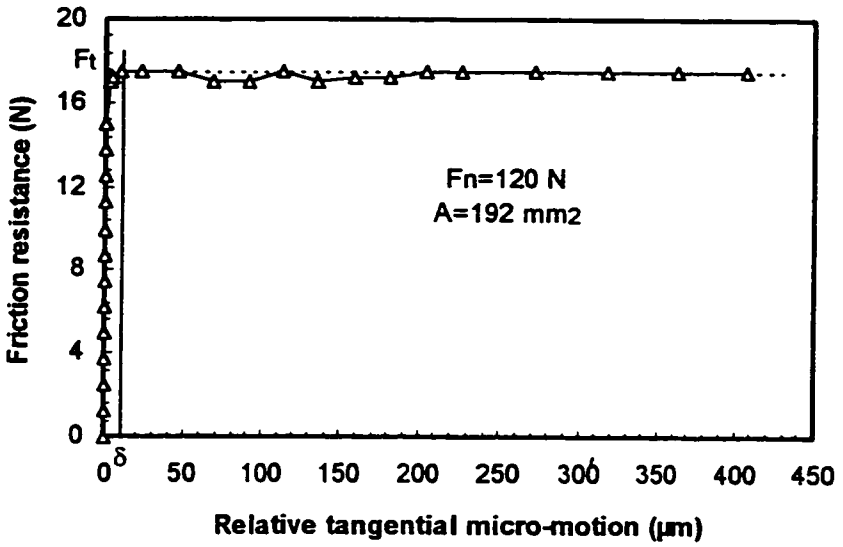


Figure 5.20: Typical relation between shearing force and displacement

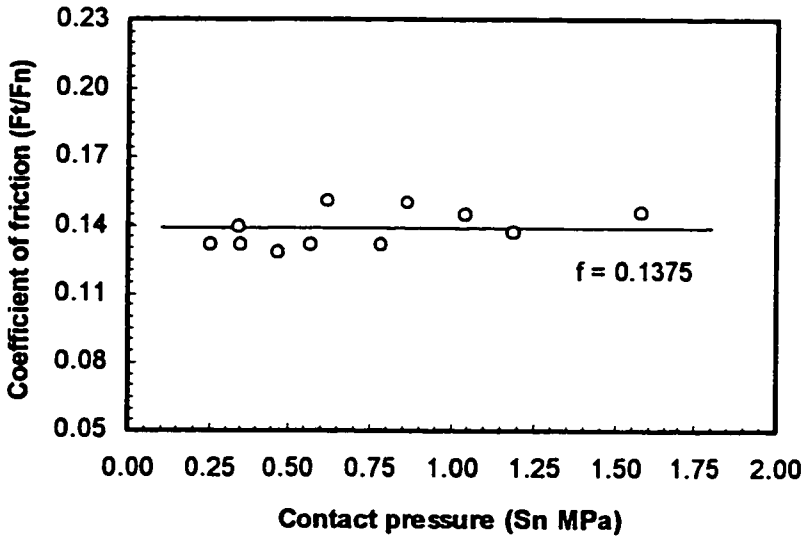


Figure 5.21: Local coefficient of friction versus normal pressure

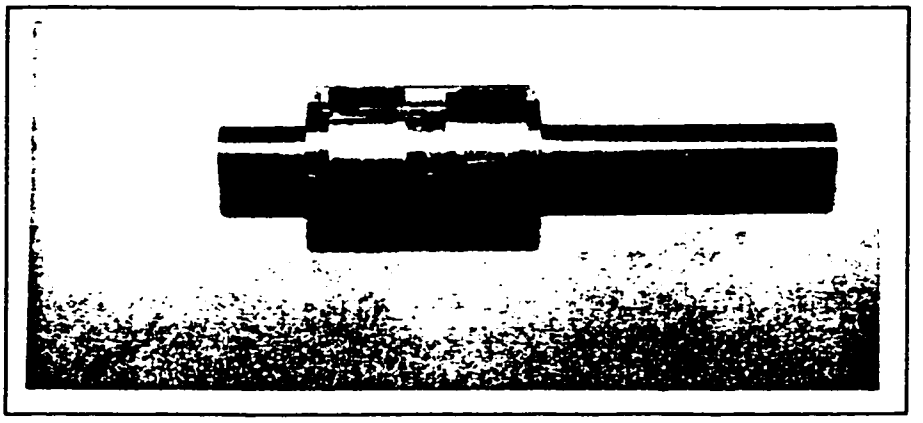


Figure 5.22: Tube-to-tubesheet joint sample

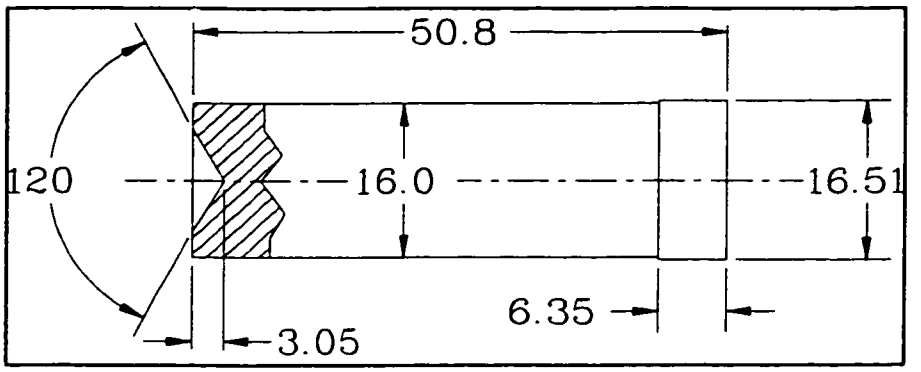


Figure 5.23: Dimensions of the locking cylinder (mm)

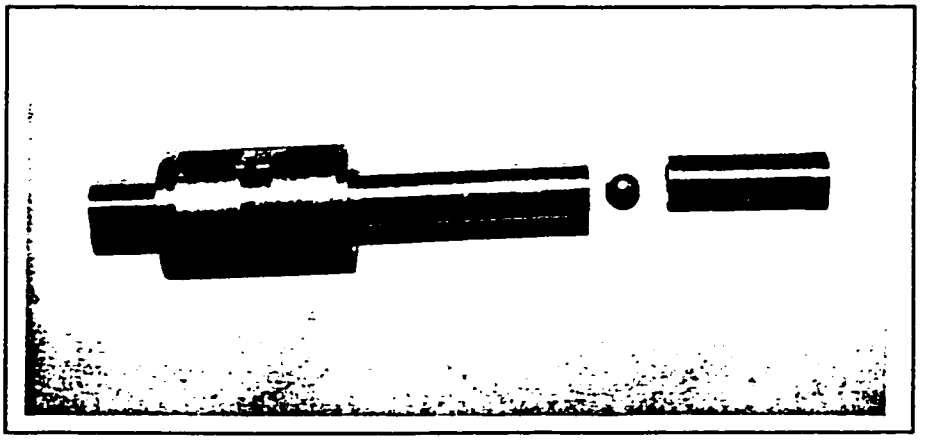


Figure 5.24: Collective picture for the test sample, locking cylinder and rigid ball

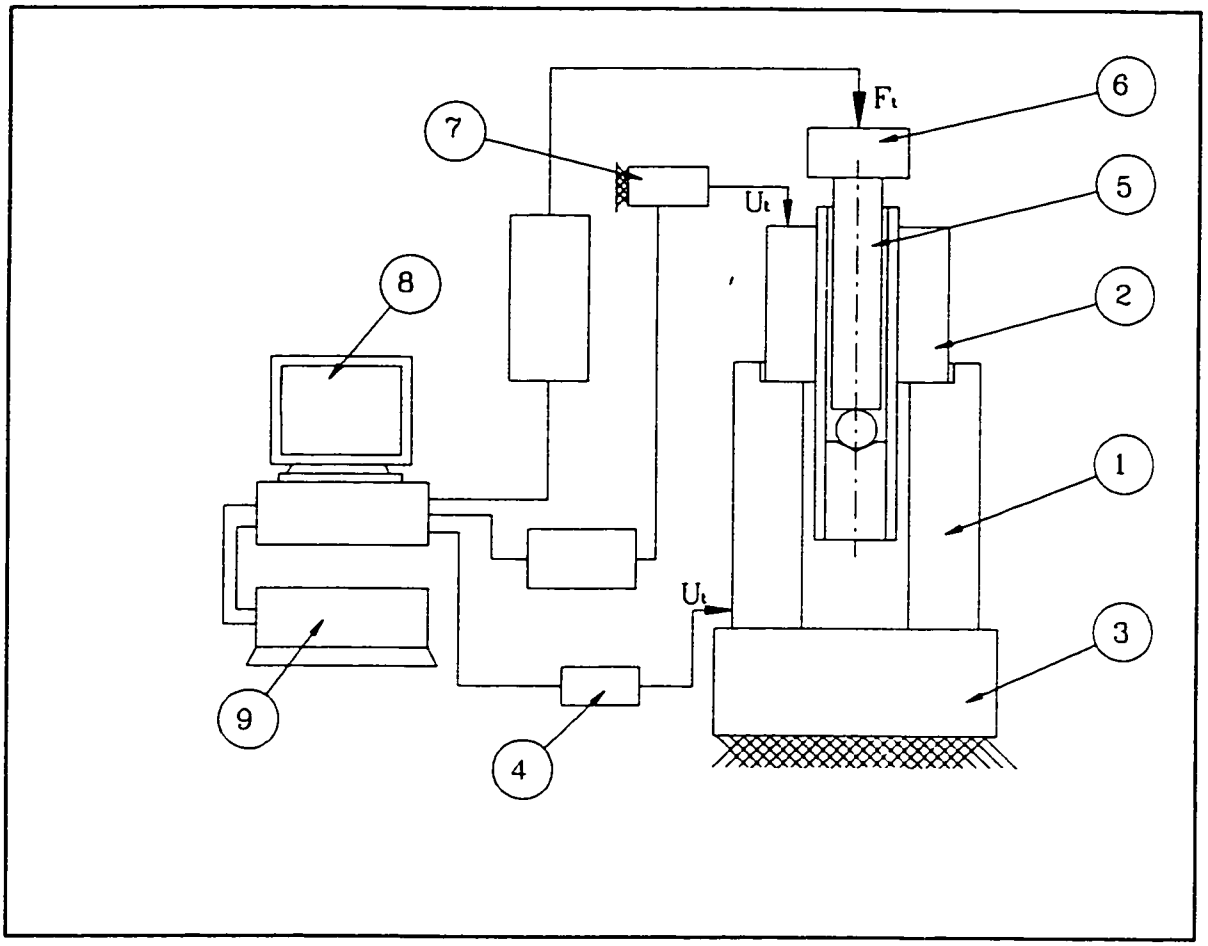


Figure 5.25: Illustration of pull-out test equipment

1-Steel cylinder
2-Sleeve
3-MTS arm
4-Displacement cell
5-Steel rod
6-Load transducer
7-Displacement transducer
8-IBM microcomputer
9-Printer

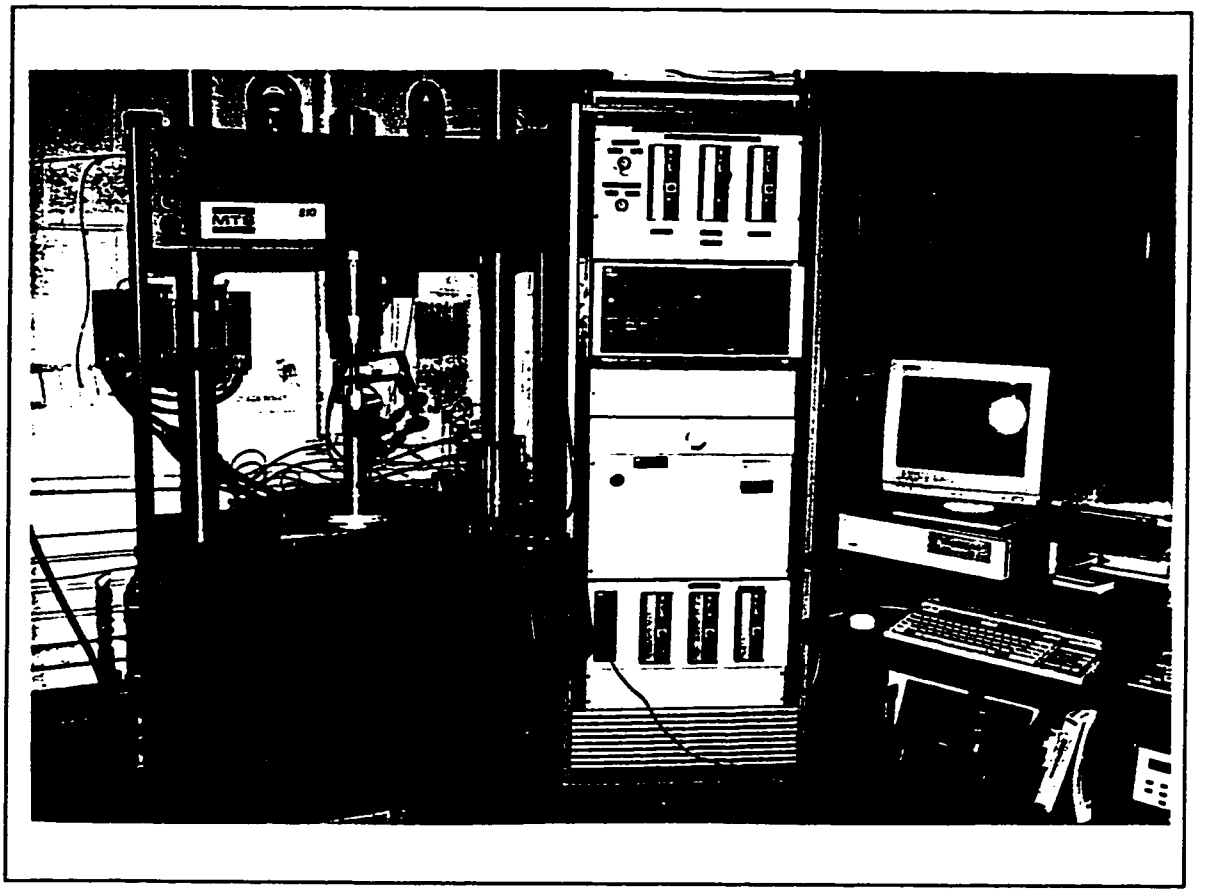


Figure 5.26: Collective picture for pull-out test rig

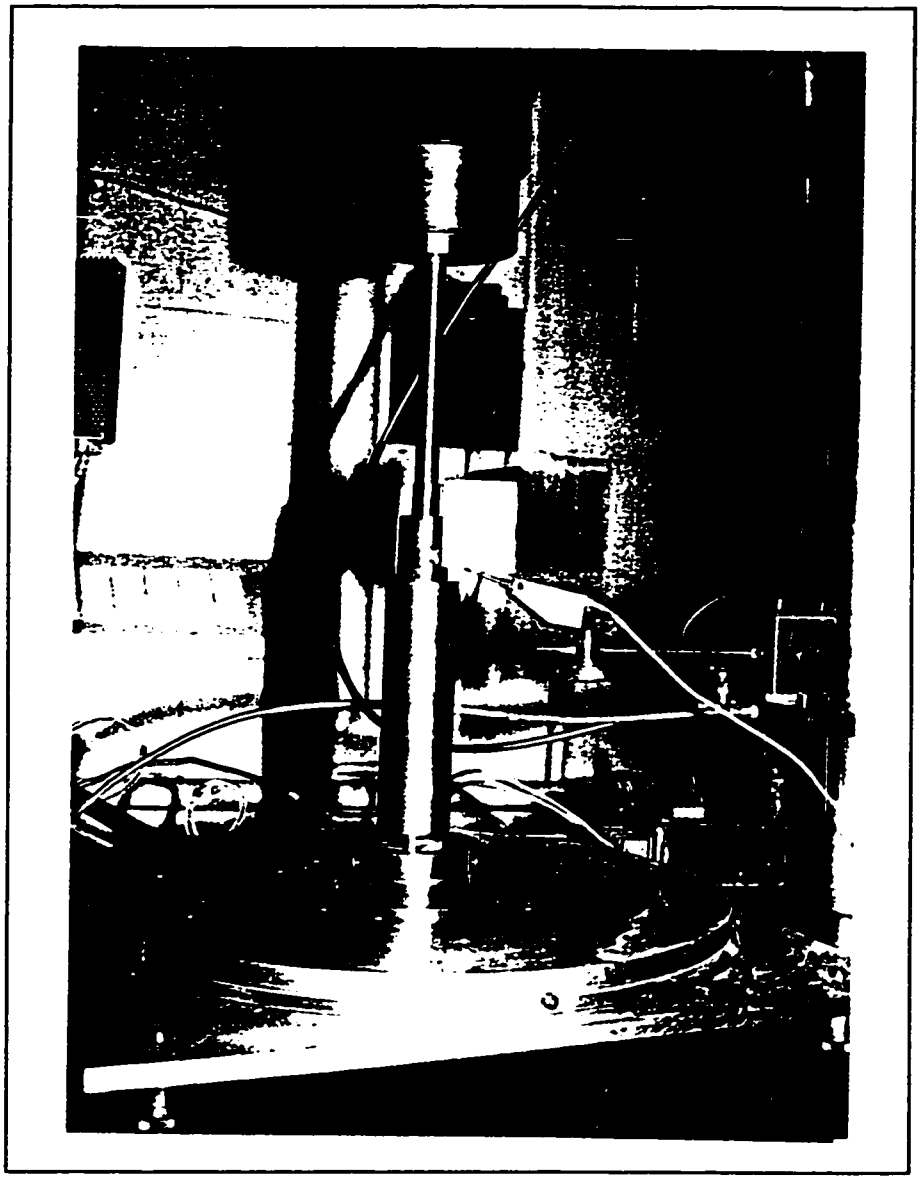


Figure 5.27: Picture showing the first arrangement of the displacement transducer

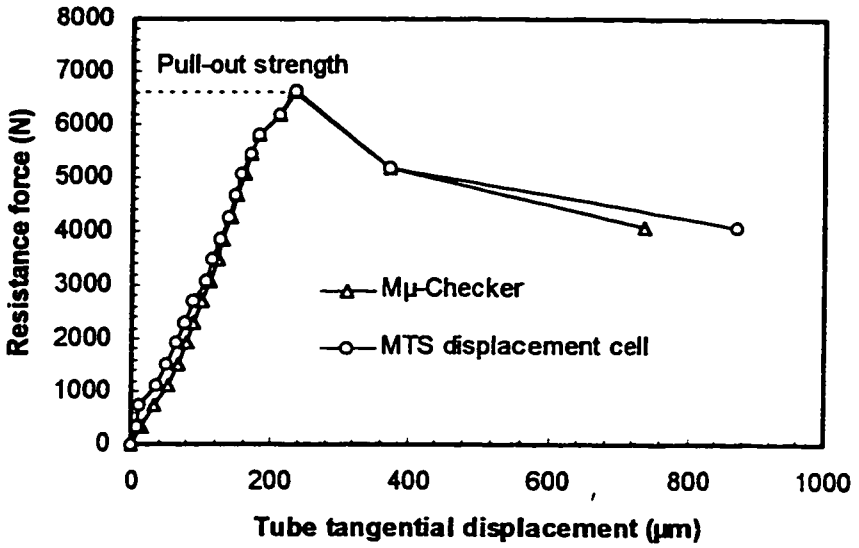


Figure 5.28: Typical relation between shearing force and relative displacement (CASE:1-1)

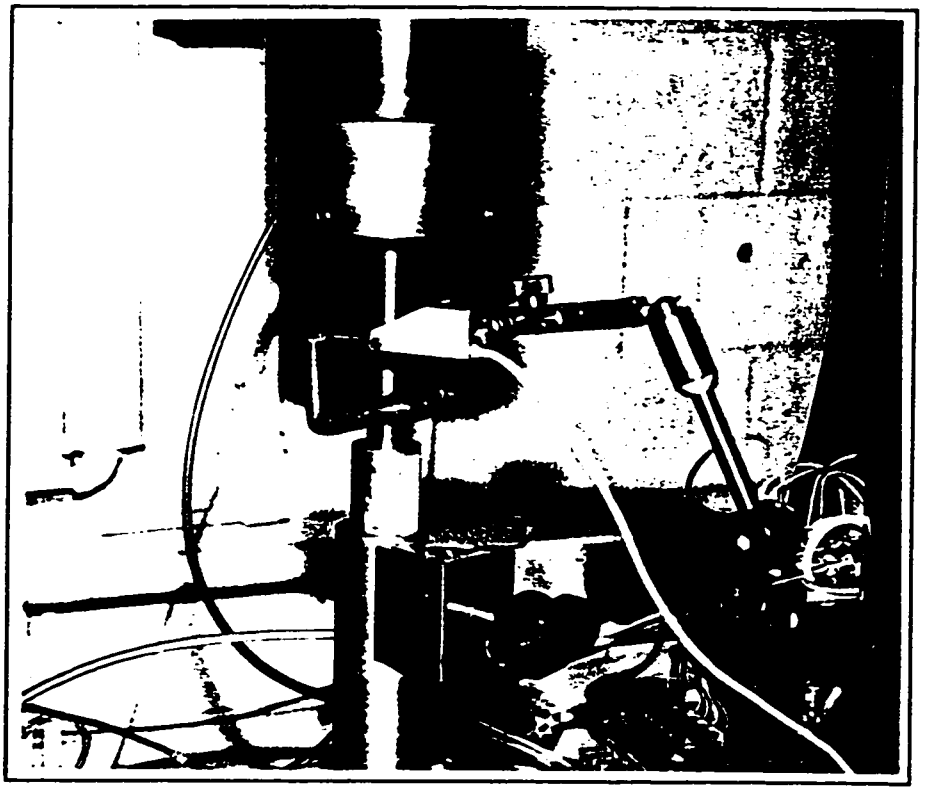


Figure 5.29: Picture showing second arrangement of the displacement transducer

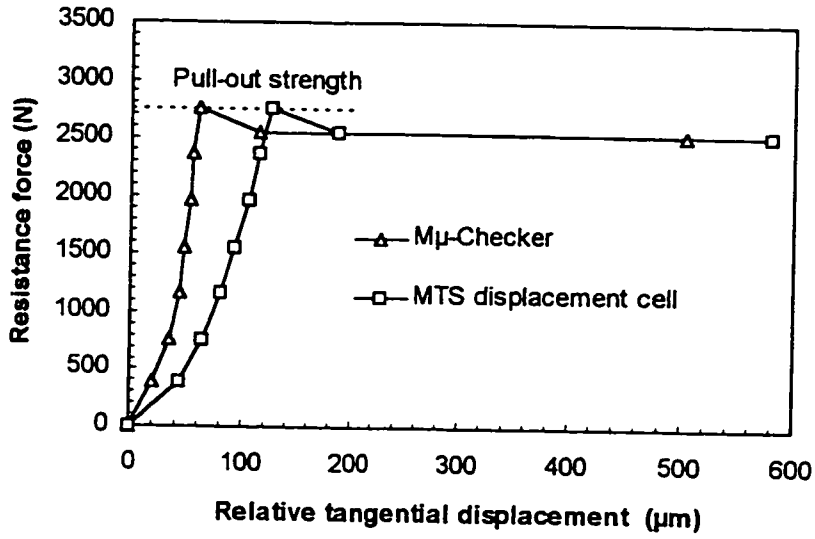


Figure 5.30: Relation between shearing force and relative displacement as given by MTS displacement cell and the Mμ-Checker; (CASE: 2-2)

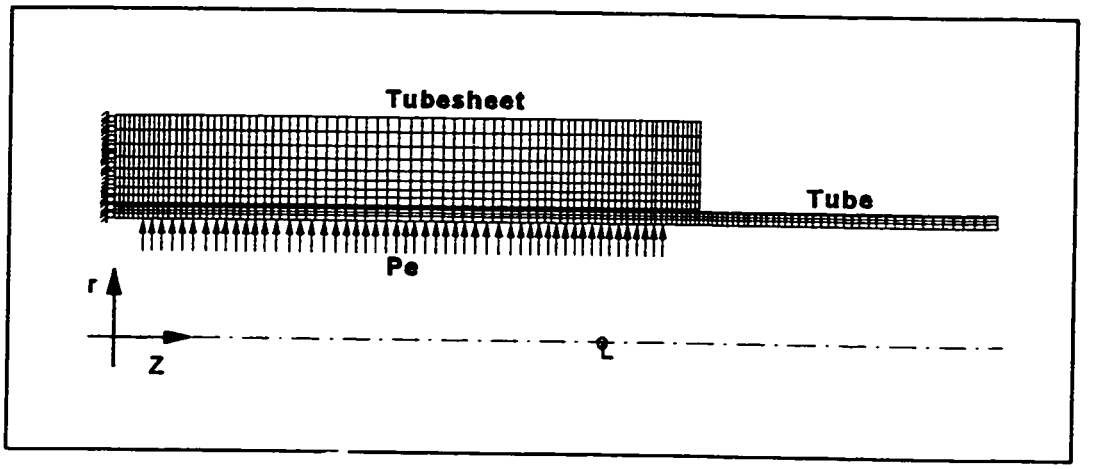


Figure 5.31: FE axisymmetric model

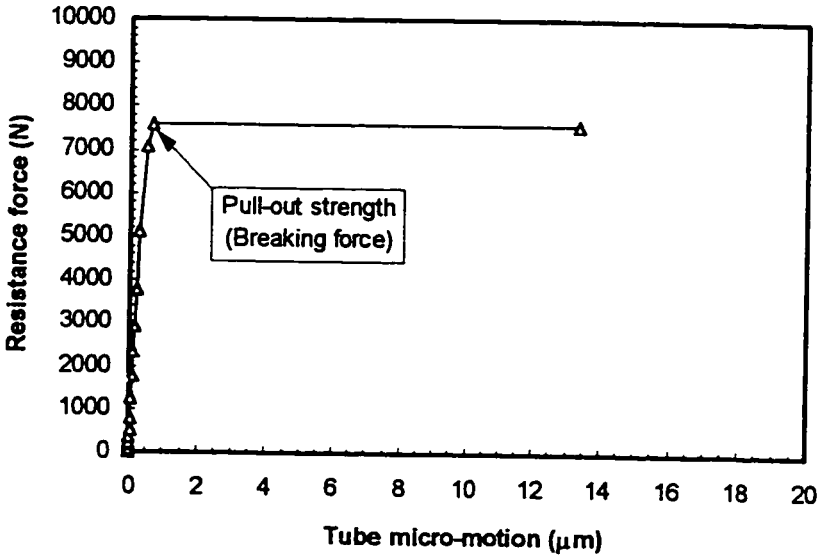


Figure 5.32: Relation between the shearing force and relative displacement as given by the finite element solution ; (CASE:1-1)

CHAPTER 6

THERMAL LOADING OF TUBE-TO-TUBESHEET JOINT

6.1 INTRODUCTION

The purpose of this chapter is to establish a simplified finite element analysis by which the behaviour of the joint under the working temperature can be predicted. The effect of the working temperature can then be added to the results of the analytical models of Chapter 4. Previous analytical studies reported by Middlebrooks (1991) showed that the creep-relaxation has no effect on joint performance as long as the temperature is less than 482.2 °C for either Alloy 600 or Alloy 690. Since such high operating temperatures are not found in practical applications, the creep- relaxation is ignored in the present. Also, because of the range of the working temperatures selected for the proposed model, material properties are assumed not to change with temperature. The ultimate motivation in this chapter is to accurately predict the final value of the residual contact pressure and residual stresses during thermal loading (e.i. when the tube and tubesheet are imposed to working temperature) and after temperature cycling (e.i. after the working temperature drops to room temperature). A new term, namely: the joint tightness coefficient (η) is introduced to characterize joint performance under the working conditions.

In the first part of this chapter, a simplified axisymmetric model is developed to investigate the effect of thermal loading and unloading on the residual contact pressure and residual stresses in the tube transition zone. In the second part, a simplified analytical solution of the joint behaviour under the effect of thermal loading and unloading is performed. The final part deals with full parametric studies to investigate the effect of the thermal loading and unloading on the level of the joint tightness coefficient and the residual stress profile in the tube transition zone. The effect of the material, thermal and geometrical properties will carefully be examined.

6.2 FE MODELLING FOR THERMAL LOADING ANALYSIS

The general purpose finite element program ABAQUS (1995) is used to simulate the working temperature behaviour of tube-to-tubesheet joint and study the change in the distribution of stresses and interference pressure as a result of the joint elevated temperature. As in other previous analyses the tube-to-tubesheet joint model can be greatly simplified by considering a single tube surrounded by an annular sleeve.

6.2.1 Validation of the Axisymmetric FE Model

In order to detect any small variation in the stresses resulting from the temperature effect, a more refined mesh at the location where high stress gradient is expected to take

place, is constructed as shown in Figure 6.1. The mesh is refined in both the tube and the sleeve at the location where the crevice zone will be located. Also, a fine mesh is used along the tube transition zone. The finite element model is developed using a total of 842, 2-D isoparametric 8-node axisymmetric elements having a total of 2348 nodes with three degrees of freedom at each node. The contact boundary conditions is also considered using 3-node axisymmetric contact elements. Since the coefficient of friction of the material used in this chapter is unknown, a value of 0.35 is assumed based on the average range of the coefficient of friction of typical materials. It is to be noted that the coefficient of friction measured in the previous chapter was for tube and tubesheet materials (Inconel 690 and SA-508 steel, respectively) which are not used in this chapter. The friction model follows Coulomb's friction law. All nodes along the tube and sleeve primary side are constrained in the axial direction while the radial displacement is conditioned by the level of the expansion pressure used. The remaining nodes in the entire model are left to move freely in the r-z plane. The expansion pressure is also applied over the part of the tube inner surface that lies under the sleeve. It is increased from zero to the maximum level required through an incremental loading step, and then removed in a following step. In addition to the mechanical and frictional properties of the tube and tubesheet materials, there are also the thermal properties that must be given in the material definition for the temperature-displacement analysis.

The equivalent sleeve diameter, given by Chaaban et all (1992) and Kohlpaintner (1995), are adopted. The validation of the equivalent axisymmetric model for the working

condition analysis, is done first by comparing its results to those obtained by using the 3-D finite element model. The 3-D model shown in Figure 3.9 with the material and geometrical data as wall as the loading conditions of the four cases listed in Tables 3.1 and 3.4 are used here. In addition to the material data of Tables 3.1 and 3.4, the thermal properties for the tube and tubesheet materials are given in Table 6.1 for each case.

First, the expansion process was simulated using each finite element model to provide the initial deformations and stresses of as-expanded joint at room temperature (20°C). Then, the joint is subjected to a temperature cycle simulated in the finite element solution, as follows: 1) change the model temperature from the initial temperature (20°C) to that of the operating condition, and then: 2) back to 20°C. So, the thermal cycling is achieved incrementally in two successive steps. For each study case, two sperate temperature cycles are performed. Table 6.2 indicates the variation in the temperature during each cycle for every case. For each thermal cycle, the 3-D and axisymmetric finite element results are compared at the maximum temperature change and after temperature cycle, on the basis of the following parameters:

1- The axial stress on the tube inner surface at distance (Z/d=1.2)

2 - Interference contact pressure between the tube and the tubesheet.

3 - Circumferential strain at the tube inner surface

4 - Circumferential strain at the tubesheet inner surface.

5- CPU (Central Processing Unit) time required on IBM 6000 workstation.

Table 6.3 presents the axial stress and interference pressure values prior and after heating and cooling temperature cycles, as calculated by the 3-D and axisymmetric finite element models. The results of strains represented in Table 6.4 compare well. Unlike the expansion process which necessarily develops a plastic deformation in the tubes and, in some cases, plastically deforms the tubesheet, the thermal loading and unloading does not produce any plastic deformation. In most cases, the axisymmetric model is executed with much less CPU time (see Table 6.5).

Due to the good agreement in the results obtained by using the 3-D and the equivalent axisymmetric models for the selected cases, one may conclude that the equivalent sleeve diameter calculated empirically by Chaaban et al (1992) and analytically by Kohlpaintner (1995) on the basis of as-expanded joint parameters, can be used satisfactorily in the single-tube model in order to predict the tube-to-tubesheet joint behaviour under thermal loading.

The same axisymmetric model was also verified by comparing its results to those obtained by the layered element model developed by Soler et al (1984). The different tube and tubesheet material combinations and particular geometries specified by Soler (1984), and listed in Table 4.3, are also used here. The thermal coefficient of expansion of each case is given in Table 6.6. The tube and tubesheet materials, the geometry and the level of expansion

pressure of Data No. 5 are similar to those of Data No. 1. In all cases, the room temperature is taken to be 20 °C and the thermal cycle is done by heating up the entire model to 200 °C and then back to the room temperature. The only exception was in Data No. 5 where the model is cooled down to -200 °C and then heated up to the room temperature. Since the mathematical solution given by Soler (1984) was for a 2-D plane stress model, the residual stresses in the tube transition zone was not calculated. Consequently, only the results related to the interference contact pressure are compared with Soler's solution for as-expanded condition and under the effect of the temperature cycle. Table 6.7 summarizes the results as provided by Soler et al (1984) and as calculated by our axisymmetric finite element model. During the thermal loading of case No. 3 the level of the residual contact pressure falls down to almost zero as predicted by both models. Also for data No. 4 the residual contact pressure was lost completely at low level of working temperature (approximately 80 °C) as also predicted by both models. In general, Table 6.7 shows that the results obtained by our axisymmetric finite element model are in good agreement with the incremental solution given by the layered element model proposed by Soler.

During the thermal loading in the second case (Data No. 2), there is no significant change in the contact pressure during heating up to operating temperature as predicted by both models. However, removal of the thermal loading causes significant reduction in the finial level of the residual contact pressure. This phenomenon will be discussed in the analytical section. Also, a considerable reduction in the contact pressure occurs for the fourth

case (Data No. 4) in which titanium and Muntz materials are used for the tube and tubesheet, respectively. Increasing the temperature in the thermal cycle essentially reduces the contact pressure due to the significant difference in the coefficient of the thermal expansion between the titanium and Muntz.

The above mentioned results indicate that the change in the level of the residual contact pressure is controlled by the sign of the term $((\alpha_t-\alpha_s)\Delta T)$ during thermal loading. However, as it will be shown later, the final value of the contact pressure is affected by the level of the thermal load as well as the plastic deformation that may develop in the tube during the thermal loading. The next section presents a simplified analytical approach to discuss in details the behaviour of the tube-to-tubesheet joint and to approximate the change in its strength during the thermal cycle.

6.2.2. Selecting the Proper Boundary Conditions

An additional point regarding the effect of the boundary conditions used in the axisymmetric model must be also verified. Up to now, the upper end of the tube was left free while applying the thermal loads. This boundary condition may be considered as a simulation of a heat exchanger having a floating tubesheet and/or U-tubes, see Figure 6.2 (BOUND-1). When, the upper end of the tube and tubesheet primary side are constrained in the axial direction, it would simulate a heat exchanger having fixed tubesheets without a shell

expansion joint, see Figure 6.2 (BOUND-2).

Both boundary conditions are applied separately to the axisymmetric finite element model on a typical case given in Table 6.8. Two different temperature cycles are simulated for heating up and cooling down the expanded joint. The change in the temperature (ΔT) with respect to the initial temperature T_o is taken to be +2 and -4 for the hot and cold working conditions. Figure 6.3 shows the tube profile for as-expanded joint, at heating thermal load and after the temperature cycle for the two different boundary conditions used. Figure 6.4 shows the same type of curves but for the cooling cycle. As expected, Figures 6.3 and 6.4 show that the change in the tube diameter is positively correlated to the temperature modification in both cases (BOUND-1 and BOUND-2). After a temperature cycle, the initial tube deformed shape is fully recovered without affecting the initial level of the residual contact pressure, specially with the first class of the boundary condition (BOUND-1). However, after the temperature cycle, with the second type of boundary condition (BOUND-2), the reduction of the tube diameter in the expanded zone was much lower than that of as-expanded joint, and the initial residual contact pressure was thus relieved completely. Figures 6.5 and 6.6 show the axial and hoop residual stress distributions on the tube inner and outer surfaces for as-expanded joint, during the thermal loading and after thermal cycle for the two types of boundary conditions (BOUND-1 and BOUND-2). Based on these figures, it seems that in BOUND-1 situations, the thermal loading and unloading of elevated temperature have no significant effect on the stress profiles. The same behaviour is also observed with the

cooling thermal cycle. However, the second type of boundary condition (BOUND-2) has a significant effect on the stress profiles depending on the tube length, as shown in Figures 6.5 and 6.6. It seems that this boundary condition is not realistic for the level of temperature considered. Therefore, the first type of the boundary condition (BOUND-1) has be selected in the subsequent finite element analysis.

6.3 ANALYTICAL APPROACH

As has been shown in the previous section, any subsequent temperature change from the initial temperature at which the joint was expanded, could modify the level of the residual contact pressure upon which the joint sealing and strength are strongly dependent. This phenomenon depends on various parameters such as temperature range, joint dimensions and material properties of the tube and the tubesheet.

6.3.1 Simplified Analytical Analysis

Again for the purpose of simplicity, the tube and the tubesheet geometries are idealized by a 2-D plane stress cylindrical element as shown in Figure 6.7. After the joint is expanded and a level of residual contact pressure is set up by the expansion process, any change in the temperature will change also the level of the residual contact pressure by (ΔP). The initial residual contact pressure is taken as a reference level for the interference pressure

calculation. According to Burgreen (1971), the change in the circumferential strain at the tube outer surface and the sleeve hole can respectively be given by:

$$\Delta\epsilon_t = -\frac{\Delta P}{E_t}\left(\frac{Y_t^2+1}{Y_t^2-1} - \nu_t\right) + \alpha_t \Delta T \qquad (6.1)$$

$$\Delta\epsilon_s = \frac{\Delta P}{E_s}\left(\frac{Y_s^2+1}{Y_s^2-1} - \nu_s\right) + \alpha_s \Delta T \qquad (6.2)$$

The absolute values of $\Delta\epsilon_t$ and $\Delta\epsilon_s$ must be the same, unless there is separation between the tube and tubesheet. By satisfying this condition, the following equation must be thus obtained;

$$\Delta P = K_t (\alpha_t - \alpha_s) \Delta T \qquad (6.3)$$

where K_t is given by:

$$\frac{1}{K_t} = \frac{1}{E_t}\left(\frac{Y_t^2+1}{Y_t^2-1} - \nu_t\right) + \frac{1}{E_s}\left(\frac{Y_s^2+1}{Y_s^2-1} - \nu_s\right)$$

Then, the final interference contact pressure during the thermal loading can be obtained as follows:

$$P_f = P^* + \Delta P \qquad (6.4)$$

the stress state on the tube outer surface can be obtained by superposition as follows:

$$\sigma_\theta = - \Delta P \left(\frac{Y_t^2 - 1}{Y_t^2 + 1} \right) + S_{r\theta} \qquad (6.5)$$

Where $S_{r\theta}$ is the residual hoop stress left on the tube outer surface as a result of the expansion process.

The radial stress on the tube outer surface is always equal to the interference contact pressure with reverse sign, thus:

$$\sigma_r = -P_f \qquad (6.6)$$

If plastic deformations take place, the stress state on the tube outer surface is assumed to follow the Von-Mises yield criterion which could be represented by the following equation:

$$\sigma_\theta^2 + P_f \sigma_\theta + P_f^2 = S_{yt}^2 \qquad (6.7)$$

.

In practice, no plastic deformations would be considered due to the working temperature. However, by including them in the present development, a better understanding of the joint behaviour may be revealed.

Figure 6.8 shows graphically the relation between σ_θ and P_f (P_f is the interference contact pressure on the tube outer surface at any loading stage) on the tube outer surface for the total cycle starting from the first point (1) at which the tube is set to be hydraulically expanded, and ending by the final operating interference pressure due to different thermal conditions. In this figure, the tube outer surface is elastically expanded from point (1) to point (2) beyond which the tube wall becomes fully plastic. At this point the tube has no more stiffness to take additional applied internal pressure. Therefore, a contact interaction between the meeting surfaces of the tube and the tubesheet takes place at the same point (2) on the σ_θ-P_f curve. Any further increase in the expansion pressure will deform the tubesheet and create an interference pressure P_f. The stress state from point (2) up to point (3) is located on the yield surface given by Equation (6.7), at which the expansion pressure reaches a peak value. When the expansion pressure is released, the tube springback linearly from point (3) to the residual state (4) which represents the as-expanded joint condition. At point (4), the residual contact pressure P^* and the residual stress $S_{r\theta}$ are introduced in the tube wall. Indeed, the thermally induced stress must first start elastically and then plastically. This means that the stresses first exhibit a linear relation (say line (A-B) that represents the relationship between σ_θ and P_f in the elastic domain as given by Equation (6.5). The direction in which the stress state is modified, depends on the final sign of the thermal term $((\alpha_t-\alpha_s)\Delta T)$ in Equation (6.3). If the sign is positive, ΔP will be also positive which should cause an increase in the interference pressure (P_f) and the stress state must go to the left hand side direction in order to satisfy the required increase in the interference pressure. A negative sign of the thermal

term will reverse the direction of the stress state towards the right hand side. Consider the first possibility by which the stress state goes elastically from point (4) to point (5) at which the interference pressure increases by ΔP. If the thermal state is taken away, the stress state will return elastically to point (4) without changing the initial level of the residual contact pressure. On the other hand, the change in the temperature could be so high that it will cause the stress state to go beyond the elastic yield surface from point (5) to point (6). If the temperature is reduced to its initial value, the stresses will drop linearly on a different elastic line that is parallel to line A-B. Therefore, the final stress state at point (7) could have a different final value of the interference pressure that could be either higher or lower than the initial residual contact pressure (Point 4). Now, If the sign of thermal term $((\alpha_t-\alpha_s)\Delta T)$ of Equation (6.3) is negative, a negative value for ΔP will result according to Equation (6.3). Consequently a reduction in the interference pressure will take place and the stress state will thus go down elastically on the same line A-B, from point (4) to point (9) beyond which the interference pressure becomes negative implying a separation between the tube and tubesheet. The stress state must be at or above point (9) depending on the joint geometry, material property, as-expanded stress state and the level of the thermal loading. Practically, in most cases the stress state does not reach point (9) and linear elastic thermal unloading moves back to point (4) with no change in the initial residual contact pressure. Thus, elastic unloading always takes place on the same line A-B leading the initial state at point (4) to be fully recovered. The condition of point (9) is identical to that of Data No. 3 in Table 6.7, at which the initial residual contact pressure is reduced to almost zero and then is fully recovered when

the temperature returns back to that of the as-expanded joint condition.

Generally, when a negative thermal term is provided ($(\alpha_t-\alpha_s)\Delta T < 0.0$), the initial residual contact pressure declines and the resulting loss can be linearly calculated from Equation (6.3). However, when a positive value is imposed ($(\alpha_t-\alpha_s)\Delta T>0.0$), the initial residual contact pressure is expected to increase and the situation becomes more complicated. If the stress state is lower or equal to that of point (5) on Figure 6.8, the resulting increase in the contact pressure can also be calculated directly from Equation (6.3). If the increase in the initial contact pressure becomes high enough to cause an additional plastic deformation in the tube, an elastic-plastic analysis is required to calculate the change in the initial residual contact pressure during and after the thermal loading. Also, in this case, the expanded joint could become weaker when the temperature is reduced to the temperature at which the joint is expanded.

6.3.2 Joint Tightness Coefficient

In order to better estimate the joint performance under operating temperature, it is proposed to replace the absolute value of the interference contact pressure during the working condition by the proposed "Joint Tightness Coefficient; (η)". It can be used to assess the quality of the tube-to-tubesheet joints and give and indication how tight they are under working conditions. It also evaluates the working condition behaviour of the joint as

compared to that of as-expanded joint for which the leakage tightness and the axial strength are already known. The value of η is expressed by the percentage change in the level of the interference contact pressure as a result of a mechanically and/or thermally induced deformation:

$$\eta = \frac{P_f - P^*}{P^*} \times 100$$

where P^* is the level of the initial residual contact pressure set up by the expansion process, and P_f is the final value of the interference contact pressure during operation. The value of η may be positive, near-zero or negative. At -100% the joint has zero interference contact pressure and therefore the initial residual contact pressure is totally released.

6.4 PARAMETRIC ANALYSIS OF THERMAL LOADING AND UNLOADING

The axisymmetric finite element model explained earlier is used here to study the effect of temperature on the residual contact pressure and residual stresses in the tube-to-tubesheet joint having different design parameters. The main purpose of this section is to perform a detailed parametric study in order to evaluate the behaviour of:

1- The joint tightness coefficient during thermal loading

2- The final residual contact pressure after the temperature cycle.

3- The maximum tensile residual stresses and their axial location during the thermal loading and after the temperature cycle.

Many calculations are carried out on three different material combinations for the tube and the tubesheet as listed in Table 6.9. As it has been shown in the analytical section, the joint behaviour under the thermal loading is depending on the level and the sign of the thermal term of Equation (6.3). Therefore, the material combinations selected in Table 6.9 are sorted out in order to provide three possible levels for the term (α_t - α_s). As shown in Table 6.10, the level of this term in material SET-1, SET-2 and SET-3 is equal to zero, greater than zero and less than zero, respectively. These material sets are also selected according to real combinations of tube and tubesheet materials that are used in industrial applications.

Three levels are selected for each of the remaining design parameters namely; tube wall thickness, initial clearance, equivalent sleeve diameter, and the level of the expansion pressure, as listed in Table 6.11. The dimensions are chosen according to the geometrical standard provided by TEMA (1988), while the expansion pressure is limited by the yield strength of the tube and tubesheet materials.

In order to save time while taking into account the effect of all possible combinations of the design parameters, the orthogonal design array is used once again. As shown in Table

4.8, nine calculations must be carried out for each material set. For each calculation, the joint is to be expanded first. It is then exposed to two separate thermal cycles (heating and cooling), so as to predicted the joint behaviour under five different conditions. The temperature change ($\Delta T/T_o$) in the heating and the cooling cycles will be +2 and -4, respectively. In spite of using the orthogonal design method, a total of 135 calculations are required to complete the finite element analysis.

6.4.1 Effect of Temperature Change on Residual Stresses in the Transition Zone

Some typical axial and hoop stresses profiles along the tube axis are shown in Figures 6.9 and 6.10 for as-expanded joints, during the operating temperature and after heating and cooling cycles. In order to compare these curves, each study case is characterized by two specific values; 1) the level of the maximum tensile axial and hoop stresses and 2) their axial locations.

Figures 6.11 and 6.12 show plots of the maximum tensile axial and hoop stresses calculated during and after the thermal loading, and compared to those of the as-expanded joint. The maximum change in the tensile residual stress as a result of the thermal loading or unloading is found to be about ±12%. The highest percentage change in the stress state is observed in the cases at which the interference contact pressure is either greatly increased or totally released during the thermal loading and after the temperature cycles. In order to

compare between those stresses, the mean values of the initial maximum tensile axial and hoop stresses and those obtained by various thermal conditions are calculated and listed in Table 6.12. Relatively lower values of the standard deviation are found. The calculation of the coefficient of variation indicates a very low level of dispersion around the means and therefore confirms the central tendency of the data. Since in all cases, the coefficients of variation are in the same order (less then 10%), the mean values can be compared directly. On this basis, it can be concluded directly that the thermal loading or unloading has a negligible effect on the level of maximum tensile residual axial and hoop stresses in the tube transition zone.

Regarding the axial location of these stresses, the results indicate that, for all cases considered, the thermal loading and unloading do not influence the axial location at which the maximum tensile axial and hoop residual stresses are initially introduced by the expansion process.

6.4.2 Effect of Thermal loading on the Joint Tightness Coefficient.

The loss of the joint tightness may result from the tube and/or tubesheet relaxation caused by thermally induced deformations. The level of the interference contact pressure is related to the difference between the rate of the radial thermal expansion in the tube and the tubesheet. The initial residual contact pressure and the change in its value during and after the

temperature cycle are calculated for each material set in Table 6.9 and for each combination of design parameters as given by the orthogonal design method (Table 4.8). As was shown in the analytical section and confirmed here by the finite element analysis, the joint tightness coefficient (η) may be used to estimate the joint performance under operating conditions. The initial value of the residual contact pressure as well as the joint tightness coefficient (η) during the heating and cooling operating temperature are calculated by the axisymmetric finite element solution and given in Table 6.13. The change in the initial level of the residual contact pressure depends on the sign of the thermal term $((\alpha_t-\alpha_s)\Delta T)$ and not on the sign of the temperature only as predicted by Yokell (1990).

Regarding the level of the joint tightness coefficient, Table 6.13 shows that the material combinations and the level of the operating temperature have a considerable effect on the value of η. This merely reflects that the joint performance at the working conditions depends on the dimensional and material design parameters and on the more obvious factors such as the level of the working temperature and the thermal coefficients of expansion of the tube and the tubesheet.

While the η factor indicates an enhancement in the joint performance under the elevated temperature for the second material set (SET-2), the lowest value of η reflecting a very bad joint behaviour is found for the same material set when exposed to cooled working temperature. On the other hand, for the material combination (SET-3), a drop in the joint

performance results when heating up the joints, and an enhanced behaviour is found when the same joints are exposed to a lower temperature. Finally, the first material set (SET-1) that has the same thermal coefficient of expansion for the tube and the tubesheet, shows almost no response for either heating or cooling temperature and provides near-zero level for η.

In general, with a positive sign for the thermal term $((\alpha_t-\alpha_s)\Delta T)$, an increase in the joint tightness coefficient reflecting an enhancement in the joint performance will result during working conditions. However, the increase in the joint tightness coefficient must be limited by the plastic deformation. Some plastic deformations are often observed in either the tube or the tubesheet when the joint tightness coefficient exceeds approximately 40%. As will be shown, when the working temperature causes plastic deformation in either the tube or the tubesheet and then drops as a result of, say, shut down conditions, the initial residual contact pressure in every tube-to-tubesheet joints could be permanently reduced to a lower level that most likely will require the joints to be reexpanded. This problem can be simply avoided by taking into account the change in the temperature and choosing proper material combination to prevent any plastic deformation to be developed in either the tube or the tubesheet. Three important limiting temperatures are given in Appendix II. On the other hand, if the thermal term $((\alpha_t-\alpha_s)\Delta T)$ is negative, a negative value of the joint tightness coefficient reflecting a bad joint behaviour is anticipated. But, when the working temperature is lowered to that of the initial condition, no loss in the initial contact pressure will be expected. For a good behaviour at working conditions, the lower value of η should be limited by -25%. In addition, the initial

contact pressure set up during the manufacturing process must be high enough to substitute the anticipated reduction in the contact pressure during the operating condition.

6.4.3 Effect of Thermal Unloading on the Initial Residual Contact Pressure

Apart from the operating temperature which imposes certain changes in the joint tightness coefficient, the thermal unloading which modifies the working temperature back to that of the initial condition, may not necessary permit the initial residual contact pressure to be fully recovered. Generally, unloading of the operating thermal condition could change the initial residual contact pressure to an unknown extent depending on the kind of deformation (elastic or plastic) at the operating temperature. Indeed, the induced-thermal elastic deformation will provoke elastic unloading by which the initial residual contact pressure could be reestablished. However, the induced-thermal plastic deformation would introduce a great reduction in the initial residual contact pressure after thermal unloading.

In order to investigate this phenomenon, the temperature is reduced from operating back to the room. The value of the final interference contact pressure after each temperature unloading is calculated using the axisymmetric finite element model and recorded for statistical analysis. The mean value and the standard deviation of this pressure are compared to the initial residual contact pressure, as shown in Table 6.14. The t-value is also calculated in order to compare between the estimated means of the different level of interference contact

pressure. The value of $t(\alpha,d)$ as provided by Dally (1983) is 2.12 with 2.5% level of significance (α) combined with the degree of freedom (d) equal to 16 in the cases being considered. The first material set (SET-1) yields approximately the same means of the interference contact pressure for the three cases considered; initial (AE), after the heating temperature cycle (AT_h) and after the cooling temperature cycle (AT_c). Consequently, a very low level of t-value is calculated and indicates that all the differences between the initial residual contact pressure and those calculated after the temperature cycles are attributed to a random error. Since the t-value is less than $t(\alpha,d)$ for the second material set (SET-2), it can be concluded with 97.5 % level of confidence that there is no change in the initial residual contact pressure after heating or cooling temperature cycle for this particular material set having ($\alpha_i > \alpha_y$). However, some cases of this material set show a significant loss in the initial residual contact pressure after a heating temperature cycle during which a plastic deformation is developed in the tube. While the cooling temperature causes a full release of the initial residual contact pressure as shown in Table 6.13 for the second material set, the initial residual contact pressure of every joint is totally recovered after the temperature cycle as shown in Table 6.14. In this case, no-plastic deformation is developed and the joint behave no-stress change (i.e. no response to the temperature) at the peak level of the cooling temperature (see Figure 6.8; Point 9). A similar behaviour is also observed with the third material set (SET-3) during the hot operating temperature. While, a very low interference contact pressure is established by the elevated temperature, the initial residual contact pressure is perfectly recovered again when the temperature is dropped to that of the initial

conditions. Thus, a small level of t-value referring to a lower difference between the mean of the initial contact pressure and that calculated after the heating cycle, is obtained. For the same material combination (SET-3), the residual contact pressure has been strongly influenced by the cooling cycle. This is merely proved by the large difference between the mean of the initial residual contact pressure and that calculated after the cooling cycles. Also, as shown in Table 6.14, the t-value is greater than $t(\alpha,d)$, and therefore a significant difference between the two means is obtained. In fact, plastic deformation is developed in every joint made from this particular material set when exposed to a lower temperature. In spite of instantaneously increasing the interference residual contact pressure, this deformation, when released as a result of a change in the temperature, negatively influences the joint elastic recovery and leads to a great reduction in the initial residual contact pressure.

Executive summary

3-D and axisymmetric finite element analyses of tube-to-tubesheet joint under working temperature were presented in this chapter. A comparison between these two finite element models indicated that the equivalent axisymmetric model might efficiently be used to investigate the effect of temperature on both the residual contact pressure and residual stresses in the tube transition zone. The results of the FEM parametric study indicated that during thermal loading and after temperature cycling, the maximum tensile residual stresses in the tube transition zone were practically unchanged. It has been also found that the joint

tightness coefficient was greatly affected by both the value and the sign of the thermal term ($(\alpha_t - \alpha_s)\Delta T$). During the working temperature, a positive value of this term would improve the joint performance and vice-versa. Finally, a comparison between the initial residual contact pressure set up by the expansion process and the final contact pressure after a temperature cycle was performed. The results showed a significant reduction in the final value of the residual contact pressure when plastic deformation was developed in the joint at the operating temperature.

Table 6.1: Thermal properties of the cases used in the 3-D model

(κ by (W/m K) and α by (1/ °C)x10^{-6})

Case	Tube			Tubesheet		
	Material	κ	α	Material	κ	α
CASE-1	*St. steel*	589.7	12.065	*steel*	589.7	12.065
CASE-2	*St. steel*	589.7	12.065	*steel*	589.7	12.065
CASE-3	*90:10 Cu Ni*	657.5	17.1	*Muntz*	1474.2	20.88
CASE-4	*70:30 Cu Ni*	401.4	16.2	*90:10 Cu Ni*	657.5	17.1

Table 6.2: Change in temperature for each involved case

	Heating Cycle				Cooling Cycle			
CASE	1	2	3	4	1	2	3	4
$\Delta T/T_o$	4.5	4.5	2	4.5	-5.5	-5.5	-5	-5.5

Table 6.3: Axial stresses and interference pressure as given by 3-D and axisymmetric FEM

Model	S_z/S_{yt}					P_f/S_{yt}				
	AE	Heating Cycle		Cooling Cycle		AE	Heating Cycle		Cooling Cycle	
		OT_h	AT_h	OT_c	AT_c		OT_h	AT_h	OT_c	AT_c
CASE-1										
3-D	0.567	0.568	0.567	0.583	0.567	0.040	0.040	0.040	0.038	0.038
Axy	0.495	0.495	0.495	0.495	0.495	0.039	0.039	0.039	0.039	0.039
CASE-2										
3-D	0.652	0.635	0.635	0.635	0.635	0.075	0.072	0.075	0.075	0.074
Axy	0.713	0.713	0.713	0.713	0.713	0.074	0.074	0.074	0.074	0.075
CASE-3										
3-D	0.663	0.772	0.708	0.593	0.632	0.110	0.053	0.102	0.215	0.067
Axy	0.770	0.823	0.770	0.599	0.750	0.107	0.046	0.093	0.206	0.052
CASE-4										
3-D	0.528	0.586	0.578	0.569	0.577	0.156	0.121	0.159	0.181	0.145
Axy	0.681	0.710	0.681	0.638	0.675	0.146	0.114	0.145	0.174	0.135

Table 6.4: Tube and tubesheet deformations as given by 3-D and axisymmetric FEM

Model	$\epsilon_s \times 10^{+3}$					$\epsilon_t \times 10^{+3}$				
	AE	Heating Cycle		Cooling Cycle		AF	Heating Cycle		Cooling Cycle	
		OT_h	AT_h	OT_c	AT_c		OT_h	AT_h	OT_c	AT_c
CASE-1										
3-D	0.062	2.176	0.062	-2.52	0.062	12.63	14.96	12.71	10.18	12.71
Axy	0.063	2.161	0.063	-2.51	0.063	12.05	14.19	12.05	9.444	12.05
CASE-2										
3-D	0.125	2.242	0.128	-2.45	0.128	13.09	15.23	13.09	10.47	13.09
Axy	0.124	2.238	0.124	-2.45	0.124	12.20	14.34	12.20	9.591	12.20
CASE-3										
3-D	0.157	1.589	0.155	-3.73	0.071	6.313	7.821	6.314	2.100	6.161
Axy	0.155	1.591	0.155	-3.76	0.071	5.969	7.481	5.970	1.765	5.830
CASE-4										
3-D	1.733	4.662	1.712	-1.90	1.690	8.898	11.88	8.876	5.174	8.841
Axy	0.789	3.738	0.789	-2.82	0.773	6.999	10.00	6.999	3.301	6.969

Table 6.5: CPU time consumed by 3-D and axisymmetric models

	Heating Cycle				Cooling Cycle			
CASE	1	2	3	4	1	2	3	4
3-D	17019	15435	13857	15975	15545	15511	14486	1569
Axy	91.2	93.39	99.13	97.55	91.91	93.4	113.78	95.43

Table 6.6: Thermal coefficient of expansion (10^{-6} x (1/ °C))for the materials used by Soler (1984); (see Table 4.2)

Data No.	Tube	Tubesheet
1	16.2	17.1
2	16.2	11.7
3	16.2	20.88
4	8.64	20.88

Table 6.7: Axisymmetric FE residual contact pressure versus the calculation of the layered model (Soler (1984)); (OT: Operating temperature, AT: After temperature cycle)

Data No.	Method Used	As-Expanded	Thermal Cycle	
			OT	AT
1	FE	0.1407	0.1059	0.1393
	Soler	0.1298	0.1096	0.1297
2	FE	0.0642	0.0858	0.0048
	Soler	0.0743	0.0744	0.0045
3	FE	0.0866	0.0017	0.0789
	Soler	0.0738	0.0069	0.0738
4	FE	0.0132	No Contact	-
	Soler	0.0192	No Contact	-
5	FE	0.1407	0.1496	0.1104
	Soler	0.1298	0.1298	0.1052

Table 6.8: Typical case used for boundary conditions verification, see Figure 6.2

Design parameters							
t/d	c/d	D_c/d	E_t/S_{yt}	S_{ys}/S_{yt}	E_s/E_t	α_s/α_t	P_c/S_{yt}
0.109	0.004	3.0	966.7	1	1	1	0.9
Operating temperature $\Delta T/T_o$							
Heating				Cooling			
2				-4			

Table 6.9: Materials used for parametric study

Material Combination	Tube	Tubesheet
SET-1	*Stainless steel*	*Carbon Steel*
SET-2	*Nu.Cu. 70:30*	*Carbon Steel*
SET-3	*Nu. Cu. 90:10*	*Muntz*

Table 6.10: Material properties of tube and tubesheet; see Table 7.9

Material Set	Tube				Tubesheet			
	Mechanical Properties		Thermal Properties		Mechanical Properties		Thermal Properties	
	S_{yt}	E_t	α_t	κ_t	S_{ys}	E_{ys}	α_s	κ_s
SET-1	206.8	200.0	12.06	589.7	206.84	200.0	12.06	589.70
SET-2	124.1	151.7	15.66	401.4	206.84	200.0	12.06	589.70
SET-3	103.4	124.1	17.10	657.5	137.90	103.4	20.88	1474.2

Table 6.11: Three levels of dimensions and expansion pressure

Level	Dimensions			Expansion pressure
	t/d	c/d	D_e/d	P_e/S_{yt}
1	0.065	0.003	2.00	0.8
2	0.087	0.007	2.67	0.9
3	0.127	0.01	3.33	1.0

Table 6.12: Maximum tensile residual axial and hoop stresses for as-expanded joint and during and after temperature cycles (Mean values and standard deviation)

Stress	Parameter	Working Conditions				
		AE	Heating Cycle		Cooling Cycle	
			OT_h	AT_h	OT_c	AT_c
S_z^*/S_{yt}	σ	0.9687	0.9690	0.969	0.9574	0.9636
	λ	0.0310	0.0297	0.0301	0.0494	0.0339
	C_v%	3.197	3.0651	3.1056	5.1584	3.5182
S_θ^*/S_{yt}	σ	0.5943	0.5960	0.5945	0.5937	0.5932
	λ	0.0185	0.0184	0.0178	0.0223	0.0183
	C_v %	3.1152	3.0797	2.9991	3.7575	3.0789

able 6.13: Residual contact pressure for as-expanded joint and η factor during thermal loading

Calculation No.	P^*/S_{yt}			Joint Tightness Coefficient (η)					
	AE			OT_h			OT_c		
	SET-1	SET-2	SET-3	SET-1	SET-2	SET-3	SET-1	SET-2	SET-3
1	0.064	0.033	0.074	-0.110	134.4	-57.5	0.198	-100	60.1
2	0.075	0.038	0.099	-0.118	150.6	-58.1	0.220	-100	76.8
3	0.094	0.051	0.121	-0.109	159.6	-62.7	0.206	-100	94.2
4	0.083	0.046	0.101	-0.188	101.50	-49.3	0.332	-100	20.1
5	0.026	0.010	0.039	-0.505	394.1	-82.5	1.155	-100	244.6
6	0.078	0.030	0.094	-0.276	246.7	-65.1	0.523	-100	109.1
7	0.041	0.008	0.056	-0.557	504.3	-77.1	0.969	-100	87.1
8	0.103	0.057	0.117	-0.264	82.01	-48.5	0.432	-100	19.8
9	0.020	0.009	0.024	-0.223	295.6	-84.9	0.387	-100	425.8

Table 6.14: Mean level of the residual contact pressure for as-expanded joint and after temperature cycles

material	SET-1			SET-2			SET-3		
Condition	AE	AT_h	AT_c	AE	AT_h	AT_c	AE	AT_h	AT_c
σ	0.065	0.065	0.065	0.031	0.026	0.033	0.081	0.083	0.037
λ	0.029	0.029	0.029	0.019	0.014	0.020	0.034	0.036	0.021
t	-	0.0003	0.0019	-	0.719	0.799	-	0.1325	3.437
$t(d,\alpha)$	2.12			2.12			2.12		

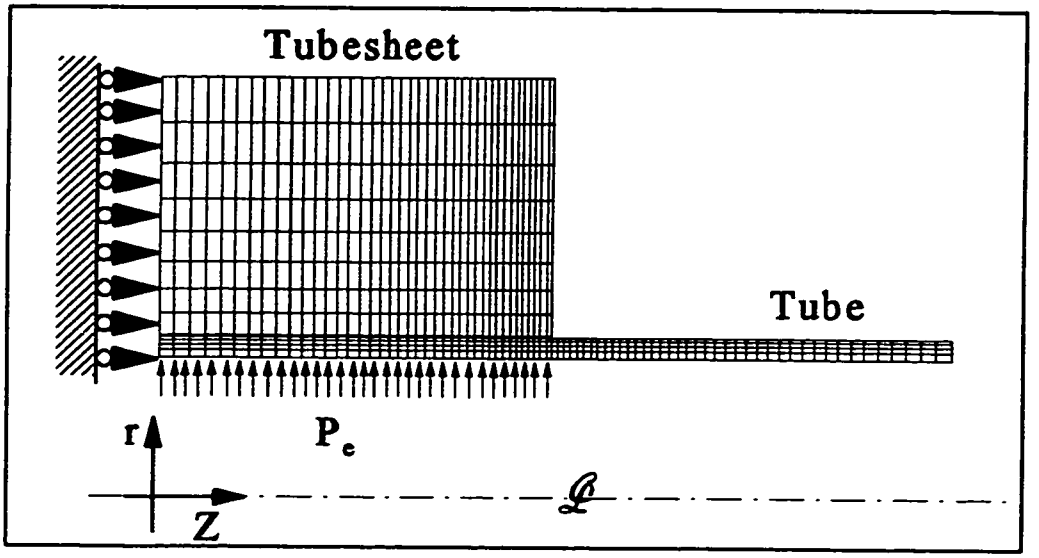


Figure 6.1: Equivalent axisymmetric model for the thermal loading analysis

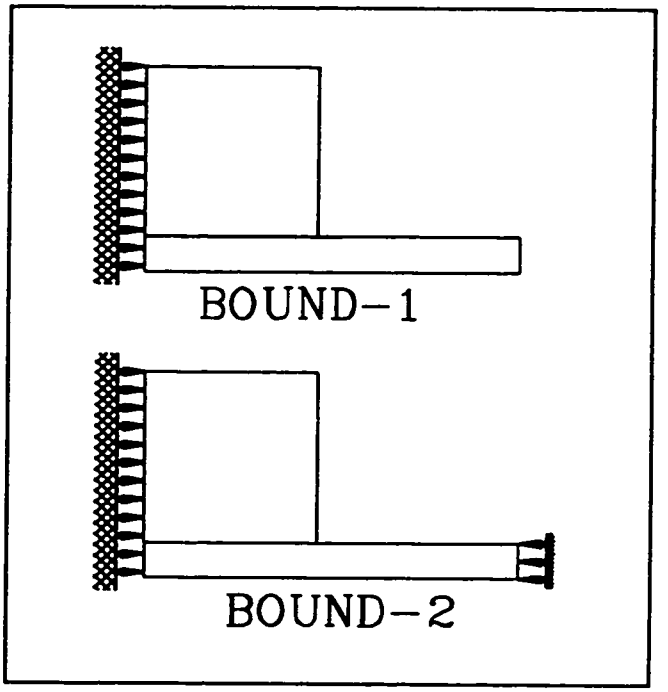


Figure 6.2:Two different boundary conditions that are applied in the axisymmetric model

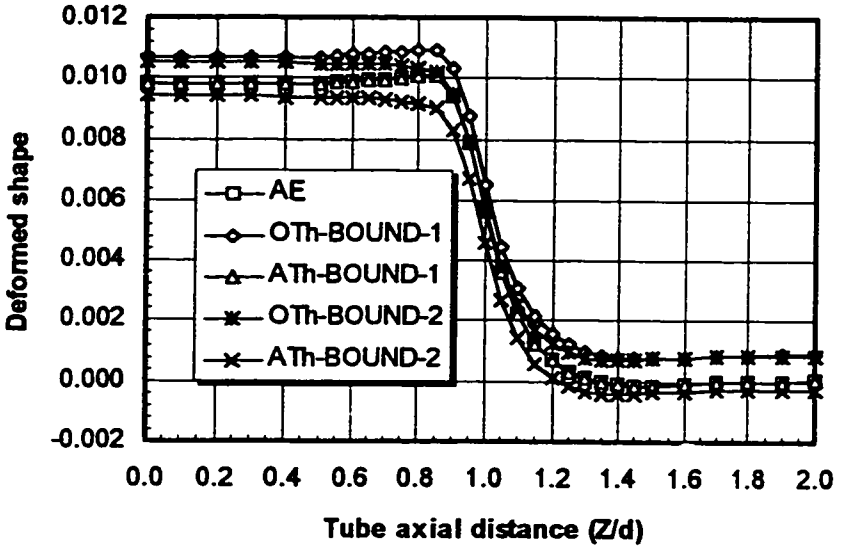


Figure 6.3: As-expanded (AE), during heating (OT_h) and after temperature cycle (AT_h), tube profile with the two boundary conditions used; see Fig.6.2

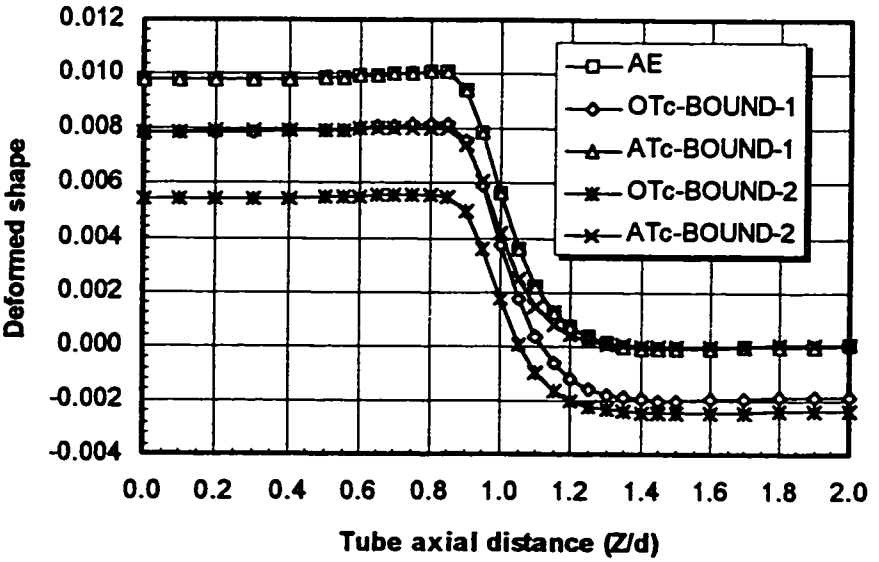


Figure 6.4: As-expanded (AE), during heating (OT_c) and after temperature cycle (AT_c), tube profile with the two boundary conditions used; see Fig.6.2

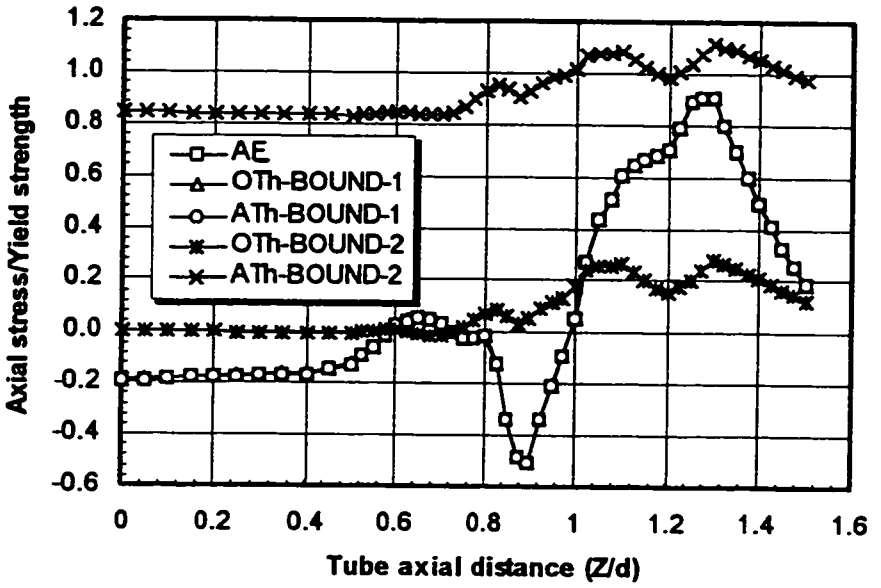


Figure 6.5: As-expanded (AE), during heating (OT_h) and after temperature cycle (AT_h) axial stress profile with the two boundary conditions used, see Fig 6.2

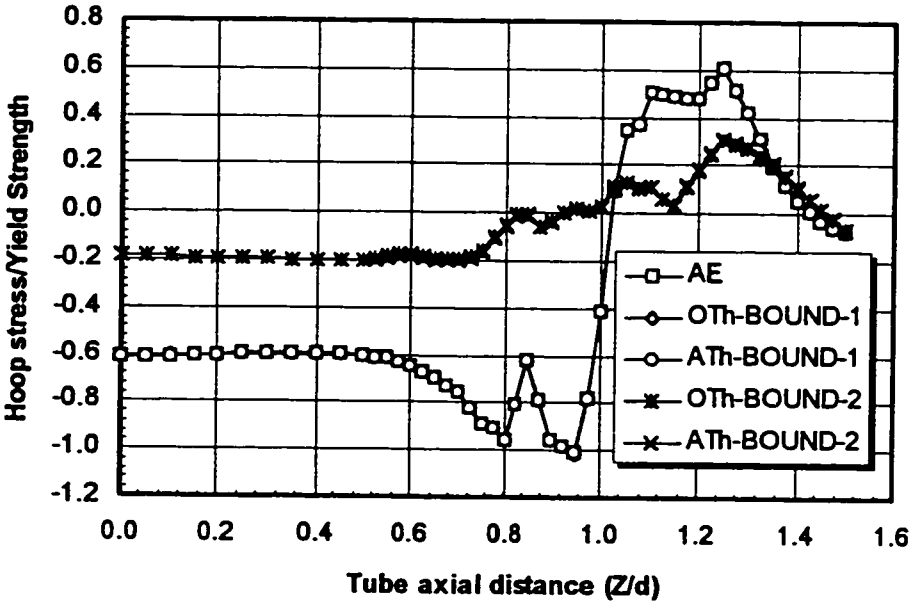


Figure 6.6: As-expanded (AE), during cooling (OT_c) and after temperature cycle (AT_c) hoop stress profile with the two boundary conditions used; see Fig 6.2

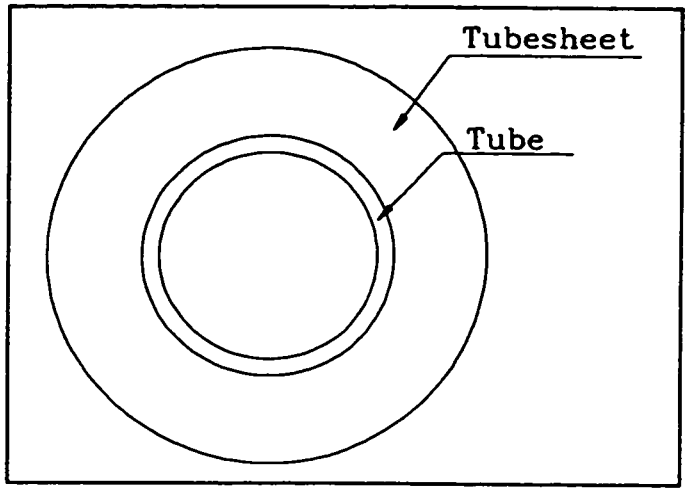


Figure 6.7: simplified plane stress model for tube-to-tubesheet joint

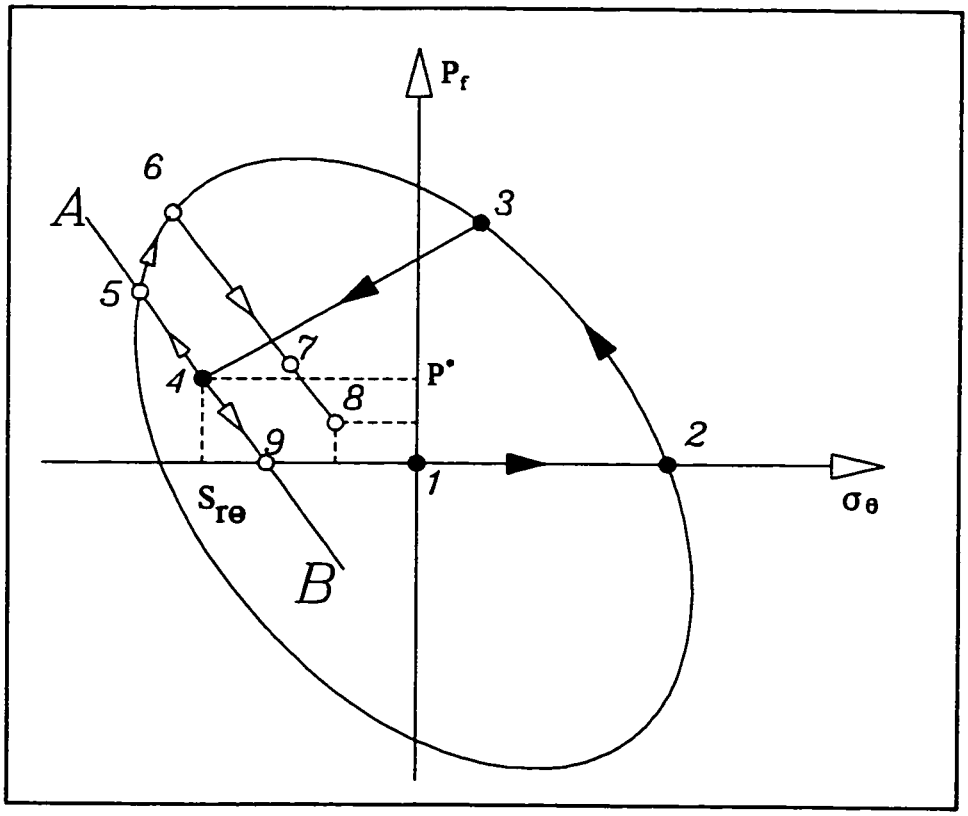


Figure 6.8: The steps for creating the expanded joint as wall as the joint response to thermal loading as presented in terms of interference contact pressure-stress relation; Yield surface assuming a perfectly plastic material

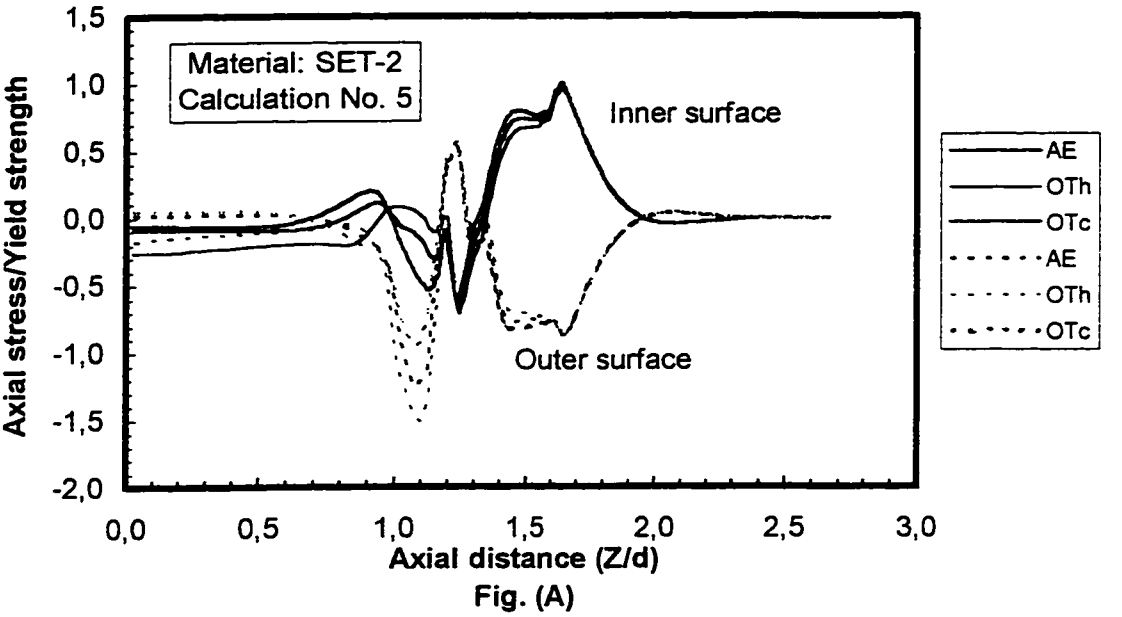


Fig. (A)

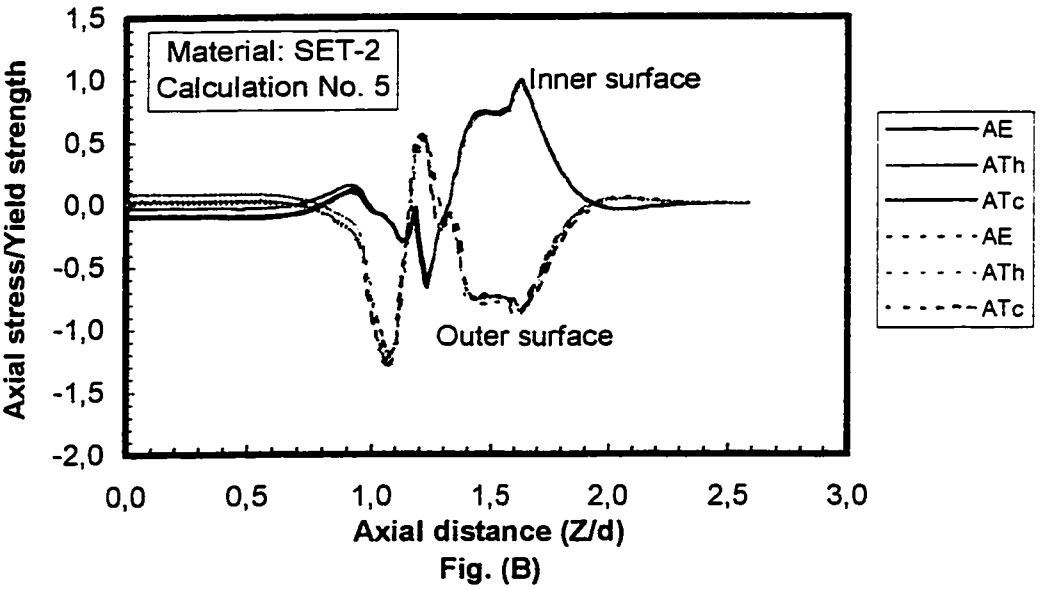


Fig. (B)

Figure 6.9: Typical axial stress profile, (A) for as-expanded joint and during thermal loading, (B) for as-expanded joint and after temperature cycling

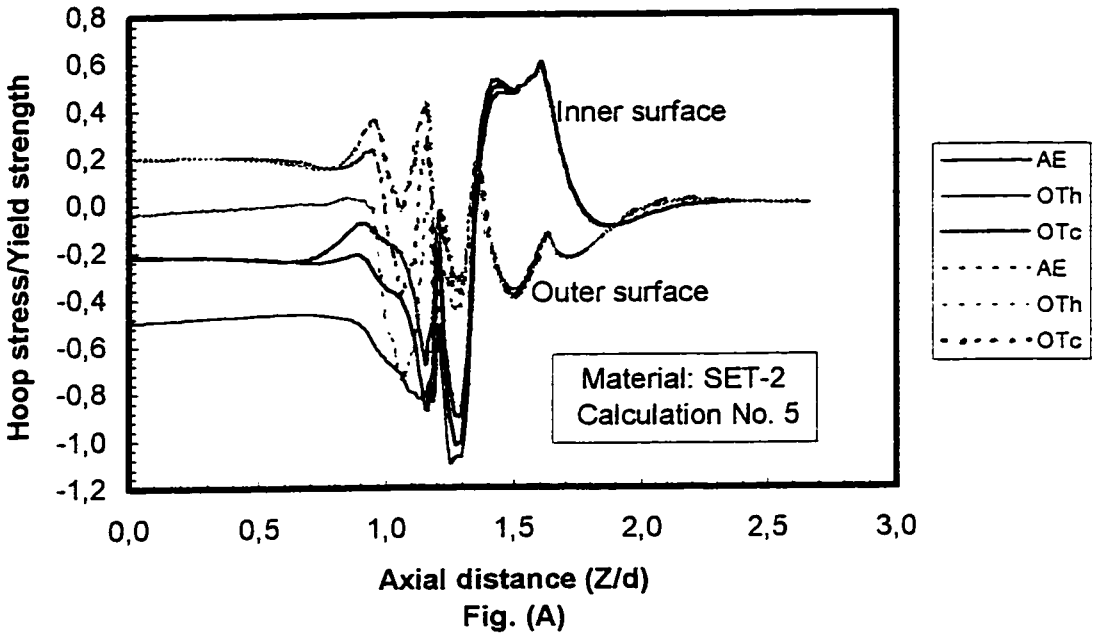


Fig. (A)

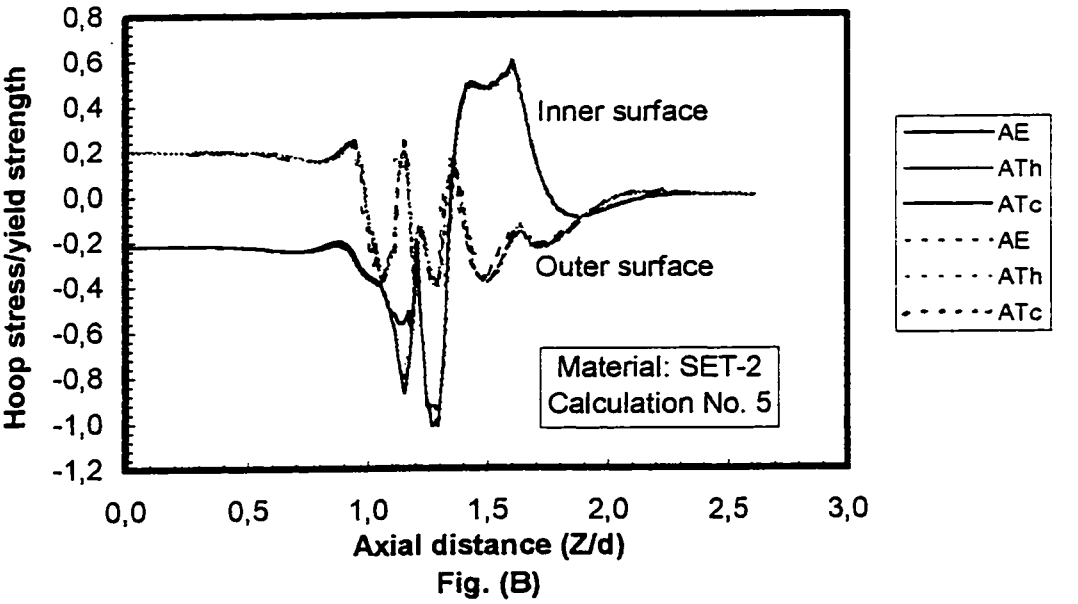


Fig. (B)

Figure 6.10: Typical hoop stress profile, (A) for as-expanded joint and during thermal loading, (B) for as-expanded joint and after temperature cycling

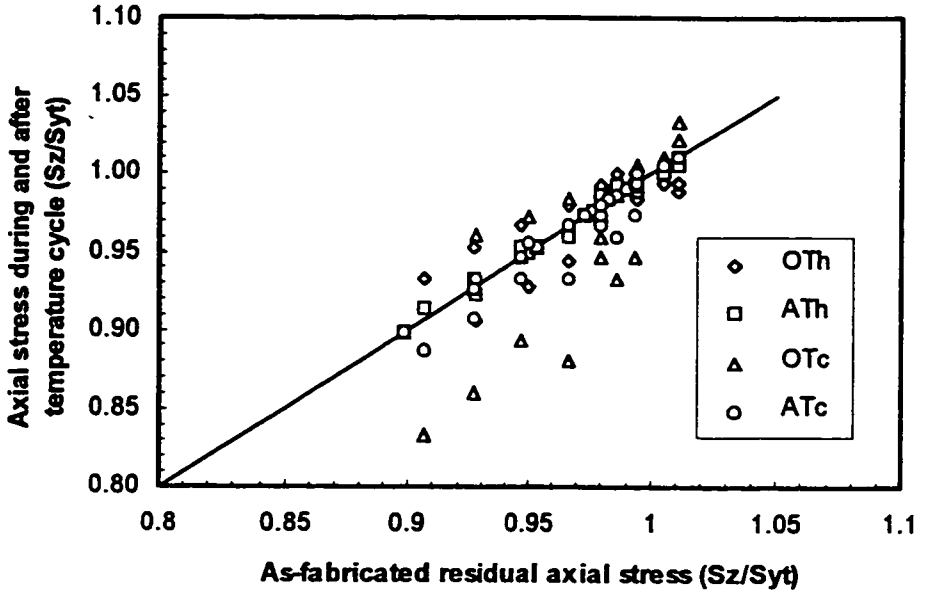


Figure 6.11: Maximum tensile axial stresses at different thermal loading versus that of as-expanded joint

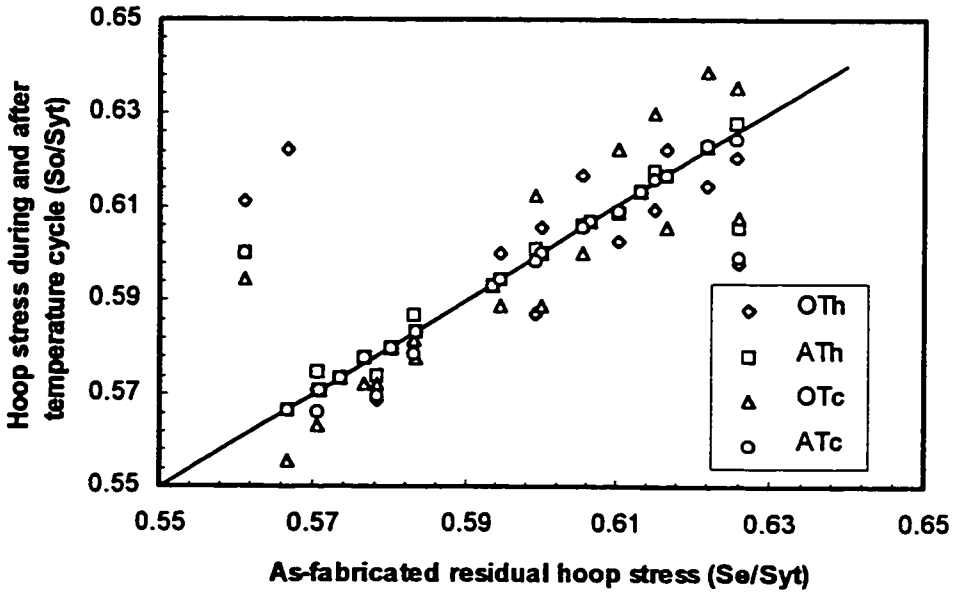


Figure 6.12: Maximum tensile axial stresses at different thermal loading versus that of as-expanded joint

CHAPTER 7

JOINT BEHAVIOUR UNDER MECHANICAL LOADING

7.1 INTRODUCTION

In this chapter a series of finite element analyses will be considered to evaluate the effect of the tubesheet deflection on the residual contact pressure and residual stress in the tube transition zone. In order to obtain a statistically significant set of results, many 3-D finite element calculations will be performed in addition to 2-D plane stress calculation to simulate the sequential and simultaneous expansion processes as well as the subsequent tubesheet deflexion.

7.2 ANALYSIS OF TUBESHEET DEFLECTION

The tubesheet is inevitably deformed as a result of the differential pressure loads between the primary and secondary sides. In addition, all nuclear steam generators must be generally installed in a vertical position causing the huge weights of both the tube bundle and the secondary-side liquid to be carried by the tubesheet and consequently introduce some important deformation in the tubesheet itself, as shown in Figure 7.1. These deformations may

greatly affect the integrity of the tube-to-tubesheet joints.

Finite element modelling for tubesheet deformation was performed (Private Communication) to assess the stresses and the deformations of this element under the working conditions of steam generators. The perforated tubesheet section is replaced by an equivalent plate having a solid section with equivalent material properties driven from the tubesheet ligament efficiency and the base material properties. Using the solid plate with the equivalent material properties, the finite element model can be greatly simplified as shown in Figure 7.2. The resulting ligaments stresses and displacements can then be recalculated from the stress and displacement fields of the equivalent solid plate.

The model shows that the differential pressure loads between the primary and secondary sides contribute to most of the bending stresses observed at the primary and secondary surfaces of the tubesheet. The ratio of stress components and that of the displacement components generally range between -0.5 and 1.0. The highest magnitude of the tubesheet deformation is observed towards the central area where the ratio approaches one. This area is considered important for the purpose of evaluating the joint strength as a function of tubesheet deformation. For the analysis of the expanded joint under this kind of loading, the bending stresses are replaced by the average displacements (**u**, **v**) in X and Y directions as shown in Figure 7.3.

7.3 METHOD OF ANALYSIS

As shown previously, the degree of the joint tightness and the level of the tensile residual stresses on the inside surface of the tube transition zone are influenced by too many variables. Some of these variables are the design factors including material, dimensional and fabrication parameters that are usually identified at the joint fabrication stage, as shown in Chapter 4. For the same design parameters the tube-to-tubesheet joint might experience different levels of working conditions where unlimited number of variables could affect the quality and integrity of the expanded joint. As it has been shown in Chapter 6, the operating temperature is one of those important working-condition parameter upon which the joint integrity was strongly dependent.

Unlike the simulation performed for the operating temperature, which was greatly simplified by using an axisymmetric finite element model, the investigation of the effect of the tubesheet deformation on the strength of expanded joint requires a full 3-D finite element analysis. Figure 7.3 shows the central region of the tubesheet where the displacement **u** and **v** are activated on the tubesheet boundaries. Simulating the real tubesheet geometry with this type of loading, by using the equivalent axisymmetric model might be associated with a high degree of uncertainty. However, if the stresses of the tube transition zone become out of interest and only joint integrity represented by the level of the interference pressure is the controlling factor, then plane stress/strain models could be used as presented in section 7.4.

7.3.1 3-D Finite Element Solution

In order to determine the effect of the tubesheet deformation on the interference contact pressure and on the residual stresses, a central hole in a finite circular tubesheet is first considered. Because of the size limitation imposed on the problem, a tubesheet with only 7 holes is considered. Only triangular tube pattern, as shown in Figure 7.3, is investigated. The tubes are assumed to be expanded simultaneously, which allows us to consider only a quarter of the total geometry for the finite element modelling. Figure 7.4 shows a typical mesh for the adopted 3-D finite element model. The width and the height of this model are equal to 1.5 and 1.732 of the hole pitch (P), respectively. A 3-D 8-node full integration solid element is chosen. Also, 4-noded surface contact elements are used between all the tubes and the tubesheet contacting surfaces. The entire 3-D model consists of 9595 nodes and 6797 continuum elements. The frictional interaction between the tube and the tubesheet is accounted for by using Coulomb's friction law with the coefficient of friction f = 0.1375 found experimentally. The normal and the shearing stresses given here are presented in the global coordinate system (X-Y-Z). Because of the periodical symmetry, all nodes located on sides of the 3-D finite element model (X=0.0 and Y=0.0) are constrained in the normal directions during the expansion process and also when the tubesheet rims are displaced to simulate the tubesheet deflection. In order to provide stability to the numerical models, the front ends of both the tubes and the tubesheet, at the tubesheet primary side, are restrained against the axial motion. This boundary conditions have no effect on the stresses in the

transition zone since it is far enough from the tubesheet secondary side. In order to avoid the interaction effect between the constrained boundary and the stresses located beyond the secondary side of the tubesheet, a tubesheet thickness taken equal to the tube outer diameter has been considered satisfactory. The length of each tube is taken to be twice the value of the tube outer diameter. A uniform internal pressure is applied simultaneously over the portions of three tubes that lie within the tubesheet.

Because of the huge time consumed and also due to the memory limitation on the RISK/6000 IBM computer utilized to solve the problem, only one typical case (Table 7.1) is considered in the current investigation. The expansion pressure is applied simultaneously to the appropriate tube elements shown in Figure 7.4 to be created simultaneously.

Figure 7.5 shows the contours of residual axial stresses generated in the whole model including the tubes and the tubesheet following the simultaneous expansion process. The level of the residual stresses in the transition zones seems independent of the tube location in the tubesheet. Also, the profile of the stress in each tube is axisymmetric. Thus, it can be re-confirmed that investigating as-expanded tube-to-tubesheet joint behaviour by using only one typical tube is quite adequate.

Tubesheet deflection is expected to strongly influence the characteristics of the tube-to-tubesheet joint. In this study, tubesheet deflection will be investigated by considering the

tubesheet rim displacement. Thus, the tubesheet deformation parameter is characterised by two factors, 1) a displacement (**u**) imposed on the tubesheet right rim placed at X=1.5 ***P***, and 2) a displacement (**v**) imposed on the tubesheet upper rim placed at Y=1.732 ***P***.

A series of calculation are undertaken to identify the effect of the tubesheet deformation on three important parameters, namely: the tensile residual axial and hoop stresses in the tube transition zone and the residual contact pressure. The initial values of the residual axial and hoop stresses measured at an axial location (Z/d =1.25) of the central tube inner surface, are given by 37.2% and 36.0% of the tube yield strength, respectively. Also, the initial residual contact pressure between the tubesheet and the central tube was about 9.16% of the tube yield strength. The change in those values are carefully examined in terms of the tubesheet deformation.

The investigation is performed by a number of calculation where four levels of each parameter are considered as shown in Table 7.2. The values of **u** and **v** presented in this table are selected to cover the range of the tubesheet displacement resulting from a real loading applied on the tubesheet of Figure 7.2 (Private Communication). Also, Table 7.2 presents the values of the tensile residual axial and hoop stresses and the level of the residual contact pressure obtained after loading. As a result of the tubesheet deformation, the highest reported magnitudes for the stress ratios in the axial and circumferential directions are 0.444 and 0.511 reflecting an increase in the stresses of as-expanded conditions by 19% and 41%, respectively.

The final values of the interference contact pressure as a result of the tubesheet deformation are found to be higher is some cases and lower in others. As shown numerically, the tubesheet deformation has a non-negligible effect on each of the joint characteristics. The coefficient of variation C_v that has relatively higher values are statistically reflecting a wide variation of the stresses and the interference contact pressure with respect to the tubesheet deformation level, as shown in Table 7.3.

In spite of the effectiveness of the 3-D finite element model, a higher cost must be payed due to the huge CPU time consumed while executing the model for tubes expansion and for the tubesheet biaxial loading calculations. Table 7.4 shows that in order to perform a full investigation it will take almost one week of actual computer execution time for one design case only. As such, the effect of the biaxial deformation of the tubesheet on the stresses created in the tube transition zone will not be investigated here and left for future studies where a simplified method might be developed. However, the effect of the tubesheet biaxial deformation on the residual contact pressure is investigated here with a plane stress finite element model.

7.4 SIMPLIFIED 2-D FINITE ELEMENT ANALYSIS

The effect of tubesheet deformation on the sealing and strength performances of the tube-to-tubesheet joint is investigated here by a 2-D plane stress model taking into account

two different techniques of manufacturing: simultaneous and sequential expansion processes.

7.4.1 Mechanical Loading with Simultaneously Expanded Joints

In order to determine the effect of the tubesheet deformation on the interference contact pressure, a central hole in the 7-tube model shown in Figure 7.3 is considered here. Since, the tubes are expanded simultaneously, a quarter of the geometry given in Figure 7.3 is sufficient for the finite element modelling. Figure 7.6 shows the 2-D finite element plane stress model that simulates the 7-hole simultaneous expansion process. As in the case of 3-D finite element model, the width and the height of this model are taken as 1.5 and 1.732 times the hole pitch, respectively. The model is constructed with 2-D, 8-node quadrilateral solid elements with some 2-D, 4-node bilinear full integration element. Also, 3-noded interference contact elements are used between all tubes and the tubesheet contacting surfaces to simulate the initial gap and the contact state when it occurs. The entire 2-D model consists of 1690 nodes and 901 continuum elements. The frictional interaction between the tubes and the tubesheet is still accounted for by using Coulomb's friction law with a coefficient of friction $f = 0.1375$. The cartesian coordinate system (X,Y) is located at the centre of the middle tube. The normal and shearing stresses are also presented in the global coordinate system (X-Y-Z). Because of the periodical symmetry, all nodes located on sides of the 2-D finite element model (X=0.0 and Y=0.0) are constrained in the normal directions during the expansion process and while applying the displacement on the tubesheet rims. The tubes all together are

simultaneously expanded in one loading step applying a pressure on the tubes inner surface.

First, let us consider the correlation between the 2-D plane stress and 3-D finite element models. The results of study case of Table 7.1 together with some induced displacements listed in Table 7.2, are compared in Table 7.5 on the basis of the interference contact pressure and the CPU time required for execution. As shown in Table 7.5, the levels of the interference contact pressure as calculated by the simplified 2-D plane stress and by the 3-D finite element models are in good agreement. Therefore, it can be concluded that, while consuming less CPU time, the 2-D plane stress model gives an accurate evaluation for the joint performance as a function of the working condition induced displacement.

The orthogonal design method is a useful tool to set the optimum combination of parameters involved during the design and operation of the joint. First, the Inconel 690 tubes and steel (SA-508 Class 3) tubesheet materials listed in Table 7.1 are considered important and thus used in the proposed parametric study. Also, the Inconel 690 tube material, used for nuclear steam generators manufacturing is commercially available with one dimensional standard (d=19.05 mm and t=1.143 mm). The initial clearance, hole pitch and the level of the expansion pressure are the remaining design parameters by which the tube-to-tubesheet joint can be installed. Upper and lower limits are selected for each of these parameters as specified by practical applications and listed in Table 7.6. In Table 7.7, four optimum combinations for these parameter are chosen for the orthogonal design method. In order to complete the

analysis for each study case, the working condition at which the joint will serve must be identified. Two important working-condition parameters are believed to be important namely: the primary-side pressure (P_{ps}) and the differential pressure induced tubesheet displacements (**u** and **v**) in X and Y directions, respectively. For each set of calculation listed in Table 7.7, two extreme levels for each working condition related parameter are selected and listed in Table 7.8. Also, the orthogonal design method is used to set the optimum combinations of these parameter as shown in Table 7.9 where the index (n) refers to the calculation number used in Tables 7.7 and 7.8. Each joint installed according to Table 7.7, must be subjected to the four different working conditions listed in Table 7.9. Each of the four working conditions consist of an application of a uniform internal pressure (P_{ps}) over the inside surface of the tubes, and tubesheet free rims displacements **u** and **v** in X and Y directions, respectively.

The initial residual contact pressure for each case listed in Table 7.7 and the corresponding joint tightness coefficient (η) resulting from each working condition applied to the joint are given in Table 7.10. The effect of the parameters will be examined statistically: The 16 observation points (4 in Table 7.7 and 4 in Table 7.9) are verified by performing a correlation analysis considering the primary-side pressure and the tubesheet rims displacements as independent variables, and the joint tightness coefficient (η) as the response (dependent variable). The correlation coefficient varies from -1 to +1; a positive value indicates that as the value of the independent parameter increases the value of the dependent variable will also tend to increase. The opposite is true for a negative value. A correlation

coefficient near zero indicates little correlation between the two variables. The results of the correlation analysis are summarized in Table 7.11. Also, the graphical correlations between the dependent parameters and the joint tightness coefficient are given in Figures 7.7, 7.8 and 7.9 where the independent parameters (**u**, **v** and P_{ps}) are labelled VAR1, VAR2 and VAR3 respectively, while the dependent parameter η is labelled VAR4.

As estimated statistically, the tubesheet rim displacements equally influence the final level of the joint tightness coefficient. In addition, they have a stronger effect than that of the primary-side pressure which has the lowest level of the correlation coefficients, as listed in Table 7.11. A positive values for the tubesheet displacement badly affects the joint performance as shown by the negative correlation coefficient between the tubesheet displacement and the joint tightness coefficient. The greater the tubesheet deformation, the worst the residual resistance. On the other hand, the primary-side pressure can help a little to improve the joint performance during service conditions. Nevertheless, increasing the primary-side pressure, for the purpose of improving the joint performance, would increase the deferential pressure load that in turn might greatly deform the tubesheet. Therefore, the use of highly rigid tubesheet is strongly recommended in order to stand the differential pressure loads and the heavy dead weights of both the tubes bundle and the secondary-side liquid of the vertically installed nuclear steam generators.

7.4.2 Mechanical Loading with Sequentially Expanded Joints

The geometry of the perforated plate given in Figure 7.3 is used for modelling the central area of tubesheet including the innermost 7-tube sections. The perforated plate deformation at the central area depends upon the surrounding ligament and tubes that are expanded sequentially. When the tubes are locked in the tubesheet holes, they provide some additional stiffness that must be considered when determining the effect of the tubesheet deformation on the central joint. In this study, the seven tubes of Figure 7.3 are sequentially expanded. Thus, the entire modelling of the geometry is required in order to obtain the solution. The finite element mesh of the model is shown in Figure 7.10. The model is discretized by using 3516, 2-D plane stress 8-node isoparametric quadrilateral elements with some 4-noded bilinear elements particularly used in the tubesheet ligament section. Also, 3-noded interference contact elements are used between the outer surface of each tube and the corresponding tubesheet hole bore. The results are given in the global coordinate system X, Y and Z. The tube and the tubesheet materials selected are Inconel 690 and SA-508 Class 3, respectively. Also, a tubes having 19.05 mm outer diameter and 1.143 mm thickness with a tubesheet having a hole with a bore diameter of 19.2532 mm and 25% ligament efficiency, are adopted. During expansion the outer four corner nodes are restrained in the X and Y direction, for numerical stability purpose. Each tube is independently expanded by applying a pressure equal to 77% of the tube yield strength. The sequence in which the tubes are expanded might significantly affect the final value of the residual contact pressure around the

cental tube as shown in Appendix III. In the present parametric study, the following order (1-4-2-5-3-6-7) is adopted. After all seven tubes are expanded, the model boundary conditions are removed and the four corner nodes become free to move in the X-Y plane. The total CPU time required to simulate the seven tubes expansion only is 7½ hours.

Following the expansion, the interference contact pressure around the central tube is evaluated in terms of the tubesheet displacement in the X-axis ($\mathbf{u}/1.5P$) and a different level of displacement ratio ($\beta = \mathbf{v}/\mathbf{u}$).

The results are represented in terms of the joint tightness coefficient (η) versus the tubesheet edge displacement ($\mathbf{u}$) and the displacement ratio (β), as shown in Figures 7.11 and 7.12. As it can be seen from Figure 7.11, the joint tightness coefficient is negatively correlated to the tubesheet displacement. This joint behaviour was also noticed in the statistical parametric study performed for the simultaneous expansion case. It seems, however, that the joint tightness coefficient is sensitive to small changes in the tubesheet deformation up to certain critical level beyond which the joint either starts to fully disintegrate ($\mathbf{u}>0.00$) or strongly contact the tubesheet ($\mathbf{u}<0.00$) where the joint has no more response to the tubesheet displacement. On the other hand, the displacement ratio factor (β) seems to be a non important parameter with the negative range of the tubesheet displacement. The joint tightness coefficient is evaluated as a function of this factor at different levels of the tubesheet displacement ($\mathbf{u}$) as shown in Figure 7.11. The joint behaviour with the displacement ratio is

dependent, of course, on the level and the sign of the tubesheet displacement (**u**). In the positive range of **u**, a negative value of β would improve the joint performance up to a certain level beyond which the joint may entirely fail as shown by the lower curve of Figure 7.12. For a negative value of **u**, a positive value of β could improve the joint behaviour and a negative one may affect badly the joint behaviour during service conditions, as show by the upper curve of Figure 7.12.

A comparison between the sequential expansion and the simultaneous expansion processes shows a little difference in terms of joint performance in service. Based on the computed joint tightness coefficient of this study case reported in this chapter, it would be possible to compare the joint behaviour under different levels of tubesheet deformation. The value of the joint tightness coefficient outside a certain range is generally combined with some plastic deformation in the tubesheet. However, before drawing any general conclusion, the analysis needs to be extended further in the future.

Executive summary

In this chapter, a series of finite element analysis was considered to investigate the effect of tubesheet rim displacement and primary side pressure on the residual contact pressure and the residual stresses in the tube transition zone. 3-D finite element analysis indicated that the tubesheet deflection has significant effect on both the residual contact

pressure and maximum tensile residual stresses. Because of the CPU time limitation with 3-D finite element modelling, the analysis was oriented toward studying the effect of tubesheet rim displacement and primary side pressure on the residual contact pressure only. A detailed 2-D finite element analysis together with statistical approach showed -0.5 correlation factor between tubesheet rim displacement and joint tightness coefficient. The effect of primary side pressure was relatively less significant.

Table 7.1: Material and dimensional properties used in 3-D model

	Tube (Inconel 690)	Tubesheet (SA-508 Class 3)
Modulus of Elasticity (GPa)	209.0	199.6
Poisson ratio	0.289	0.300
Yield Strength (MPa)	294.0	458.0
Tangent Modulus (GPa)	2.090	1.996
Expansion Pressure (MPa)	191.0	
Tube outer diameter (mm)	19.05	
Tube wall thickness (mm)	0.045	
Hole diameter (mm)	19.177	
Hole pitch (mm)	25.4	

Table 7.2: Effect of tubesheet rim displacements on the central joint characteristics

Calculation No.	Tubesheet deformation		Joint characteristics		
	$u/1.5P$	$v/1.732P$	S_z/S_{yt}	S_θ/S_{yt}	P_f/S_{yt}
As-expanded	0.00E+00	0.00E+00	0.377791	0.361628	0.091558
1	6.67E-03	5.00E-04	0.400721	0.290163	0.052558
2	1.33E-03	1.00E-03	0.444512	0.279395	0.00000
3	-6.67E-03	-5.00E-04	0.245488	0.34893	0.118442
4	-1.33E-03	-1.00E-03	0.168791	0.363256	0.12900
5	-6.67E-03	5.00E-04	0.337465	0.415419	0.103209
6	-1.33E-03	1.00E-03	0.355349	0.511116	0.118767
7	6.67E-03	-5.00E-04	0.325512	0.21386	0.103186
8	1.33E-03	-1.00E-03	0.332023	0.107488	0.114767

Table 7.3: Mean and standard deviation of investigated parameters (see Table 7.2)

Statistical parameter	Joint characteristics		
	S_z/S_{yt}	S_θ/S_{yt}	P_f/S_{yt}
σ	0.331961	0.321251	0.092388
λ	0.082323	0.116738	0.041189
C_v %	24.79904	36.33872	44.58288

Table 7.4: CPU time required for 3-D model

Calculation No.	CPU Time (sec)	Calculation No.	CPU Time (sec)
Expansion	25192	5	9882.1
1	10568	6	10400
2	15543	7	9950
3	10728	8	12939.7
4	13775	Total	33:02:57.8 hr.

Table 7.5: Comparison between 2-D and 3-D finite element solutions

Calculation No.	Tubesheet Deformation		P_f/S_{yt}		CPU Time (sec)	
	$u/1.5P$	$v/1.732P$	3-D	2-D	3-D	2-D
Expansion	0.00E+00	0.00E+00	0.0916	0.0950	25192	368.6
1	6.67E-04	5.00E-04	0.0526	0.0589	10568	92.2
2	1.33E-03	1.00E-03	0.0000	0.0000	15543	127.3
3	-1.33E-03	-1.00E-03	0.1290	0.1345	13775	159.7
4	-1.33E-03	1.00E-03	0.1188	0.1210	10400	161.1

Table 7.6: Upper and lower limits of involved parameters

Limits	P/d	c/d	P_c/S_{yt}
Upper	2	0.0067	0.7698
Lower	1.333	0.0033	0.6279

Table 7.7: Optimum combination of involved parameter; Taguchi (1982)

Calculation	Parameter involved		
	P/d	c/d	P_e/S_{yt}
1	1	1	1
2	1	2	2
3	2	1	2
4	2	2	1

Table 7.8: Upper and lower limits of working condition parameters (Calculation No. According to Table 7.7)

Calculation	u/1.5*P*		v/1.732*P*		P_{ps}/S_{yt}	
	Upper	Lower	Upper	Lower	Upper	Lower
1	2.00E-03	-2.00E-03	1.50E-03	-1.50E-03	0.05	0.00
2	1.33E-03	-1.33E-03	1.00E-03	-1.00E-03	0.05	0.00
3	1.60E-03	-1.60E-03	3.50E-04	-3.50E-04	0.05	0.00
4	2.00E-04	-2.00E-04	1.00E-03	-1.00E-03	0.04	0.00

Table 7.9: Optimum combination of working condition parameters; Taguchi (1982)

Calculation n	Parameter involved		
	u/1.5*P*	v/1.732*P*	P_{ps}/S_{yt}
n-1	1	1	1
n-2	1	2	2
n-3	2	1	2
n-4	2	2	1

Table 7.10: Initial residual contact pressure and joint tightness coefficient (η) at working conditions

Calculation	P^*/S_{yt}	η	Calculation	P^*/S_{yt}	η
1-1	0.09497	-99.95	3-1	0.09635	-99.72
1-2		52.076	3-2		-75.83
1-3		67.81	3-3		51.91
1-4		42.53	3-4		28.82
2-1	0.08103	-99.19	4-1	0.05302	-99.75
2-2		-49.79	4-2		181.99
2-3		29.51	4-3		-72.32
2-4		80.31	4-4		130.18

Table 7.11: Results of the correlation analysis for the joint tightness coefficient (η)

	Independent parameter		
	u	**v**	P_{ps}
Correlation coefficient	-0.52	-0.53	+0.19

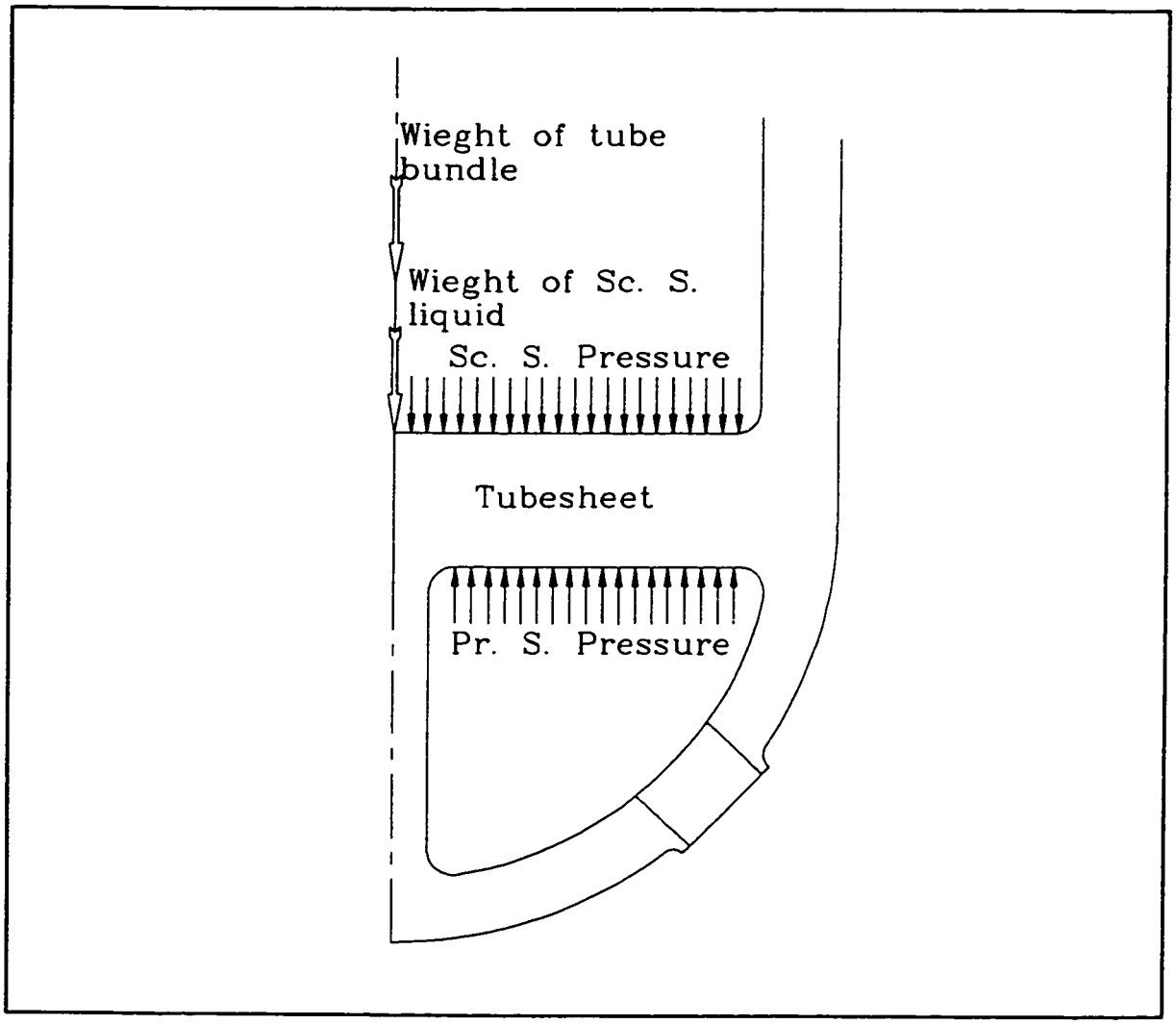


Figure 7.1: Some mechanical loads acting on the tubesheet surfaces

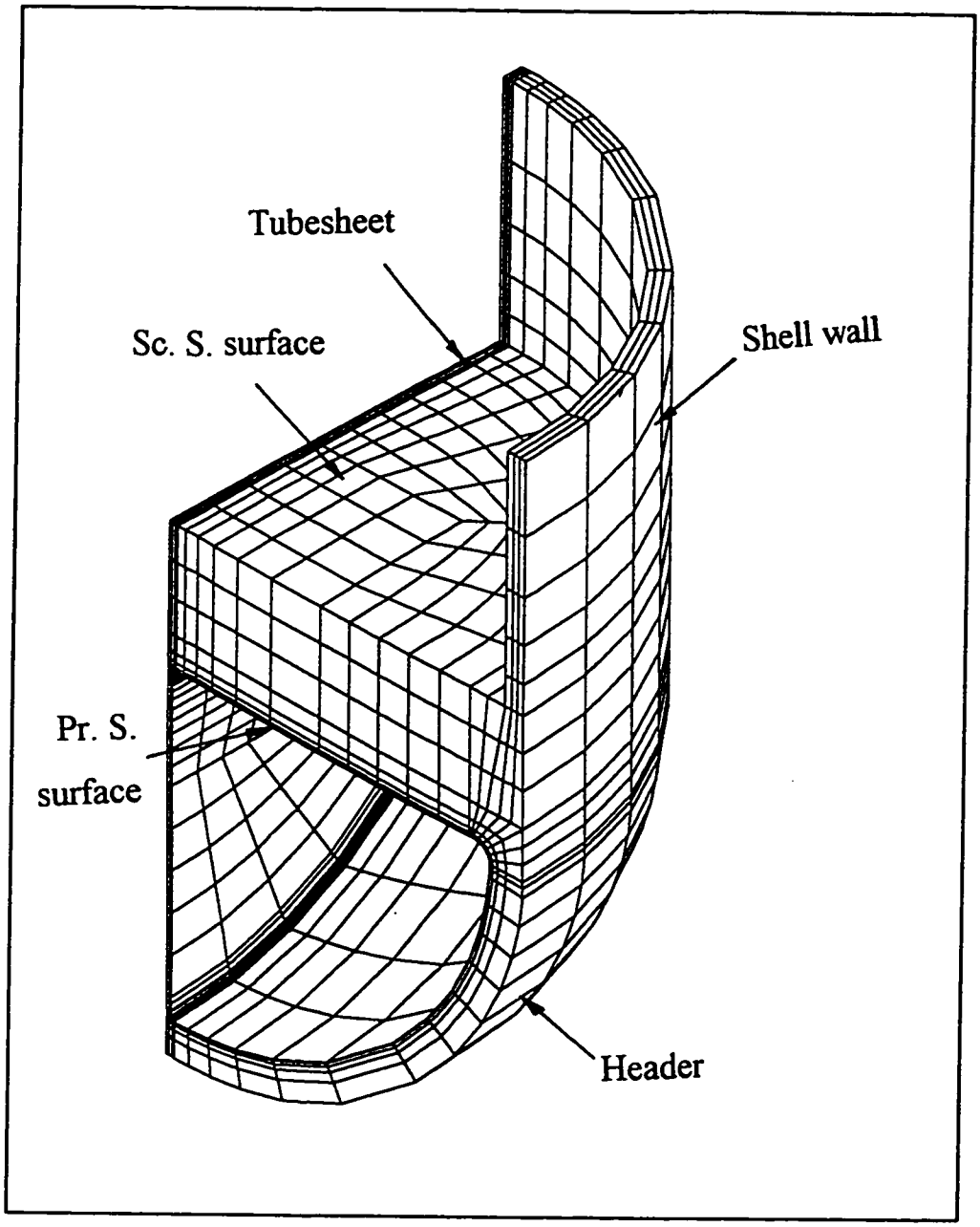


Figure 7.2: 3-D finite element model used for tubesheet deformation analysis (Private Communication)

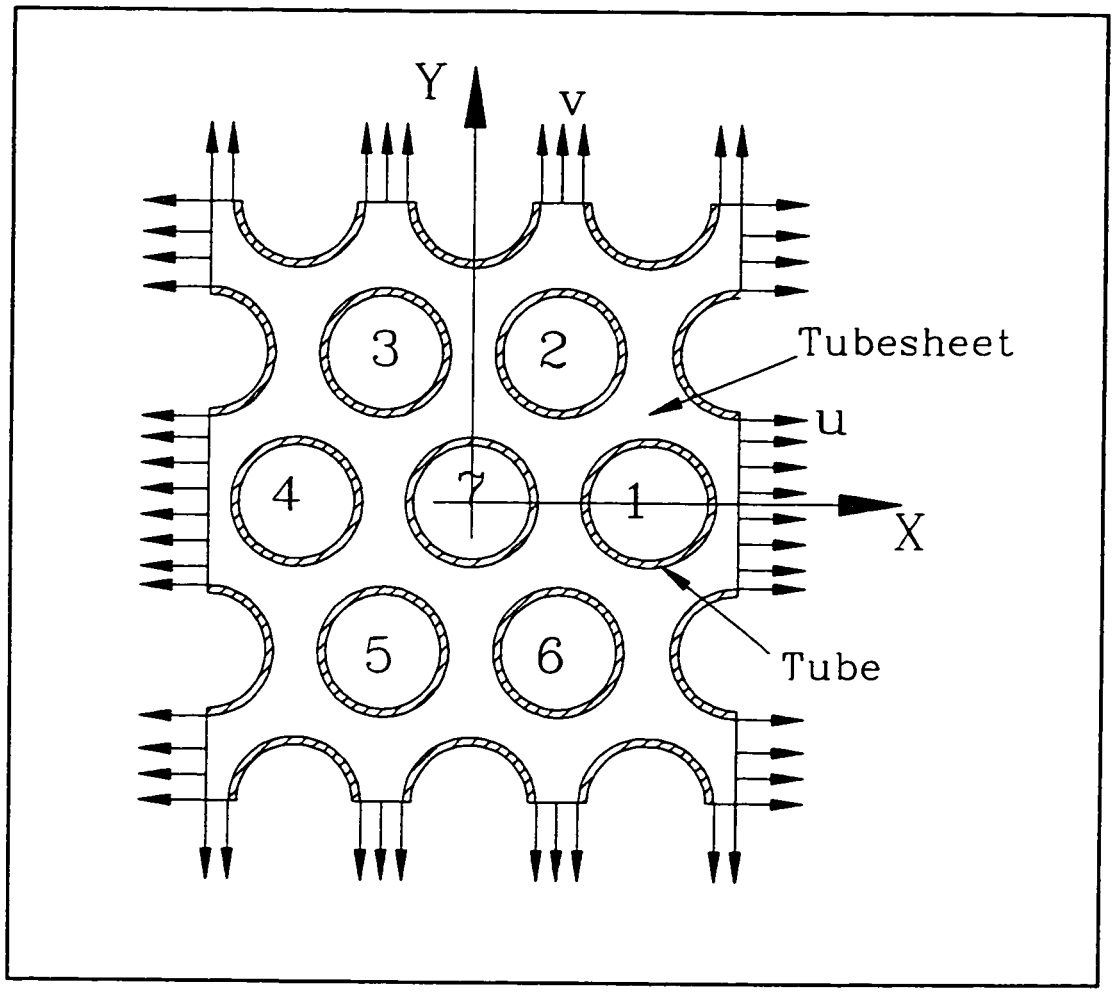
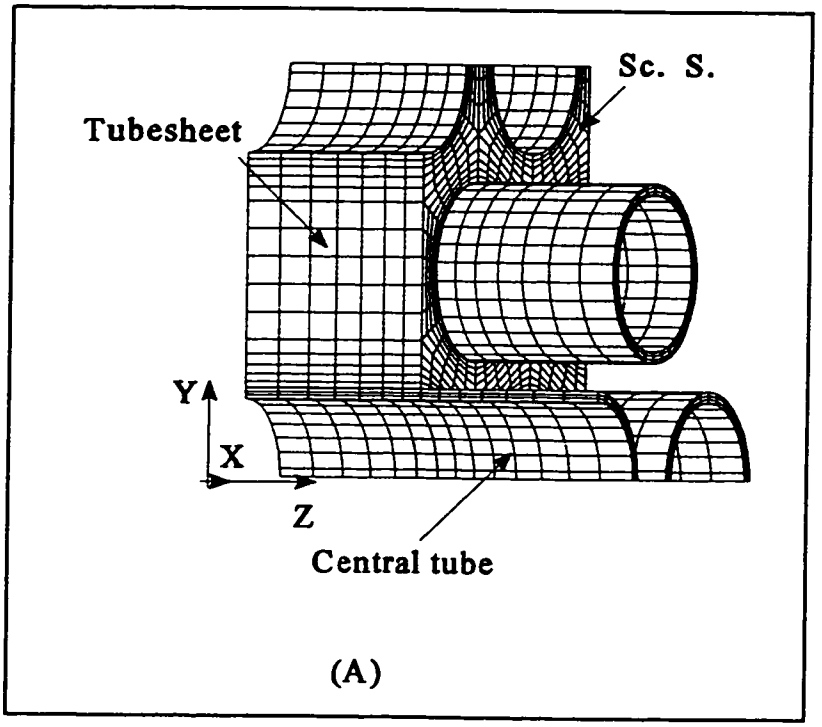


Figure 7.3: Central region of the perforated plate



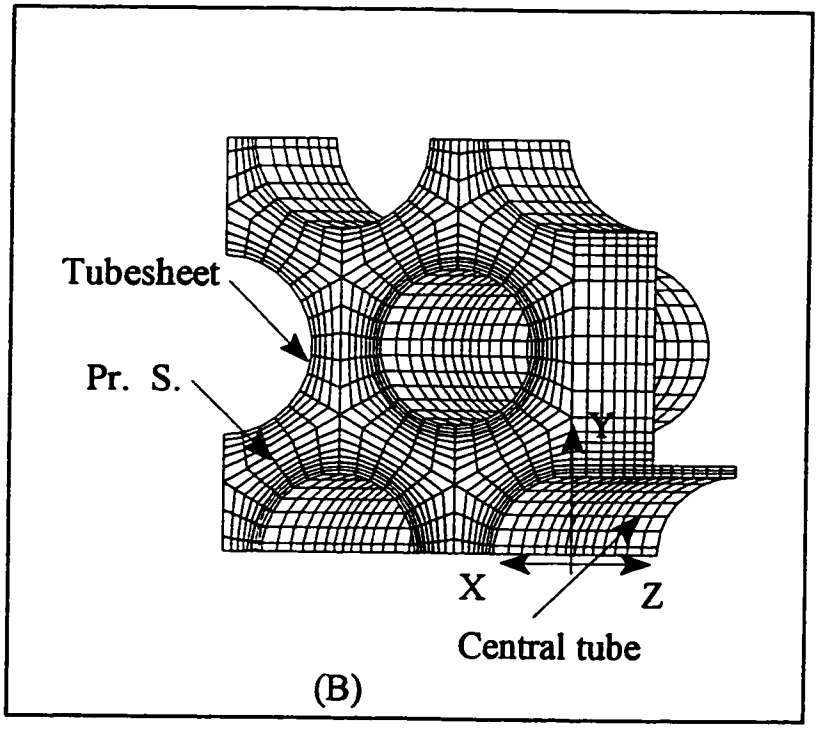


Figure 7.4: 3-D finite element model

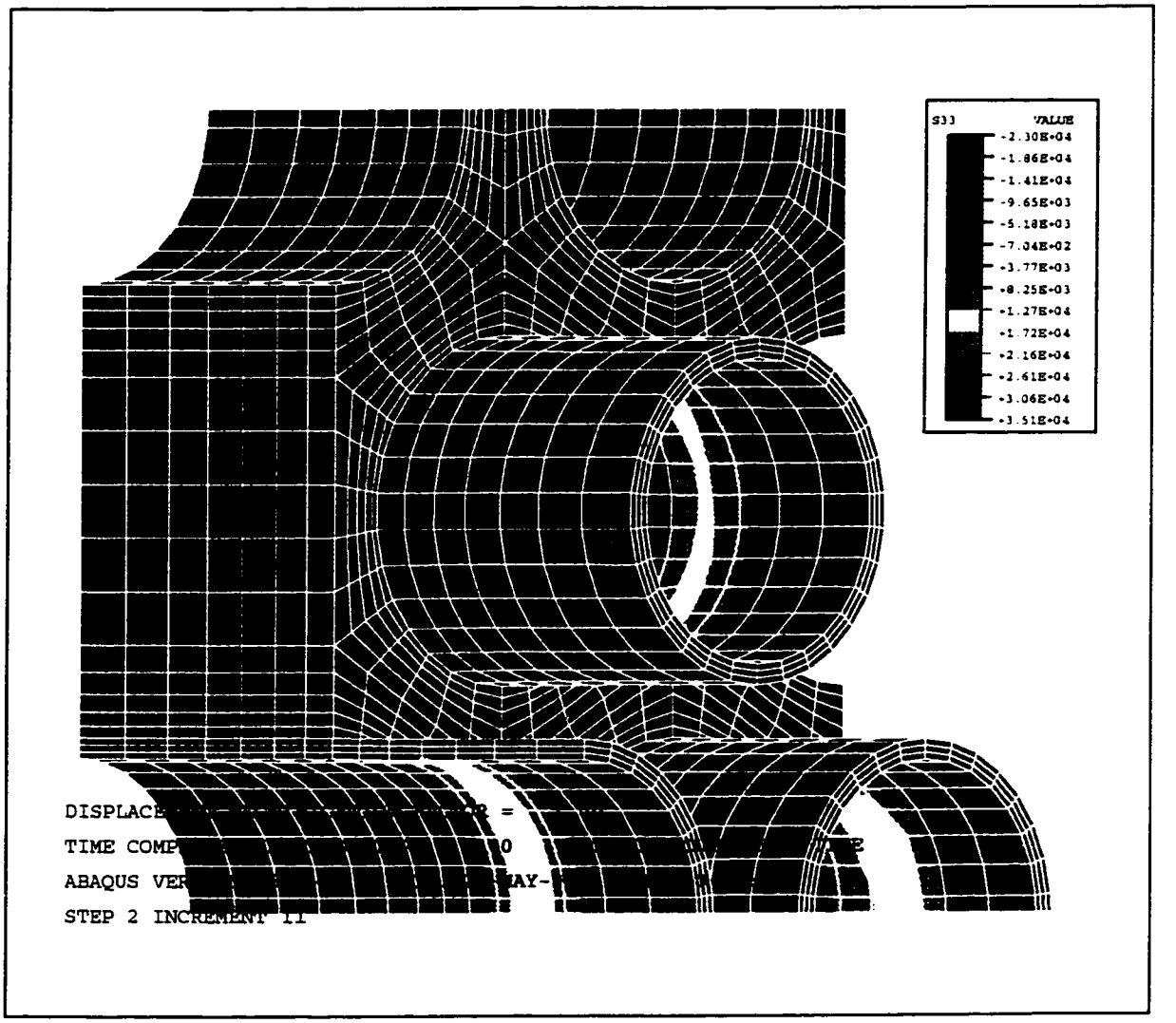


Figure 7.5: 3-D residual axial stress contour on the tubes transition zone

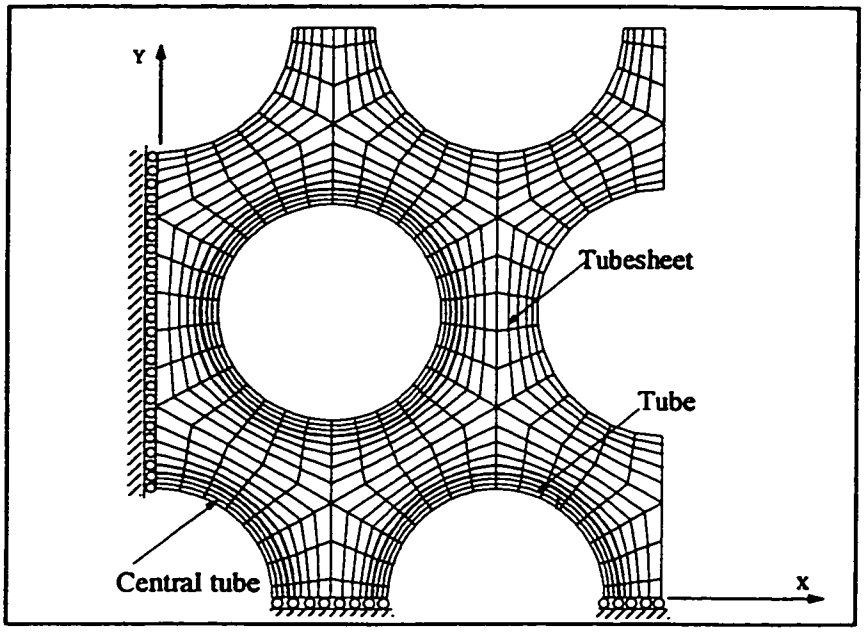


Figure 7.6 : Finite element model for simultaneous expansion case

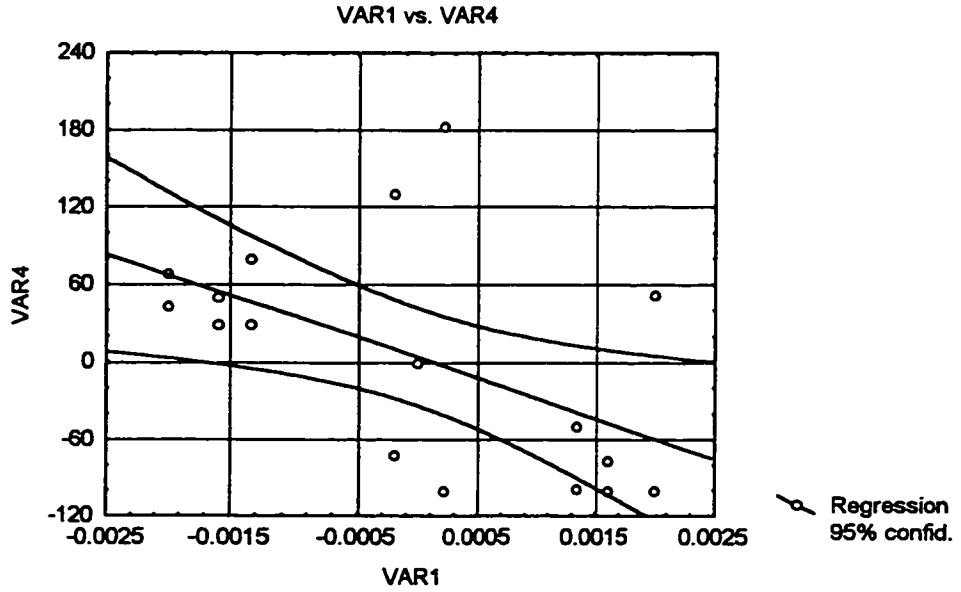


Figure 7.7 Statistical relation between the joint tightness coefficient (VAR4) and the displacement (u) (VAR1)

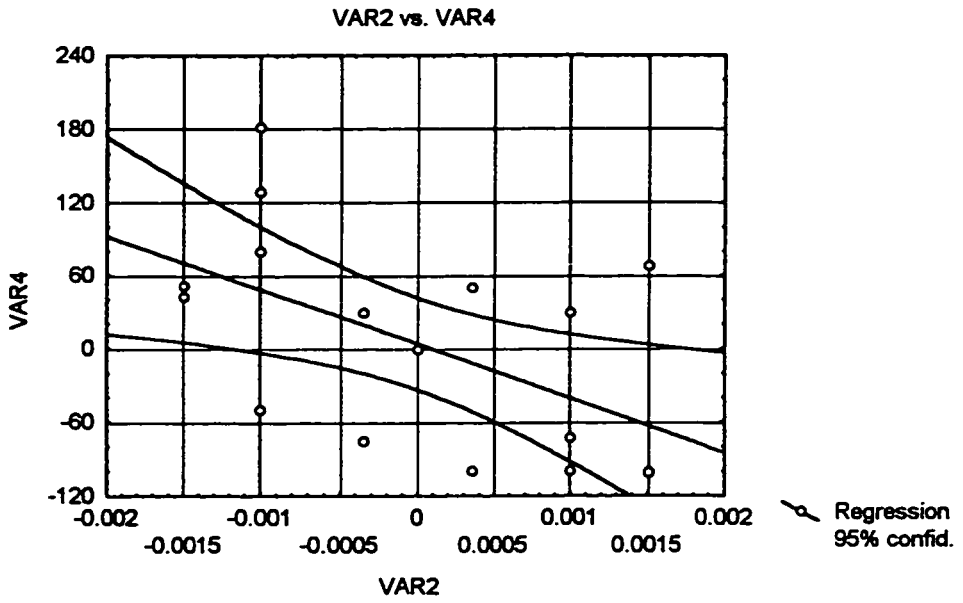


Figure 7.8: Statistical relation between the joint tightness coefficient (VAR4) and the displacement (v) (VAR2)

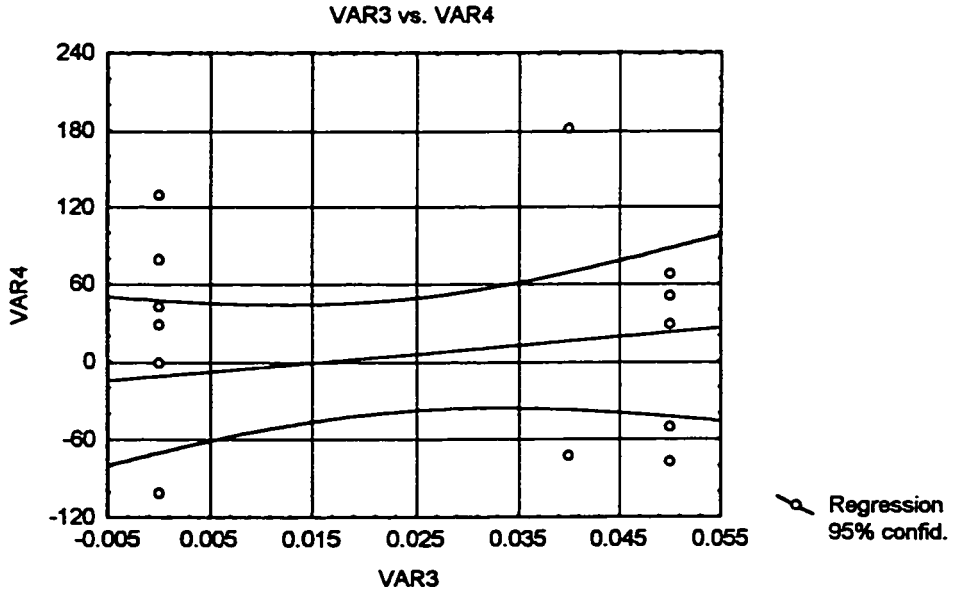


Figure 7.9 Statistical relation between the joint tightness coefficient (VAR4) and the primary side pressure (P_{ps}) (VAR3)

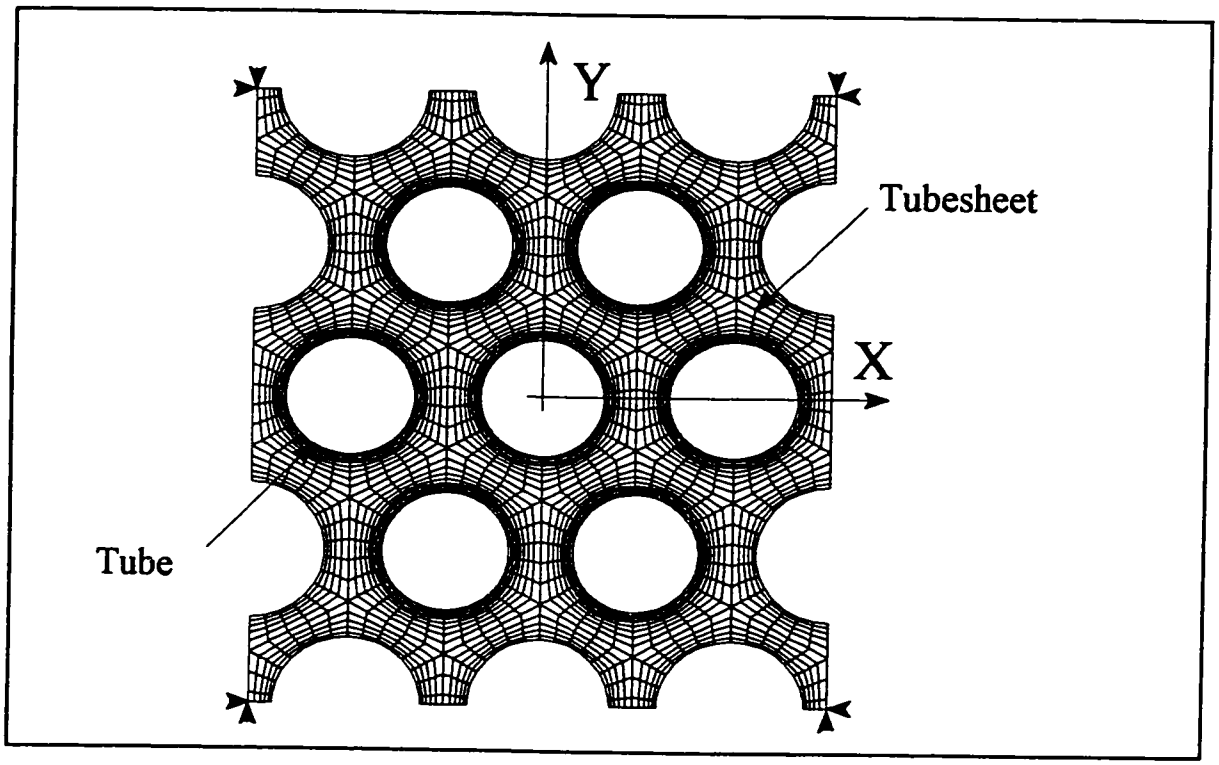


Figure 7.10: 2-D finite element model for sequential expansion case

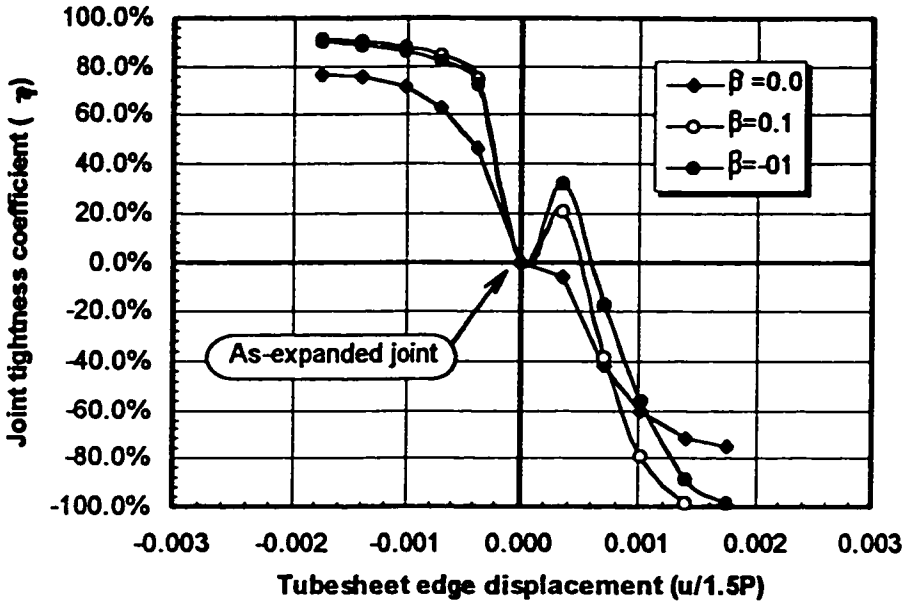


Figure 7.11: Relation between joint tightness coefficient and displacement (u) at different levels of displacement bi-axialty (β)

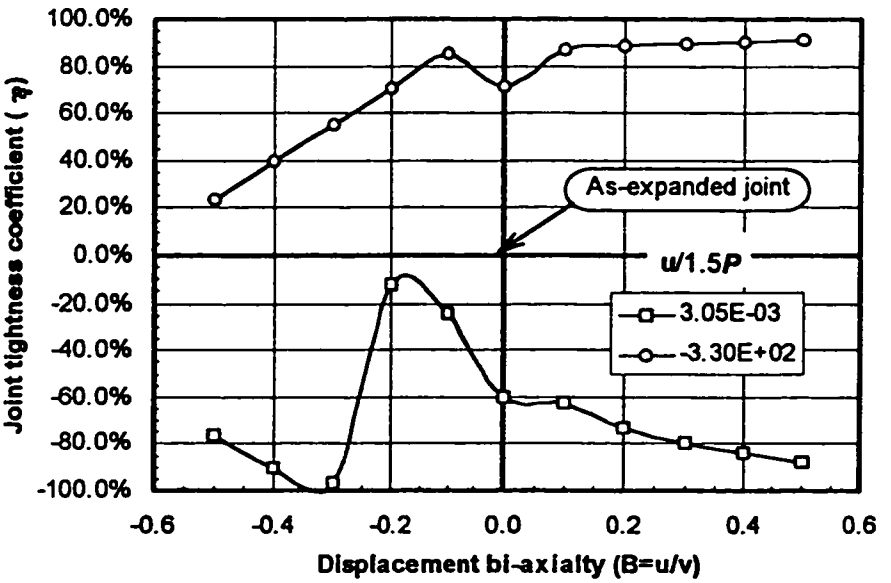


Figure 7.12: Relation between joint tightness coefficient and displacement ratio at different levels of displacement (u)

CHAPTER 8

MULTI-STEP OF EXPANSION

8.1 INTRODUCTION

The multi-step tube expansion technique for very thick tubesheet is very common in the industry of nuclear steam generators. Studying the difference between single-step and multi-step expansion processes is thus of interest for industrial application and will be performed in this chapter.

With the progressive needs for more powerful and economical nuclear power plants, designs have been oriented towards not only efficient but also highly productive steam generators. Consequently, a large massive tubesheet with large pressure area and thickness is used for such requirements. In currently manufactured steam generators, the thickness of the tubesheet may vary between 0.735 and 1.27 m. Expanding the tubes against a very thick tubesheet, is not always possible to be achieved by a single expansion technique. Figure 8.1 shows a part of tubesheet where some difficulties could be encountered while expanding the tubes that are close to the shell wall (Zone B) because the expansion mandrel is much longer than the space available between the tubesheet surface and the header of the steam generator. In such case, a multi-step expansion process using a shorter mandrel is proposed. The expansion is initiated form the tubesheet primary surface and applied over a portion of the

tube equal to the length of the mandrel. After the first step of expansion, the mandrel is then pushed forward and the process repeated. An over-lap zone between the two subsequent expansion portions is introduced and its length must be carefully controlled (see Figure 8.2). The length of the mandrel used in multi-step expansion is calculated according to the minimum space available between the tubesheet surface and the header, the number of steps to be applied, and the length of the over-lap zone.

The multi-step expansion is usually limited to a very thick tubesheet that is located in a very restrained area such as nuclear steam generator. Therefore, less attention was focused on this analysis. The profile of residual stresses and the deformed shape resulting form the two step of expansion are examined. The axisymmetric finite element solution was performed by using ANSYS 5.4 (1995) -licensed to B&W, Cambridge, Ontario. Also, a microscopic examination for some tubes expanded by two-step expansion is carried out.

8.2 AXISYMMETRIC FINITE ELEMENT ANALYSIS

A 2-D axisymmetric finite element model was used for two-step expansion of single tube placed freely inside the hole of an equivalent sleeve, Figure 8.3. The analysis will focus only on the over-lap zone. The same geometry used for Inconel 690 tube given in the previous chapter is used again here. According to Chaaban et al (1992), a 34.036 mm equivalent diameter for the sleeve should be used in the axisymmetric model. A cartesian coordinate system is placed on the tube axis and having its origin at a distance 228.6 mm

measured from the tubesheet primary surface. A length of 101.6 mm for both the tube and the sleeve was found adequate for the analysis of two-step expansion. All nodes along the side, Y=0.0, are constrained against the axial motion. This boundary condition is applied for the nodes of both the tube and the sleeve. The friction effect is also accounted for by using Coulomb's friction law with a typical value of the coefficient of friction (f = 0.1375). The expansion pressure is applied first over a portion of the tube located in the secondary side. The length of this potion is taken as 63.5 mm. After the expansion of this part of the tube, the expansion pressure is then applied over 63.5 mm of the tube primary side. The length of the over-lap zone is thus equal to 25.4 mm.

Figures 8.4 and 8.5 show the stress profiles on the tube outer and inner surfaces after the first step of expansion. The stress profiles are similar to those of the tube transition zone. Figures 8.6 and 8.7 show the final stress profiles on the outer and inner tube surfaces after the second expansion. The residual stress distribution is almost uniform along the tube surface except for those acting near the point located at the end of the first-expanded tube portion. The final deformed shape of the tube represented by the residual hoop strain is also shown in Figure 8.6 and 8.7. Some irregularities on the tube inner surface at the first location of first-expanded tube portion can be observed. Figure 8.8 is a picture taken to a real tube that was expanded against the tubesheet block by two-steps expansion and then cut longitudinally for microscopic examination. From a practical point of view, the tube inner surface is considered free from any irregularities resulting from two-expansion process.

Since the length of the expansion is much longer than that of the over-lap region, the final level of the residual contact pressure may be considered uniform. The only scattered variation in the residual contact pressure is observed in the over-lap zone due to the double expansion of the material in this portion.

Some study cases have been investigated to address the importance of the length of the over-lap region. Figures 8.9 and 8.10 show the final residual stress profiles on the tube inner surface of the expanded parts at different level of over lap length. Shorter over-lap region provides more irregular tube surface with very high level of tensile residual stresses and a remarkable reduction in the meeting surfaces between the tube and the tubesheet.

Executive Summary

The analysis of tube-to-tubesheet joint was finally extended to explore the difference between single pass and two-step expansions. A simplified axisymmetric finite element method was used. With two-step expansion, the results indicated the existence of tensile residual stresses on the inside surface of the tube. The levels of these stresses were dependent on the length of the over-lap region. The effect of the over-lap length on the level of tensile residual stresses was significant. When a shorter over-lap length was used, higher tensile residual stresses were developed. However, due to time limitation, this subject was not investigated in more details. It will be left for future studies.

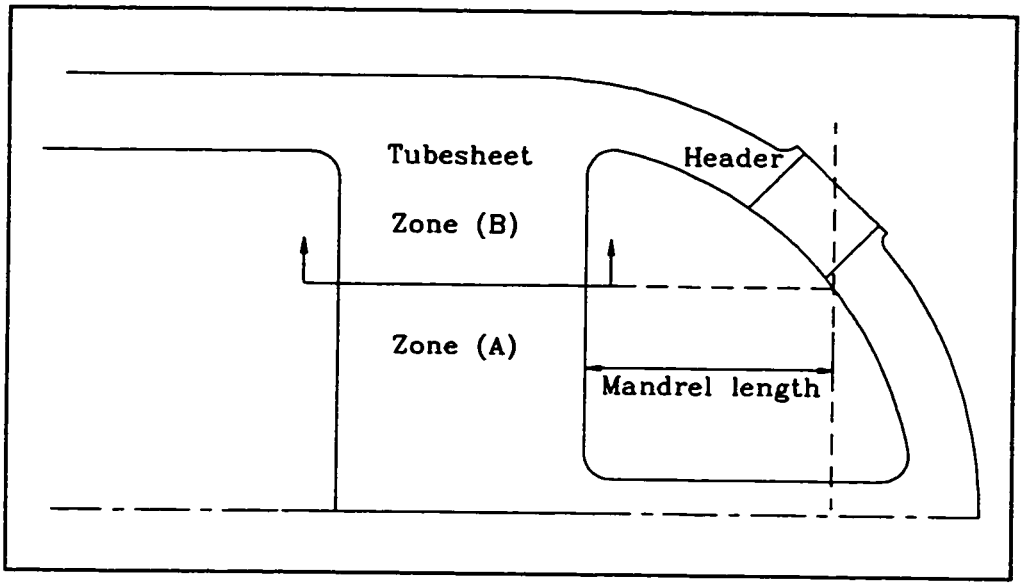


Figure 8.1: Difficulty in expanding tube in a very thick tubesheet; Zone (A) full expansion, Zone (B) Multi-expansion

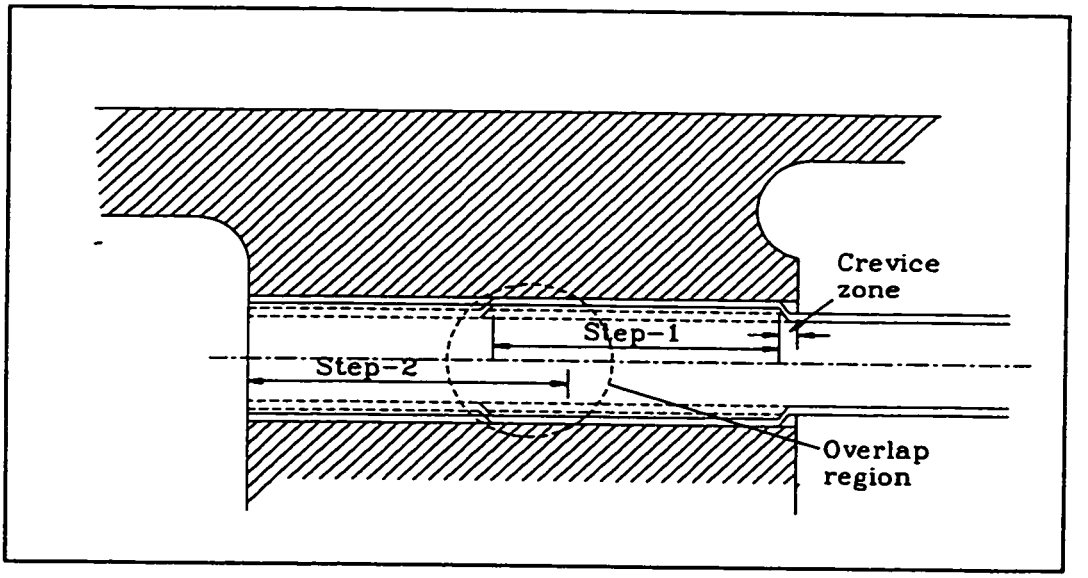


Figure 8.2 Two-step expansion process

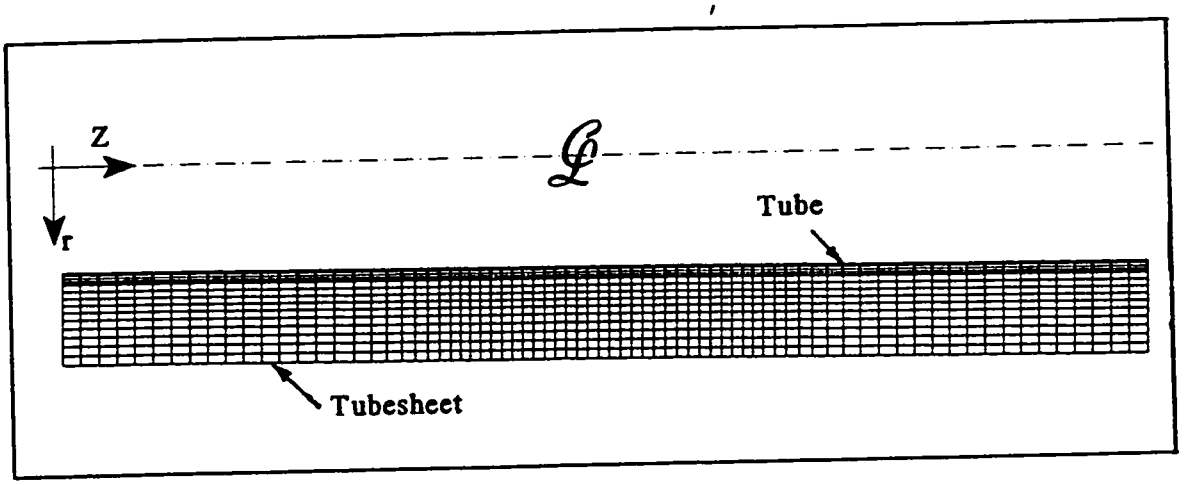


Figure 8.3: Near-overlap region axisymmetric model

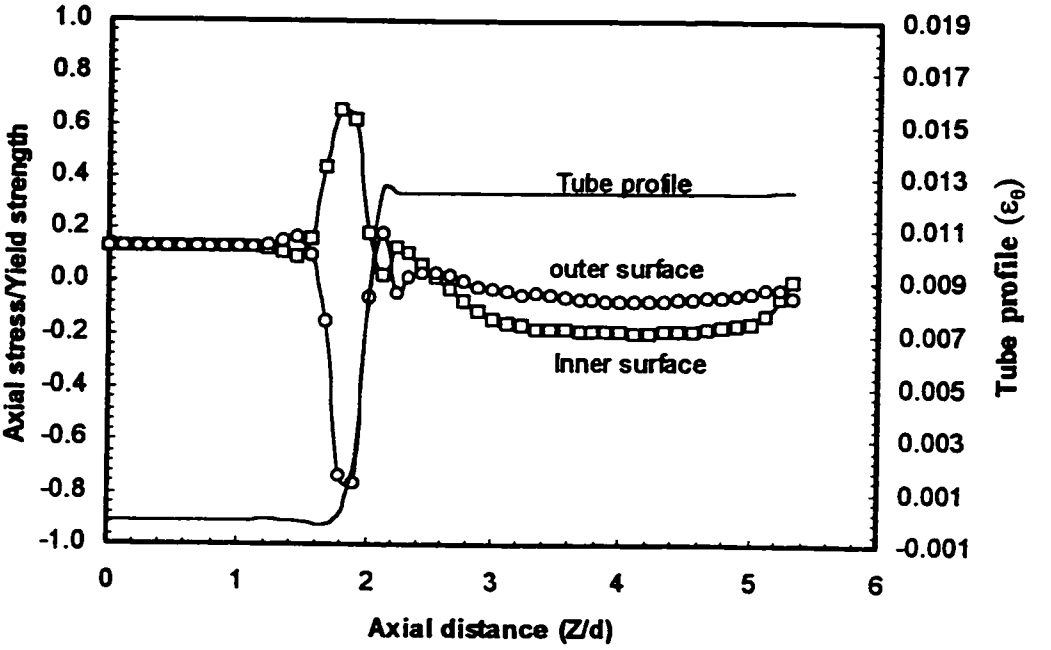


Figure 8.4: Axial stress and tube deformation profiles after first step of expansion

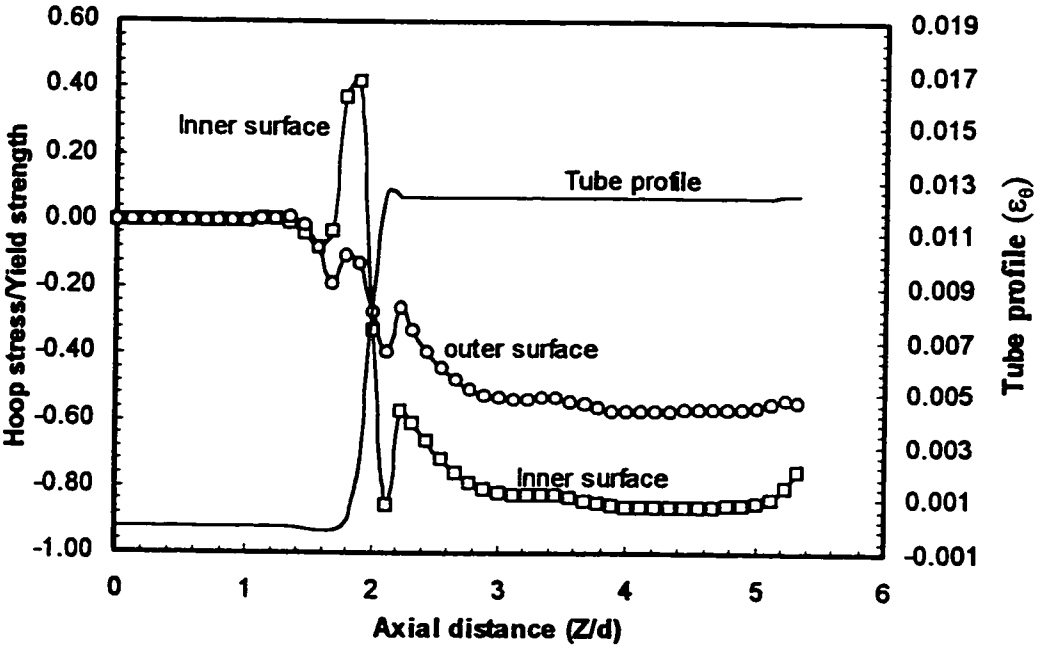


Figure 8.5: Hoop stress and tube deformation profiles after first step of expansion

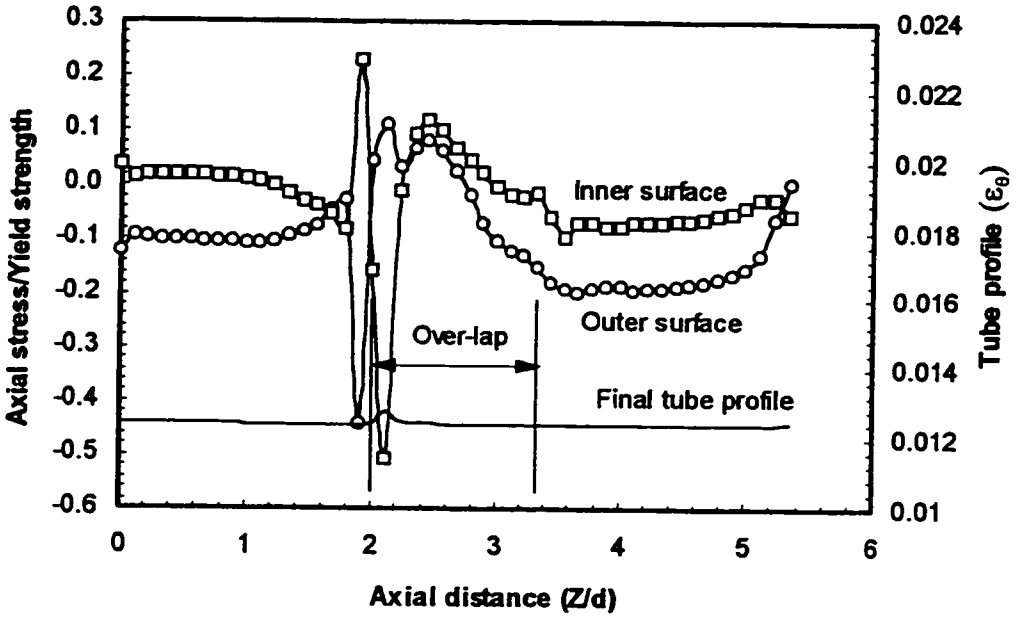


Figure 8.6: Axial stress and tube profiles after second step of expansion

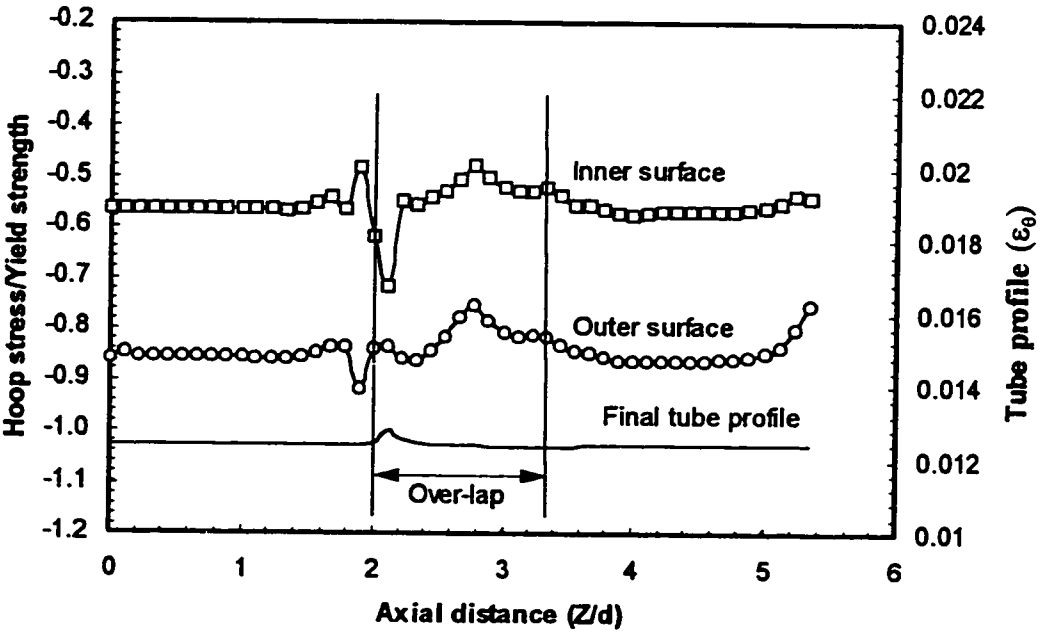


Figure 8.7: Hoop stress and tube profiles after second step of expansion

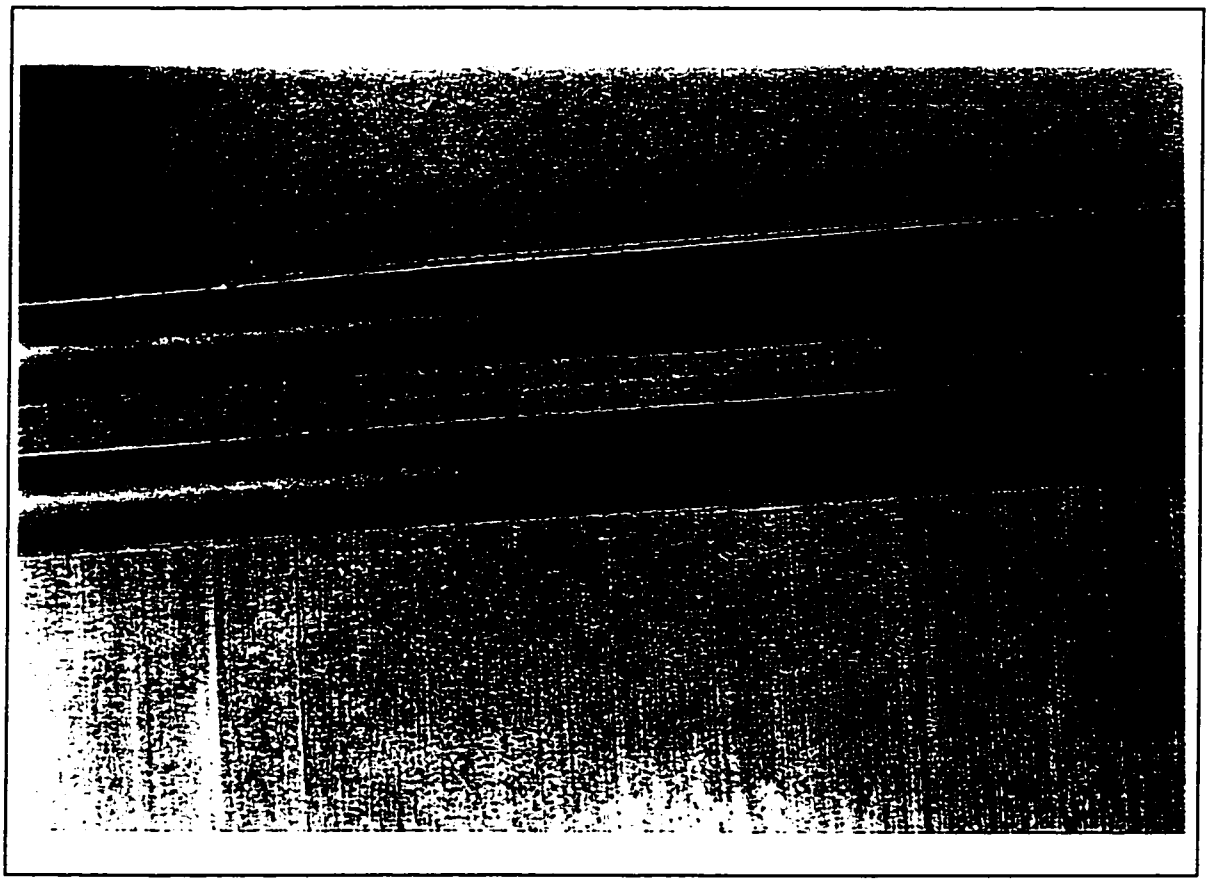


Figure 8.8: Section through two tubes expanded by 2-step expansion process indicating that the tube inner surfaces are free from any irregularities

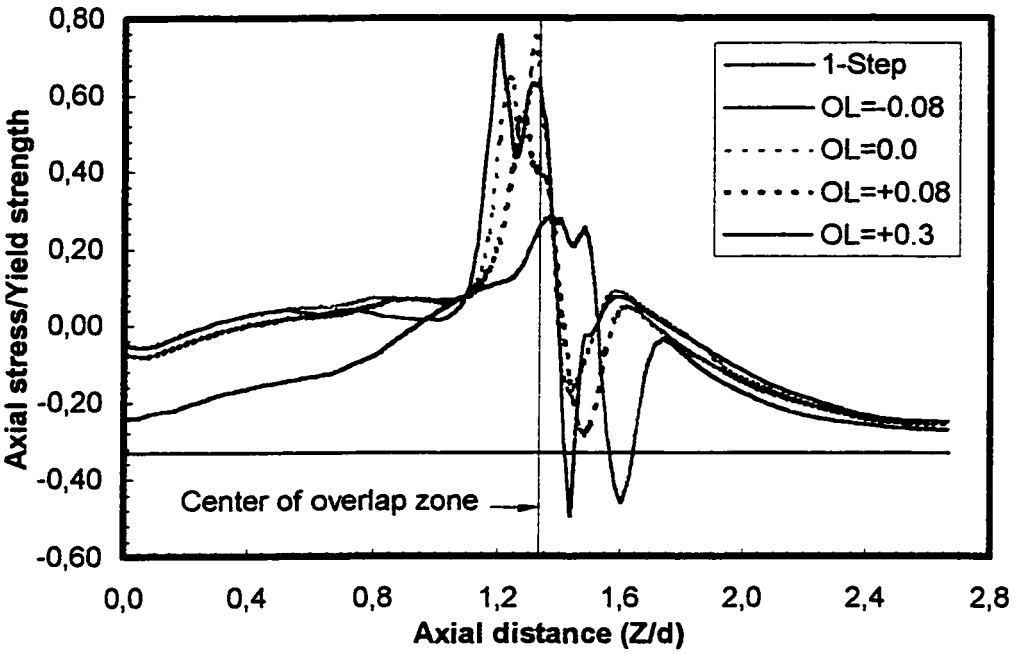


Figure 8.9: Axial stress profile on the tube inner surface with different levels of overlap length (OL=Overlap length/d)

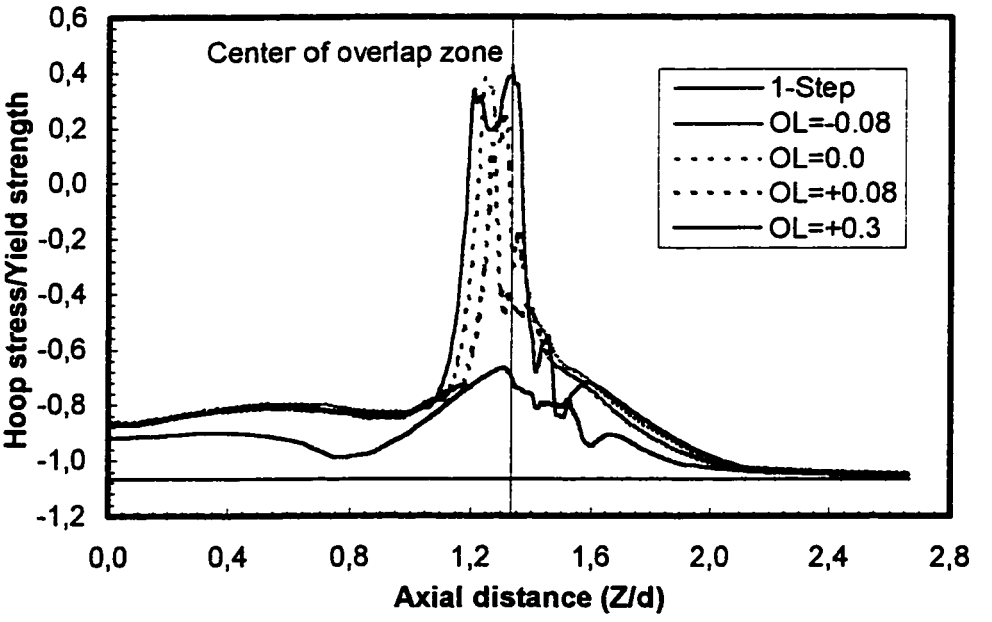


Figure 8.10: Hoop stress profile on the tube inner surface with different levels of overlap length (OL=Overlap length/d)

CHAPTER 9

CONCLUSIONS AND RECOMMENDATIONS

9.1 MAJOR FINDINGS

A) A 3-D finite element model was developed for tube-to-tubesheet joint analysis. A comparison with the axisymmetric finite element simulation indicates that the latter would greatly simplify the analysis with good accuracy, when an appropriate equivalent sleeve diameter is chosen. The comparison between the two models is in very good agreement as long as the tubesheet remains elastic during loading. In addition, numerical verification indicates that the axisymmetric finite element model has the capability of economically replacing 3-D model, while overcoming the limitation of 2-D plane stress/plain strain models.

B) A parametric study was performed to show the effect of all involved design parameter on residual contact pressure and maximum tensile residual stresses in the tube transition zone. The general finding can be summarised as follows:

1- Most dimensional and material parameters have a strong influence on the level of the residual contact pressure but have less effect on the maximum tensile residual stresses.

2- The initial tube radial clearance has a strong effect on the level of residual contact pressure when the strain hardening parameter is taken into account. However, when elastic perfectly plastic material behaviour is assumed, the effect becomes much less important.

3- Within the practical range of the dimensional parameters, the maximum tensile residual stresses for either strain hardening or elastic-perfectly plastic material assumptions, are not correlated to the initial radial clearance.

C) A closed-form solution for the hydraulic expansion process of tube-to-tubesheet joints has been developed based on elastic-plastic stress analysis. Three general equations were proposed for the minimum and maximum recommended expansion pressure and residual contact pressure. A comparison between these proposed solutions and those available in the literature has shown good agreement. On the basis of an extensive analytical analysis, some specific conclusions may be drawn:

1- The maximum tensile residual stress could be either in the axial or in the circumferential direction depending on expansion pressure level.

2 - The best joint expansion is achieved when the inner surface of the tubesheet is on the onset of yielding.

3 - After 25% of plastic overstrain in the tubesheet, further expansion does not produce a proportional increase in the residual contact pressure.

4 - Attention should be paid to the choice of joint material properties. A smaller modulus of elasticity ratio between tubesheet and tube yields higher residual contact pressure and vice-versa.

5 - The relationship between the residual contact pressure and the tube wall thickness ratio (t/d) is approximately linear.

6 - The analytical model was enhanced to calculate accurately the residual contact pressure by introducing a new factor taking into account the combined effect of both the strain hardening parameter and the initial radial clearance.

D) A detailed parametric finite element investigation for the loading, unloading, and residual stress profiles in the tube transition zone was performed. Some specific conclusions follow:

1- In all cases considered, the entire transition zone of the tube was deformed plastically during the expansion process.

2- The maximum tensile residual stresses, in both the axial and circumferential directions, are always located on the inner surface of the tube.

3- The crevice zone has a tensile residual stress on the tube outer surface

4- Within the range of the expansion pressure considered, the maximum value of the axial tensile residual stresses ranges approximately between 86% and 109% of the tube yield stress, and located almost at the end of the transition zone along the tube.

5- The maximum value of the residual hoop stresses ranges approximately between 55% and 68% of the tube yield stress, and is located almost at the beginning of the transition zone.

E) A simplified analytical approach was established to evaluate the residual stress profiles in the tube transition zone. Elastic-plastic plane-stress and beam-on-elastic-foundation theories were adopted in the development of the model. This model was verified against some numerical and experimental results reported in the literature.

F) A closed form equation to approximate the optimum recommended expansion pressure was proposed. The axisymmetric finite element analysis together with the statistical approach, *t*-test, have indicated that the level of expansion pressure is likely to increase the residual contact pressure, without significantly affecting the level of the tensile residual stresses in the tube transition zone. In addition, an analytically based empirical solution to approximate the level of the residual contact pressure introduced by applying the proposed optimum recommended expansion pressure, was developed and verified.

G) The analytical theory was extended to calculate the axial strength of tube-to-tubesheet joints. The analysis shows a large difference between the levels of the joint pull-out and push-out strengths. Both are linearly correlated to the level of the residual contact

pressure. The finite element results indicate that the pull-out strength is about 40% lower than that of the push-out.

H) Two different experimental rigs were set up for evaluating the frictional characteristics between the tube and tubesheet materials, and for evaluating the joint pull-out strength. The surface examination of both the tube and tubesheet have indicated some change in the surface roughness as a results of the expansion process, and consequently the coefficient of friction was greatly affected. For the tested material, a coefficient of friction of about 0.1375 was measured and the friction model followed Coulomb's friction law. The axisymmetric finite element model used to calculate the joint axial strength was also verified experimentally. On the basis of the pull-out strength, a good agreement between the results of the finite element model and those of the experimental measurements was obtained.

I) The 2-D and 3-D finite element models were used to investigate the effect of the working temperature on the joint tightness coefficient and the re-distribution of the residual stresses along the tube transition zone. On the basis of the analytical and finite element analysis of thermal effect, the main findings were:

1- The equivalent sleeve diameter evaluated on the basis of a number of variables related to the initial deformation and contact pressure is also valid in the analysis of working temperature application.

2-The axisymmetric finite element model simulation gives the change in the level of the residual contact pressure resulting from the temperature change. The numerical results compare well to those reported in the literature.

3-All cases considered in the present study indicate that during thermal loading and after a temperature cycle, the maximum tensile residual stresses in the tube transition zone are practically unchanged.

4- The level of the joint tightness coefficient is greatly affected by both the sign and the value of the thermal term $((\alpha_t - \alpha_s)\,\Delta T)$; a positive value of the joint tightness coefficient must be limited by the plastic deformation resulting in the tube and tubesheet and the negative value should be limited by -25% for an acceptable joint performance at working temperature.

J) The finite element method together with correlation analysis approach were used to perform a parametric study of the joint behaviour under mechanical loading:

1- From the 3-D finite element analysis, it is observed that the tubesheet rim displacement has an important effect on both the residual contact pressure and the residual stresses in the tube transition zone.

2- From the 2-D finite element together with statistical analysis for simultaneous and sequential expansion processes, a -0.5 correlation factor is found to exist between the tubesheet rim displacement and the joint tightness coefficient. The primary side

pressure is relatively less significant.

3- The finite element analysis shows that a joint tightness coefficient outside a certain range is always combined with some plastic deformation in the tubesheet ligament. As such, it is recommended that the joint tightness coefficient resulting from the mechanical loading effect should be limited by approximately ±25%.

K) The study of the hydraulic expansion process was extended further to explore the difference between single step expansion and 2-step expansion techniques. The results have shown the importance of the length of the overlap expansion region that must be adopted.

1- A shorter overlap length results in a tensile residual stresses as high as those of the tube transition zone.

2- When an adequate length of overlap region is selected, the tube inner surface appears to practically free from irregularities; also much lower tensile residuals stresses are developed in the overlap region.

2- Expanding either primary then secondary side or vice-versa introduces exactly the same level of residual stress and tube profiles.

Figure 9.1 provides a flow chart for the purpose of following the procedure and the appropriate figures and equations presented in this thesis. Starting from the basic available design data, joint performance may thus be evaluated.

9.2 RECOMMENDATIONS FOR FUTURE RESEARCH

The literature survey indicates that the mechanical rolling is sill widely used in industry. The difference between the hydraulic expansion and the mechanical rolling should be investigated using a 3-D finite element modelling. Possibly, an equivalent sleeve diameter applicable for both processes could be established, although the non-symmetrical nature of the roller-expansion process may render this approach inadequate.

Preliminary experimental testing has shown that the expansion process has a great effect on the coefficient of friction between the tube and the tubesheet. As such, further experimental work is required to provide a realistic set of data for this coefficient as a function of the material, dimensional and manufacturing variables. A more practical experimental apparatus to measure the friction characteristic must be designed and built in order to introduce in the specimen the same level of residual contact pressure that is created during expansion. In addition, the frictional measurement must take into account the effect of the elevated temperature on the friction characteristic of the contacting bodies.

The working condition joint behaviour relies on a large number of variables that are difficult to predict and control: temperature, differential pressure, tubesheet deflection and tube axial and non-axial loads. The proposed 2-D and 3-D finite element analyses are believed to be capable of predicting with some acceptable accuracy the tube-to-tubesheet joint

behaviour in terms of some of these variables. However, additional 3-D finite element analyses are required to investigate the effect of the tubesheet deformation and the non-symmetrical loading on the residual stresses in the tube transition zone.

Finally, regarding the multi-step expansion process, further study is required to explore the effect of the overlap region on the joint characteristic. A closed form equation to approximate the optimum overlap length would be helpful for industrial applications.

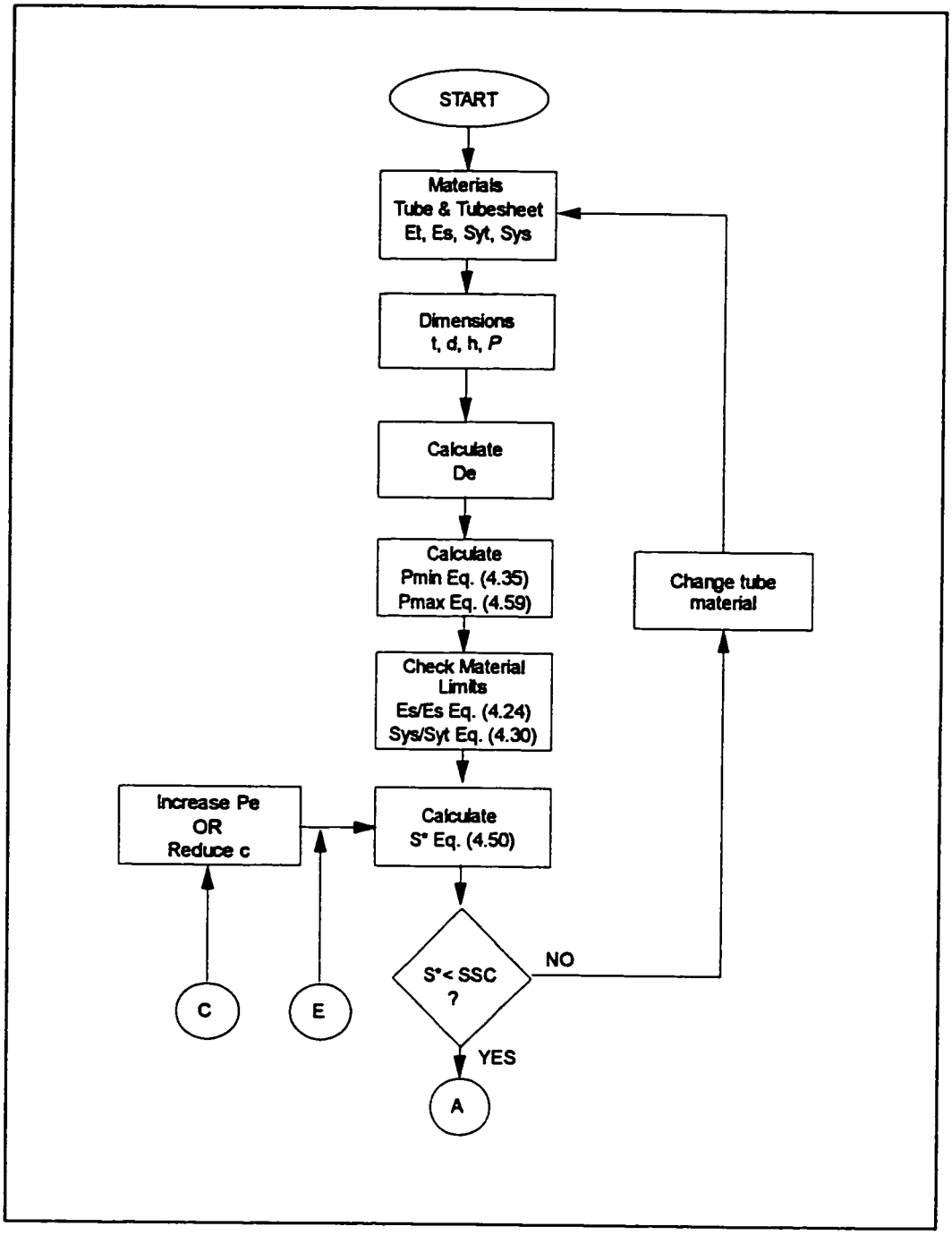


Figure 9.1: Proposed design procedures of tube-to-tubesheet joint

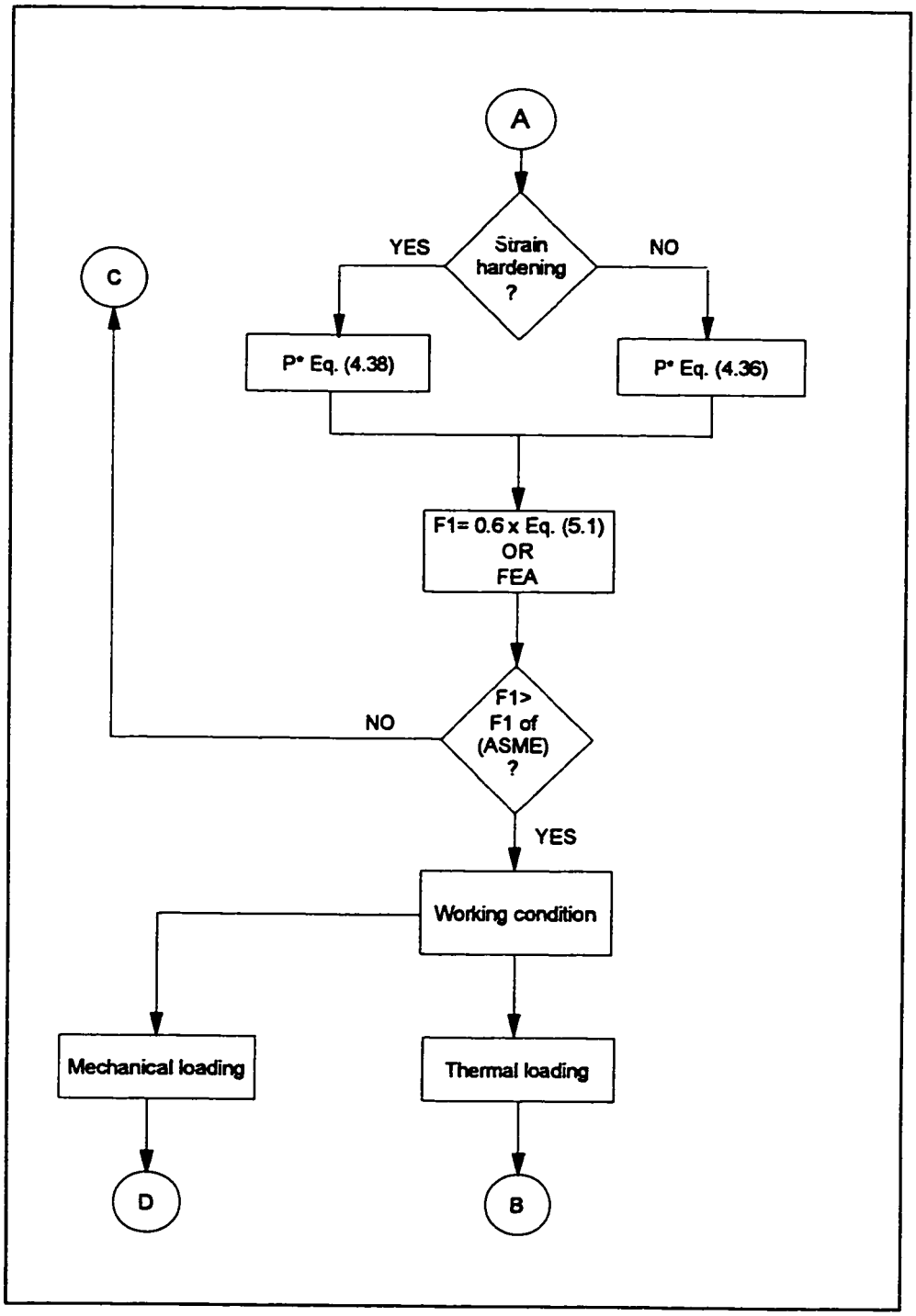


Figure 9.1: (Cont.)

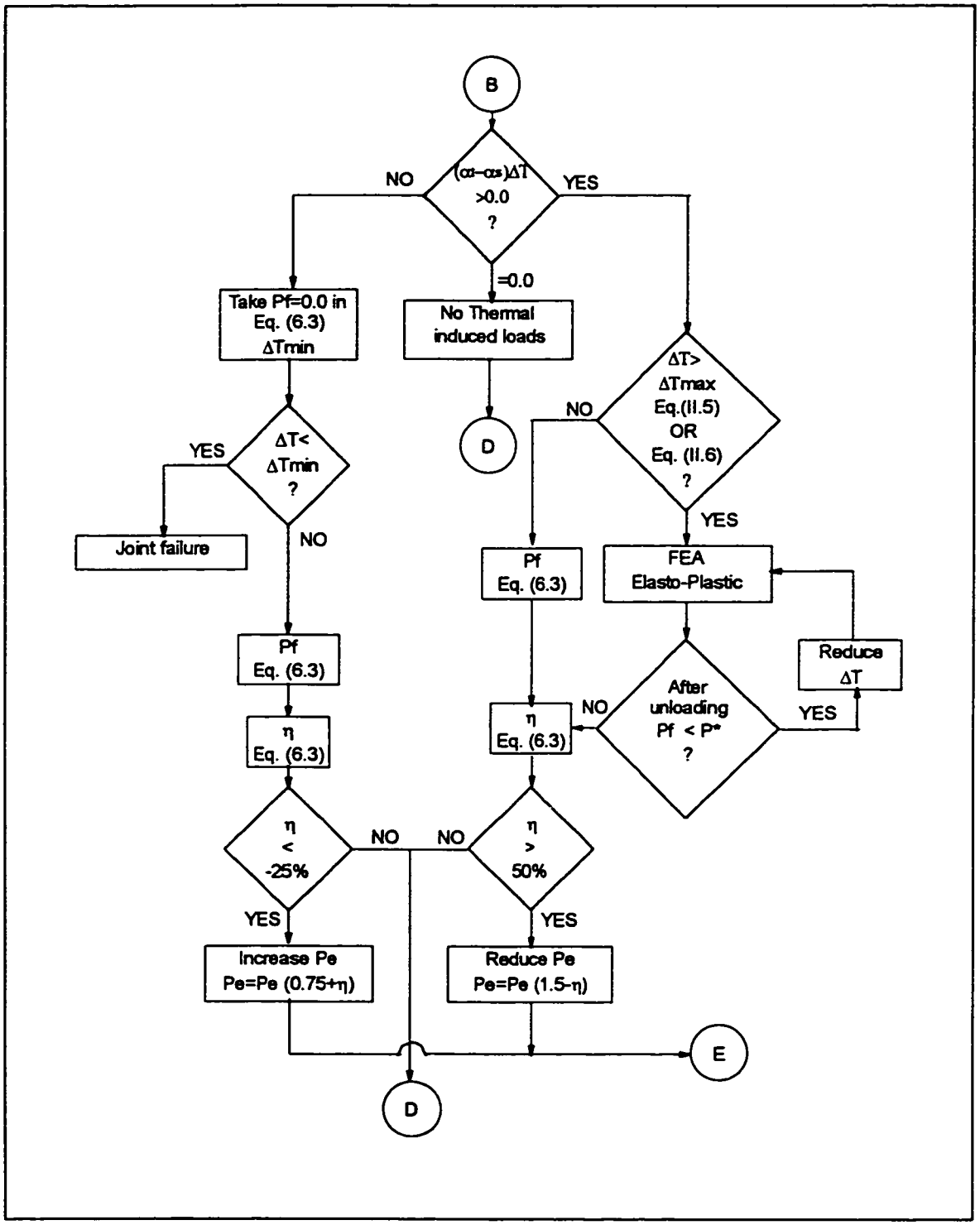


Figure 9.1: (Cont.)

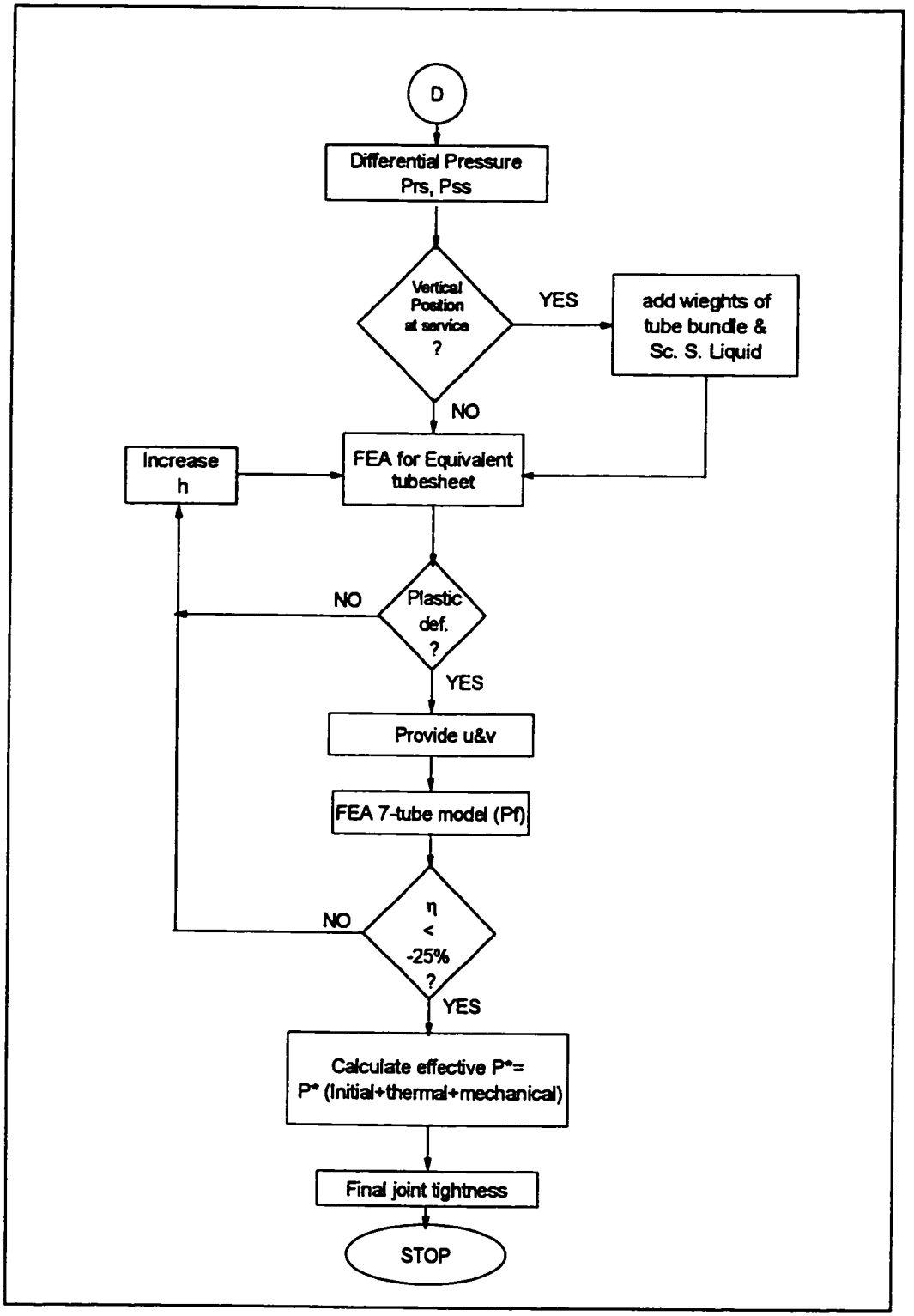


Figure 9.1: (Cont.)

BIBLIOGRAPHY

ABAQUS Version 5.4, (1995). Hibbitt, Karlson & Sorenson, Inc.

ABDELSALAM, U. and DOKAINISH, M. (1993). Hydraulic Expansion of Tube-To-Tubesheet Joints: A Finite Element Analysis. International Conferences on Expanded and Rolled Joint Technology, Toronto, CANADA, D41-D52.

ALDRED, D. L. (1984). Hydraulic Expansion of Tube-to-Tubesheet Joints. U. K. National Conference on Heat Transfer, Institut of Chemical Engineering, 1235-12254.

ALEXANDER, J. M. and FORD, H. (1956). Experimental Investigation of The Process of Expanding Boiler Tubes. Proceeding of Institut of Mechanical Engineering., Vol. 171, 351-367.

ALLAM, M., CHAABAN, A. and BAZERGUI, A. (1995). Residual Contact Pressure of Hydraulically Expanded Tube-to-Tubesheet Joint: Finite Element and Analytical Analyses. ASME Conference, PVP-Vol. 305.

ALLAM, M., CHAABAN, A. and BAZERGUI, A. (1996). Estimation of Residual Stresses in Hydraulically Expanded Tube-to-Tubesheet Joint. Submitted to Transaction of the ASME, Journal of Pressure Vessel Technology.

ANSYS Version 5.4. (1995). Swanson Analysis Systems, Inc.

APPENDIX A, SECTION VIII-DIVISION I OF ASME BOILER AND PRESSURE VESSEL CODE. (1992). Basics for Establishing Allowable Loads for Tube-to-Tubesheet Joints. ASME Code.

AUFAUR, M., BOUDOT, R., ZACHARIE G. and PROIX, J. M. (1987). Analysis of residual stresses due to roll-expansion: Finite element computation and validation by experimental tests. Transactions of the 9th International Conference of SmiRT, Vol. B, 499-503.

BAZERGUI, A. and LEMARQUIS, J. P., (1976). Residual Stress Measurement on Sanicro-30 Tube Sample. Center de Development Technolgique de L'Ecole Polytechnique de Montreal, Report No. 2384.

BURGREEN, D., (1971), Elements of Thermal Stress Analysis, Jamaica, NY, C.P Press.

CHAABAN, A., MA, H. and BAZERGUI, A. (1992). Tube-Tubesheet Joint: A Proposed Equation For The Equivalent Sleeve Diameter Used in Single-Tube Model. Transactions of the ASME, Journal of Pressure Vessel Technology, Vol. 114, 19-22.

CHAABAN, A., MORIN, E., MA, H., and BAZERGUI, A., (1989). Finite Element Analysis of Hydraulically Expanded Tube-To-Tubesheet Joints: A Parametric Study. ASME PVP Conference, 19-25.

CHAABAN, A. (1985). Static and Fatigue Design of High Pressure Vessels With Blind-Ends and Cross-Bores. Ph.D Thesis, University of Waterloo.

CHAABAN, A., ALLAM, M., BAZERGUI, A. and MA, H. (1993). Hydraulic Expansion of Tube-to-Tubesheet Joint. International Conferences on Expanded and Rolled Joint Technology, Toronto, CANADA, D1-D13.

COPE, E. T. (1943). Discussion-Expanded Tube Joints. Transactions of the ASME, 515-522.

CULVER, L. E. and FORD, H. (1959). Experimental Study of Some Variables of the Tube-Expanding Process. Proceeding of Institute of Mechanical Engineering, Vol. 173, 399-413.

DALLY, J. W., RILEY, W.F. and McCONNELL, K. G. (1994). Instrumentation for Engineering Measurements. John Wiley & Sons, NY.

DRUEZ, J. (1983). Détermination des Contraintes résiduelles dans des Tubes d'Echangeur de Chaleur. Ph.D. Thesis, Ecole Polytechnique De Montréal.

DRUEZ, J., BAZERGUI, A. and PETTIGREW, M. J. (1985). Residual Stresses in Roller-Expanded Thin Tubes. Journal of Experimental Mechanics, 316-324.

DUDLEY, F. E. (1954). Electronic-Control Method for the Precision Expanding of Tubes. Transaction of ASME, 577-584.

FENDER, D. A., WILLIAMS, G. J. and DICKER, E. P. (1985). Current Development in the On-Going Investigation of Steam Surface Condenser roller Expanded Tube-to-Tubesheet Joints. Joint Power Generation, ASME Paper No. 85-JPGC-Pwr-15.

FISHER, F. F. and COPE, E. T. (1935). Rolling-in of Boiler Tubes. Transaction of ASME, Vol. 57, 145-152.

FISHER, F. F. and COPE, E. T. (1943). Automatic Uniform Rolling -In of Small Tubes. Transaction of ASME, Vol. 65, 53-60.

FISHER, F. F. and BROWN, G. J. (1954). Tube Expanding and related subjects. Transaction of ASME, Vol. 75, 563-584.

FLESCH, B., VIDAL, P., CHABRERIE, J. and BRUNET, J. P. (1993). Operating Stresses and Stress Corrosion Cracking in Steam Generator Transition Zones (900-MWe PWR). International Journal of Pressure Vessel & Piping, 46, 213-228.

GAFFOGLIO, C. J. and THIELE, E. W. (1981).Tube to Tubesheet Joint Strengths. ASME 81-JPGC-Pwr-7, 1-6.

GOODIER, J. N. and SCHOESSOW, G. J. (1943). The Holding Power and Hydraulic Tightness of Expanded Tube Joints: Analysis of the Stress and Deformation. Transaction of ASME, Vol. 65, 489-496.

GRIMISON, E. D. and. LEE, G. H, (1943). Experimental Investigation of Tube Expanding. Transaction of ASME, Vol. 65, 497-505.

HALLING, J. (1975). Principles of Tribology, London, MacMillan.

HASLINGER, K. H. and HEWITT, E.W. (1983). Leak Tight, High Strength Joints for Corrosion Resistant Condenser Tubing. Joint Power Generation, ASME paper 83-JPGC-Pwr-39.

HASLINGER, K. H. and FISHER, F. M. (1985). Performance of High Strength, Corrosion Resistant Condenser Tubing and Muntz Tubesheet Joints Under Simulated Operational Loadings. Joint Power Generation, ASME Paper No. 85-JPGC-Pwr-63.

HULBERT, L. E. and NIEDENFUHER, F. W. (1965). Accurate Calculation of Stress Distributions in Multi holed Plates. ASME Journal of Engineering for Industry, Vol.87, 331-335.

HWANG, J., HARROD, D. and MIDDLEEBROOKS, W. (1993). Analytical Evaluation of The Hydraulic Expansion of Stream Generator Tubing in to Tubesheet. International Conferences on Expanded and Rolled Joint Technology, Toronto, CANADA, C98-C113.

JANTSCHA, R. (1929). Ueber das Einwalzen und Einpressen von Kessel-und Ueberhitzerrohren bei Verwendung Verschiedener Werkstoffe. Ph.D thesis, technical university of darmstadt.

JAWAD, M. H., CLARKIN, E. J. and SCHUESSLER, R. E. (1987). Evaluation of Tube-to-Tubesheet Junctions. Transaction of the ASME, Journal of Pressure Vessel Technology, Vol 109, 19-26.

KALNINS A. and UPDIKE, D. P. (1988). K-SHEL Manual for Incremental Plasticity

Analysis with a Personal Computer. Department of Mechanical Engineering and Mechanics, Lehigh University, Bethlehem PA 18015.

KASRIAE, B., POROWSKI, J. S. and O'DONNEL, W. J. (1983). Elastic-Plastic Analysis of Tube Expansion in Tubesheet. Pressure Vessel and Piping Conference, Portland, Ore.

KRIPS, H. and PODHORSKY, M. (1976). Hydraulic Expansion -A New Method for the Anchoring of Tubes. VGB KRAFTWERKSTECHNIK, Number 7, 418-426.

KOHLPAINTNER, W. R. (1995). Calculation of Hydraulically Expanded Tube-to-Tubesheet Joints. Transaction of ASME, Journal of pressure vessel technology, Vol.117, 24-30.

MA, H., CHAABAN, A. and BAZERGUI, A. (1990). Tube-To-Tubesheet Joints Analysis: A Proposed Method. ASME PVP Conference, Vol. 194.

MA, H. (1992). Parametric Study of Hydraulic Expanded Joint. Ph.D Thesis, Ecole Polytechnique de Montréal.

MAXWELL,C. A. (1943). Practical Aspects of Making Expanded Joints. Transaction of ASME, Vol. 65, 507-514.

METZGER, D. R. and SAUVE, R. G. (1993). Numerical Simulation of a Rolled Joint Formation Process. International Conferences on Expanded and Rolled Joint Technology, Toronto, CANADA, C2-C33.

METZGER, D. R., SAUVE, R. G. and NADEAU, E. (1995). Predication of Residual Stress

by Simulation of the Rolled Joint Manufacturing Process for Steam Generator. ASME PVP Conference, Vol. 305, 67-74.

MIDDLEBROOKS, W. B., HARROD, D. L. And GOLD R.E. (1991). Residual Stresses Associated with the Hydraulic Expansion of Steam Generator Tubing into Tubesheets. Transaction of the 11th. International Conference on Structural Mechanics in Reactor Technology, Atomic Energy Society of Japan, Vol. F.

NADAI, A. (1931). Plasticity. McGraw-Hill Book Company Inc., New York, N.Y.

NADAI, A. (1943).Theory of the Expanding of Boiler and Condenser Tube Joints Through Rolling. Transaction of ASME, Vol. 65, 865-880.

OPPENHEIMER, P. H. (1927). Rolling Tubes in Boiler Plates. Power, 300-303.

PODHORSKY, M. and KRIPS, H. (1979). Hydraulic Expansion of Tubes. VGB KRAFTWERKSTECHNIK, Number 1, 77-83.

RAMU, S. A.,KRIHNAN, A. and DXIT, K. (1987). Finite Element Analysis of Elastic-plastic Stresses in Channel Rolled Joints. 9th. International Conference on Structural Mechanics in Reactor Technology, Vol.8, 359-368.

REINIS, K. A. and SOLER, A. (1985). Tube-to-Tubesheet Joint Interface Pressure: PART II-Experimental Testing. ASME PVP Conference, Vol. 89-90, 235-242.

SACHS, G. (1947). Note on the Tightness of expanded tube joints. Journal of Applied Mechanics, A285-A286.

SAS Version 5.18. (1982). Statistical Analysis System Institute, USA.

SCOTT, D., WOLEMUTH G. and AIKIN, J. (1984). Hydraulic Expanded Tube-to-Tubesheet joints. Transactions of ASME, Journal of Pressure vessels Technology, Vol. 106, 104-109.

SHIRAZI-ADL, A., DAMMAK, M. and PAIEMENT, G. (1993). Experimental Determination of Friction Characteristics at the Tabular Bone/Porous-Coated Metal Interface in Cementless Implants. Journal of Biomedical Materials Research, Vol. 27, 167-175.

SINGH, K. P. and SOLER, A. I. (1984). Mechanical Design of Heat Exchanger and Pressure Vessel Components. Arcturus Publishers, Cherry Hill, N.J.

SOLER, A. I. and XU HONG (1984). Analysis of Tube-to-Tubesheet Joint Loading Including Thermal Loading. Transactions of ASME, Journal of Applied Mechanics, Vol. 51, 339-344.

TEMA (1988). STANDARDS OF TUBULAR EXCHANGER MANUFACTURES ASSOCIATION, Seventh Edition.

TAGUCHI. (1982). System of Experimental Design, Kraus International Publications.

TOBA, A. (1966). Residual Stress and Stress Corrosion Cracking in the Vicinity of Expanded Joint of Aluminum Brass Tube Condensers. Journal of Japan Petroleum Institute, Vol. 9, No. 5, 30-34.

UPDIKE, D. P., KALNINS, A. and CALDWELL, S. M. (1988). A Method for Calculating Residual Stresses in Transition Zones of Heat Exchanger Tubes. ASME PVP Conference, Vol. 139.

UPDIKE, D. P., KALNINS, A. and CALDWELL, S. M. (1989). Residual Stresses In Transition Zones of Heat Exchanger Tubes. ASME PVP Conference, Vol. 175.

UPDIKE, D. P., KALNINS, A. and CALDWELL, S. M. (1989). Contact Pressure in Rolled Tube-Tubesheet Joints. Transactions of the 10th International Conference on Structural Mechanics in Reactor Technology, Vol. L, 195-200.

UPDIKE, D. P., KALNINS, A. and CALDWELL, S. M. (1990). Analysis of Tube-Tubesheet Joints with Grooves. ASME PVP Conference, Vol. 194, 71-76.

UPDIKE, D. P. and KALNINS, A. (1991). Elastic-Plastic Analysis of Shells of Revolution Under Axisymmetric Loading. Welding Research Council Bulletin, 364, 46-56.

UPDIKE, D. P., KALNINS, A. and CALDWELL, S. M. (1992). Residual Stresses in Tube-Tubesheet with Grooves. Transaction of the ASME, Journal of Pressure Vessel Technology, Vol.114, 249-251.

URAGAMI, K. et al (1982). Experimental Residual Stress Analysis of Tube to Tube Sheet Joints During Expansion. Pressure Vessel and Piping, ASME, 82-PVP-61.

WALKER, C. A., MCDONACH, A. et al (1985). Dynamic Moiré Measurement of Strains Induced in a Titanium Tube Plate During the Rolling of a Series of Tubes. Journal of the Society for Experimental Mechanics, Vol. 25, No. 1.

WANG, C. (1953). Applied Elasticity. McGraw-Hill.

WANG, Y. and SOLER, A. I. (1988). Effect of Boundary Conditions on The Tube-Tubesheet Joint Annulus Model- Finite Element Analysis. ASME PVP Conference, Vol. 139.

WEINSTOCK, S. and SOLER, A. I. (1985). Tube-Tubesheet Interface Pressure: PART I-Theoretical Analysis with Strain Hardening and Temperature Dependent Properties. ASME PVP Conference, Vol. 89-90, 227-234.

WEINSTOCK, S., REINIS K. and SOLER, A. (1987) .Tube-To-Tubesheet Joint Interfacing Pressure: Analysis and Experiments. Transaction of the ASME, Journal of pressure Vessel Technology, Vol.109, 193-194.

WILSON, R. M. (1978).The Elastic-Plastic Behaviour of a Tube During Expansion. ASME paper 78-PVP-112.

YOKELL, S. (1982). Hyrdoexpanding: The Current State of Art. Joint Power Generation, ASME Paper No. 80-JPGC-1.

YOKELL, S. (1987). Calculation of Interference Required to Produce Maximum Strength in Expanded Tube-to-Tubesheet Joints. Joint Power Generation, ASME Paper No. 87-JPGC-24.

YOKELL, S. (1990). A Working Guide to Shell-and-Tube Heat Exchangers. McGraw-Hill, NewYork.

YOKELL, S. (1992). Expanded and Welded-and-Expanded Tube-to-Tubesheet Joints. Transaction of ASME, Journal of Pressure Vessel Technology, Vol. 114, 157-165.

YOSHITOMI, Y. et al (1979). Tube-Hole Structure for Expanded Tube-to-Tubesheet Joints. U.S. Patent No. 4, 142, 581.

APPENDIX I

EVALUATION OF THE EFFECTIVE COEFFICIENT OF FRICTION

Axial equilibrium for tube element shown in Figure I.1 provides

$$\frac{dF_z}{dz} + \pi d f P_f = 0 \tag{I.1}$$

On application of the pull-out force, the initial residual contact pressure P^* is reduced to P_f which increases the tube outer diameter and reduces the tubesheet inner bore. The change in the tube and tubesheet diameters is given respectively by;

$$\frac{U_t}{d} = \frac{P^* - P_f}{2E_t}\left(\frac{Y_t^2 + 1}{Y_t^2 - 1} - \upsilon\right) \tag{I.2}$$

$$\frac{U_s}{d} = \frac{P^* - P_f}{2E_s}\left(\frac{Y_s^2 + 1}{Y_s^2 - 1} + \upsilon\right) \tag{I.3}$$

Additional reduction in the tube outer diameter is resulted in by the tensile force F_z thus

$$\frac{U_t}{d} = \frac{P^* - P_f}{2E_t}\left(\frac{Y_t^2 + 1}{Y_t^2 - 1} - \upsilon\right) + \frac{\upsilon F_z}{2A_t E_t} \qquad \text{(I.4)}$$

where A_t is tube wall area and given by;

$$A_t = \pi\left(td - t^2\right) \qquad \text{(I.5)}$$

By assuming $E_t = E_s$, and equating the net increase of the tube outer diameter to the final decrease of the hole diameter, the following equation can be obtained:

$$F_z = 2A_t(P^* - P_f)\left(\frac{Y_t^2\, Y_s^2 - 1}{\upsilon\,(Y_t^2 - 1)\,(Y_s^2 - 1)}\right) \qquad \text{(I.6)}$$

Substituting Equation (I.6) into Equation (I.1), then we can obtain the following differential equation:

$$\frac{dP_f}{dz} - \alpha f P_f = 0 \qquad \text{(I.7)}$$

with the following boundary conditions:

$$\begin{array}{lll} \textbf{At} & Z=0.0 \ ; & F_z=F_1 \\ & Z=l \ ; & F_z=0.0 \end{array}$$

where α is given by:

$$\alpha = \frac{2\upsilon}{d}\left(\frac{Y_t^2\, Y_s^2 - Y_t^2}{Y_t^2\, Y_s^2 - 1}\right) \tag{I.8}$$

The final integral solution of Equation (I.7) is given by:

$$P_f = A\ e^{\alpha f Z} \tag{I.9}$$

Then Equation (I.6) can be written by:

$$F_z = \frac{\pi d}{\alpha}\,(P^* - A\, e^{\alpha f Z}) \tag{I.10}$$

By using the boundary condition, the value of the pull-out force can be given by:

$$F_1 = P \cdot \frac{\pi d}{\alpha} \left(1 - e^{-\alpha \mu l}\right) \tag{I.11}$$

The effective coefficient of friction is then:

$$\mu_1 = \frac{1}{\alpha l} \left(1 - e^{-\alpha \mu l}\right) \tag{I.12}$$

By reversing the sign of F_z in all previous equations, a closed form solution for push-out load can be obtained. The results may be written as follows:

$$F_2 = P \cdot \frac{\pi d}{\beta} \left(e^{-\beta \mu l} - 1\right) \tag{I.13}$$

where;

$$\beta = \frac{2\upsilon}{d} \left(\frac{Y_t^2 \, Y_s^2 - Y_t^2}{Y_t^2 \, Y_s^2 - 1} \right) \tag{I.14}$$

Then the effective coefficient of friction μ_2 can be given by:

$$\mu_2 = \frac{1}{\beta l} \left(e^{-\beta \mu l} - 1\right) \tag{I.15}$$

Soler et al (1984) performed an analytical solution to obtain more precise equations

for calculating the joint axial strength. The theory starts with two equilibrium equations in term of the normal and shearing stress components in r-z plane. By using a mathematical approach makes use of an energy minimization principle providing a lengthy integral and differential coupled equations, the joint axial strength (Pull-out or Push-out load) was obtain and represented here as follows:

$$F = \pi l d_t f P^{\bullet} \left(\frac{1 + \lambda}{1 + \lambda + \upsilon \Phi} \right) \tag{I.16}$$

where,

$$\lambda = (1 + \upsilon) \frac{E_t}{E_s} \frac{\bar{t}}{(1 - \bar{t})^2} \tag{I.17}$$

$$\Phi = \frac{\cosh(\theta f) - 1}{\sinh(\theta f)} \tag{I.18}$$

$$\theta = 2 \frac{l}{d(1 - \bar{t})} \tag{I.19}$$

$$d_t = d - t \tag{I.20}$$

By using Equation (I.16), the effective coefficient of friction (μ_3) can be written as follows:

$$\mu_3 = \frac{d_t}{d} f \left(\frac{1 + \lambda}{1 + \lambda + \upsilon \Phi} \right) \tag{I.21}$$

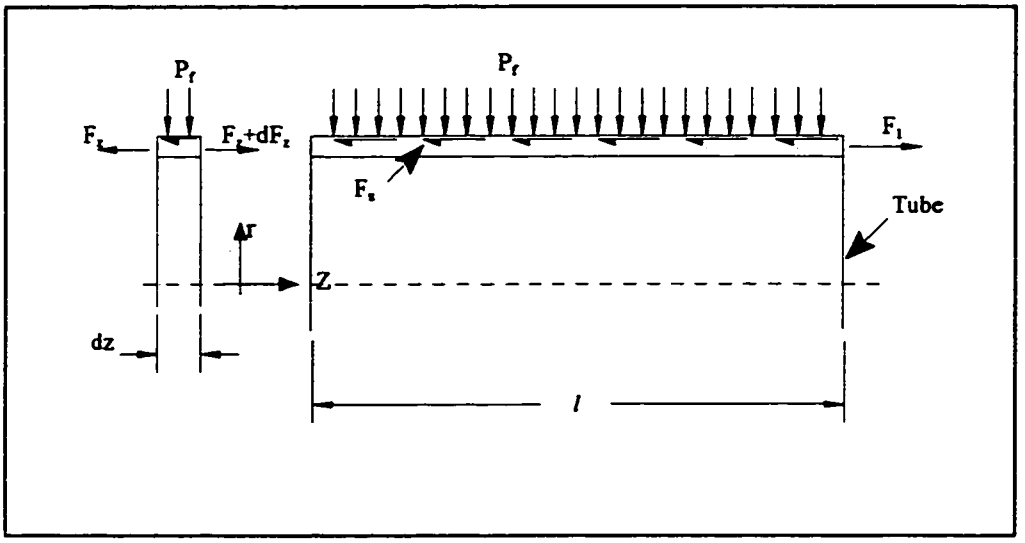


Figure I.1: Forces on tube subjected to an axial load

APPENDIX II

SUGGESTED TEMPERATURE LIMITS

Joint relaxation resulting from a relatively large change in the temperature may relieve the initial residual contact pressure set up by the expansion process. The initial residual contact pressure may fully release within the ASME Code's permitted metal temperature. Table II.1 which was suggested by Yokell (1990) provides the limits of the elevated temperature on the basis of ASME Code's permitted creep temperature of tube and tubesheet materials having similar thermal coefficient of expansions.

Table II.1: Suggested temperature limits for expanded tube-to-tubesheet joint with similar tube and tubesheet metals

Material	Suggested Creep limits	
	°F	°C
Low-carbon steel	700	370
Stainless Type 304	1000	535
Stainless Type 304	1050	565
Stainless Type 304	1050	565
Nickel 200	600	315
Inconel 600	750	400
Incoloy 800	1025	550
Monel 400	750	400

It seems that the range of the temperature specified in Table II.1 is limiting only the

heating temperature, while cooling temperature received no attention. In fact, based on the analytical and finite element analyses represented in Chapter 6, the cooled operating temperature has exactly the same effect as that of elevated temperature. Yet, if the tube and tubesheet thermal coefficients of expansion are different, the expanded joint could be lost at much lower temperature than that of creep limits given by Yokell (1990).

According to the analytical and finite element solutions represented in Chapter 6, the initial residual contact pressure may release under loading temperature that provides a negative sign to the thermal term $((\alpha_t-\alpha_s)\Delta T)$. The maximum temperature change at which the initial residual contact pressure is totally released can be given by:

$$\Delta T = \frac{P^*}{K_t\,(\alpha_t - \alpha_s)} \qquad \text{(II.1)}$$

Also, in order to prevent a dramatic loss of the initial residual contact pressure after a temperature cycle that has a positive thermal term $((\alpha_t-\alpha_s)\Delta T)$, the sum of the thermally induced stress and the room temperature residual stress resulted from the expansion process must not initiate a plastic deformation neither in the tube nor in the tubesheet materials.

The total stresses on the tube outer surface during the thermal loading can be written as follows:

$$\sigma_r = -P^* - \Delta P \tag{II.2}$$

$$\sigma_\theta = -\left(P^* + \Delta P \right) \frac{Y_t^2 - 1}{Y_t^2 + 1} + S_{t\theta} \tag{II.3}$$

$$\sigma_z = 0.0 \tag{II.4}$$

where P^* is the initial residual contact pressure and $S_{t\theta}$ is the room-temperature residual hoop stress on tube outer surface resulted from the elastic-plastic deformation of the tube during the expansion process. Evaluating this value of the stress can be obtained from elastic-plastic analysis of as-expanded tube-to-tubesheet joint. By using Tresca yield criterion and substituting from Equation (7.3) for the value of ΔP, the maximum temperature change can be given by:

$$\Delta T = \frac{\left(S_{yt} - S_{t\theta}\right)\left(Y_t^2 + 1\right) - P^*\left(Y_t^2 - 1\right)}{K_t\left(Y_t^2 - 1\right)\left(\alpha_t - \alpha_s\right)} \tag{II.5}$$

By a similar way the limit of the temperature on the basis of the tubesheet stress can be given

by:

$$\Delta T = \frac{(S_{ys} - S_{s\theta})(Y_s^2 + 1) - 2P^* Y_s^2}{2 K_t Y_s^2 (\alpha_t - \alpha_s)} \qquad \textbf{(II.6)}$$

where $S_{s\theta}$ is the room-temperature residual hoop stress created in the tubesheet inner surface as a result of the expansion process. The temperature at which the tube or the tubesheet first yields may then be set as the limiting temperature. Thus, a working condition ranged between the room temperature and the limiting temperature may increase the interference contact pressure without an anticipated loss of the initial residual contact pressure after the temperature cycle. A lower level of the expansion pressure can be also used to slightly expand the tube so as to create a lower level of the initial residual contact pressure which will, of course, increase due to the operating temperature. Consequently, the tube-to-tubesheet joint will serve well under working condition.

APPENDIX III

EFFECT OF SEQUENCE OF EXPANSION

The level of the residual contact pressure around the central tube of the 7-tube model represented in Chapter 7, is affected by the sequence of expansion. The average value of the residual contact pressure around the central tube is given for two different sequences. First, the sequence 7-1-4-2-5-3-6 of tube expansion is considered (see Figures 7.3 and 7.10). The result for this case which is shown in Figure III.1 indicates that the expansion of the surrounding tube has a great effect on the level of the residual contact pressure of the central joint (7). The value of the residual contact pressure around the cental tube is reduced by almost 20% due to the expansion of the neighbouring tubes. In order to avoid such reduction in the residual contact pressure around the central tube-to-tubesheet joint which is considered the ideal joint for the parametric study, the expansion of the central tube is achieved after expanding the surrounding tubes by the sequence 1-4-2-5-3-6-7. A detailed investigation on the effect of sequence of expansion has been already achieved by Chaaban, Bazergui and others (1989).

For more verification for the finite element model, a pull-out test for 7-tube block model pictured in Figure III.2 was carried out and the results was provided by (Private

communication). The experimental test was done on an MTS machine as pictured in Figure III.3 and the experimental procedures were approximately similar to those of the experimental technique explained in Chapter 5. The comparison between the value of the pull-out load measured experimentally for the central joint and that calculated by Equation (5.1) using the residual contact pressure of the finite element model represented in Figure 7.10, indicated approximately 40% difference. As illustrated in Chapter 5, this is attributed in part to change the level of the interference contact pressure while applying the pull-out loads. Also, the level of the residual contact pressure calculated based on plane stress finite element model, was expected to be higher than that of the real model pictured in Figure III.2. This is because of the resistance of the transition zone and non-expanded part of the tube which naturally cannot be represented by plane stress model. Finally, the ends of the tubes that are near to the tubesheet surface were closed by welding process as shown in Figure III.2. Thus, the elevated temperature created by the welding process could affect the level of the residual contact pressure of the real model. As such, the welding process was not recommended to close the tube end of the joint specimens used in the experimental procedures presented in this thesis as explained in Chapter 5.

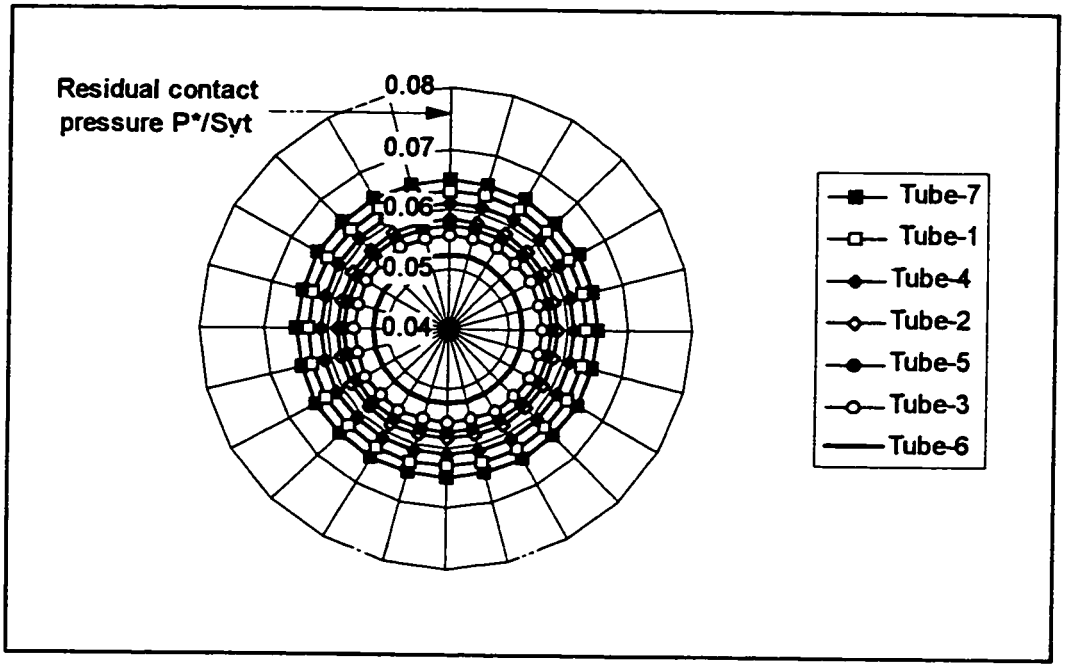


Figure III.1: Residual contact pressure around central tube (7)after expanding the neighbouring tubes

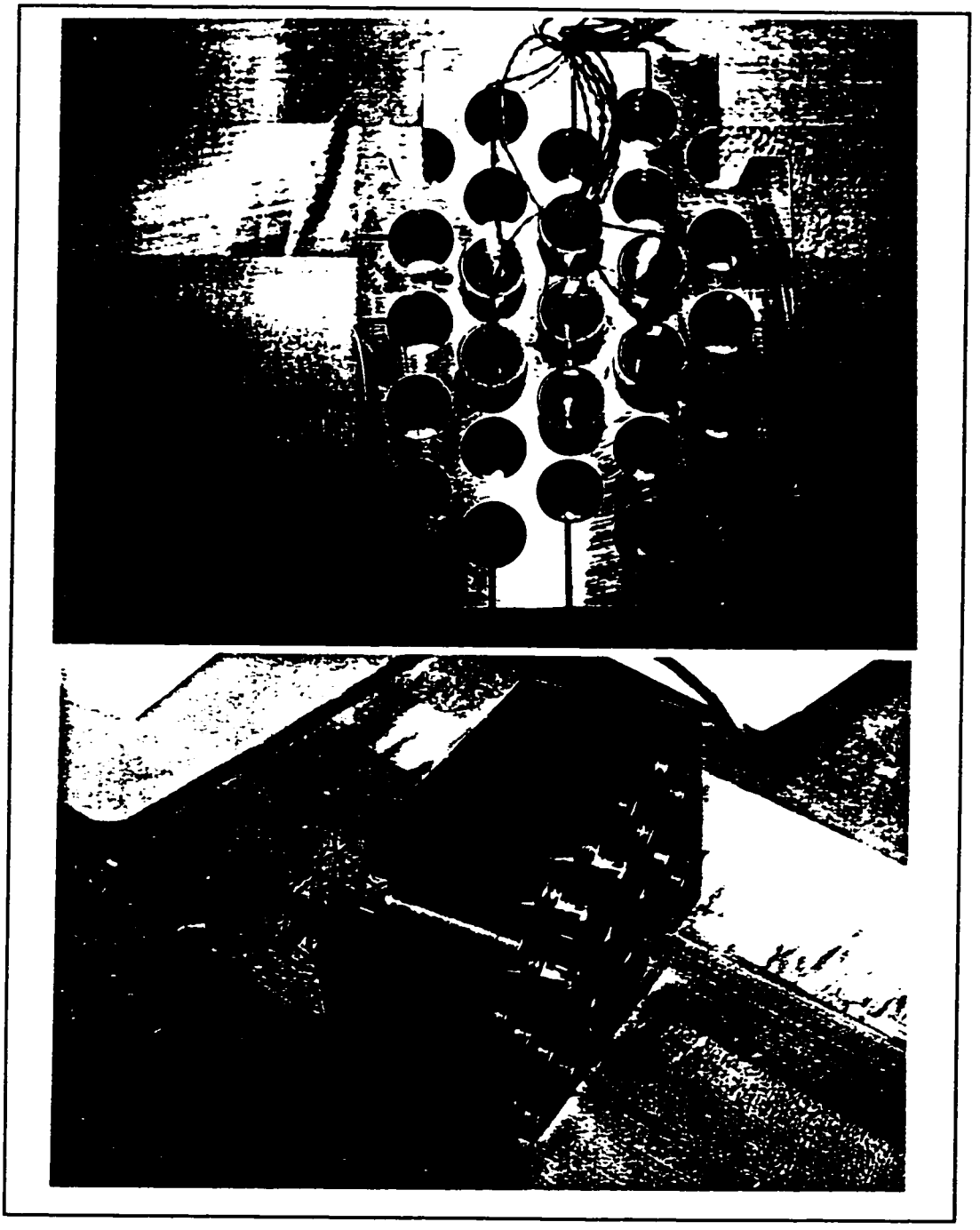


Figure III.2: 7-tube block

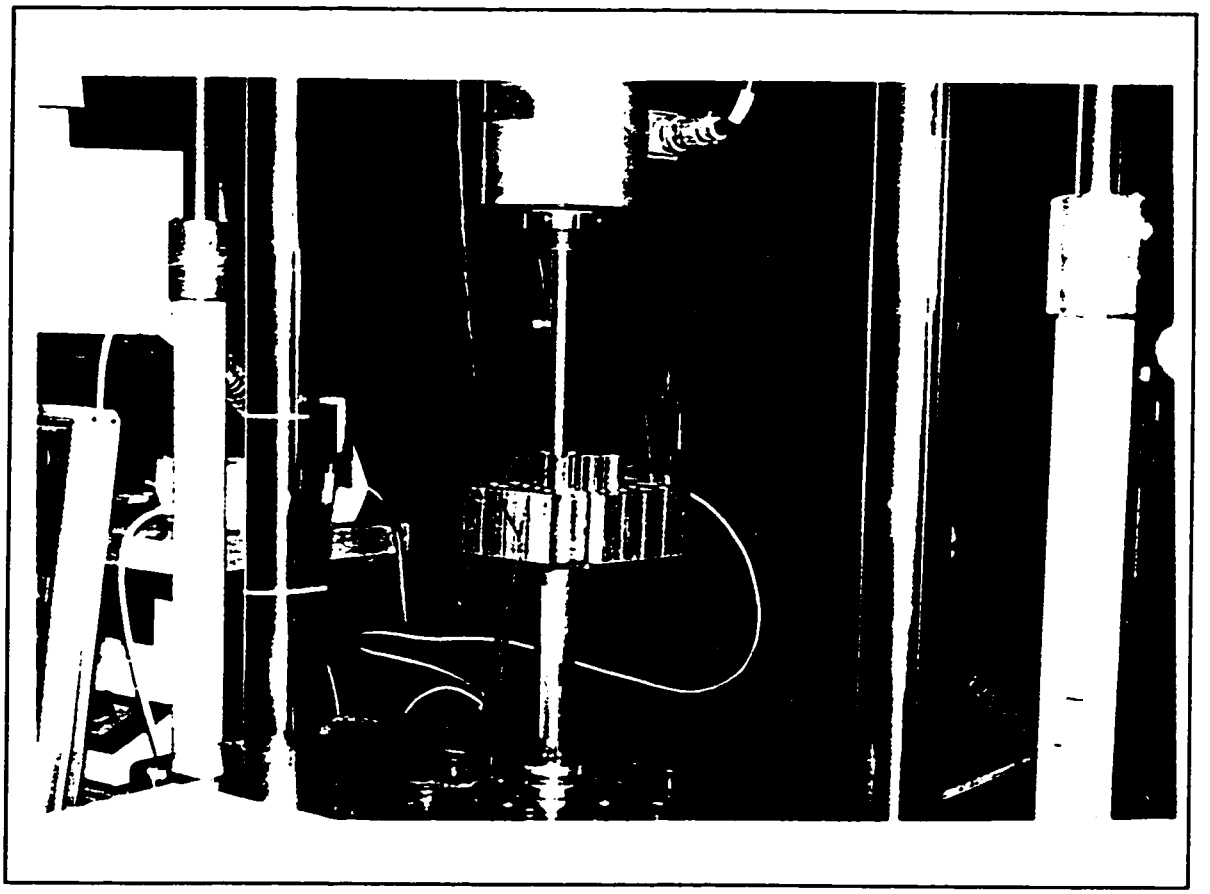
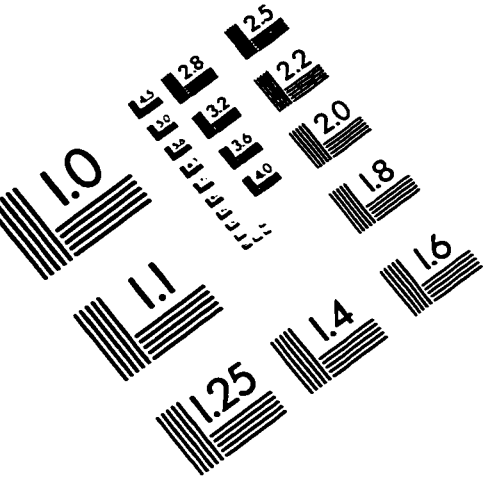
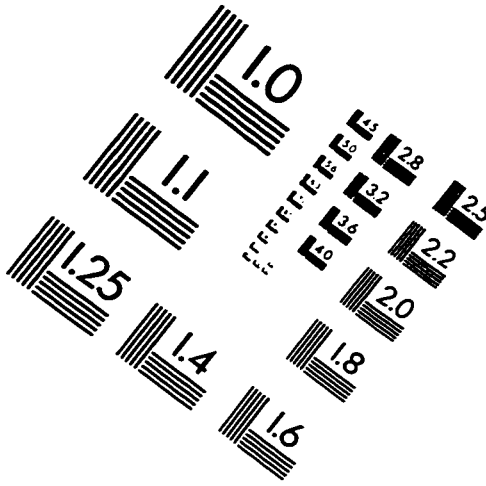
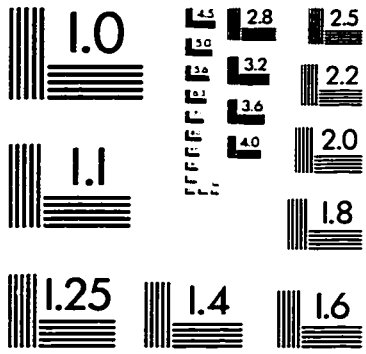


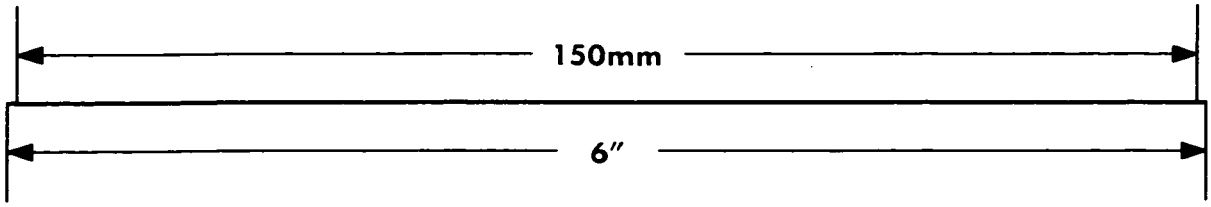
Figure III.3: Pull-out test for 7-tube block

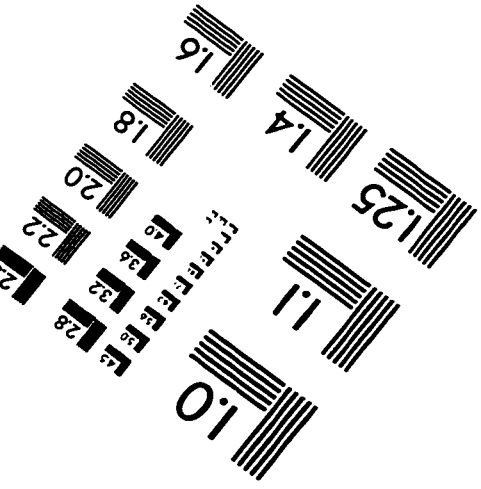
IMAGE EVALUATION
TEST TARGET (QA-3)

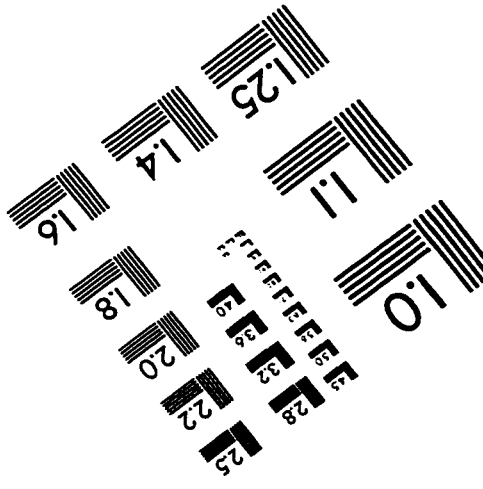












APPLIED IMAGE, Inc
1653 East Main Street
Rochester, NY 14609 USA
Phone: 716/482-0300
Fax: 716/288-5989

© 1993, Applied Image, Inc., All Rights Reserved